INVESTIGATION OF TRANSITION BETWEEN KINETIC THEORY AND DISSIPATIVE HYDRODYNAMIC FORMALISMS

Dissertation
zur Erlangung des Doktorgrades
der Naturwissenschaften

vorgelegt beim Fachbereich Physik
der Goethe-Universität
in Frankfurt am Main

von
Andrej El
aus Minsk

Frankfurt am Main 2011
(D30)

vom Fachbereich Physik (13) der Goethe-Universität
als Dissertation angenommen.

Dekan: Prof. Dr. Michael Huth

Gutachter: Prof. Dr. C. Greiner, Prof. Dr. D. H. Rischke

Datum der Disputation: ....

Contents

0.1. Einleitung vii
0.2. Herleitung und Erweiterung von dissipativen hydrodynamischen Gleichungen ix
0.3. Diskussion der Ergebnisse xi
  0.3.1. Berechnung der Scherviskosität xi
  0.3.2. Anwendbarkeit von hydrodynamischen Formalismen xii

1. Introduction 1
1.1. This work 1
1.2. Quantum Chromodynamics. 1
1.3. Heavy-ion research: on the way to a 'Big Bang'. 3
1.4. Phase diagram of QCD. 4
1.5. Heavy-Ion phenomenology: a short overview 5
  1.5.1. Jet Quenching. 5
  1.5.2. J/Ψ suppression. 6
  1.5.3. Collective Flow. 6
  1.5.4. Scaling of elliptic flow. 7
1.6. Theoretical tools to description of Heavy-Ion phenomenology 8
1.7. The Roadmap. 9
1.8. Notation 10

2. Construction of the hydrodynamic framework. 11
2.1. Basic tensorial decompositions. 11
2.2. Choice of the reference frame. 13
2.3. Equation of state. 14
2.4. Grad's 14-moment theory 14
  2.4.1. Approximation of off-equilibrium distribution 14
  2.4.2. Matching conditions 16
  2.4.3. Moments of the Boltzmann Equation 18

3. Derivation of the relativistic dissipative hydrodynamic equations. 21
3.1. Hydrodynamic equations from the entropy principle. 21
  3.1.1. Preface 21
  3.1.2. First-order equations 23
  3.1.3. Second-order equations 24
  3.1.4. Third-order equations 26

3.1.5. Second-order hydrodynamic equations for a multi-component system 29
3.2. Other known approaches 32
3.2.1. Second-order hydrodynamics from kinetic approach using method of moments. 33
3.2.2. Conformal second-order hydrodynamics from gradient expansion method. 34
3.2.3. Second-order hydrodynamic equations from kinetic theory. 35

4. Shear viscosity of a Boltzmann gas. 37
4.1. Review of theoretical methods. 37
4.2. Shear viscosity from Grad's 14-moment theory 39
4.2.1. One-component system. 39
4.2.2. Multi-component system. 40

5. Bjorken's picture of heavy-ion collisions 43
5.1. Bjorken's assumptions 43
5.2. Velocity field in Bjorken's model 44

6. Relativistic hydrodynamics for one-dimensional boost-invariant expanding systems. 47
6.1. Thermodynamic coefficients β_2 and α 49
6.2. Evolution equations for the energy and particle densities with particle number conservation. 50
6.3. Ideal hydrodynamics in Bjorken's model 51
6.4. Dissipative hydrodynamics in Bjorken's model with conserved particle number 51

7. Partonic cascade BAMPS 53
7.1. Numerical solution of Boltzmann Equation 53
7.2. Boost-invariant expansion in BAMPS. 56
7.3. Implementation of Leading Order pQCD processes in BAMPS 57
7.4. Application of BAMPS to heavy-ion phenomenology 58
7.4.1. Thermalization of gluon matter in BAMPS 58
7.4.2. Jet suppression. 62
7.4.3. Flow phenomena. 63

8. Off-equilibrium distribution function in BAMPS. 65
8.1. Generic properties of Grad's approximation. 65
8.2. Deviations of transverse particle distributions in BAMPS from equilibrium. 67
8.3. Deviations of transverse particle distributions in BAMPS from Grad's approximation. 69

9. Shear viscosity of a pQCD interacting gluon gas. 73
9.1. Shear viscosity of a gluon gas from BAMPS. 73

9.2. Shear viscosity to entropy density ratio as function of α_s. 76
9.3. Applicability limits of the second-order hydrodynamic formalism. 80
9.4. Limits of the transport approach. 82

10. Hydrodynamics vs BAMPS 85
10.1. Relevant observables. 86
10.2. Comparison of numerical results. 89
    10.2.1. Effect of initial time. 89
    10.2.2. Effect of shear viscosity to entropy density ratio. 94
    10.2.3. Beyond-third-order terms 97

11. Hydrodynamic evolution of a chemically equilibrating Gluon Plasma. 103
11.1. Bjorken's model including particle production and annihilation processes . 105
    11.1.1. Rate equation for particle production in anisotropic systems. . . . 105
    11.1.2. Second-order hydrodynamic evolution equations including number changing processes. 107
    11.1.3. Third-order hydrodynamic evolution equations including number changing processes. 107
11.2. Results of hydrodynamic calculations. 108
    11.2.1. Constant Knudsen number and inelastic cross section with chemically and kinetically equilibrated initial condition. 109
    11.2.2. Constant η/s and time-dependent inelastic cross section with chemically and kinetically equilibrated initial condition. 110
    11.2.3. Constant η/s, chemically and kinetically disequilibrated initial condition. 112
    11.2.4. Effect of chemical evolution on transverse spectra. 113
11.3. Comparison between dissipative hydrodynamic calculations and BAMPS results for a system with non-conserved particle number. 116

12. Hydrodynamic evolution of a two-component system 125
12.1. Hydrodynamic equations for a two-component system in one dimension. . 125
12.2. Effective shear viscosity of a multi-component system. 127
12.3. Comparison with kinetic transport calculations. 128

13. Summary, Conclusions and Outlook 137

A. Components of the off-equilibrium distribution function in Grad's 14-moment theory. 141

B. Entropy current up to third order in shear stress tensor. 145

C. Hydrodynamic equations for one-dimensional boost-invariant systems 149
C.1. Systems with conserved particle number 149
C.2. Systems with particle creation and annihilation processes 150
C.3. System of two components with conserved particle numbers. 151

D. Evolution equation for particle density in presence of inelastic processes. **153**

E. Shear viscosity coefficients for a multi-component fluid. **157**

Bibliography **158**

Index **173**

Curriculum Vitae **177**

Zusammenfassung

0.1. Einleitung

Die Erforschung von Schwerionnenkollisionen bei hohen Energien ist eines der aktivsten Felder der modernen Kern- und Elementarteilchenphysik. In Kollisionen von schweren Ionen an den modernen Beschleunigeranlagen RHIC an der Brookhaven National Laboratory (BNL) und LHC am CERN in Genf wird Kernmaterie zu extremen Energiedichten und Temperaturen komprimiert. Da die Kopplungskonstante der starken Wechselwirkung auf kurzen Längenskalen und bei hohen Energien kleiner wird, kann extreme Verdichtung der normalen (kalten) Kernmaterie zu ihrem 'Schmelzen' führen. Aus der hadronischen Materie entsteht dabei ein ungebundener Zustand von Quarks und Gluonen, den elementaren Konstituenten von Neutronen und Protonen. Dieser Zustand der stark wechselwirkenden Materie ist extrem kurzlebig und entzieht sich jeglicher direkter Beobachtung. Schlussfolgerungen über seine kurzzeitige Existenz und Eigenschaften können ausschließlich anhand von Messungen von sekundären Teilchen deduziert werden. Die dabei gemessenen Teilchen entstehen, wenn die Temperatur des Quark-Gluonischen Mediums unter die kritische Temperatur sinkt und so der umgekehrte Phasenübergang stattfindet. Die extremen Dichten und Temperaturen, die so im Labor erzeugt werden, sind dem Zustand des frühen Universums ähnlich, und die Erforschung des ungebundenen Zustandes der stark wechselwirkenden Materie, des sogenannten 'Quark-Gluon-Plasmas' (QGP) [1] ist somit von fundamentaler Bedeutung sowohl für die Kern- als auch für die Astrophysik. Die aktive Erforschung der Eigenschaften des QGP läuft seit den späten 70er Jahren (vgl. beispielsweise Referenzen [2, 3, 1]) bis heute.

In der Erforschung von Eigenschaften der Kernmaterie in hochenergetischen Schwerionenkollisionen kamen hydrodynamische Modelle bereits sehr früh zum Einsatz [2, 4, 5]. Analysen der Ergebnisse aus den Schwerionenexperimenten an den Beschleunigern RHIC und LHC haben in der letzten Dekade dazu geführt, dass Hydrodynamik mittlerweile zu einem Standardmodell zur Beschreibung der Eigenschaften des in diesen Experimenten erzeugten Mediums geworden ist. Dabei handelt es sich um eine relativistische Formulierung der hydrodynamischen Gleichungen, welche auch außerhalb der hochenergetischen Schwerionenphysik Anwendung finden. Messungen der Winkelabhängigkeit von Multiplizitäten der sekundären Teilchen [6, 7] und deren gute Übereinstimmung mit Ergebnissen hydrodynamischer Rechnungen [8, 9, 10, 11, 12] sind ein Hinweis darauf, dass der in Schwerionenkollisionen erzeugte ungebundene Zustand der stark wechselwirkenden Materie, bestehend aus Quarks und Gluonen, sich kollektiv verhält. Diese These wird von weiteren Beobachtungen unterstützt, wie beispielsweise Unterdrückung der gebundenen Zustände von Charm und Anti-Charm Quarks (sog. Quarkonia) [13, 14, 15] oder Unterdrückung von hochenergetischen Teilchen (sog. Jets), welche durch das Medium propagieren [16, 17, 18, 19, 20, 21, 22] . Aus dem direkten Vergleich aus den hydrodynamischen Modellen gewonnener Ergebnisse mit den experimentellen Daten wurde die Scherviskosität η des Quark-Gluonischen Gases extrahiert. Die mit der Entropiedichte s reskalierte Scherviskosität, η/s, ist eine dimensionslose Grösse und ein Maß für die stärke der dissipativen Effekte im Medium. Es zeigt sich, daß das η/s Verhältnis des Quark-Gluon Plasmas kleiner ist, als die entsprechenden Werte für die kalten Atomgase – die kältesten unter den bekannten Flüssigkeiten [23, 24]. Der kleine, jedoch endliche η/s Wert von QGP liegt nah an der universellen unteren Grenze $\hbar/(4\pi k_B)$, welche von Kovtun, Son und Starinets gefunden wurde [25]. Dadurch wurde das Paradigma der Entdeckung der 'perfekten Flüssigkeit' am RHIC [26], welches aus den frühen erfolgreichen Anwendungen der idealen Hydrodynamik [8] resultierte, zwar relativiert, jedoch gilt das Quark-Gluon Plasma als die womöglich 'perfekteste' unter den bekannten Flüssigkeiten. Der Wert von η/s des QGP darf als ein Kandidat für die Aufnahme ins sogenannte 'Particle Data Book' gelten, ein Standard-Nachschlagewerk mit den wichtigsten Werten und Zusammenhängen für die Elementarteilchenphysik.

Neben der dissipativen Hydrodynamik ist die kinetische Theorie das am meisten benutzte Mittel zur Modellierung der Dynamik von Schwerionenkollisionen. Die kinetische Transporttheorie basiert auf der Boltzmannschen Gleichung, welche die Evolution der Phasenraumverteilung unter Berücksichtigung von Wechselwirkungsprozessen beschriebt. In der Form, in der sie am häufigsten verwendet wird, beschreibt die Boltzmann-Gleichung die Ein-Teilchen Verteilungsfunktion. Sie ist somit die erste Approximation der sogenannten Bogolyubov-Born-Green-Kirkwood-Yvon (BBGKY) Hierarchie. In Kaskadesimulationen [27, 28, 29, 30, 31] sind die Konstituenten des QGP – Quarks und Gluonen – durch Quasi-Teilchen, d.h. punktförmige Teilchen, repräsentiert. Die kinetische Transporttheorie ist also eine *mikroskopische* Theorie, welche Prozesse auf der kurzen Skala der mittleren freien Weglänge der Teilchen beschreiben vermag. Im Gegensatz dazu ist die hydrodynamische Theorie eine *makroskopische* Theorie. Die hydrodynamischen Gleichungen folgen aus den Erhaltungssätzen für die Energie und den Impuls des Systems zusammen mit weiteren, ebenfalls makroskopischen Eigenschaften des Systems wie die Zustandsgleichung. Damit ist Hydrodynamik nicht in der Lage, die Prozesse auf kürzesten Längenskalen zu beschreiben, denn die hydrodynamischen Gleichungen basieren auf einer Mittlung über alle im System vorhandenen mikroskopischen Längenskalen.

Das Ziel dieser Arbeit besteht darin, in einer Reihe von Beispielen zu untersuchen, welche Unterschiede zwischen der dissipativen hydrodynamischen und kinetischen Beschreibung eines ultrarelativistischen Systems gibt. Diese Frage ist von großer Relevanz für die hochenergetische Schwerionenphysik, da dort die relativistische dissipative Hydrodynamik als ein Standard Modell zur Beschreibung der frühen Dynamik unmittelbar nach dem Kollisionsprozess gilt. Indem die Grenzen der Gültigkeit der dissipativen hydrodynamischen Beschreibung untersucht werden, wird zugleich auch die Gültigkeit der auf hydrodynamischer Beschreibung basierenden Erkenntnisse kritisch hinterfragt.

Eines der Ziele Dieser Arbeit besteht auch darin, die existierenden dissipativen hydrodynamischen Formalismen zu erweitern, sodaß ihr Anwendungsbereich nach Möglichkeit erweitert wird. Die kinetische Theorie wird in dieser Arbeit verwendet um, einerseits , die dissipativen hydrodynamischen Gleichungen herzuleiten und um , andererseits, eine Referenzlösung für die dissipativen hydrodynamischen Berechnungen zu finden.

Die vorliegende Dissertation basiert auf den folgen Publikationen:

- [32] Thermalization of a color glass condensate and review of the 'Bottom-Up' scenario. *A. El, Z. Xu, and C. Greiner, Nucl. Phys. A, 2008, 806, 287-304.*
- [33] Shear viscosity and out of equilibrium dynamics. *A. El, A. Muronga, Z. Xu and C. Greiner, Physical Review C, 2009, 79, 044914.*
- [34] Extension of relativistic dissipative hydrodynamics to third order. *A. El, Z. Xu and C. Greiner, Phys. Rev. C, 2010, 81, 041901*
- [35] A Relativistic dissipative hydrodynamic description for systems including particle number changing processes, *A. El, A. Muronga, Z. Xu and C. Greiner, Nucl.Phys.A, 2010, 848, 428-442*
- [36] Dissipative hydrodynamics for relativistic multi-component systems. *A. El,I. Bouras, F. Lauciello, Z. Xu and C. Greiner, 2011, arxiv: 1103.4038 [hep-ph]*

0.2. Herleitung und Erweiterung von dissipativen hydrodynamischen Gleichungen

Ideale hydrodynamische Gleichungen folgen direkt aus den Erhaltungsgleichungen für die Energie- und Impulsdichten (d.h.,Erhaltungsgleichung für den Energie-Impulstensor $T^{\mu\nu}$) sowie der Zustandsgleichung, welche den Zusammenhang zwischen den Zustandsgrössen eines Systems angibt, z.B. zwischen der Energiedichte und dem Druck eines idealen ultrarelativistischen Gases. Werden die dissipativen Terme berücksichtigt, so reichen die oben genannten Gleichungen nicht mehr aus und es müssen weitere fundamentale Gleichungen herangezogen werden. Die dissipativen Terme sind durch tensorielle Strukturen in den Darstellungen des Energie-Impulstensors $T^{\mu\nu}$ und des Teilchenfluss-Vektors N^{μ} repräsentiert – entsprechend den Gleichungen (2.4), (2.5) und den Definitionen (2.11) – (2.18). Die makroskopischen 'Felder' $T^{\mu\nu}(x,p)$ und $N^{\mu}(x,p)$ sind jedoch als integrale über die mikroskopische Phasenraumverteilungsfunktion $f(x,p) = \frac{dN}{d^3pd^3x}$ zu verstehen. Die sogenannte Gradsche Methode stellt den Zusammenhang zwischen den Komponenten des Energie-Impuls Tensors und der Teilchenfluss-Vektors und der entsprechenden Verteilungsfunktion $f(x,p)$ in konsistenter Weise her. Diese Zusammenhänge werden im 2 erklärt.

Für die Herleitung der Raum- und Zeit-Evolution der dissipativen Anteile des Energie-Impuls Tensors und des Teilchenfluss-Vektors wird, neben den Erhaltungssätzen und der Zustandsgleichung, eine zusätzliche Gleichung benötigt. Diese Gleichung kann die Boltzmann-Gleichung sein, wie beispielsweise in den Referenzen [37, 38, 39] ausgeführt.

Im Rahmen dieser Arbeit wird jedoch ein anderer Weg eingeschlagen. Die zusätzlich benötigte Gleichung, oder viel mehr Prinzip, ist das zweite Gesetz der Thermodynamik, welcher besagt, daß die Entropie eines abgeschlossenen Systems nicht abnehmen kann. Um dieses Prinzip in expliziter Form für die Herleitung dissipativer hydrodynamischer Gleichungen nutzen zu können, wird der Entropiedichte-Strom s^μ basierend auf der Kenntnis der Verteilungsfunktion $f(x,p)$ berechnet. Im klassischen, als Standard geltenden Ansatz von Israel und Stewart [40] wird angenommen, dass der Entropiedichte-Strom eines nicht-idealen Systems Korrekturen zweiter Ordnung in dissipativen Grössen (wie Schertensor, Wärmefluss oder Volumenviskosität) enthält. Diese Annahme basiert auf einer Reihenentwicklung, bei der die entsprechend reskalierten dissipativen Grössen als Kleinheitsparameter dienen. Damit der so konstruierte Entropie-Strom den zweiten Hauptsatz der Thermodynamik in Form der Ungleichung $\partial_\mu s^\mu \geq 0$ erfüllt, müssen die Evolutionsgleichungen für die dissipativen Grössen eine bestimmte Form haben. Die gleichzeitige Forderung der Konvergenz zur Navier-Stoke'schen Theorie (welche auch in der nicht-relativistischen Physik bekannt ist) führt auf die sog. dissipativen hydrodynamischen Gleichungen zweiter Ordnung. In dieser Arbeit wir die klassische Theorie von Israel und Stewart erweitert. Der Reihenentwicklung bei der Berechnung des Entropiedichtestromes wird bis zur *dritten Ordnung* in dissipativen Grössen durchgeführt. Dadurch entstehen neue Terme in der Evolutionsgleichung für den Schertensor $\pi^{\mu\nu}$ – dies wird in **Abschnitt 3.1.4** diskutiert (der Wärmefluss sowie Volumenviskosität werden in dieser Arbeit zur Vereinfachung vernachlässigt). Des weiteren ist in der klassischen, Israel-Stewart'schen Hydrodynamik, die Teilchenzahl stets konstant. In dieser Arbeit werden im **Abschnitt 11** Teilchenproduktion und Teilchenvernichtung in den dissipativen hydrodynamischen Formalismus eingebaut. Des weiteren wird in **Abschnitt 3.1.5** ein dissipativer hydrodynamischer Formalismus für binäre Mischungen entwickelt. Solche Systeme sind in der nicht-relativistischen Physik bekannt und können beispielsweise als Modell für Mischungen von einatomigen Gasen dienen. In dieser Arbeit werden hydrodynamische Gleichungen für ein relativistisches massenloses Gas entwickelt, welches aus Teilchen mit unterschiedlichen Wirkungsquerschnitten zusammengesetzt ist.

Die in den **Abschnitten 3.1.4**, **3.1.5** und **11** behandelten Erweiterung der 'klassischen' relativistischen dissipativen Hydrodynamik haben große Relevanz für das Feld der hochenergetischen Schwerionenphysik. Das System, welches durch relativistische dissipative Hydrodynamik beschrieben wird – das QGP – durchläuft unmittelbar nach ihrer Entstehung eine rasche Expansion und befindet sich weit weg vom Gleichgewicht. Unter solchen Bedingungen sind die dissipativen Effekte stark und die Fähigkeit der hydrodynamischen Gleichungen, die Evolution eines solchen Systems zu beschreiben hängt davon ab, welche Korrekturen und Terme in der Herleitung berücksichtigt und welche vernachlässigt worden sind. Berücksichtigung von Termen höherer Ordnung in dissipativen Grössen erscheint daher notwendig. Durch berücksichtigung von Teilchenproduktion und Annihilation wird der aus der pertubativen Quanten-Chromodynamik (QCD) bekannte Effekt der pQCD Brehmsstrahlung modelliert. Sowohl die Brehmsstrahlung als auch der umgekehrte Prozess der Annihilation (oder, Absorption) sind inhärente eigenschaften eines QCD Mediums. Die entsprechenden Matrixelemente können im pertubativen Regime analytische Berechnet werden.

Das quark-gluonische Plasma ist eine Mischung. Die Quarks und Gluonen haben, im Sinne der pertubativen QCD, unterschiedliche Wechselwirkungsraten. Auch sind die Energie- und Teilchendichten für Gluonen und Quarks stark unterschiedlich. Bei sehr hohen Energien werden die partonischen Verteilungsfunktionen im Inneren von Nukleonen klar durch die Gluonen dominiert. Im quark-gluonischen Plasma werden Quarks und Antiquarks jedoch produziert. Es stellt sich daher die Frage, inwiefern eine Mischung, in der die Spezies stark unterschiedliche Wechselwirkungsraten und Dichten aufweisen, durch einkomponentige Hydrodynamik beschrieben werden kann. Bleibt die innere Dynamik eines solchen Systems versteckt oder hat sie direkten und beobachtbaren Einfluss auf die mikro- und makroskopischen Observablen wie die Energie- und Impulsdichten, Flussanisotropien und Viskosität? Das QGP wird derzeit durch einkomponentige Hydrodynamik beschrieben. Eine Formulierung der dissipativen Hydrodynamik ist daher von großer Relevanz.

0.3. Diskussion der Ergebnisse

0.3.1. Berechnung der Scherviskosität

Aus dem sog. Entropieprinzip, auf welchem in dieser Arbeit die Herleitung hydrodynamischer Gleichungen basiert, folgen die Ausdrücke für die Transportkoeffizienten wie die Scherviskosität, Wärmeleitfähigkeit und Volumenviskosität. In dieser Arebit ist lediglich die Scherviskosität vom Interesse gewesen. Für die Berechnung von Transportkoeffizienten muss aber – im Gegensatz zu den hydrodynamischen Gleichungen – zusätzlich eine mikroskopische Gleichung verwendet werden, welche die Wechselwirkungsprozesse im System beschreibt. Der im **Kapitel 4** hergeleitete Ausdruck für die Scherviskosität η entält den Kollisionsterm aus der Boltzmann-Gleichung. Dieser Term enthält die Information übder die differenziellen Wirkungsquerschnitte für die Prozesse im System. Für pertubative QCD Prozesse muss der Ausdruck für die Viskosität numerisch ausgewertet werden. Dafür wurden die numerischen Methoden benutzt, die in der partonischen Kaskadesimulation BAMPS [30, 41] – Boltzmann Approach to Multi-Parton Scattering – zum Einsatz kommen. BAMPS ist ein mikroskopisches Modell, welches die partonische Phase einer Schwerionenkollision beschreiben kann. Es beschreibt also die Dynamik eines quark-gluonischen Gases und enthält einer Reihe von auf pQCD Matrixelementen basierten Wechselwirkungsprozessen. Unter Verwendung von Matrixelementen aus BAMPS wurde in **Kapitel 9** die Abhängigkeit der Scherviskosität eines *rein gluonischen* Gases von der Kopplungskonstanten α_s berechnet. Es zeigt sich, dass für die Werte von $\alpha_s = 0.2..0.6$, welche für die Schwerionenexperimente am RHIC und LHC relevant sind, die Viskosität pro Entropiedichte η/s zwischen 0.2 und 0.08, und somit nah am unteren physikalischen Limit, liegt. Der Grund für die niedrigen Werte des dimensionslosen η/s wurde in den Teilchenerzeugung und -vernichtungsprozessen gefunden. Durch den sog. Landau-Pomeranchyk-Migdal (LPM) Effekt, welcher kollineare Abstrahlung im QCD Medium unterbindet, wirken die Erzeugungs- und Vernichtungsprozesse stark isotropisierend [42, 41, 33]. Die in dieser Arbeit berechneten Werte für $\eta/s(\alpha_s)$ wurden vor kurzen durch zwei unabhängige, auf der Green-Kubo Formel [43] sowie der Betrachtung eines Scherflusses [44] basierte, Arbeiten mit hoher Genauigkeit bestätigt. Die Bedeutung von inelastischen Prozessen, womit der Bremsstrahlungsprozess und der umgekehrte Kanal gemeint sind, wurde bereits aus der Studie des Äquilibrierungsprozesses in der partonischen Kaskade BAMPS deutlich und wird im **Kapitel 7** diskutiert.

Extraktion von Transportkoeffizienten aus einer kinetischen Transportsimulation ist von zentraler Bedeutung für die Erforschung von Transportprozessen in der Schwerionenphysik. Damit wird die Brücke zwischen den beiden Ansätzen – dem makroskopischen, hydrodynamischen und dem mikroskopischen, kinetischen – geschlagen. Nur unter genauer Kenntnis der Korrespondenz zwischen den Werten von Wirkungsquerschnitt und Viskosität sind konsistente und direkte Vergleiche zwischen den beiden Ansätzen möglich. Die im **Kapitel 4** hergeleitete Formel für die Scherviskosität kann auch analytisch ausgewertet werden, falls der differentiale Wirkungsquerschnitt winkelunabhängig ist. Das erlaubt, zum Beispiel, die Viskosität unter Berücksichtigung von inelastischen Prozessen als Funktion des inelastischen Wirkungsquerschnittes zu berechnen.

0.3.2. Anwendbarkeit von hydrodynamischen Formalismen

Um die Grenzen der Anwendbarkeit von hydrodynamischen Formalismen zu untersuchen, wird in dieser Arbeit ein Spezialfall gewählt – ein longitudinal expandierendes System mit transversaler Isotropie. Somit beschränken sich die dissipativen Korrekturen auf eine Dimension. Die longitudinale Expansion wird in Form des sog. Bjorken'schen Flusses [45] realisiert. Ein solches System in analog zu einem in einer Dimension expandierenden Hubble-Universum. Eine detaillierte Beschreibung dieses von Bjorken geprägten Szenario's von Schwerionenkollisionen ist in **Kapitel 5** gegeben. Reduktion der hydrodynamischen Gleichungen auf einer Dimension wird in **Kapitel 6** diskutiert.

In einem longitudinal expandierenden System sorgt die Expansionsrate für Abweichung vom globalen Gleichgewicht. Der Energie-Impuls Tensor (und die mikroskopische Impulsraumverteilung) wird anisotrop und der longitudinale Druck sinkt. Dem entgegen wirken im kinetischen Bild die mikroskopischen Kollisionsprozesse bzw. Relaxation zum Gleichgewicht im hydrodynamischen Bild. Falls die Expansionsrate über die Äquilibrierungsrate dominiert, wird das System immer weiter weg vom Gleichgewicht getrieben. Lösungen von hydrodynamischen Gleichungen zweiter Ordnung können unter solchen Umständen zu unphysikalischen negativen Werten für den longitudinalen Druck führen, wie im **Kapitel 10** gezeigt wird. In einem voll-dimensionalen numerischen hydrodynamische Algorithmus führen negative Werte für den Druck sofort zu einem Zusammenbruch des Codes. Im **Kapitel 10** wird demonstriert dass dieses Problem in der Lösung der erweiterten hydrodynamischen Gleichungen nicht auftritt. Eine Erweiterung der dissipativen hydrodynamischen Gleichungen über die standardmäßige zweite Ordnung hinaus kann also zu einer erhöhten Stabilität von numerischen Algorithmen führen und unphysikalische Ergebnisse vermeiden helfen. Für die dissipativen hydrodynamischen Berechnungen stellen die kinetischen Transportsimulation mit BAMPS eine Benchmark dar. Dissipative Hydrodynamik wird als anwendbar erachtet, falls die relative Abweichung zwischen den hydrodynamischen und BAMPS Ergebnissen unter 10% liegt. Diese spezielle Wahl der Fehlertoleranz ist durch frühere Publikation [46] bedingt. Für die Anfangszeit $\tau_0 = 0.4\ fm/c$, d.h. eine typische Anfangszeit für die meisten dissipativen hydrodynamischen Simulationen [47], kann man feststellen dass die standardmäßige dissipative hydrodynamische Theorie zweiter ordnung für $\eta/s \leq 0.2$ anwendbar ist. Dieser Wert liegt in der Nähe der Physikalischen Viskosität des QGP (welche auch in dieser Arbeit bestimmt wurde). Die erweiterte Theorie dritter Ordnung kann hingegen auch für größere Viskositäten im Bereich $\eta/s \leq 0.4$ angewendet werden.

In **Kapitel 11** werden die Ergebnisse dissipativer hydrodynamischer Rechnungen für ein System mit Teilchenproduktion und Annihilation diskutiert. Es wird gezeigt, dass die Berücksichtigung dieser Prozesse im hydrodynamischen Formalismus einen großen effekt auf die Spektren und Temperatur des Mediums hat, auch wenn der Effekt auf andere Observablen, wie die Energiedichte eher gering ist.

Die hydrodynamischen Gleichungen für ein mehrkomponentiges System unterscheiden sich von denen für einkomponentiges System durch die Präsenz von mehreren Relaxationszeitskalen. Dies ist die Folge davon, dass die Wirkungsquerschnitte für Kollisionen von Teilchen unterschiedlicher Sorten unterschiedlich groß sind. Wie in **Kapitel 12** ausgeführt, unterscheidet sich das Verhalten eines mehrkomponentigen Systems vom Verhalten eines einkomponentigen Systems, wenn man die Evolution des Schertensors betrachtet. Man stellt auch fest, dass, unabhängig von der Anfangsbedingung, sich ein bestimmtes Verhältnis zwischen den Komponenten des Schertensors der Mischungskonstituenten einstellt. Dieses spezifische Verhältnis ist eine Charakteristik der Mischung und hängt nur von den Dichten und Wirkungsquerschnitten ab. Auch hier bringen die Vergleiche mit BAMPS Ergebnissen eine Bestätigung der hydrodynamischen Berechnungen. Ebenfalls in **Kapitel 12** wird gezeigt, wie sich die Viskosität einer Mischung berechnen lässt, falls die differenziellen Wirkungsquerschnitte winkelunabhängig sind.

1. Introduction

The farther you go, the less you know.

Lao Tzu (6th century BCE),
philosopher of ancient China.

1.1. This work

This work is dedicated to a study of various aspects of the theory of relativistic dissipative hydrodynamics. In high-energy heavy-ion physics hydrodynamic framework has become a standard theoretical tool, providing quite accurate description of a number of phenomena observed in the experimantal facilities. Still work on proper formulation of hydrodynamic formalisms for physical systems created in heavy-ion collisions is a continous processes and a very active research field. This work aims to contribute to a deeper understanding of the relativistic hydrodynamic formalism, its applicability limits and intrinsic parameters.

1.2. Quantum Chromodynamics.

Quantum Chromodynamics (QCD) is the theory of the strong interaction, which is one of the four fundamental interactions of nature – along with the electromagnetic, weak and gravitational interactions. For three of these interactions – strong, weak and electromagnetic – quantum field theories have been formulated. Together they constitute the Standard Model of elementary particle physics. A quantum theory of gravity is still to be developed. The 'quantum fields' of QCD are quarks and gluons. Gluons are the mediators of the strong interaction, in a similar way to which the photons are the mediators of the electromagnetic force, which is represented by the simplest of the quantum field theories. But in contrast to the photons, gluons can interact with each other. This property of QCD, if formulated in a mathematical way, follows from its non-Abelian structure. Analogous to the electromagnetic interaction, which exists between carriers of the electric charge, strong interacting objects carry a so-called color charge, or simply Color. Whereas there is only one charge – namely *the* electric charge – in (Abelian) electromagnetic quantum field theory, there are three colors in (non-Abelean) QCD, symbolically labeled 'red', 'green' and 'blue'. Gluons, the carriers of the strong force, rotate the color of the interacting objects. Thus, in contrast to the electromagnetic force which is represented by the symmetry group $U(1)$ and has one gauge field, the photon, the strong force is represented by the non-Abelian $SU(3)$ group and has $3^2 - 1 = 8$ gauge fields – the gluons.

In nature the carriers of color charge do not exist in an isolated form. All objects observed by any direct measurement – e.g. protons and neutrons – are color-neutral. If one were to try to separate the two constituents of a quark–anti-quark pair, the most simple color-neutral object, the attraction and potential energy between them would increase with the distance. As the potential increases, it becomes more favorable to create a new quark–anti-quark pair, so that another color-neutral object appears – but color stays 'confined'. Color confinement is one of the basic properties of the strong interaction. In this example, increasing the distance corresponds, by virtue of Heisenberg's uncertainty principle, to decreasing the energy scale. Thus, color confinement means that the coupling of the strong interaction increases with decreasing energy scale. In a macroscopic world of large spacial and accordingly small energy scales strong coupling is indeed infinitely strong. This conclusion can be made from the simple fact that single quarks and gluons cannot be observed *outside* of protons and neutrons. One particular implication of this conclusion is very intriguing – on the other end of the energy spectrum, on large energy and small length scale – color confinement should disappear and quarks and gluons should become asymptotically free .

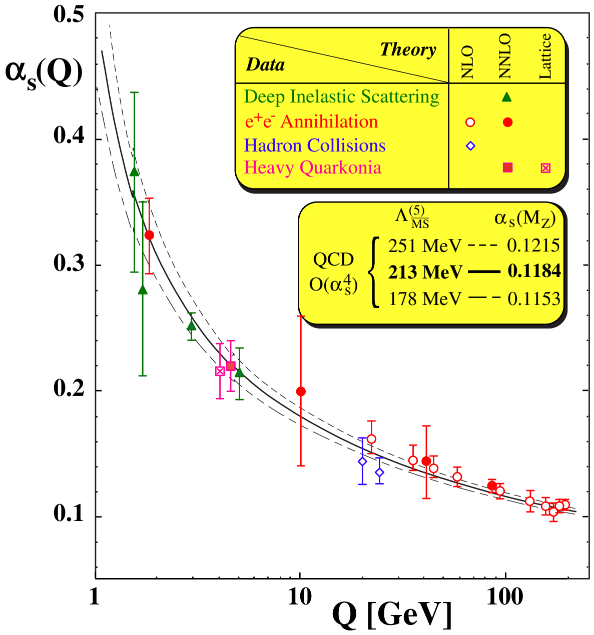

Figure 1.1.: Strong coupling constant $\alpha_s(Q)$ extracted from different experimental measurements. Figure is taken from Ref. [48].

The two properties of QCD, confinement and asymptotic freedom, can be tested in a variety of experiments, in which the strong coupling constant α_s can be determined at a specific energy scale Q, which is associated with the momentum transfer involved into the scattering considered process. To determine the coupling constant α_s one needs to investigate particle reactions involving quarks and gluons in either in- or outgoing states. Due to confinement, they manifest themselves as hadrons during the measurement. Examples of such processes are deep inelastic scattering, electron – anti-electron annihilation, hadronic collisions or decays of heavy quark – anti-quark particles [49]. All these processes are characterized by a specific energy scale Q, which is the momentum transfer involved. The results of $\alpha_s(Q)$ measurements in different experiments are summarized in Fig. 1.1 [48]. The dependence of α_s on the energy scale is referred to as 'running coupling' and qualitatively demonstrates the concepts of color confinement and asymptotic freedom. The intriguing implication of the asymptotic freedom is the possibility to study a dynamic system of weakly coupled quarks and gluons at extremely high energies. The search for this state of matter, which is believed to describe the very early moments after the 'Big Bang', is pursued in high energy hadronic colliders.

Here is a short story of a fast-forward journey to the origin of the universe.

1.3. Heavy-ion research: on the way to a 'Big Bang'.

In the year 2000 a CERN press release announced the discovery of a new state of matter, which became known as the Quark Gluon Plasma (QGP). Underlying this discovery have been a number of phenomenological observations, which revealed the properties of the new created medium. One of the most prominent of these properties is its collective, or fluid-like, behavior.

The starting point for experimental research of heavy-ion collisions was the BEVALAC at Berkeley, where in the mid-70s for the first time collisions of heavy atomic nuclei were explored. The unique feature of such experiments is the possibility to investigate nuclear matter at densities and temperatures which are much higher than the normal state of so called 'cold' matter, which we live in. However, with the establishment of a novel fundamental theory of strong interactions – Quantum Chromodynamics – it became clear that energies accessible at BEVALAC experiments were not high enough to observe a transition between the hadronic phase and a deconfined phase of quarks and gluons, predicted by QCD. Such a 'melting' of the nucleons at extreme densities and temperatures would imply not just an extreme, but a completely new state of matter, which, until the start of heavy-ion research at high energies, could only exist in early universe.

The theoretical possibility to re-create a 'Big Bang' in an experimental facility has thus motivated heavy-ion research and the design of new experiments with higher available energies. Though the challenge was not only to access higher collision energies, since these were already possible in proton-proton collisions at the CERN, Geneva and the BNL, Long Island, but as well to create higher densities at same time. This challenge was solved at already existing facilities such as the Alternating Gradient Synchrotron (AGS) at BNL and Super Proton Synchrotron (SPS) at CERN, where for the first time heavy nuclei where accelerated to ultra-relativistic energies, i.e. kinetic energies much larger than the rest mass of the constituents. In the year 1986 at the SPS accelerator two ^{16}O beams with 60 GeV per nucleon (AGeV) where collided. Until 1993 the highest possible energy was at 200 AGeV for experiments with sulfur nuclei and different targets. In 1994, with the development of a new ion source, operation with ^{207}Pb beams at 160 AGeV started and the led beam program was pursued until 2002. The next big step was done in June 2000 with the start of the Relativistic Heavy-Ion Collider (RHIC) at BNL. In this next generation collider, utilizing 20 years of experience at AGS and SPS, the maximal available energy was 200 AGeV for $Au + Au$ collisions in the center of mass frame of the colliding nuclei. Now the next, and probably the last of its art, facility has started its heavy-ion program – the LHC at CERN. With 27 km circumference, which tops RHIC by factor of 7, it will provide center of mass energies up to 5.5 ATeV for $Pb + Pb$ collisions. For some time to come it will probably stay world's largest and most powerful machine.

1.4. Phase diagram of QCD.

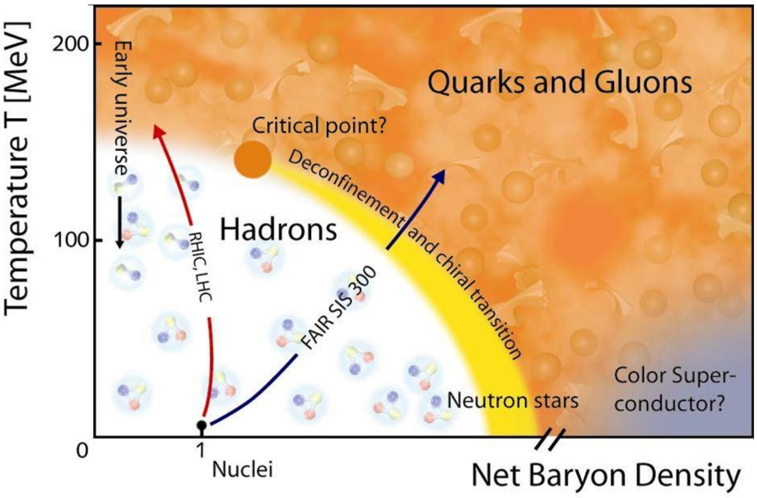

Figure 1.2.: Schematic phase diagram of strongly interacting matter. The net baryon density on the x-axis is normalized to the net baryon density in normal nuclear matter [50].

From the properties of QCD it follows that a deconfined state of strongly interacting matter can be created at conditions of extreme temperature (going to large energy scales) and particle density (going to small spacial dimensions). A schematic view of the phase diagram of QCD is presented in Fig. 1.2. The normal state of matter in the present state of the universe is located at very low temperature around unity on the x-axis. The collisions of heavy-ion at RHIC and LHC are supposed to create a fireball of a deconfined state with high temperature and low baryon density – in other words, a charge-neutral system of highly energetic quarks (q), anti-quarks ($\bar{q}$) and gluons with $N_q - N_{\bar{q}} \approx 0$. This is believed to be the state of the early universe, before quarks and gluons combined into hadrons. The very low net baryon density found in RHIC and LHC heavy-ion experiments is due to the onset of transparency with increasing collision energy. At highest energies, the colliding nuclei pass through each other creating a highly-excited mixture of gluons and pairs of quarks and anti-quarks. Other experimental facilities, like the upcoming projects FAIR at GSI in Darmstadt or NICA at JINR in Dubna, operate at lower energies and thus in the regime where the transparency effect is reduced and a high net baryon density can be created [51, 52].

The critical temperature $T_c \approx 160-180$ MeV, at which a free gas of hadrons undergoes a transition to a deconfined QGP phase at zero baryon density can be obtained by lattice calculations – numerical solutions of QCD field equations[53, 54, 55].

The evidence of the existence of a short-lived deconfined phase of quarks and gluons in heavy-ion collisions can only be of indirect nature. Studies of the final state of these collisions, represented by high numbers of baryons, mesons and leptons, can give insight into the evolution and properties of the QGP. The detector collaborations involved into the investigation of QGP at RHIC are BRAHMS[56], PHOBOS[57], STAR[58] and PHENIX[59]. At LHC these are ALICE, ATLAS and CMS.

1.5. Heavy-Ion phenomenology: a short overview

> *If you see a 'Buffalo' sign on an elephant's cage, do not believe your eyes.*
>
> Koz'ma Proutkov (1801 – 1863), russian writer (translated from Russian by author).

Here I will give a short overview of some of the phenomena which are regarded as signatures of the QGP phase.

1.5.1. Jet Quenching.

Upon collision of two nuclei, the constituent quarks and gluons (*partons*) of the nucleons can undergo hard collision processes in which a highly energetic partons can be created. Such partons can be observed since they give rise to a shower of hadrons in the finals state. For every of such high-energy jet events detected in an experimental device, one would expect to detect a correlated event at an azimuthal angle of 180 °. However, it was observed that the correlated jet signal of jets with high transverse momentum component (high-p_T) at 180 ° is suppressed in a heavy-ion system. This observation is known as *jet quenching* [16, 20, 21, 22]. If a jet pair is created at some point inside the QGP medium, the two jets have to cover different distances as they travel outside. If one jet ('near side jet') is able to quickly escape the QGP medium, the other jet will pass through more QGP matter and thus will most likely lose most of its energy to the medium due to scattering processes with partons.

The observation of the jet quenching phenomenon is consistent with observed suppression of high-p_T particles in $Au + Au$ collisions. This suppression is quantified by the *nuclear modification factor* R_{AA}, which is a ratio of particle yield measured in heavy-ion (e.g. $Au + Au$) collision to the corresponding yield in a proton-proton collisions rescaled by the estimated number of binary scatterings. R_{AA} as function of the transverse momentum p_T is found to be well below unity for hadrons [17, 18, 19], indicating a very effective suppression of high-p_T particles by the QGP medium. This is an indication of a rather strong coupling inside the medium.

1.5.2. J/Ψ suppression.

Quarkonia, e.g. the particles J/Ψ and Υ, are bound states of a quark and its anti-quark (charm–anti-charm for J/Ψ and bottom–anti-bottom for Υ). These particles are expected to 'melt' in a deconfined QCD medium due to the screening of their binding potential. This screening is analogous to the Debye screening of electric charges in non-relativistic plasmas. Thus, observation of a suppression of Quarkonia in the final state can be seen as an indication of existence of a deconfined QCD plasma, as was proposed 1986 by Satz and Matsui [13]. Analysis of the experimental data from RHIC demonstrated that several puzzling features of the J/Ψ suppression [14]. The suppression at mid-rapidity proved to be qualitatively the same at RHIC (measured by PHENIX) and SPS (mesured by NA50) energies for same number of participants. Furthermore, a stronger degree of suppression was observed at RHIC at forward rapidities in comparison to the central rapidity region. Observation of these two effects places special emphasis on the role of initial state effects and the role of possible secondary J/Ψ production from recombination of charm quarks produced in heavy-ion collisions. Moreover, these effects are expected to be more pronounced at LHC energies [14, 15]. Whereas a detailed understanding of the interplay of suppression, initial state effects and regeneration of charomonia is an actual subject of theoretical research [15], the presense of suppression due to melting of J/Ψ in a quark-gluon medium is an indication of presence of strong collectivity.

1.5.3. Collective Flow.

Observation of collective flow is related to observation of anisotropies in angular momentum and spacial particle distributions. The particle yield at different azimuthal angles is not constant, i.e. the flow pattern of the QGP medium is anisotropic. This anisotropy was interpreted by Ollitrault [60] as a signature of collective behavior of the QGP.

The overlap region of the two colliding nuclei has a prolongated, roughly ellipsoidal shape if the collision is off-central. As the created elliptic region starts expanding, pressure gradients build up. In the direction of minor axis the pressure gradient is stronger than in the direction of the major axis. Thus, the expansion will proceed faster in direction of the minor axis, transforming the initially present spacial anisotropy into a momentum-space anisotropy. Particles will be pushed into the direction of strongest pressure gradient. Of course, such a behavior can only be expected in case the medium does behave in a collective way.

To obtain a quantitative measure of flow anisotropy the transverse momentum distribution is expanded into a Fourier series, which for a perfect ellipsoidal form can be written as

$$\frac{dN}{p_T\ dp_T\ dy\ d\varphi} = \frac{dN}{2\pi\ p_T\ dp_T\ dy}\big(1 + 2v_2(p_T)\cos 2(\varphi - \Psi_{RP}) + \dots\big) \quad . \tag{1.1}$$

The decomposition is done with respect to the *reaction plane* orientation angle Ψ_{RP}, which is different for each event. For a perfect ellipsoidal form the coefficient v_2 is the first non-vanishing coefficient to be taken into account. Experimentally v_2 can be obtained by weighting the measured particle multiplicities with $\cos 2(\varphi - \Psi_{RP})$ and averaging over the angle φ. The coefficient $v_2(p_T)$ is usually referred to as the differential elliptic flow . The integrated elliptic flow v_2 is an average over transverse momenta.

The ability of ideal hydrodynamics to reproduce the first differential v_2 measurements at RHIC [6] at small $p_T < 1.5$ GeV (i.e. for more than 98% of all particles), reported in 2001 in Ref. [8] and later in Refs. [9, 10], was considered a startling success. This success lead to the two paradigms of ideal fluid creation at RHIC and early thermalization [26]. The latter conclusion is based on the rather low initialization time for hydrodynamic calculations. However, the quality of the matching of experimentally measured $v_2(p_T)$ with ideal hydrodynamic calculations is dependent on the choice of initial time, energy density and temperature values [12]. More importantly, the assumption of full thermalization of produced matter in heavy-ion collisions is rather unrealistic. Full thermalization would require an infinitely strongly coupled medium. A step away from the ideal hydrodynamics paradigm was made as TEANEY [61] and later HEINZ and SONG [11] demonstrated that viscous effects can significantly suppress $v_2(p_T)$. These findings were later confirmed by a number of non-ideal hydrodynamic calculations (e.g. in Refs. [62], [47], [63]). However, the switch from ideal to viscous hydrodynamics brings an additional unknown – along with the initial conditions – the values of the dissipative coefficients in hydrodynamic theory. These have to be understood from first principles. Calculation of the transport coefficients (in particular the shear viscosity η) of a partonic medium is one of the central aspects of this work.

1.5.4. Scaling of elliptic flow.

Some properties of the medium, in which the anisotropic flow is built up, can be deduced from scaling properties of $v_2(p_T)$. As was demonstrated by the PHENIX collaboration in Ref. [64], by scaling the measured $v_2(p_T)$ of mesons and baryons by the number n_q of constituent quarks (2 resp. 3) and relating it to the transverse kinetic energy E_T scaled by same factor, one obtains a universal curve, on which the measurements for all particle species lie. The obtained universal $v_2/n_q(E_T/n_q)$ increases at small kinetic energy and saturates towards larger energies. This universality can be interpreted as an indication, that hadronic elliptic flow is built up in the deconfined partonic phase and the hadrons are produced by a coalescence of flowing partons (the so called recombination model)[65, 66, 67, 68].

Observations of the elliptic flow, its properties and other indications of the existence of a strongly coupled medium during the early stages of heavy-ion collisions turned the attention of theory community to the deconfined phase of QCD matter and its dynamics.

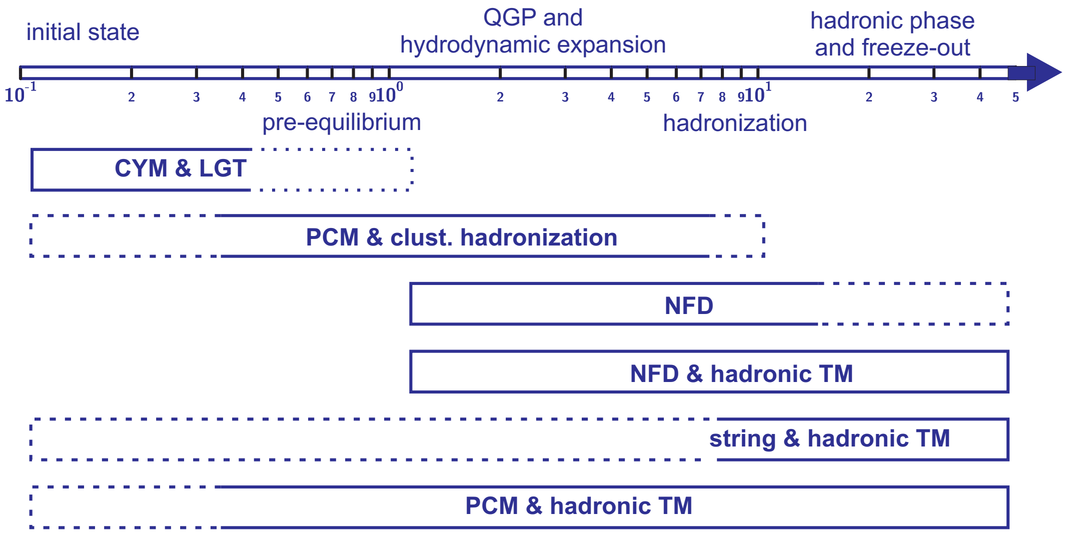
initial state
QGP and
hydrodynamic expansion
hadronic phase
and freeze-out
10^{-1}
2
3
4
5
6
7
8
9
10^{0}
2
3
4
5
6
7
8
9
10^{1}
2
3
4
5
pre-equilibrium
hadronization
CYM & LGT
PCM & clust. hadronization
NFD
NFD & hadronic TM
string & hadronic TM
PCM & hadronic TM

Figure 1.3.: Time evolution of a heavy-ion collision and ranges of applicability of theoretical tools [69]

1.6. Theoretical tools to description of Heavy-Ion phenomenology

The different stages through which a heavy-ion collision goes are characterized not only by different time scales but as well by different energy scales and associated degrees of freedom of the produced matter constituents. It is thus not possible to find a universal modelling approach for heavy-ion collisions – the different stages rather have to be understood within different theoretical approaches.

The initial and the early pre-equilibrium states are characterized by a anisotropic momentum distribution. A very prominent example of a model approach for the initial state is the Color Glass Condensate [70, 71, 72], which will be discussed later in this work. another popular approach to initial state distribution is the Glauber model, as e.g. employed in Ref. [8]. The very early pre-equilibrium stage is often modelled in terms of plasma instabilities [73]. The appropriate theoretical concepts for such modelling of early stages are formulated in the Classical Yang-Mills theory (CYM) or Lattice Gauge Transport (LGT). These theories are able to describe the initial coherence of the produced fields and can be employed to model the initial conditions for dynamical models used at later stages. Examples of these approaches can be found for instance in Refs. [74, 75].

The late pre-equilibrium stage can be investigated by means of kinetic theory using transport models (TM). Partonic Cascade Models (PCM), e.g. [27, 28, 29, 30, 31] are based on a quasi-particle approach, i.e. the relevant degrees of freedom for these models are (light) quarks and gluons, which are treated as an ultra-relativistic gas. The advantage of the PCM approaches is their ability to describe the microscopic dynamics of the quark-gluon gas basing on relevant cross sections, which for small coupling are known from the perturbative theory (perturbative QCD). PCMs are thus equally based on the kinetic transport theory [76].

In this work the partonic cascade BAMPS will be employed. BAMPS is a Monte-Carlo approach to solving the Boltzmann transport Equation

$$p^{\mu}\partial_{\mu}f = C[f]\,. \tag{1.2}$$

Here f represents the phase-space particle distribution and the functional $C[f]$ accounts for collisional processes between quasi-particles. BAMPS and related technical aspects of numerical implementation of the Boltzmann Equation will be discussed in detail in Chapter 7.

The range of applicability of a PCM approach can be extended to the hadronization and freeze-out phases once the partonic degrees of freedom are translated into hadronic ones. Using an appropriate procedure to model the phase transition, the hadronic phase can be again investigated by means of the Monte-Carlo transport theory using the experimentally known hadronic decay ratios and cross sections in a hadronic transport model, as for example done in UrQMD [77, 78] or HSD [79].

Whereas transport models are microscopic approaches, a macroscopic description of the evolution of the QGP can be given by a hydrodynamic models (nuclear fluid dynamics, NFD), as already discussed in the context of heavy-ion phenomenology. A significant difference between these two descriptions is the fact, that a hydrodynamic description is only applicable if the considered system is close to local equilibrium, whereas the kinetic transport theory can also be used to describe non-equilibrated systems. This shrinks the applicability range of the hydrodynamic description considerably. In particular, hydrodynamics can most likely not be applied at early times when the medium is highly anisotropic. One of the aims of this work is to investigate the applicability of relativistic hydrodynamics to non-equilibrated systems by a direct comparison of hydrodynamic calculations with results of kinetic transport calculations.

This work is dedicated to the investigation of the transition between the kinetic transport and dissipative hydrodynamic theories for ultrarelativistic systems. The existing hydrodynamic formalisms are improved in order to better extent their spectrum of applications to a broader class of transport scenarios. These improvements are related to the inclusion of new terms neglected in previous works, the possibility of particle production and annihilation and the possibility of descriprion of mixtures, i.e. fluids of several distinguishable components. A formal way to extract the transport coefficients from kinetic transport theory has been established. Validity and limitations of hydrodynamic equations are demonstrated by direct comparisons of their solutions with kinetic transport calculations. All these aspects can contribute to a better understanding of applications of dissipative hydrodynamics to the description of the QGP dynamics.

1.7. The Roadmap.

This work is organized as follows: I will begin with a basic discussion of the formulation of relativistic hydrodynamics in Chapter 2. In this Chapter also the mapping of hydrodynamic theory onto kinetic theory – the so called Grad's method of moments – will be introduced. In Chapter 3 derivation of relativistic dissipative hydrodynamic equations from the entropy principle will be discussed. After a review of the well-known first- and second-order equations, derivation of a novel, third-order evolution equation for shear tensor will be discussed. Both second- and third-order formalisms will be extended with the possibility of particle creation and annihilation. In the same Chapter a novel dissipative formalism for a multi-component system is derived. After the derivation of the hydrodynamic evolution equations, in Chapter 4 I introduce an expression that allows to calculate the shear viscosity coefficient in scope of kinetic transport theory. In Chapter 5 Bjorken's picture of heavy-ion collisions is introduced; this picture constitutes the framework for the analytic calculations discussed in the following. In Chapter 6 hydrodynamic equation derived in Chapter 3 are given in one-dimensional boost-invariant geometry from Bjorken's scenario. The kinetic transport model BAMPS is introduced in Chapter 7. An overview of heavy-ion phenomena that can be studied with BAMPS is given in the same Chapter. In Chapter 8 I investigate whether Grad's approach, discussed in Chapter 2, is consistent with the results of BAMPS calculations. Results of calculation of the shear viscosity coefficient of a QCD medium employing BAMPS are presented in Chapter 9. In Chapters 10 and 11 I compare solutions of second- and third-order dissipative hydrodynamic equations with BAMPS results for a one-dimensional expanding system with conserved net particle number and including particle production and annihilation. In Chapter 12 solutions of the hydrodynamic equations for a two-component system are compared with BAMPS calculations and some properties of the multi-component equations are discussed.

1.8. Notation

In this work I will be using the following standard conventions

- Natural units $\hbar = c = k_B = 1$.
- The metric tensor is $g^{\mu\nu} = diag(1, -1, -1, -1)$.
- For any second-rank tensor the symmetrization operation is defined as

  $$A^{(\mu\nu)} = \frac{1}{2}(A^{\mu\nu} + A^{\nu\mu})\,.$$

  The anti-symmetrization is defined as

  $$A^{[\mu\nu]} = \frac{1}{2}(A^{\mu\nu} - A^{\nu\mu})\,.$$

2. Construction of the hydrodynamic framework.

Panta Rei (from greek: everything flows)

Name of a bar in Frankfurt am Main

In this Chapter the basic *fields* and tensorial structures of the relativistic hydrodynamic framework are introduced. Without yet considering the dynamics of these fields, I will discuss their basic mathematical properties and physical interpretation. The two basic choices of the computational frame – Eckart and Landau frames – are introduced. Grad's 14-moment theory is introduced in order to establish a connection between the hydrodynamic, i.e. macroscopic, and kinetic, i.e. microscopic, descriptions.

The concepts introduced in this Chapter will be needed in the following Chapters to derive dissipative hydrodynamic equations for applications in high-energy heavy-ion physics.

2.1. Basic tensorial decompositions.

Relativistic hydrodynamics can be interpreted as an effective theory of the fields $T^{\mu\nu}(x)$, which is the energy-momentum tensor, $N_B^{\mu}(x)$, which is the particle number four-current, and u^{μ}, which is the fluid four-velocity. In heavy-ion collisions the particle four-current is usually associated with the net baryon number (indicated by the subscript B) and thus is conserved due to baryon number conservation. The energy-momentum tensor is conserved due to energy and momentum conservation in a closed system. Thus, the hydrodynamic equations can be written in form of the conservation laws

$$\partial_{\mu} T^{\mu\nu} = 0 \ , \ \ \partial_{\mu} N_B^{\mu} = 0 \, . \tag{2.1}$$

For a dissipation-free (i.e. ideal) fluid, these two equations are the only ones needed to describe the evolution of the system. However the focus of this work is on derivation and analysis of dissipative hydrodynamic equations, since theoretical studies of the early stages of heavy-ion collisions do provide certain indications, that dissipation is present in the produced system. In a ideal fluid entropy is conserved, but if dissipation is present, entropy is produced and an additional equation is needed to describe the amount of entropy production, which is proportional to the strength of the dissipation. All these aspects will be addressed later in this work. At this stage it is necessary to discuss in more detail the constructs $N_B^\mu(x)$, $T^{\mu\nu}(x)$ and u^μ.

The energy-momentum tensor and particle number four-current can be decomposed into orthogonal components with respect to the four-vector u^μ. The vector u^μ is normalized to unity, i.e.

$$u_\mu u^\mu = u_\mu u_\nu g^{\mu\nu} = 1 \,. \tag{2.2}$$

Here $g^{\mu\nu}$ ist the metric tensor as intoduced in Section 1.8. Using this property of u^μ, the projector

$$\Delta^{\mu\nu} = g^{\mu\nu} - u^\mu u^\nu \,, \tag{2.3}$$

can be shown to be orthogonal to u^μ, i.e. $\Delta^{\mu\nu}u_\mu = 0$. With these definitions, the most general orthogonal decompositions of $T^{\mu\nu}$ and N^μ can be written as

$$T^{\mu\nu} = eu^\mu u^\nu - (p+\Pi)\Delta^{\mu\nu} + W^\mu u^\nu + u^\mu W^\nu + \pi^{\mu\nu} \,, \tag{2.4}$$

$$N^\mu = nu^\mu + V^\mu \,. \tag{2.5}$$

Note, that in the latter equations the subscript B, indicating that the number four-current is related to the net baryon number, has been dropped. The particle four-current could be defined via any charge, as e.g. the baryon number or also electrical charge and strangeness. In a one-component system of particles without charge, the net particle four-current is associated with the net particle number. In contrast to the *net baryon number*, the *net particle number* is not necessary conserved in a system produced in heavy-ion collisions.

The quantities Π, W^μ, V^μ and $\pi^{\mu\nu}$ are dissipative quantities, also referred to as *dissipative fluxes* or *dissipative fields.* For systems in equilibrium they vanish, leading to the following form of the energy-momentum tensor and particle number four-current:

$$T^{\mu\nu}_{eq} = eu^\mu u^\nu - p\Delta^{\mu\nu} \,, \tag{2.6}$$

$$N^\mu_{eq} = nu^\mu \,. \tag{2.7}$$

The requirement of orthogonality leads to the following relations between the introduced tensorial structures and u^μ:

$$u_\mu V^\mu = u_\mu W^\mu = 0 \;\;, \;\; u_\mu \pi^{\mu\nu} = 0 \,. \tag{2.8}$$

The scalar and tensorial quantities entering the decompositions (2.4) and (2.5) can be obtained as projections of $T^{\mu\nu}$, N^μ and their deviation from the equilibrium

$$\delta T^{\mu\nu} = T^{\mu\nu} - T^{\mu\nu}_{eq} \,, \tag{2.9}$$

$$\delta N^\mu = N^\mu - N^\mu_{eq} \,. \tag{2.10}$$

The projections of $T^{\mu\nu}$, N^{μ}, $\delta T^{\mu\nu}$ and δN^{μ} attain the following interpretation [80]:

$$\begin{aligned}
n &= u_{\mu} N^{\mu} && \text{net particle density ,} && (2.11)\\
e &= u_{\mu} u_{\nu} T^{\mu\nu} && \text{energy density ,} && (2.12)\\
\Pi &= -\frac{1}{3}\Delta_{\mu\nu}\delta T^{\mu\nu} && \text{bulk pressure ,} && (2.13)\\
p &= -\frac{1}{3}\Delta_{\mu\nu} T^{\mu\nu} - \Pi && \text{equilibrium pressure ,} && (2.14)\\
V^{\mu} &= \Delta^{\mu}_{\nu}\delta N^{\nu} && \text{net particle flow (relative to } u^{\mu}\text{),} && (2.15)\\
W^{\mu} &= u_{\nu}\Delta^{\mu}_{\lambda}\delta T^{\nu\lambda} && \text{energy flow (relative to } u^{\mu}\text{),} && (2.16)\\
q^{\mu} &= W^{\mu} - \frac{e+p}{n} V^{\mu} && \text{heat flow (relative to } u^{\mu}\text{),} && (2.17)\\
\pi^{\mu\nu} &= \delta T^{\langle\mu\nu\rangle} && \text{shear stress tensor .} && (2.18)
\end{aligned}$$

with $\delta T^{\langle\mu\nu\rangle} = \left[\frac{1}{2}\left(\Delta^{\mu}_{\alpha}\Delta^{\nu}_{\beta} + \Delta^{\mu}_{\beta}\Delta^{\nu}_{\alpha}\right) - \frac{1}{3}\Delta^{\mu\nu}\Delta_{\alpha\beta}\right]\delta T^{\alpha\beta}$.

Now the mathematical notation and relevant physical quantities have been discussed. We are now in a position to discuss the choice of the reference frame, which will be used for all calculations throughout this work.

2.2. Choice of the reference frame.

For a given 'field' configuration $N^{\mu}(x)$, $T^{\mu\nu}(x)$ the reference frame of a fluid element is defined by the fluid four-velocity $u^{\mu}(x)$, which now has to be determined in terms of the components of $N^{\mu}(x)$ and $T^{\mu\nu}(x)$. In the set of Eq. (2.11) – (2.18) two independent vectorial structures were introduced, the particle number flow V^{μ} and the energy flow W^{μ} (which in principle can be replaced by q^{μ}). The velocity field u^{μ} can be associated either with particle flow (in which case V^{μ} vanishes) or the energy flow (W^{μ} vanishes) [76].

Eckart frame

If u^{μ} is chosen to be parallel to the particle number flow N^{μ} than due to $u_{\mu}u^{\mu} = 1$ it becomes

$$u^{\mu} = \frac{N^{\mu}}{\sqrt{N_{\mu}N^{\mu}}} \,. \tag{2.19}$$

With this choice the net particle flow V^{μ} vanishes, since the reference frame follows the flow of net particle number so that energy flow W^{μ} becomes identical with the heat flow q^{μ}. This frame is known as Eckart or particle frame. If the particle four-current is defined via the baryon number, Eckart's frame is ill-defined in a system with vanishing net baryon number, like the one produced at RHIC or LHC. However, for any other non-vanishing net charge this definition can be applied.

Landau frame

Alternatively, the velocity field u^μ can be chosen to be parallel to the energy flow $u_\nu T^{\mu\nu}$. Than it can be written as

$$u^\mu = \frac{T^\mu_\nu u^\nu}{\sqrt{u^\alpha T^\alpha_\beta T^\beta_\gamma u^\gamma}} \,. \tag{2.20}$$

With this definition the reference frame follows the flow of energy density. The energy flow W^μ vanishes and the heat flow q^μ becomes proportional to the particle flow V^μ. This frame is known as Landau and Lifshitz or energy frame. Due to the shortcoming of Eckart frame, which is not applicable in systems with vanishing net baryon charge, Landau frame is the first choice in applications of relativistic hydrodynamics. The disadvantage of the energy frame is its implicit form, which leads in a general case to a polynomial equation for the components of u^μ.

2.3. Equation of state.

The equation of state relates pressure to the other thermodynamic variables such as the energy density e and particle density n (or alternatively the temperature T:

$$p = p(e, n)\,. \tag{2.21}$$

For QCD medium the equation of state can be obtained from lattice calculations. The method and results of such calculations are reviewed by KARSCH in Ref. [54] and FODOR and KATZ in Ref. [81]. In this work the most simple equation of state will be used – the one of an ideal ultrarelativistic gas:

$$e = 3p\,. \tag{2.22}$$

This equation models a non-interacting gas of massless quarks and gluons. For analytic calculations this choice is often the standard simplistic choice. For numerical implementations of hydrodynamic evolution, the major disadvantage of this equation of state is its inability to describe the phase transition between partonic and hadronic phases. In order to account for the latter, different equations of state can be chosen. The effect of equation of state on hydrodynamic evolution is studied for instance in Ref. [47].

2.4. Grad's 14-moment theory

2.4.1. Approximation of off-equilibrium distribution

A connection between the microscopic Boltzmann Equation (1.2), which is the underlying equation of the kinetic theory, and the macroscopic hydrodynamic description is based on the method of moments introduced by GRAD [82]. and adopted for relativistic systems by ISRAEL and STEWART [40]. A macroscopic description of a system requires knowledge of the independent components of the particle four-current N^μ and the energy-momentum tensor $T^{\mu\nu}$, as discussed in Section 2.1. In contrast to that, in kinetic theory the system is characterized by the distribution function $f(x,p)$, which describes the occupation number in the phase-space. For a system in thermodynamic equilibrium the phase space occupation density can be calculated analytically. For systems off thermal equilibrium an exact analytic expression for the particle distribution is unknown. Moreover, the distribution could have a highly non-trivial analytic form. In this case the kinetic theory has a major advantage, since in a numerical kinetic transport model, which simulates the dynamics of an ensemble of microscopic constituents, the particle distribution is known implicitly.

In order to establish a connection to the macroscopic theory of hydrodynamics, an analytic expression for the off-equilibrium distribution function has to be found. Formally an off-equilibrium distribution function can be written as [83, 84, 85]

$$f(x,p) = A_0 e^{y(x,p)} . \tag{2.23}$$

In the latter equation A_0 denotes the normalization factor dependent on the number of degrees of freedom; in the presented form, Eq. (2.23) does not take into account quantum effects like Bose enhancement or Fermi blocking – strictly it only applies to a system of Boltzmann particles. Note that in Ref. [83] an analogous equation is given for Fermi/Bose systems. For a system in thermal equilibrium the function $y(x,p)$ is

$$y_{eq}(x,p) = \ln(A_0^{-1} f_{eq}) = \mu(x) - \beta_\nu(x) p^\nu . \tag{2.24}$$

with $\beta^\nu(x) = u^\nu/T$, i.e. the equilibrium distribution is a Boltzmann distribution.

For a system off thermal equilibrium the deviation of the exponent can be formally written as

$$y(x,p) = y_{eq}(x,p) + \phi(x,p). \tag{2.25}$$

The deviation of the exponent from its equilibrium form, $\phi(x,p) = y(x,p) - y_{eq}(x,p)$, is a function of momentum and space and can be expanded in terms of momentum in a most general form as follows [83, 84]

$$\phi(x,p) \approx \epsilon(x) - \epsilon_\mu(x) p^\mu + \epsilon_{\mu\nu}(x) p^\mu p^\nu + \dots . \tag{2.26}$$

The latter expression is second order in momentum.

The unknowns needed for a complete determination of the macroscopic state of the system are now the independent components of the new variables $\epsilon(x)$, $\epsilon_\mu(x)$ and $\epsilon_{\mu\nu}(x)$ together with the chemical potential $\mu(x)$ and the vector $\beta^\mu(x) = u^\mu/T$.

Next, Eq.(2.23) can be linearized via Eqs. (2.25) and (2.26):

$$f(x,p) \approx f_{eq}(x,p)(1 + \epsilon(x) - \epsilon_\mu(x) p^\mu + \epsilon_{\mu\nu}(x) p^\mu p^\nu) . \tag{2.27}$$

Using the linearized expression for the off-equilibrium distribution function (2.27) one can calculate the first and second moments of the latter. These moments are identical with the kinetic definition of the particle number four-current and the energy-momentum tensor:

$$\begin{aligned} N^{\mu} = \int p^{\mu} f(x,p) d\Gamma = N^{\mu}_{eq} &+ \epsilon \int f_{eq}(x,p) p^{\mu} d\Gamma - \epsilon_{\nu} \int f_{eq}(x,p) p^{\nu} p^{\mu} d\Gamma \\ &+ \epsilon_{\sigma\nu} \int f_{eq}(x,p) p^{\sigma} p^{\nu} p^{\mu} d\Gamma \end{aligned} \tag{2.28}$$

$$\begin{aligned} T^{\mu\nu} = \int p^{\mu} p^{\nu} f(x,p) d\Gamma = T^{\mu\nu}_{eq} &+ \epsilon \int f_{eq}(x,p) p^{\mu} p^{\nu} d\Gamma - \epsilon_{\sigma} \int f_{eq}(x,p) p^{\sigma} p^{\mu} p^{\nu} d\Gamma \\ &+ \epsilon_{\lambda\sigma} \int f_{eq}(x,p) p^{\sigma} p^{\lambda} p^{\mu} p^{\nu} d\Gamma \end{aligned} \tag{2.29}$$

where $d\Gamma$ denotes the integration measure $d\Gamma = \frac{d^3p}{(2\pi)^3 p_0}$. Using the above equations, the deviations of particle flow N^{μ} and energy-momentum tensor $T^{\mu\nu}$ from equilibrium values N^{μ}_{eq} and $T^{\mu\nu}_{eq}$ can be now written in a compact form

$$\delta N^{\mu} = \epsilon \tilde{N}^{\mu}_{eq} - \epsilon_{\nu} \tilde{T}^{\nu\mu}_{eq} + \epsilon_{\lambda\nu} \tilde{F}^{\lambda\nu\mu}_{eq} \tag{2.30}$$

$$\delta T^{\mu\nu} = \epsilon \tilde{T}^{\mu\nu}_{eq} - \epsilon_{\lambda} \tilde{F}^{\lambda\mu\nu}_{eq} + \epsilon_{\lambda\sigma} \tilde{R}^{\lambda\sigma\mu\nu}_{eq}. \tag{2.31}$$

with $\tilde{N}^{\mu}_{eq}$, $\tilde{T}^{\mu\nu}_{eq}$, $\tilde{F}^{\lambda\nu\mu}_{eq}$ and $\tilde{R}^{\lambda\sigma\mu\nu}_{eq}$ denoting the first, second, third and fourth moments of the equilibrium distribution function $f_{eq}(x,p)$ respectively. Note that these moments of the equilibrium distribution can easily be calculated analytically.

2.4.2. Matching conditions

In order to obtain a closed expression for the off-equilibrium distribution function, the unknown tensorial structures $\epsilon, \epsilon^{\mu}, \epsilon^{\mu\nu}$ in Eqs. (2.30) – (2.31) have to be calculated in terms of $T^{\mu\nu}$, N^{μ} and the fluid velocity field u^{μ}. In order to identify these unknowns one can use equations (2.30) – (2.31) together with the decompositions of the dissipative fluxes from Eqs. (2.4) – (2.5).

But, before one starts calculating ϵ, ϵ^{μ} and $\epsilon^{\mu\nu}$, the following two additional equation are needed:

$$u_{\mu} \delta N^{\mu} = u_{\mu} u_{\nu} \delta T^{\mu\nu} = 0\,. \tag{2.32}$$

The meaning of these two equations, known as the Landau matching conditions [83, 84] becomes apparent if one rewrites them using the decompositions (2.4) – (2.5) as follows:

$$e = e_{eq}\,, \tag{2.33}$$

$$n = n_{eq}\,. \tag{2.34}$$

where e and n denote the energy and particle densities in the local rest frame and same quantities with a subscript 'eq' refer to an equilibrium state. The above equations match the actual energy and particle densities in a system to the energy and particle densities of a fictitious equilibrated state. If the particle distribution in equilibrium state is given by the Boltzmann distribution of massless particles, the *effective* temperature of a non-equilibrium state can be defined by virtue of Landau matching conditions as a temperature of a equilibrium state with the same energy and particle densities:

$$T = \frac{e}{3n} = \frac{e_{eq}}{3n_{eq}} \tag{2.35}$$

The latter equation implies for the energy and particle densities of as Boltzmann gas

$$\begin{aligned} e &= \frac{3\lambda g}{\pi^2} T^4 \equiv e_{eq} && (2.36) \\ n &= \frac{\lambda g}{\pi^2} T^3 \equiv n_{eq}. && (2.37) \end{aligned}$$

where g denotes the degeneracy factor. The factor λ, which is interpreted as fugacity, accounts for deviations from the chemical equilibrium state. $\lambda = 1$ for an equilibrated system. Fugacity is essentially needed to distinguish between a chemically equilibrated and non-equilibrated states, as will be demonstrated later in Chapter 11.

Note that Landau matching conditions are essentially needed in order to define the temperature no matter what reference frame – either Landau's or Eckart's – has been chosen.

Using Eqs. (2.30) – (2.31) together with the definitions (2.11) – (2.18) and the properties (2.32), one can find the solutions for $\epsilon(x)$, $\epsilon_\mu(x)$ and $\epsilon_{\mu\nu}(x)$ in Eckart frame:

$$\begin{aligned} \epsilon_{\mu\nu} &= A_2(3u_\mu u_\nu - \Delta_{\mu\nu})\Pi - B_1 u_{(\mu} q_{\nu)} + C_0 \pi_{\mu\nu} && (2.38) \\ \epsilon_\nu &= A_1 u_\nu \Pi - B_0 q_\nu && (2.39) \\ \epsilon &= A_0 \Pi && (2.40) \end{aligned}$$

The values of the thermodynamic coefficients A_i, B_i and C_i were calculated for example in [83, 84]. They are combinations of moments of the equilibrium distribution and thus are known analytically. Derivation of $\epsilon_{\mu\nu}$, ϵ_ν, ϵ and calculation of the coefficients A_i, B_i and C_i are presented in Appendix A of this work.

The fields $\epsilon_{\mu\nu}$, ϵ_ν and ϵ together have 14 independent components, which corresponds to 14 unknowns in the set of Eqs. (2.4) – (2.5). Indeed, e and p are connected via the chosen equation of state (which need not be the one of an ideal gas). In Eckarts frame W^μ is equivalent to q^μ, which has only 3 independent components due to orthogonality property $q_\mu u^\mu = 0$. $\pi^{\mu\nu}$ is diagonal-symmetric and $\pi^{00} = 0$ by virtue of the matching condition 2.32, which leaves only 9 independent $\pi^{\mu\nu}$ components. In addition, shear tensor is traceless, $\pi^\nu_\nu = 0$, and there are only 8 independent components left. In total, the number of unknowns in Eqs. (2.4) – (2.5) is

$$\underbrace{8}_{\pi^{\mu\nu}} + \underbrace{3}_{q^\mu} + \underbrace{1}_{\Pi} + \underbrace{1}_{n} + \underbrace{1}_{e,p} = 14\,. \tag{2.41}$$

Using these 14 unknowns, the hydrodynamic fields can be constructed.

The off-equilibrium distribution is thus determined within the Grad's theory of moments in terms of dissipative fluxes Π, q_μ , $\pi_{\mu\nu}$ and the thermodynamic coefficients A_i, B_i, C_i according to Eqs. (2.38), (2.39), (2.40) together with Eqs. (2.27):

$$f = f_{eq}\big[1 + A_0\Pi - \big(A_1 u_\nu \Pi - B_0 q_\nu\big)p^\nu + \big(A_2(3u_\mu u_\nu - \Delta_{\mu\nu})\Pi - B_1 u_{(\mu}q_{\nu)} + C_0\pi_{\mu\nu}\big)p^\mu p^\nu\big] \tag{2.42}$$

Hence any distribution $f(x,p)$ now can be expressed in terms of the macroscopic fields describing the system.

2.4.3. Moments of the Boltzmann Equation

Hydrodynamic equations can be derived from the Boltzmann Equation (1.2) using the moments of its left and right hand side. Such derivations were reported e.g. in Refs. [86, 38]. Although this particular approach to derivation of hydrodynamic equations is not a subject of this work, the moments of the Boltzmann Equation will be needed to derive an expression for the shear viscosity coefficient. 0th, 1st and 2nd moments of the Boltzmann Equations are accordingly given by the following set of equations:

$$\int p^\mu \partial_\mu f(x,p) d\Gamma = \partial_\mu N^\mu = \int C[f] d\Gamma = J \tag{2.43}$$

$$\int p^\mu p^\nu \partial_\mu f(x,p) d\Gamma = \partial_\mu T^{\mu\nu} = \int p^\nu C[f] d\Gamma = J^\nu \tag{2.44}$$

$$\int p^\mu p^\nu p^\lambda \partial_\mu f(x,p) d\Gamma = \partial_\mu F^{\mu\nu\lambda} = \int p^\nu p^\lambda C[f] d\Gamma = P^{\nu\lambda} \tag{2.45}$$

In the latter set of equations J and J^ν can be physically understood as the source terms for particle production and energy-momentum deposition accordingly. For a closed system $J^\nu = 0$ and Eq.(2.44) simply states the conservation of energy and momentum. In this work I will consider energy-momentum conservation, i.e. closed systems without external source-terms, $J^\nu = 0$. In a multi-component system energy and momentum exchange between the species is possible, but the total energy-momentum tensor is still conserved. In Eq.(2.43) $J = 0$ if the particle number is conserved. However, this is not true in a gluonic system, where the bremsstrahlung and absorption processes have an influence on the net particle number. Thus, in presence of bremsstrahlung and the reverse channel J has to be calculated by evaluating the integral over the collision term in Eq.(2.43). This will be done in Chapter 11. The second moment of the Boltzmann Equation is in general not conserved, i.e. $P^{\nu\lambda} \neq 0$. To give an analytical expression for $P^{\nu\lambda}$ one can consider its tensorial decomposition in terms of the dissipative fluxes, which in most general form can be written as follows

$$P^{\mu\nu} = \frac{4}{3}\mathcal{C}_\Pi A_2 (3u^\mu u^\nu - \Delta^{\mu\nu})\Pi + 2\mathcal{C}_q B_1 q^{(\mu}u^{\nu)} + \frac{1}{5}\mathcal{C}_\pi C_0 \pi^{\langle\mu\nu\rangle}. \tag{2.46}$$

Again, the decomposition above is introduced in the Eckart or particle frame. The tensorial structures introduced in the latter equation are the same as in Eq. (2.42) for the momentum-independent parts of the distribution function. The coefficients $\mathcal{C}_{\Pi,q,\pi}$

are dependent on the transport coefficients bulk viscosity, heat conductivity and shear viscosity accordingly. This becomes clear since they can be obtained as projections of the left hand side of Eq. (2.46), which is an integral over the collision term:

$$\begin{aligned} -4\mathcal{C}_{\Pi} A_2 \Pi &= u_\mu u_\nu P^{\mu\nu}, && (2.47)\\ \mathcal{C}_q B_1 q^\mu &= \Delta^\mu_\nu u_\lambda P^{\nu\lambda}, && (2.48)\\ \frac{1}{5}\mathcal{C}_\pi C_0 \pi^{\langle\mu\nu\rangle} &= P^{\langle\mu\nu\rangle}. && (2.49) \end{aligned}$$

Since the collision term and thus its moments depend on the collision cross section, the right hand side of Eqs. (2.47) – (2.49) must depend on the transport coefficients bulk viscosity, heat conductivity and shear viscosity. These equations will be needed later, when I derive an expression for the shear viscosity coefficient (comp. Section 4.2.1).

Now that the basic mathematical concepts and physical quantities have been discussed and an analytic expression for off-equilibrium distribution has been constructed, derivation of dissipative hydrodynamic equations can be discussed.

3. Derivation of the relativistic dissipative hydrodynamic equations.

Wonder, rather than doubt, is the root of knowledge.

Abraham Heschel (1907 – 1972),
Jewish theologian and philosopher.

3.1. Hydrodynamic equations from the entropy principle.

In this section I will first introduce derivation of the well-known first and second-order dissipative hydrodynamic equations from the entropy principle. The approach I will be using here is a phenomenological one. Its main advantage is that obtained equations automatically satisfy the second law of thermodynamics, since they are obtained from this requirement. One of the flaws of this approach is however its inability to recover some terms, which can be obtained in scope of different approaches discussed in previous section and at the end of this one. Derivation of hydrodynamic equations from the entropy principle has been discussed by MURONGA in Ref. [80] and originates from the earlier works by ISRAEL and STEWART [40]. Israel and Stewarts formulation of hydrodynamic equations has for a long time been the standard hydrodynamic theory for relativistic systems. After discussing the established theories I will derive a novel, third-oder relativistic hydrodynamic equation, which has been reported in Ref. [34], as well as novel second-order hydrodynamic equations for a multi-component system [36]. At the end of this Chapter I will also review other approaches to derivation of hydrodynamic equations.

3.1.1. Preface

In this Section I partly follow the procedure introduced by MURONGA in Refs. [80, 83, 87]. The approach used in these works is based on the entropy production principle and requires knowledge of the entropy current S^{μ}. From the phenomenological point of view it can be written in the most general form as

$$s^{\nu} = p\beta^{\nu} - \frac{\mu}{T}N^{\nu} + \beta_{\alpha}T^{\alpha\nu} + Q^{\mu}(\delta N^{\nu}, \delta T^{\alpha\nu}) \tag{3.1}$$

with $\beta^\nu = u^\nu/T$. N^ν and $T^{\mu\nu}$ are the particle current and the energy-momentum tensor, defined in Section 2.1 in terms of the energy density n, particle density e and isotropic pressure p and dissipative fields. μ the the chemical potential and is often replace by the fugacity $\lambda = \ln(\mu/T)$. $Q^\mu(\ldots)$ is the dissipative contribution to the entropy current. Its exact form will be specified in the next Sections and is irrelevant for now.

In order to calculate the divergence $\partial_\nu s^\nu$ of the entropy vector constructed above one sometimes uses the so-called Gibbs-Duham relation (which is a generalized form of Gibbs equation in non-relativistic thermodynamics)

$$\partial_\nu (p\beta^\nu) = N^\nu_{eq}\partial_\nu \left(\frac{\mu}{T}\right) - T^{\alpha\nu}_{eq}\partial_\alpha \beta_\nu\,, \tag{3.2}$$

as for instance done in Ref. ([80]). To verify this relation one can use the definition of the particle number four-vector

$$N^\nu_{eq} = \int p^\nu e^{-\beta_\alpha p^\alpha + \mu\beta} d\Gamma \tag{3.3}$$

with $\beta = 1/T$ and $\beta^\nu = \beta u^\nu$. μ denotes the chemical potential and is related to the fugacity λ via $e^\mu = \lambda$. The divergence $\partial_\nu N^\nu_{eq}$ can be expressed in terms of the derivative of the exponent:

$$\begin{aligned}\partial_\nu N^\nu_{eq} &= \int d\Gamma p^\nu \partial_\nu \left(-\beta_\alpha p^\alpha + \mu\beta\right) \cdot e^{-\beta_\alpha p^\alpha + \mu\beta} = \\ &= -\int d\Gamma p^\nu p^\alpha \partial_\nu \beta_\alpha e^{-\beta_\alpha p^\alpha + \mu\beta} + \int d\Gamma p^\nu \partial_\nu \left(\mu\beta\right) e^{-\beta_\alpha p^\alpha + \mu\beta} = \\ &= -T^{\nu\alpha}_{eq}\partial_\nu \beta_\alpha + N^\nu_{eq}\partial_\nu \left(\frac{\mu}{T}\right)\,. \end{aligned} \tag{3.4}$$

On the other hand, in Eckart frame the particle number four-vector can be written using the ideal equation of state as follows:

$$N^\nu = n u^\nu = \frac{p}{T} u^\nu = p\beta^\nu\,. \tag{3.5}$$

Taking the divergence of the above equations together with calculations performed prior to it, one verifies the Gibbs-Duham relation (3.2).

For the divergence of the entropy current (3.1) one now obtains

$$\begin{aligned}\partial_\alpha s^\alpha &= \partial_\alpha \left(p\beta^\alpha\right) - N^\alpha \partial_\alpha \left(\frac{\mu}{T}\right) - \frac{\mu}{T}\partial_\alpha N^\alpha + \beta_\mu \partial_\alpha T^{\mu\alpha} + T^{\mu\alpha}\partial_\alpha \beta_\mu + \partial_\alpha Q^\alpha = \\ &= -\delta N^\alpha \partial_\alpha \frac{\mu}{T} + \delta T^{\alpha\nu}\partial_\alpha \beta_\nu - \frac{\mu}{T}\partial_\alpha N^\alpha + \partial_\alpha Q^\alpha\,. \end{aligned} \tag{3.6}$$

The definitions of $\delta N^\mu = N^\mu - N^\mu_{\rm eq}$ and $\delta T^{\mu\nu} = T^{\mu\nu} - T^{\mu\nu}_{\rm eq}$ have been used together with the conservation equation $\partial_\mu T^{\mu\nu} = 0$ to obtain the latter relation. For the derivations of hydrodynamic equations presented in this work, Equation (3.6) plays the most central role. It has to satisfy the second law of thermodynamics, stating that the entropy production $\partial_\alpha s^\alpha$ must be non-negative, which requires a specific mathematical form of Eq. (3.6) which will be discussed in the following.

At this point I want to notice that the evolution of the particle number current N^α enters the entropy production *explicitly* via the term $-\frac{\mu}{T}\partial_\alpha N^\alpha = -\ln\lambda\partial_\alpha N^\alpha$. Hydrodynamic approaches – e.g. MOLNAR and HUOVINEN in Ref. [46] and MURONGA in [80] – often assume conservation of the particle number current, $\partial_\alpha N^\alpha = 0$. In Section 11.1.1 and Appendix D I will demonstrate that the divergence of the particle number current can be written in the form of a rate equation $\partial_\alpha N^\alpha = n\left(\frac{1}{2}R_{23} - \frac{1}{3}R_{32}\right)$ [87, 35, 88, 89], where R_{23} and R_{32} are the rates of particle production and annihilation with the factors 1/2 and 1/3 accounting for the number of colliding particles in each process. The fugacity λ is a measure of deviation from chemical equilibrium. $\lambda > 1$ denotes the oversaturated regime characterized by particle annihilation, i.e. $1/3R_{32} > 1/2R_{23}$. The undersaturated regime $\lambda < 1$ is characterized by particle production, i.e. $1/3R_{32} < 1/2R_{23}$. Thus, the term $-\ln\lambda\partial_\alpha N^\alpha$ is always a *non-negative* contribution to the entropy production in a closed system.

3.1.2. First-order equations

I will begin the derivation of a first-order equation for dissipative fluid dynamics with an *ansatz* for the entropy current, which is at most first order in dissipative currents:

$$s^\mu = su^\mu + \frac{q^\mu}{T}\,. \tag{3.7}$$

The above expression is given in the Eckart frame. Note, that this is the only possible four-vector which can be constructed from the available tensors u^μ, q^μ and $\pi^{\mu\nu}$ and contains only first-order terms in dissipative corrections. The scalar quantity s denotes the local rest frame equilibrium entropy density. Comparing Eqs. (3.7) and (3.1), one can identify $Q^\mu = q^\mu/T$. In order to calculate the divergence of the first-oder entropy current one can use Eq. (3.6) with $Q^\mu = q^\mu/T$ and $\delta T^{\mu\nu} = -\Delta^{\mu\nu}\Pi + \frac{1}{2}\left(q^\mu u^\nu + q^\nu u^\mu\right) + \pi^{\mu\nu}$ (which is valid in Eckart frame). Note, that $\delta N^\mu = 0$ in Eckart frame. Thus Eq. (3.6) leads to the following form of the divergence of the entropy current:

$$\partial_\alpha s^\alpha = \left(-\Delta^{\mu\nu}\Pi + \frac{1}{2}\left(q^\mu u^\nu + q^\nu u^\mu\right) + \pi^{\mu\nu}\right)\partial_\mu\beta_\nu - \frac{\mu}{T}\partial_\alpha N^\alpha\,. \tag{3.8}$$

With the defintion $\beta^\mu = u^\mu/T$ and the properties $\pi^{\mu\nu}u_\mu = 0$, $q^\mu u_\mu = 0$ as well as $\Delta^{\mu\nu}u_\mu = 0$ the latter equation can be rewritten as follows:

$$\partial_\alpha s^\alpha = -\frac{1}{T}\cdot\Pi\cdot\Delta^{\mu\nu}\partial_\mu u_\nu + \frac{1}{2}q^\mu\left(\partial_\mu\beta + \beta u^\nu\partial_\nu u_\mu\right) + \frac{1}{T}\pi^{\mu\nu}\partial_\mu u_\nu - \ln\lambda\cdot J\,. \tag{3.9}$$

where I have used the general from of the particle number current evolution equation, $\partial_\mu N^\mu = J$, as motivated in the previous Section. In the limit of vanishing dissipative currents Π, q^μ and $\pi^{\mu\nu}$ and chemical equilibrium $\lambda = 1$ the entropy production (3.9) vanishes which means that entropy of equilibrium state is conserved. For a non-ideal (off-equilibrium) system, the entropy production must be non-negative

$$\partial_\mu s^\mu \geq 0 \tag{3.10}$$

which is satisfied in Eq. (3.9) if one postulates following linear relations

$$\begin{aligned}\Pi &= -\zeta\nabla_\mu u^\mu\,, && (3.11)\\ q^\mu &= \kappa T\left(\beta^{-1}\partial^\mu\beta + u^\nu\partial_\nu u^\mu\right)\,, && (3.12)\\ \pi^{\mu\nu} &= 2\eta\partial^{\langle\mu}u^{\nu\rangle} = 2\eta\nabla^{\langle\mu}u^{\nu\rangle}\,. && (3.13)\end{aligned}$$

The covariant gradient operator ∇^μ means $\nabla^\mu = \Delta^{\mu\nu}\partial_\nu$. Note that in the last of these relations the projection $\langle..\rangle$ has been applied to the gradient in order to obtain a traceless symmetric tensor since the shear stress tensor $\pi^{\mu\nu}$ also has this property. Application of the projector $\langle..\rangle$ has no effect on the entropy production $\partial_\mu s^\mu$ since, as one can easily check, $\pi_{\mu\nu}\partial^\mu u^\nu = \pi_{\mu\nu}\partial^{\langle\mu}u^{\nu\rangle}$. Equations (3.11) – (3.13) for dissipative fluxes in relativistic systems are known as Eckart/Landau-Lifschitz theory. For non-relativistic systems first-order hydrodynamic theory is known as Navier-Stokes theory. However, relativistic first-order equations are often referred to by this name as well.

With the relations postulated above the entropy production takes the non-negative form

$$\partial_\mu s^\mu = \frac{\Pi^2}{\zeta T} - \frac{q_\mu q^\mu}{\kappa T} + \frac{\pi_{\mu\nu}\pi^{\mu\nu}}{2\eta T} - \ln\lambda\cdot J\,. \tag{3.14}$$

The proportionality factors in Eqs. (3.11) – (3.13) are the transport coefficients bulk viscosity ζ, heat conductivity κ and shear viscosity η and have to be non-negative in order to satisfy the second law of thermodynamics.

Equations (3.11) – (3.13) are of first order in gradients of thermodynamic variables and velocity fields. Moreover, they can be interpreted as a linear relation between dissipative thermodynamic forces and corresponding fluxes. The forces are

$$\nabla_\mu u^\mu,\ \ -T\partial^\mu\frac{1}{T} - u^\nu\partial_\nu u^\mu,\ \ \nabla^{\langle\mu}u^{\nu\rangle}\,. \tag{3.15}$$

The algebraic Eqs. (3.11) – (3.13) imply that thermodynamic forces can be switched on and off instantaneously. Indeed, if one considers an initially equilibrated system which is driven off equilibrium by expansion, the dissipative fluxes (and thus the related forces as well) evolve from 0 to a finite value instantaneously, thus violating causality. The acausal nature of first-order relativistic hydrodynamic equations as well as their instability under small perturbations have been demonstrated by HISCOCK in [90, 91, 92]. The problem of acausality can be solved by introducing new terms into equations for dissipative fluxes which turn them to equations of relaxation type. This was done for relativistic systems by Israel and Stewart.

3.1.3. Second-order equations

The entropy current introduced in the previous section was up to first order in dissipative currents. Second-order corrections can be introduced in a most general form as follows[40, 80]

$$s^\mu = su^\mu + \frac{q^\mu}{T} - \left(\beta_0\Pi^2 - \beta_1 q_\nu q^\nu + \beta_2\pi_{\alpha\beta}\pi^{\alpha\beta}\right)\frac{u^\mu}{2T} - \frac{\alpha_0\Pi q^\mu}{T} + \frac{\alpha_1\pi^{\mu\nu}q_\nu}{T}\,. \tag{3.16}$$

The dissipative corrections have to be constructed in such way that the local rest frame entropy density is maximal in equilibrium, i.e.

$$\beta_0 \Pi^2 - \beta_1 q_\nu q^\nu + \beta_2 \pi_{\alpha\beta} \pi^{\alpha\beta} \geq 0 \,. \tag{3.17}$$

This leads to requirement $\beta_{0,1,2} \geq 0$. β_i are thermodynamic functions, i.e. in general they are functions of energy and particle densities: $\beta_i(e, n)$. Note that the argumentation introduced so far is rather heuristic. An exact derivation of the entropy current in the scope of Grad's formalism is given in Appendix B. However the result of an exact derivation is identical with the expression obtained here.

For the following derivations I will neglect heat conductivity and bulk pressure. A complete discussion of second-order equations is given by MURONGA in Ref. [80]. In this work I will investigate systems, for which bulk pressure and heat will vanish identically and will thus concentrate on shear viscous corrections only.

The divergence of the second-order entropy current Eq.(3.16) can be written in a factorized form

$$\partial_\mu s^\mu = \pi_{\alpha\beta} \left[\frac{1}{T} \sigma^{\alpha\beta} - \pi^{\alpha\beta} \partial_\mu \left(\frac{\beta_2}{2T} u^\mu \right) - \frac{\beta_2}{T} \dot{\pi}^{\alpha\beta} \right] - \frac{\ln \lambda}{T} \cdot J \,. \tag{3.18}$$

with $\sigma^{\alpha\beta} = \nabla^{\langle\alpha} u^{\beta\rangle}$. The first term in Eq. (3.18) has been as well obtained from the divergence of the first-order entropy current in Section 3.1.2 using Gibbs equation. The last two terms cannot be recovered from first-order *ansatz*. To obtain an equation for the shear tensor I will, in direct analogy to the procedure introduced in Section 3.1.2, use the second law of thermodynamics Eq. (3.10). Equation (3.18) satisfies the second law if one identifies

$$\pi^{\mu\nu} = 2\eta T \left[\frac{1}{T} \sigma^{\mu\nu} - \pi^{\mu\nu} \partial_\alpha \left(\frac{\beta_2}{2T} u^\alpha \right) - \frac{\beta_2}{T} \dot{\pi}^{\mu\nu} \right] . \tag{3.19}$$

The choice of proportionality coefficient guarantees reduction of the obtained equation to the first-order equation (3.13) if second-order terms are neglected. Again, in analogy to the first-order theory, the expression in angular brackets in Eq. (3.19) can be understood as an extended thermodynamic force. Dividing in Eq. (3.19) both parts by $2\eta\beta_2$ and rearranging the terms, one obtains a dynamic equation for the shear tensor

$$\dot{\pi}^{\mu\nu} = -\frac{\pi^{\mu\nu}}{\tau_\pi} + \frac{\sigma^{\mu\nu}}{\beta_2} - \pi^{\mu\nu} \frac{T}{\beta_2} \partial_\alpha \left(\frac{\beta_2}{2T} u^\alpha \right) . \tag{3.20}$$

In the latter equation the relaxation time

$$\tau_\pi = 2\eta\beta_2. \tag{3.21}$$

has been introduced. The notation $\dot{\pi}^{\mu\nu}$ denotes the co-moving derivative $\dot{\pi}^{\mu\nu} = u^\alpha \partial_\alpha \pi^{\mu\nu}$, i.e. derivative with respect to proper time τ in the local rest frame. Different from the constitutive equation of the first-order theory (3.13), Eq. (3.20) is a dynamic equation and has to be solved together with the equations for the energy and particle densities, which follow from the conservation laws Eqs. (2.43) and (2.44).

The dynamic equation (3.20) has an advantage of modelling relaxation processes since it is a differential equation, whereas equation (3.13) is of algebraic form. The necessity of a relaxation-type theory was indicated by acausal character of the first-order order theory. A purely phenomenological *ansatz* to cure the causality violation in Navier-Stokes equations was to introduce a $\tau_\pi \dot{\pi}^{\mu\nu}$ term on the left hand side of Eq. (3.13). Introducing this term one obtains a relaxation equation for the shear tensor

$$\dot{\pi}^{\mu\nu} = \frac{2\eta \nabla^{\langle\mu}u^{\nu\rangle} - \pi^{\mu\nu}}{\tau_\pi} \tag{3.22}$$

which is also known as the 'truncated Israel-Stewart equation' and is of covariant Maxwell-Cattaneo form. Indeed, Eq. (3.22) can be obtained from the Israel-Stewart Eq. (3.20) neglecting the last term in it. However, its neglect due to any power counting arguments proves to be not legitimate. Moreover, this term proves to be essential in order to achieve a good agreement between hydrodynamic and kinetic transport calculations. These issues will be addressed later in this work.

Equation (3.22) allows a very clear understanding of the role of relaxation time τ_π: this is the time scale on which the shear stress tensor relaxes to the first-order value which in turn converges to the equilibrium state where all dissipative corrections are zero in the limit of vanishing viscosity $\eta \to 0$. Although the Israel-Stewart theory contains one term not included in Eq. (3.22), the interpretation of the relaxation time in Israel-Stewart equation (3.20) is the same.

Recently it has been demonstrated that Israel and Stewart's second-order hydrodynamic equations are not complete. In fact a number of further terms can be recovered if hydrodynamic equations are derived directly from the Boltzmann equation, as demonstrated in [37, 38, 93]. Among others these are terms evolving the vorticity

$$\omega_{\mu\nu} = \frac{1}{2}\left(\nabla_\mu u_\nu - \nabla_\nu u_\mu\right) \equiv \nabla_{[\mu}u_{\nu]} \,. \tag{3.23}$$

In the expression for the entropy production (3.18) a term of the form $\pi^{\mu\nu}\nabla_{[\mu}u_{\alpha]}\pi^\alpha_\nu$ can be added since it is identically zero, as can be easily shown using Eq. (3.23). If $\pi^{\mu\nu}$ is factored as happens in transition from Eq. (3.18) to Eq. (3.19), the contribution due to terms involving vorticity is not zero any more in the equation for $\pi^{\mu\nu}$. However, terms involving the vorticity (3.23) do not contribute to the entropy production and thus cannot be recovered in scope of the entropy approach presented in this work. An overview of second-order equations obtained by methods different from the entropy based one will be given in Section 3.2 below.

3.1.4. Third-order equations

An extension of the Israel-Stewart approach to a third-order theory has been presented recently by me together with Zhe Xu and Carsten Greiner in [34]. I extend the expression for the equilibrium current by terms third-order in shear tensor:

$$s^\mu = s_0 u^\mu - \frac{\beta_2}{2T}\pi_{\alpha\beta}\pi^{\alpha\beta}u^\mu + \alpha\frac{\beta_2^2}{T}\pi_{\alpha\beta}\pi^\alpha_\sigma\pi^{\beta\sigma}u^\mu\,. \tag{3.24}$$

The first two terms are already present in the entropy current from the second-order theory. Note that the second and third-order terms are the only possible non-vanishing contractions of the shear tensor $\pi^{\mu\nu}$ and the velocity field u^μ which are, in absence of heat flow, the only tensorial structures present. However the entropy current constructed here can also be derived directly using the Grad's approximation for the distribution function Eq. (2.27). This derivation is given in Appendix B.

In the last term of Eq. (3.24) a new dimensionless coefficient α is introduced. I will assume α to be a constant. This will be demonstrated later in this work when explicit expressions for both α and β_2 will be derived in Section 6 resp. Appendix B. To guarantee that the entropy density is maximal in equilibrium the following requirement on the third-order term must be imposed:

$$\alpha\frac{\beta_2^2}{T}\pi_{\alpha\beta}\pi^\alpha_\sigma\pi^{\beta\sigma}u^\mu \leq 0\,. \tag{3.25}$$

Now the entropy production for the third-order theory can be calculated:

$$\begin{aligned}\partial_\mu s^\mu &= \frac{1}{T}\pi_{\alpha\beta}\sigma^{\alpha\beta} - \pi_{\alpha\beta}\pi^{\alpha\beta}\partial_\mu\left(\frac{\beta_2}{2T}u^\mu\right) - \frac{\beta_2}{T}\pi_{\alpha\beta}\dot{\pi}^{\alpha\beta}\\ &+ \alpha\partial_\mu\left(\frac{\beta_2^2}{T}u^\mu\right)\pi_{\alpha\beta}\pi^\alpha_\sigma\pi^{\beta\sigma} + 3\alpha\frac{\beta_2^2}{T}\pi_{\alpha\beta}\pi^\alpha_\sigma\dot{\pi}^{\beta\sigma} - \frac{\ln\lambda}{T}\cdot J\,.\end{aligned} \tag{3.26}$$

Here again the Gibbs-Duham relation Eq. (3.2) has been used. The next to last term in Eq. (3.26) is different in its structure from the rest of the equation and should be analyzed separately. It can be split into two parts in the following way:

$$3\alpha\frac{\beta_2^2}{T}\pi_{\alpha\beta}\pi^\alpha_\sigma\dot{\pi}^{\beta\sigma} = 3\left(1-\tau_\pi\theta\right)\alpha\frac{\beta_2^2}{T}\pi_{\alpha\beta}\pi^\alpha_\sigma\dot{\pi}^{\beta\sigma} + 3\tau_\pi\theta\alpha\frac{\beta_2^2}{T}\pi_{\alpha\beta}\pi^\alpha_\sigma\dot{\pi}^{\beta\sigma}\,. \tag{3.27}$$

In the latter equation $\theta = \partial_\mu u^\mu$ denotes the so-called expansion scalar and τ_π denotes the relaxation time already known from the second-order theory. The expansion scalar is a measure for the expansion rate of the system and should be compared to the relaxation rate τ_π^{-1}. The relaxation rate should be dominant over the expansion rate in a non-equilibrated system which relaxes to the equilibrium. A ratio of the two characteristic scales - the relaxation time scale and the inverse of the expansion rate - thus can be used to quantify the ability of the system to relax to equilibrium. This ratio is called the (local) Knudsen number [94] and has to be small for hydrodynamic approach to be applicable

$$Kn = \tau_\pi\theta \equiv \tau_\pi\partial_\mu u^\mu \ll 1\,. \tag{3.28}$$

For the first term on the right hand side of Eq. (3.27) two regimes can be considered. As long as $\tau_\pi\theta > 1$, i.e. $\tau_\pi > \theta^{-1}$, the expansion dominates over the relaxation and the Knudsen number is larger than 1. An expansion-dominated system will be driven out of equilibrium, since it cannot relax towards the equilibrium state. In this regime $\alpha\pi_{\alpha\beta}\pi^{\alpha}_{\sigma}\dot{\pi}^{\beta\sigma}$ will have same sign as $\alpha\pi_{\alpha\beta}\pi^{\alpha}_{\sigma}\pi^{\beta\sigma}$ which is negative as follows from the discussion of Eq. (3.24). Since $1-\tau_\pi\theta$ is negative as well, in this regime the first term on the left hand side of Eq. (3.27) will be overall positive. The other regime to be considered is $\tau_\pi\theta < 1$, i.e. $\tau_\pi < \theta^{-1}$. In this regime the relaxation dominates the evolution of the system driving it towards equilibrium state. For a relaxation dominated system $\alpha\pi_{\alpha\beta}\pi^{\alpha}_{\sigma}\dot{\pi}^{\beta\sigma}$ will have an opposite sign than $\alpha\pi_{\alpha\beta}\pi^{\alpha}_{\sigma}\pi^{\beta\sigma}$ and thus will be positive. Since $1-\tau_\pi\theta$ is positive as well, in this regime the first term on the left hand side of Eq. (3.27) will be again positive. One can thus conclude that

$$3\left(1-\tau_\pi\theta\right)\alpha\frac{\beta_2^2}{T}\pi_{\alpha\beta}\pi^{\alpha}_{\sigma}\dot{\pi}^{\beta\sigma} \geq 0 \tag{3.29}$$

holds throughout the entire evolution of the system. Rewriting Eq. (3.26) as

$$\begin{aligned}\partial_\mu s^\mu &= \frac{1}{T}\pi_{\alpha\beta}\sigma^{\alpha\beta} - \pi_{\alpha\beta}\pi^{\alpha\beta}\partial_\mu\left(\frac{\beta_2}{2T}u^\mu\right) - \frac{\beta_2}{T}\pi_{\alpha\beta}\dot{\pi}^{\alpha\beta} \\ &+ \alpha\partial_\mu\left(\frac{\beta_2^2}{T}u^\mu\right)\pi_{\alpha\beta}\pi^{\alpha}_{\sigma}\pi^{\beta\sigma} + 3\tau_\pi\theta\alpha\frac{\beta_2^2}{T}\pi_{\alpha\beta}\pi^{\alpha}_{\sigma}\dot{\pi}^{\beta\sigma} \\ &+ 3\left(1-\tau_\pi\theta\right)\alpha\frac{\beta_2^2}{T}\pi_{\alpha\beta}\pi^{\alpha}_{\sigma}\dot{\pi}^{\beta\sigma}\end{aligned} \tag{3.30}$$

one thus realizes that the second law of thermodynamics can be satisfied by the requirement

$$\begin{aligned}\partial_\mu s^\mu &= \frac{1}{T}\pi_{\alpha\beta}\sigma^{\alpha\beta} - \pi_{\alpha\beta}\pi^{\alpha\beta}\partial_\mu\left(\frac{\beta_2}{2T}u^\mu\right) - \frac{\beta_2}{T}\pi_{\alpha\beta}\dot{\pi}^{\alpha\beta} \\ &+ \alpha\partial_\mu\left(\frac{\beta_2^2}{T}u^\mu\right)\pi_{\alpha\beta}\pi^{\alpha}_{\sigma}\pi^{\beta\sigma} + 3\tau_\pi\theta\alpha\frac{\beta_2^2}{T}\pi_{\alpha\beta}\pi^{\alpha}_{\sigma}\dot{\pi}^{\beta\sigma} \geq 0\end{aligned} \tag{3.31}$$

since the last term in Eq. (3.30) is always non-negative. Splitting the expression for the entropy production into two parts and requiring non-negativeness of each of them implicitly assumes that entropy production is maximal.

Writing Eq. (3.31) in a factorized form one obtains

$$\pi_{\alpha\beta}\left[\frac{1}{T}\sigma^{\alpha\beta} - \pi^{\alpha\beta}\partial_\mu\left(\frac{\beta_2}{2T}u^\mu\right) - \frac{\beta_2}{T}\dot{\pi}^{\alpha\beta} + \alpha\partial_\mu\left(\frac{\beta_2^2}{T}u^\mu\right)\pi^{\langle\alpha}_{\sigma}\pi^{\sigma\beta\rangle} + 3\tau_\pi\theta\alpha\frac{\beta_2^2}{T}\pi^{\langle\alpha}_{\sigma}\dot{\pi}^{\sigma\beta\rangle}\right] \geq 0\,. \tag{3.32}$$

Note that the projection introduced in the last two terms the brackets represents the symmetrized spatial and traceless part of the tensors. The second law of thermodynamics is now satisfied if the dissipative flux is proportional to the expression in the brackets:

$$\begin{aligned}\pi^{\alpha\beta} &= 2\eta T\left[\frac{1}{T}\sigma^{\alpha\beta} - \pi^{\alpha\beta}\partial_\mu\left(\frac{\beta_2}{2T}u^\mu\right) - \frac{\beta_2}{T}\dot{\pi}^{\alpha\beta}\right. \\ &+ \left.\alpha\partial_\mu\left(\frac{\beta_2^2}{T}u^\mu\right)\pi^{\langle\alpha}_{\sigma}\pi^{\sigma\beta\rangle} + 3\tau_\pi\theta\alpha\frac{\beta_2^2}{T}\pi^{\langle\alpha}_{\sigma}\dot{\pi}^{\sigma\beta\rangle}\right]\,.\end{aligned} \tag{3.33}$$

The proportionality factor, in analogy to the Israel-Stewart theory discussed in Section 3.1.3, is chosen in such way that the obtained equation reduces to the Navier-Stockes equation (3.13) if higher-order terms are neglected.

The order of each term in Eq. (3.33) can be estimated from the following quantitative analysis. The coefficient β_2, for which an explicit expression will be derived later in this work, is a purely thermodynamic quantity. From dimensional reasons it has to be proportional to T^{-4} and thus roughly inversely proportional to the isotropic pressure: $\beta_2 \propto 1/p$. The dissipative corrections, in particular the shear pressure, must be small compared to the isotropic pressure in order for the Eqs. (3.16) and (3.24) to be valid. One thus can conclude, that $\beta_2 \pi^{\mu\nu}$ has to be small (component wise). The gradients of the velocity field, which appear in Eqs. (3.13), (3.19) and (3.33) can be roughly approximated by the expansion scalar θ and thus the product of τ_π and gradient of u^μ is of order $Kn = \theta\tau_\pi$ for which $Kn \ll 1$ must hold [comp. Eq. (3.28)]. Derivatives of $\pi^{\mu\nu}$ with respect to proper time, $\dot{\pi}^{\mu\nu}$ are roughly of order $\theta\pi^{\mu\nu}$. Multiplying Eq. (3.33) by β_2 and using $\tau_\pi = 2\eta\beta_2$ like in the second-order theory one thus can estimate the order of its terms:

$$\begin{aligned}\underbrace{\beta_2\pi^{\alpha\beta}}_{\mathcal{O}(1)} &= \underbrace{\tau_\pi\sigma^{\alpha\beta}}_{\mathcal{O}(1)} \underbrace{- \pi^{\alpha\beta}\tau_\pi\partial_\mu\left(\frac{\beta_2}{2T}u^\mu\right)T}_{\mathcal{O}(2)} - \underbrace{\beta_2\dot{\pi}^{\alpha\beta}\tau_\pi}_{\mathcal{O}(2)} \\ &+ \underbrace{\alpha\tau_\pi\partial_\mu\left(\frac{\beta_2^2}{T}u^\mu\right)T\pi_\sigma^{\langle\alpha}\pi^{\sigma\beta\rangle}}_{\mathcal{O}(3)} + \underbrace{3\tau_\pi\theta\alpha\beta_2^2\tau_\pi\pi_\sigma^{\langle\alpha}\dot{\pi}^{\sigma\beta\rangle}}_{\mathcal{O}(4)} . \end{aligned} \tag{3.34}$$

One thus realizes that the last term is of fourth order and has to be neglected for consistency, since further terms of this order are still missing within the presented approach.

Finally, dividing Eq. (3.33) by $2\eta\beta_2 = \tau_\pi$ and neglecting the last term one obtains the third-order evolution equation for shear tensor

$$\dot{\pi}^{\alpha\beta} = -\frac{\pi^{\alpha\beta}}{\tau_\pi} + \frac{\sigma^{\alpha\beta}}{\beta_2} - \pi^{\alpha\beta}\frac{T}{\beta_2}\partial_\mu\left(\frac{\beta_2}{2T}u^\mu\right) + \alpha\frac{T}{\beta_2}\partial_\mu\left(\frac{\beta_2^2}{T}u^\mu\right)\pi_\sigma^{\langle\alpha}\pi^{\sigma\beta\rangle} . \tag{3.35}$$

The last term is the only third-order term which comes from the extension of the entropy current. The thermodynamic coefficients α and β_2 are evaluated in Appendix B.

Recently the third-order hydrodynamic equations were derived independently from this work by MURONGA [95]. The equations reported there confirm the result of this work and contain contributions from heat flow and bulk pressure neglected here.

3.1.5. Second-order hydrodynamic equations for a multi-component system

In this subsection I introduce a derivation of second-order hydrodynamic equations for a system of multiple components. Fluid dynamical descriprion of systems of multiple components is a highly interesting topic gaining a lot of attention in different fields of physics, like for example in physics of materials (physics of polymeric fluids [96]), biophysics [97] or plasma physics [98], just to name some. Since the systems investigated in high-energy heavy-ion research are mixtures of several particle species, there has always existed a strong interest for physics of multi-component systems in heavy-ion community as well (comp. for instance the discussion of hadronic mixture in Ref. [99]).

The derivation of dissipative hydrodynamic equations for multi-component systems presented here is a generalization of the procedure discussed in Section 3.1.3. Let us assume a mixture of N components, to which we refer as *Flavor* $1..N$. The phase-space distributions $f_i(x,p)$ have small deviations $\phi_i(x,p)$ from the equilibrium distributions $f_{0,i}$:

$$f_i(x,p) = f_{0,i}(x,p)\,(1+\phi_i(x,p))\,. \tag{3.36}$$

The equilibrium distributions $f_{0,i}$ in the latter equation are Boltzmann distributions

$$f_{0,i} = \lambda_i d_i e^{-u_\mu p^\mu / T_i}\,, \tag{3.37}$$

were d_i are the respective degeneracy factors, λ_i are the fugacities and T_i are the effective temperatures. u_μ is the *common* velocity field of the considered fluid, which allows to define a reference frame for further calculations. The total energy-momentum tensor and particle flow four-vector can be obtained as sums over contributions from all components:

$$T^{\mu\nu} = \sum_i^N T_i^{\mu\nu} = \sum_i^N \int p^\mu p^\nu f_i d\Gamma \tag{3.38}$$

$$N^\mu = \sum_i^N N_i^\mu = \sum_i^N \int p^\mu f_i d\Gamma\,. \tag{3.39}$$

For the partial energy-momentum tensors and particle flow four-vectors one assumes the standard decomposition in Eckart's frame:

$$T_i^{\mu\nu} = e_i u^\mu u^\nu - (p_i + \Pi_i)\Delta^{\mu\nu} + q_i^{(\mu} u^{\nu)} + \pi_i^{\langle\mu\nu\rangle}\,, \tag{3.40}$$

$$N_i^\mu = n_i u^\mu\,. \tag{3.41}$$

The partial dissipative fluxes $\pi_i^{\mu\nu}$, q_i^μ, Π_i and thermodynamic quantities n_i, e_i, p_i in the latter decompositions were already defined in Section 2.1. In analogy to the one-component case discussed in Section 2.4.2, one can impose the matching conditions on the partial energy-momentum tensors and particle flow four-vectors:

$$n_i = u_\mu N_i^\mu = n_{i,eq} = \lambda_i \frac{d_i}{\pi^2} T_i^3 \tag{3.42}$$

$$e_i = u_\nu u_\mu T_i^{\mu\nu} = e_{i,eq} = 3\lambda_i \frac{d_i}{\pi^2} T_i^4\,. \tag{3.43}$$

With these matching conditions and decompositions in Eqs. (3.40) – (3.41) and neglecting heat flow and bulk pressure one obtains for the deviations $\phi_i(x,p)$

$$\phi_i(x,p) = \frac{1}{2(e_i+p_i)T_i^2}\pi_{i,\mu\nu} p^\mu p^\nu\,. \tag{3.44}$$

This is a generalization of the one-component result obtained in Section 2.4.2. One thus easily realizes that the partial entropy currents can be obtained in the same way as for a one-component fluid in Section 3.1.3:

$$s_i^\alpha = s_{0,i} u^\alpha - \frac{\beta_{2,i}}{2T} \pi_{i,\mu\nu} \pi_i^{\mu\nu} u^\alpha \,, \tag{3.45}$$

with

$$s_{0,i} = 4n_i - n_i \ln \lambda_i \,. \tag{3.46}$$

In analogy to the formalism presented in Section 3.1.3, the evolution equation for the hydrodynamic equations can be obtained for a multi-component system from the requirement that the *total* entropy production must be non-negative

$$\partial_\mu s^\mu \geq 0 \,. \tag{3.47}$$

This is nothing else but the second law of thermodynamics applied to the total system. To calculate the entropy production from Eq. (3.45) one now needs to specify which conservation laws apply in the system. Due to possible energy and momentum exchange between the particles of different Flavors the partial energy momentum tensors are not conserved. On the other hand the total energy-momentum tensor is always conserved in closed system. For the formalism presented here particle number conservation for each Flavor will be considered, i.e. the partial particle flow vectors are conserved. To summarize, one has the following balance equations:

$$\partial_\mu T_i^{\mu\nu} = S^\nu \,, \tag{3.48}$$

$$\partial_\mu T^{\mu\nu} = 0 \,, \tag{3.49}$$

$$\partial_\mu N_i^\mu = 0 \,. \tag{3.50}$$

The source term S^ν in Eq. (3.48) must be derived from the kinetic theory. In scope of the entropy principle based approach used here this source term is unknown. Hence, only Eqs. (3.49) – (3.50) will be used for the further derivation. This means, in a most general case the formalism is not able to describe energy balance for each of the components correctly – only the total energy balance is known – and thus evolution of the effective temperatures T_i also cannot be described. However, one can assume a *common* effective temperature for all components:

$$T_i = T \,. \tag{3.51}$$

This assumption is only valid if all Flavors thermalize on the same time scale and is a good approximation in case the time scales are comparable. This will be proven in comparisons of the solutions of hydrodynamic equations with kinetic transport calculations in Section 12. With Eqs. (3.42) – (3.43) the assumption of a common effective temperature immediately leads to the following expression:

$$T = \frac{e}{3n} = \frac{\sum e_i}{\sum n_i} \,. \tag{3.52}$$

With the definition of the common effective temperature T and with the conservation laws (3.49) – (3.50) the entropy production now can be calculated:

$$\partial_\alpha s^\alpha = \partial_\alpha \sum_i^N s_i^\alpha = \frac{\pi_{\mu\nu}\sigma^{\mu\nu}}{T} - \sum_i \left(\pi_{i,\mu\nu}\pi_i^{\mu\nu}\partial_\alpha\left(\frac{\beta_{2,i}}{2T}u^\alpha\right) + \frac{\beta_{2,i}}{T}\pi_{i,\mu\nu}\dot{\pi}_i^{\mu\nu}\right) . \tag{3.53}$$

Note that the divergences of the partial entropy currents $\partial_\alpha s_i^\alpha$ cannot be calculated since the partial energy-momentum tensors are not conserved. The right-hand side of Eq. (3.53) is explicitly non-negative if the entropy production has the following algebraic structure:

$$\partial_\alpha s^\alpha \overset{!}{=} \sum_{i=1}^N \frac{\pi_{i,\mu\nu}\pi_i^{\mu\nu}}{2\eta_i T} \geq 0 \,. \tag{3.54}$$

Splitting the first term in Eq. (3.53) into a sum over N Flavors and one can write

$$\partial_\alpha s^\alpha = \sum_i \pi_{i,\mu\nu}\left(\frac{\sigma^{\mu\nu}}{T} - \pi_i^{\mu\nu}\partial_\alpha\left(\frac{\beta_{2,i}}{2T}u^\alpha\right) + \frac{\beta_{2,i}}{T}\dot{\pi}_i^{\mu\nu}\right) . \tag{3.55}$$

Comparing Eqs. (3.54) and (3.55) one obtains the constitutive evolution equations for the partial shear tensors in accordance with the second law of thermodynamics:

$$\pi_i^{\alpha\beta} = 2\eta_i\left(\sigma^{\alpha\beta} - \pi_i^{\alpha\beta}T\partial_\mu\left(\frac{\beta_{2,i}}{2T}u^\mu\right) - \beta_{2,i}\dot{\pi}_i^{\alpha\beta}\right) . \tag{3.56}$$

The obtained evolution equations are analogous to the Israel-Stewart Equation (3.20) for the one-component case.

In contrast to the formalism presented recently by Monnai and Hirano in Ref. [100], the formalism presented here introduces separate transport coefficients η_i and shear stress tensors $\pi_i^{\mu\nu}$ for each component of the fluid. This allows to quantify the equilibrium deviations for each component and thus, the effect of dissipation on the phase-space distribution (and spectra) can be quantified for each component according to the ansatz for the off-equilibrium distribution function. The shear viscosity coefficients η_i and the thermodynamic coefficients $\beta_{2,i}$ yet must be specified. This will be done in Sections 4.2.2 and 12.1.

One also realizes that Eqs. (3.56) in principle can be summed into an effective one-component equation of form (3.19) with only one shear viscosity coefficient describing the multi-component system as a whole. This will be discussed for the special case of a one-dimensional system in Section 12.1.

3.2. Other known approaches

In Sections 3.1.2 – 3.1.4 I introduced a phenomenological way to obtain hydrodynamic equations up to third order in small deviations from equilibrium with the focus on shear viscous effects only. The approach I discussed is based on the entropy principle and the evolution equations for dissipative quantities are obtained from the requirement of a particular algebraic form of divergence of the entropy current which guarantees that the second law of thermodynamics is satisfied. The advantages of the introduced approach is that the second law is explicitly fulfilled and a functional relation between the relaxation time and shear viscosity follows directly from the derivation (same is true for bulk viscosity and heat conductivity). The obtained equations naturally had a relaxation type form and thus could be reduced to the Navier-Stokes equation in the limit of small equilibrium deviations. A disadvantage of the entropy production based derivation is that it is not obvious whether the obtained evolution equations are fully compatible with the underlying microscopic equation such as the Boltzmann Equation. Thus it might be necessary to derive hydrodynamic equations directly from the Boltzmann Equation. This can be done either by using the method of moments or by a systematic expansion of the collision term. In addition, the equation of motion for dissipative quantities can be obtained from a gradient expansion of the dissipative fluxes. This method does not yield the expressions for the transport coefficients which have to be obtained from matching of the derived equation to known solutions obtained from kinetic theory. Here I will review the most significant works in which the hydrodynamic equations were derived by some of these methods.

3.2.1. Second-order hydrodynamics from kinetic approach using method of moments.

The starting point for this approach is an approximation for the off-equilibrium distribution function, which can be seen as a truncated Taylor expansion in terms of small deviations from equilibrium $\phi(x,p)$:

$$f(x,p) = f_0(x,p) \cdot (1 + \phi(x,p)) \ . \tag{3.57}$$

The tensor decomposition of the deviation function $\phi(x,p)$ has been already introduced in Eq. (2.26), Section 2.4.1, in this work. In this method, the hydrodynamic equations are obtained from the conservation equations for the particle number current, $\partial^\mu N^\mu = 0$ and the energy momentum tensor $\partial_\mu T^{\mu\nu} = 0$, which can be rewritten using moments of the Boltzmann Equation as given by Eqs. (2.43) – (2.45). The collision term is replaced by the so-called relaxation time approximation

$$C[f] = -p_\mu u^\mu \frac{f - f_0}{\tau_\pi} \, . \tag{3.58}$$

The relaxation time τ_π is assumed to be momentum independent for the following derivation. This is a strong assumption since the different momentum scales can be expected to relax toward equilibrium distribution on different time scales as was demonstrated for example in Refs. [32, 30] for a gluon gas with leading order pQCD cross sections. Introducing the simplified form of the collision term from Eq. (3.58) into the expressions for the moments Eqs. (2.43) – (2.45) one obtains for a massless Boltzmann gas the evolution equation for the shear tensor [37]:

$$\Delta^{\mu}_{\alpha}\Delta^{\nu}_{\beta}\dot{\pi}^{\alpha\beta} = -\frac{\pi^{\mu\nu}}{\tau_\pi} - \frac{4}{3}\pi^{\mu\nu}\nabla_\alpha u^\alpha + \frac{2\eta}{\tau_\pi}\nabla^{\langle\mu}u^{\nu\rangle} - 2\pi^{\alpha[\mu}\omega^{\nu]}_{\alpha}\,. \tag{3.59}$$

This equation is similar to the second-order equation obtained from the entropy production, Eq. (3.20), but contains the vorticity terms which cannot be obtained from the entropy based method since their contributions vanish as discussed in Section 3.1.3. The relation between the shear viscosity coefficient η and the relaxation time τ_π follows directly from the calculation and reads $\tau_\pi = \frac{6\eta}{sT}$ for a massless Boltzmann gas. Eq. (3.59) is a kinetic version of the Israel-Stewart equations [38].

An alternative derivation of hydro equations up to second order in terms of the Knudsen Number $Kn \equiv \tau_\pi\theta$, which was introduced in Section 3.1.4, is presented in [38]. In this derivation, the method of moments is used and the equations are consistently expanded up to second order in Kn. Neglecting the heat conductivity and the bulk pressure, the evolution equation for shear tensor reported in [38] takes the form

$$\dot{\pi}^{\langle\mu\nu\rangle} = -\frac{\pi^{\mu\nu}}{\tau_\pi} - \frac{2\eta}{\tau_\pi}\delta_2\theta\pi^{\mu\nu} + \frac{2\eta}{\tau_\pi}\nabla^{\langle\mu}u^{\mu\rangle} + 2\pi^{\langle\mu}_{\alpha}\omega^{\alpha\nu\rangle} - 2\pi^{\langle\mu}_{\alpha}\sigma^{\alpha\nu\rangle}\,. \tag{3.60}$$

This latter equation differs from Eq. (3.19) obtained from the entropy principle by the last two terms, whereas in (3.59) only the last term is not present. This term can be written in a different way if one makes use of the first-order relation $\pi^{\mu\nu} \propto \sigma^{\mu\nu}$ [comp. Eq. (3.13)]. Then the last term in Eq. (3.60) takes the form $\frac{1}{\eta}\pi^{\langle\mu}_{\alpha}\pi^{\alpha\nu\rangle}$. It is noteworthy to mention that, if modified in such way, the last term in Eq. (3.60) is similar in its from to the third-order term in Eq. (3.33) but is of second order in gradients.

3.2.2. Conformal second-order hydrodynamics from gradient expansion method.

In Ref. [101] the evolution equation for the shear tensor is derived using conformal symmetry constrains. From the requirement of conformal symmetry all possible terms second order in gradients are constructed. The number of such terms found in [101] is 8. The conformal symmetry is defined by the Weyl transformations and only 5 combination of the 8 possible terms transform homogeneously. From these combinations a general decomposition of the shear tensor is found in [101] for flat space:

$$\pi^{\mu\nu} = -\eta\sigma^{\mu\nu} + \eta\tau_\pi\left(D\sigma^{\langle\mu\nu\rangle} + \frac{1}{3}\sigma^{\mu\nu}(\nabla_\alpha u^\alpha)\right) + \lambda_1\sigma^{\langle\mu}_{\alpha}\sigma^{\alpha\nu\rangle} + \lambda_2\sigma^{\langle\mu}_{\alpha}\omega^{\alpha\nu\rangle} + \lambda_3\omega^{\langle\mu}_{\alpha}\omega^{\alpha\nu\rangle}\,. \tag{3.61}$$

An evolution equation for $\pi^{\mu\nu}$ is obtained from the latter equation by replacing $\pi^{\mu\nu} = \eta\sigma^{\mu\nu}$, i.e. using the first-order expression for $\pi^{\mu\nu}$:

$$\dot{\pi}^{\langle\mu\nu\rangle} = -\frac{\pi^{\mu\nu}}{\tau_\pi} - \frac{4}{3}\theta\pi^{\mu\nu} + \frac{\eta}{\tau_\pi}\sigma^{\mu\nu} + \frac{\lambda_1}{\eta^2}\pi^{\langle\mu}_{\alpha}\pi^{\alpha\nu\rangle} - \frac{\lambda_2}{\eta}\pi^{\langle\mu}_{\alpha}\omega^{\alpha\nu\rangle}. \tag{3.62}$$

This equation is similar to Eq. (3.60) and 3.59, both obtained from the kinetic approach. Again, the last two terms constitute the difference to the Israel-Stewart equation (3.19).

3.2.3. Second-order hydrodynamic equations from kinetic theory.

Dissipative hydrodynamic equations can be derived from the Boltzmann Equation (1.2) in a direct way by inserting a parametrization for the off-equilibrium distribution function on the left and right-hand sides. A possible way to parametrize the off-equilibrium distribution function is Grad's approximation (2.42) used in this work. The results of a derivation of this type were reported by Denicol, Koide and Rischke in Ref. [39]. Formally, the obtained equation is similar to the one derived in Ref. [38]. However, the expressions for the transport coefficients differ slightly from the forms, given in the standard Israel-Stewart theory [102].

There are as well alternative ways of parametrization of the off-equilibrium distribution. One of them was reported by Martinez and Strickland in Ref. [103]. The second-order hydrodynamic equations obtained inserting this particular parametrization of anisotropic distribution function into the Boltzmann Equation were discussed in Ref. [86]. The other approach by Denicol criticizes Grad's approximation as being incomplete due to truncation of the momentum power series. The authors demonstrate that by considering more than 14 unknowns in the off-equilibirum distribution function, one can obtain a better approximation of the solution of Boltzmann Equation.

These two approaches by Martinez, Strickland and Denicol and Rischke are highly interesting since they naturally lead to analytical expressions for the transport coefficients. Moreover, the number of the transport coefficients appearing in the hydrodynamic equations is different form what is known form the Israel and Stewart's theory. Solutions of equations reported in Ref. [39] are in remarkably good agreement with direct solutions of the Boltzmann Equation obtained from the partonic cascade BAMPS, which will be employed in this work.

4. Shear viscosity of a Boltzmann gas.

The observed good matching between ideal hydrodynamic calculations of flow and data taken at RHIC can be interpreted as a indication that QGP is a nearly perfect fluid with a very small shear viscosity η. The shear viscosity is often rescaled by the entropy density s and the ratio η/s is used as a universal measure of the strength of dissipation in the fluid. Fluids with low η/s ratio values are known outside the ultrarelativistic heavy-ion physics. For instance, for helium, nitrogen and water under large pressures the η/s ratio as function of temperature has a pronounced minimum in the vicinity of the liquid-gas transition [25, 24]. Similar to the hot quark-gluon plasma, cold atomic gases are as well known to exhibit a hydrodynamic behavior and have a small η/s ratio [24].

In this Chapter I address the question what approaches can be used to calculate the shear viscosity of a massless Boltzmann gas consisting of one or several components.

4.1. Review of theoretical methods.

In the classical Newtonian mechanics the shear viscosity coefficient is defined in as the proportionality coefficient between shear stress τ and the velocity gradient existing between two layers in a fluid:

$$\tau = \eta \frac{\partial v_x}{\partial y} \,.$$

In the classical gas theory this definition leads to the expression of shear viscosity coefficient in terms of the mean particle velocity $\langle v \rangle$ and the cross section σ:

$$\eta = \frac{m\langle v \rangle}{3\sqrt{2}\sigma} \,.$$

For a ultra-relativistic gases one obtains [104]

$$\eta \approx \frac{3}{2}\pi n T \lambda_{\mathrm{mfp}} \tag{4.1}$$

with n denoting the particle density, T the local temperature and λ_{mfp} the mean free path.

For relativistic systems the Newtonian definition of shear viscosity corresponds to the first-oder equation, which is often referred to as the Navier-Stokes equation

$$\pi^{\mu\nu} = 2\eta \nabla^{\mu} u^{\nu} \,.$$

Derivation of this equation was already discussed in this work (Section 3.1.2). Using these considerations, which are based on the classical Newtonian picture, the shear viscosity of a gluonic gas has been recently calculated using the partonic cascade BAMPS[105].

It is important to calculate the shear viscosity coefficient of the deconfined QCD matter from first principles, i.e. from the underlining field theory. A formalism based on the fluctuation-dissipation theorem and allowing to calculate the shear viscosity coefficient in a standard field theory was introduced in by HOSOYA, SAKAGAMI and TAKAO in Ref. [106]. According to the Green-Kubo formalism, the linear transport coefficients are related to the time dependence of equilibrium fluctuations in the conjugate flux via the integral over its autocorrelation function in the zero frequency limit.

A number of approaches to calculate the shear viscosity coefficient are based on the Chapman-Enskog method [76], which employs relaxation time approximation of Boltzmann equation, as was introduced in section 3.2.1. Such calculations for a quark-gluonic system were first reported by HOSOYA and KAJANTIE in Ref. [107]. Further relaxation time approximation based approaches are by CHAKRABARTY[108], by CZYZ and FLORKOWSKI for a quark–anti-quark system [109], by VON OERTZEN for a pure quark and gluon matter, quark–anti-quark mixture and a zero baryon number quark–anti-quark-gluon plasma [110], by THOMA for a quark-gluon plasma taking into account screening effects by using an effective perturbation theory for the finite temperature QCD in the weak coupling limit [111], by ILYIN, PANFEROV and SINYUKOV using a Kubo-type formula for a QCD plasma in one-loop order [112]. The drawback of relaxation time calculations is the often neglected momentum dependence of the relaxation time itself.

A more appropriate treatments are based on solutions of the Boltzmann equation with the full collision term, which allows to take into account the momentum dependence of the collisional process. Using the linearized form of the Boltzmann equation, BAYM, MONIEN, PETHICK and RAVENHALL calculated the shear viscosity of a weakly coupled QCD plasma in Ref. [113]. By solving the Boltzmann equation analytically for quarks and gluons including screening, the viscosity is calculated to leading orders in α_s by HEISELBERG in Ref. [114]. Finally, ARNOLD, MOORE and YAFFE obtained in their leading-log calculations in Ref. [115] a result which essentially agrees with the one obtained by BAYM et al. and HEISELBERG earlier.

A recent calculation of the shear viscosity coefficient in BAMPS reported by XU and GREINER demonstrated that the η/s ratio is low for $\alpha_s \sim 0.3$ if the pQCD bremsstrahlung processes are implemented together with the particular treatment of the Landau-Pomeranchyk-Migdal effect (cf. section 7.3). At the same time, the results obtained from BAMPS calculations cannot be directly compared with those, reported in Refs. [113, 111, 115, 114] due to different treatments of the Landau-Pomeranchyk-Migdal effect and of regularization of infrared divergence in the perturbative cross sections.

A constrain on upper value of shear viscosity to entropy density ratio in q QGP can be obtained from a direct comparison of hydrodynamic calculations with experimental data. From a comparison of v_2 calculations with RHIC data, ROMATSCHKE together with LUZUM [116] and HEINZ together with SONG [47] deduced the upper limit $\eta/s < 0.5$. The lower limit $\eta/s = 1/(4\pi)$ was calculated by POLICASTRO, STARINETS and SON for the strongly coupled finite-temperature $N = 4$ supersymmetric Yang-Mills theory using the gravity/gauge theory duality of the AdS/CFT prescription [117]. This lower boundary is valid for a large class of strongly interacting quantum-field theories.

4.2. Shear viscosity from Grad's 14-moment theory

4.2.1. One-component system.

In this Section I will derive an expression for the shear viscosity coefficient for a one-component gas using the 14-moments method by Grad [33]. The advantage of the method introduced here is its compatibility with the kinetic transport models which are constructed to solve the Boltzmann equation.

I start the derivation with the kinetic expression for entropy four-current [33, 76, 83]

$$s^{\mu} = -\int d\Gamma p^{\mu} f(x,p) \left[\ln(f(x,p)) - 1\right] . \tag{4.2}$$

The divergence of the entropy current leads to the entropy production

$$\partial_{\mu} s^{\mu} = -\int d\Gamma p^{\mu} \partial_{\mu} f(x,p) \ln f(x,p) = -\int d\Gamma C[f(x,p)] \ln f(x,p) . \tag{4.3}$$

For the last equality the Boltzmann equation has been used to replace the derivative of the distribution function. The logarithm on the right hand side can be simplified by introducing the linearized form of the off-equilibrium distribution function $f = f_{eq}\,(1+\phi)$:

$$\begin{aligned} \partial_{\mu} s^{\mu} &= -\int d\Gamma C[f] \ln\left[f_{eq}\,(1+\phi)\right] \\ &= -\int d\Gamma C[f] \ln f_{eq} - \int d\Gamma C[f] \ln\,(1+\phi) \ . \end{aligned} \tag{4.4}$$

Now the logarithm can be expanded in terms of ϕ up to first order. This expansion is in particular legitimated by the assumption that $\phi(x,p)$ has to be small, which underlies the linearization in Eq. (2.27). With the explicit form of ϕ from Eq. (2.26) and the logarithm of the equilibrium distribution from Eq. (2.24) the expression for entropy production becomes

$$\begin{aligned} \partial_{\mu} s^{\mu} &= -\mu \int d\Gamma C[f] + \int d\Gamma \frac{u_{\mu} p^{\mu}}{T} C[f] \\ &- \epsilon \int d\Gamma C[f] + \epsilon_{\mu} \int d\Gamma p^{\mu} C[f] - \epsilon_{\mu\nu} \int d\Gamma p^{\mu} p^{\nu} C[f] . \end{aligned} \tag{4.5}$$

In the latter equation moments of the collision term appear, of which the 1st is zero due to energy-momentum conservation stated by Eq. (2.44). Thus the second and the fourth terms vanish in Eq.(4.5). Introducing ϵ and $\epsilon_{\mu\nu}$ from Eqs. (2.40) and (2.38) into Eq.

(4.5) and using the short notation for the moments from Eqs. (2.43) – (2.45) one thus obtains

$$\partial_\mu s^\mu = -\mu J - \left[A_2\left(3u_\mu u_\nu - \Delta_{\mu\nu}\right)P^{\mu\nu} - A_0 J\right]\Pi + B_1 u_{(\mu} q_{\nu)} P^{\mu\nu} - C_0 \pi_{\mu\nu} P^{\mu\nu}\,. \tag{4.6}$$

Assuming conservation of net particle number, i.e. setting $J = 0$, Eq. (4.6) reduces to the form obtained in Ref. [83]. In the form presented here the entropy production splits into 4 parts, which account for entropy production due to particle production, bulk viscosity , heat conductivity and shear viscosity. In a general form the entropy production can be written in a non-negative form [118]

$$\partial_\mu s^\mu = \beta\mu J + \beta\zeta^{-1}\Pi^2 - \beta\kappa^{-1} q_\nu q^\nu + \beta(2\eta)^{-1}\pi_{\mu\nu}\pi^{\mu\nu} \tag{4.7}$$

with ζ, κ and η denoting the transport coefficients bulk viscosity, heat conductivity and shear viscosity. A more detailed motivation for Eq. (4.7) was already given in Chapter 3, where I discussed derivation of the Israel-Stewart equations from the entropy principle. Here it is sufficient to mention that the expression in Eq. (4.7) is non-negative by construction and thus satisfies the second law of thermodynamics. It is now straight forward to identify the expression for the shear viscosity coefficient from Eqs. (4.6) and (4.7):

$$\eta = \frac{\beta}{2}\frac{\pi_{\mu\nu}\pi^{\mu\nu}}{C_0 \pi_{\mu\nu} P^{\mu\nu}}\,. \tag{4.8}$$

The expression presented here is similar to the one presented by Xu and Greiner in Ref. [42]. First aspect to mention is that both approaches are based on calculation of moments of the collision term. Approach in Ref. [42] is explicitly based on Navier-Stokes, i.e. first-order, relativistic fluid equation. The approach presented here is based on Grad's method and thus, implicitly, on second-order relativistic hydrodynamics. A more detailed comparison of the two approaches will be given in Chapter 9, where I apply Eq. (4.8) to a special case of one-dimensional boost-invariant expanding system.

4.2.2. Multi-component system.

In this Section the expression for the shear viscosity coefficients in a multi-component system will be derived as generalization of the one-component expression (4.8). Let us consider a system of N components, to which I refer as Flavor i. Let us furthermore assume that the phase-space distribution functions f_i of each component obey the Boltzmann Equations

$$p^\mu \partial_\mu f_i = C[f_i] + \sum_{j\neq i} C[f_i, f_j]\,. \tag{4.9}$$

In the latter equation the collision term $C[f_i]$ accounts for collisions of particles of same Flavor. These collisions will be called *self-collisions*. The collision term $C[f_i, f_j]$ accounts for collisions of particles of different Flavors and these processes will be called *inter-collisions*. The N Boltzmann Equations describing a multi-component system are thus coupled to each other via the collision terms. The off-equilibrium distribution functions

f_i are approximated by Eq. (3.36). The partial entropy currents are given by Eq. (4.2) and the total entropy production can be obtained by summing the divergences of the partial entropy currents. One then obtains an expression which is a sum of Equations of form (4.4). Neglecting heat flow and bulk pressure contributions, one can obtain the total entropy production in terms of partial shear stress tensors and chemical potentials:

$$\partial_\mu s^\mu = -\sum_i^N \mu_i J_i - \sum_i^N C_{0,i} \pi_{i,\mu\nu} P_i^{\mu\nu} \,. \tag{4.10}$$

with

$$P_i^{\mu\nu} = \int p^\mu p^\nu \left(C_i + \sum_j C_{ij} \right) d\Gamma \tag{4.11}$$

where C_i denotes the self-collision term and C_{ij} – the inter-collision term. Considering only particle number conserving processes, i.e. neglecting $J_i \equiv \partial_\mu N_i^\mu$ in accordance with Eq. (3.50), one obtains by comparing Eq. (4.10) with (3.54):

$$\eta_i = \frac{\pi_{i,\mu\nu} \pi_i^{\mu\nu}}{2C_{0,i} \pi_{i,\mu\nu} \int p^\mu p^\nu C_{ii,ij}[f_i, f_j] d\Gamma} \,. \tag{4.12}$$

with

$$C_{ii,ij}[f_i, f_j] \equiv C[f_i] + \sum_{j \neq i} C[f_i, f_j] \,. \tag{4.13}$$

The obtained expression proves to be a straight-forward generalization of the one-component result: the shear viscosity coefficients are inversely proportional to the second moment of the respective collision terms, which include elastic particle number conserving (i.e. Flavor symmetric in initial and final states) self- and all possible inter-collision terms. It is important to stress that the obtained expression is only valid in systems with conserved particle flow vectors, i.e. in systems with constant particle numbers for each component.

5. Bjorken's picture of heavy-ion collisions

> *Make everything as simple as possible, but not simpler.*
>
> Albert Einstein (1879 - 1955), physicist.

5.1. Bjorken's assumptions

The CERN SPS results on charged particle multiplicities published 1981 by the $UA5$ collaboration indicated for $p-p$ collisions that the pseudo-rapidity distributions dN_{ch}/dy were almost flat for different intervals of N_{ch} up to $N_{ch} \approx 30$ [119]. Starting with $N_{ch} \approx 30$ the distribution still could be considered constant for $|y| < 3$ but revealed an enhancement at $y \approx 1.5$. Based on this observation, Bjorken proposed a scenario for the evolution of the central rapidity region in heavy-ion collisions [45].

The main assumptions made by Bjorken in his scenario for heavy-ion collisions are the following

- The collision of two nuclei has to be transparent. This means that the net-baryon content, $N(B) - N(\bar{B})$, ends up at forward rapidities after the collision – i.e., the mid-rapidity region is completely void of original baryons thus having a zero net-baryon density and high energy density. The complete transparency of the collision proposed by Bjorken is an idealized assumption. The opposite limit is the full stopping scenario, in which at central rapidity ($y \approx 0$) an excess of net-baryon density is expected. A schematic picture of the rapidity distributions expected in both full stopping and transparency scenarios is given in Fig.5.1. The experimental data presented several years after Bjorken's publication indicates that stopping is observed for $Au + Au$ collisions at AGS energies ($\sqrt{s_{NN}} \approx 5$ GeV). A similar scenario of non-zero net baryon density can be expected for the upcoming FAIR project at GSI. The onset of transparency can be observed at higher energies in lead collisions at SPS ($\sqrt{s_{NN}} \approx 17$ GeV). However the assumption of zero net-baryon density in the mid-rapidity region derived by Bjorken from $p + p$ results is by far not always realized in collisions of heavy nuclei but can be expected to be valid at high energies[51, 52].

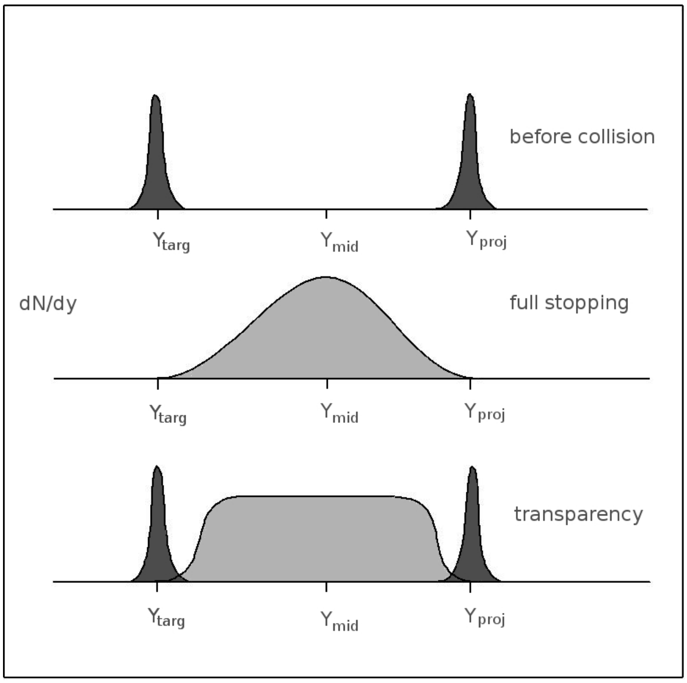

Figure 5.1.: Schematic picture of the particle rapidity distributions before and after the collision for the full stopping and complete transparency (Bjorken) scenarios.

- The second essential assumption of Bjorken scenario is the existence of a central rapidity plateau in the inclusive particle production as function of the rapidity. I.e. the yield dN/dy is expected to be independent of the rapidity. This assumption can be formulated as boost-invariance of the particle production, since the yield is independent of the choice of reference frame characterized by the rapidity y. Such a plateau has been observed for $p + p$ collisions at SPS[119]. For the nucleus-nucleus collisions at RHIC energies ($\sqrt{s_{NN}} = 200$ GeV) the BRAHMS Collaboration could observe an onset of boost-invariance in a rather small rapidity interval $y < 1$ in charged meson rapidity distributions[120]. The conclusion made based on BRAHMS data is that a certain degree of transparency can be observed in heavy-ion collisions at high energies and the boost-invariance assumption holds in a narrow rapidity range.

5.2. Velocity field in Bjorken's model

Here the mathematical implications of the Bjorken assumptions will be discussed. The existence of a plateau in particle yields as a function of rapidity leads according to Bjorken to the conclusion, that throughout the central rapidity region the initial conditions are invariant with respect to Lorentz transformations in longitudinal direction and the subsequent evolution of the system as well possesses this symmetry. Moreover, in the

Bjorken model the evolution of the QGP is assumed to be one-dimensional, i.e. the created medium expands in longitudinal direction and is isotropic in transverse plane. This assumption is reasonable only at very early times after the collision as long as transverse expansion does not set in (i.e. on time scales comparable to the transverse size of the collision region, which is the radius of the nuclei in central collisions).

The natural variables to describe an ultrarelativistic system are not the Cartesian space coordinates $\vec{x}$ and time t but rather the space-time rapidity η and the proper time τ connected to the Cartesian coordinates via

$$\eta = \frac{1}{2}\ln\frac{t+z}{t-z}, \tag{5.1}$$

$$\tau = \sqrt{t^2 - z^2}. \tag{5.2}$$

For the definition above, the z axis has been chosen as the expansion axis and the xy plane is isotropic. For massless particles travelling at speed of light with $v_z = z/t$ the space-time rapidity is equal to the momentum rapidity y of a particle (often referred to as *the rapidity*):

$$y = \frac{1}{2}\ln\frac{E+p_z}{E-p_z} = \frac{1}{2}\ln\frac{t+z}{t-z} \tag{5.3}$$

All physical quantities now depend on this set of variables:

$$A(\vec{x}, t) \rightarrow A(\eta, \tau). \tag{5.4}$$

However, according to Bjorken's assumption the dependence on rapidity is trivial, since all physical quantities are assumed to posses the symmetry of boost-invariance and thus one can write

$$A(\eta, \tau) \rightarrow A(\tau). \tag{5.5}$$

The most important feature of Bjorken's model is the special form of the velocity field u^μ. For a one-dimensionally expansing medium it has a general form

$$u^\mu = (u_0, 0, 0, u_z) \tag{5.6}$$

and is normalized

$$u_\mu u^\mu = 1, \tag{5.7}$$

which leads to

$$u_0^2 - u_z^2 = 1. \tag{5.8}$$

This relation is satisfied for the following parametrization of u^μ in terms of the space-time rapidity η:

$$u^\mu = (\cosh\eta, 0, 0, \sinh\eta). \tag{5.9}$$

Using the definitions of the rapidity and proper time, Eqs. (5.1) and (5.2), one thus obtains the so called one-dimensional Bjorken flow

$$u^\mu = \frac{1}{\tau}(t, 0, 0, z). \tag{5.10}$$

Thus in any point and at any time the velocity field is defined solely by its four-coordinate.

For the Bjorken flow velocity Eq.(5.9) one obtains

$$\partial_\nu u_\mu = \frac{1}{\tau} g_{\mu\nu} - \frac{1}{\tau^3} x_\mu x_\nu = \frac{1}{\tau}(g_{\mu\nu} - u_\mu u_\nu) \tag{5.11}$$

which in particular leads to

$$\partial_\mu u^\mu = \frac{1}{\tau}. \tag{5.12}$$

Bjorken's flow (5.9) is often referred to as “one-dimensional Hubble flow”, since regions further away from a certain point move faster than the closer ones.

6. Relativistic hydrodynamics for one-dimensional boost-invariant expanding systems.

In this chapter hydrodynamic equations derived in chapters 2.4.3 and 3.1.2 – 3.1.4 will be rewritten for a one-dimensionally expanding gas of massless Boltzmann particles. I assume a longitudinally expanding system following the Bjorken flow according to Eq. (5.9). For a massless Boltzmann gas the ideal equation of state holds (comp. Section 2.3)

$$e = 3p\,. \tag{6.1}$$

The equation presented in this Chapter are given for a one-component system.

I will consider the Eckart frame for the discussion to follow in this Chapter. As already discussed in Chapter 2.2, in the Eckart frame the particle four-current and the energy-momentum tensor are decomposed as follows:

$$\begin{aligned} N^\mu &= n u^\mu\,, & (6.2)\\ T^{\mu\nu} &= e u^\mu u^\nu - (p+\Pi)\Delta^{\mu\nu} + 2q^{(\mu}u^{\nu)} + \pi^{\mu\nu}\,. & (6.3) \end{aligned}$$

It is straightforward to demonstrate that for a massless Boltzmann gas undergoing a one-dimensional expansion with boost-invariance both bulk pressure and heat flux vanish identically. According to the definitions in Eqs. (2.11) – (2.18) one obtains for the bulk pressure

$$\Pi = -\frac{1}{3}\Delta_{\mu\nu}T^{\mu\nu} - p = -\frac{1}{3}T^\mu_\mu + \frac{1}{3}u_\mu u_\nu T^{\mu\nu} - p = 0 \tag{6.4}$$

since the trace of $T^{\mu\nu}$ is equal to the rest mass of the particles and the ideal equation of state (6.1) is assumed. For the heat flow one obtains

$$q^\mu = u_\nu \Delta^\mu_\lambda T^{\nu\lambda} = u_\nu T^{\mu\nu} - e u^\mu = \int p_0 p^\mu f d\Gamma - e u^\mu\,. \tag{6.5}$$

Boost-invariance implies symmetry of the distribution $f(p_T, p_z) = f(p_T, -p_z)$, which means that the integral in Eq. (6.5) does not vanish only if $\mu = 0$. On the other hand for $\mu = 0$ both terms in (6.5) cancel, so that heat flow q^μ vanishes component-wise in a one-dimensional boost-invariant case.

In the local rest frame the energy-momentum tensor

$$T^{\mu\nu} = e u^\mu u^\nu - (e+p)\Delta^{\mu\nu} + \pi^{\mu\nu} \tag{6.6}$$

is diagonal and traceless for massless particles:

$$T^{\nu}_{\nu} = \int p_\nu p^\nu f(x,p) \mathrm{d}\Gamma = \int (p_0^2 - \vec{p}^{\,2}) f(x,p) \mathrm{d}\Gamma = 0 \tag{6.7}$$

and thus $\pi^{\mu\nu}$ has this property as well. Off-diagonal components of the energy-momentum tensor vanish due to the longitudinal symmetry $f(p_T, p_z) = f(p_T, -p_z)$ and transverse isotropy:

$$T_{\mathrm{ij,LRF}} = \int \frac{p_i p_j}{p_0} f(x,p) d^3p = 0, \quad i \neq j;\ i,j = 0,1,2,3\,. \tag{6.8}$$

Thus the energy-momentum and the shear tensors take the form

$$T^{\mu\nu} = \begin{pmatrix} e & 0 & 0 & 0 \\ 0 & p + \frac{\pi}{2} & 0 & 0 \\ 0 & 0 & p + \frac{\pi}{2} & 0 \\ 0 & 0 & 0 & p - \pi \end{pmatrix} \tag{6.9}$$

$$\pi^{\mu\nu} = \begin{pmatrix} 0 & 0 & 0 & 0 \\ 0 & \frac{\pi}{2} & 0 & 0 \\ 0 & 0 & \frac{\pi}{2} & 0 \\ 0 & 0 & 0 & -\pi \end{pmatrix} \tag{6.10}$$

The fourth diagonal component of the shear tensor is negative and $\pi \geq 0$ denotes the shear pressure. For a one-dimensionally expanding system the *longitudinal pressure* $T_{33} = p - \pi$ is thus reduced due to dissipation whereas in transverse directions the effective pressure is enhanced.

Since the heat flow q^μ and the bulk pressure Π vanish for one-dimensional geometry and massless particles the expression for the off-equilibrium distribution function simplifies to

$$f = f_{eq} \big(1 + C_0 \pi_{\mu\nu} p^\mu p^\nu \big)\,. \tag{6.11}$$

Introducing the diagonal form of the shear tensor, Eq. (6.10), into the latter equation one finds for a boost-invariant expansion

$$f(\tau, p) = f_0(\tau, p) \left(1 + C_0(\tau) \pi(\tau) \big(p_z^2 - \frac{1}{2} p_T^2 \big) \right), \tag{6.12}$$

where $f_0(\tau, p)$ is the Boltzmann distribution

$$f_0(\tau, p) = g \lambda e^{-\frac{p_0}{T}} \tag{6.13}$$

with the fugacity λ and the degeneracy factor g.

The coefficient C_0 was already calculated for a general case in Appendix A. Alternatively, in the one-dimensional geometry chosen here C_0 can be obtained from the condition $T_{33} = T_{33}^{eq} - \pi$ according to Eq. (6.9):

$$T_{33} = \frac{16\lambda}{(2\pi)^3} \int e^{-p_0/T} p_z^2 \left(1 + C_0 \pi \big(p_z^2 - \frac{1}{2} p_T^2 \big) \right) \frac{d^3p}{p_0} \overset{!}{=} p - \pi\,, \tag{6.14}$$

where the degeneracy factor $g = 2(N_c^2 - 1)$ has been set to 16 for gluon gas with $N_c = 3$. For the coefficient C_0 one thus obtains

$$C_0 = \frac{3}{8eT^2}\,. \tag{6.15}$$

Although obtained using a one-dimensional geometry, this value of C_0 is universal for a gas of massless Boltzmann particles since it is consistent with the results obtained in Appendix A and Refs. [33, 83]. With the known factor C_0 the approximation for the one-dimensional form of the off-equilibrium distribution function, Eq. (6.12), is determined completely.

6.1. Thermodynamic coefficients β_2 and α

In order to give the one-dimensional form of second and third-oder hydrodynamic equations, (3.20) and (3.35), the thermodynamic coefficients β_2 and α need to be specified. Since they are purely thermodynamic functions, i.e. dependent only on e and T, their functional form does not depend on the symmetry of the system. One thus can choose a one-dimensional expanding system of Bjorken type to find the functional forms for β_2 and α[33]. The entropy current in Eq. (3.24) can be rewritten using the one-dimensional representation of the shear tensor, Eq. (6.10), as follows:

$$s^\mu = \left(s_0 - \frac{\beta_2}{T}\pi^2 + \frac{\alpha\beta_2^2}{T}\pi^3\right)u^\mu\,. \tag{6.16}$$

On the other hand the entropy density can be calculated using the kinetic theory approach. The kinetic definition of the entropy density [76]

$$s = u_\mu s^\mu = -\int u_\mu p^\mu f(\ln f - 1)\mathrm{d}\Gamma\,. \tag{6.17}$$

is based on Boltzmann's H-function. The distribution $f(x,p)$ in Eq. (6.17) is a off-equilibrium phase-space distribution and has been discussed for a one-dimensional boost-invariant expansion in the previous section. Writing Eq. (6.12) in a compact form

$$f = f_0(1+\phi)\,, \tag{6.18}$$

and introducing this compact form into Eq. (6.17) one obtains

$$s = -\int p_0 f_0\,(1+\phi)\,(\ln\left[f_0(1+\phi)\right] - 1)\,\mathrm{d}\Gamma\,. \tag{6.19}$$

The deviation from equilibrium, $\phi(x,p)$, is supposed to be small and thus the logarithm can be expanded up to *third* order in ϕ. Introducing $\phi = C_0\pi(p_z^2 - p_T^2)$ into Eq. (6.19) after expanding the logarithm, one obtains for the entropy density[33]

$$s \approx s_0 - \frac{27}{16}\frac{\pi^2}{eT} - \frac{27}{8}\frac{\pi^3}{e^2T}\,. \tag{6.20}$$

The equilibrium entropy s_0 in Eqs. (6.16) and (6.20) is given by

$$s_0 = 4n - n \ln \lambda \,. \tag{6.21}$$

Comparing the two equations, (6.16) and (6.20), one can identify the unknown thermodynamic coefficients

$$\beta_2 = \frac{9}{4e} \,, \tag{6.22}$$

$$\alpha = -\frac{8}{9} \,. \tag{6.23}$$

These coefficients are pure thermodynamic functions and thus do not depend on the symmetry properties of the considered system. The obtained expressions are consistent with calculation of the third-order entropy current from Grad's approximation for the distribution function in Appendix B.

6.2. Evolution equations for the energy and particle densities with particle number conservation.

The evolution equations for the particle and energy densities follow from the conservation laws Eqs. (2.43) and (2.44). At this point both source terms for particle production and energy-momentum deposition will be set to zero, i.e. I assume particle number conservation and energy conservation

$$\partial_\mu T^{\mu\nu} = 0 \,, \tag{6.24}$$

$$\partial_\mu N^\mu = 0 \,. \tag{6.25}$$

From the conservation of particle four-number via Eq. (6.2) then follows

$$u^\mu \partial_\mu n \equiv \dot{n} = -n \partial_\mu u^\mu \,. \tag{6.26}$$

The $\dot{x}$ notation denotes the co-moving derivative $u_\mu \partial^\mu$, i.e. derivative with respect to τ in the local rest frame. Energy conservation follows from Eqs. (2.44) or (6.25):

$$u_\nu \partial_\mu T^{\mu\nu} = 0 \,. \tag{6.27}$$

For a one-dimensional boost-invariant expansion, in absence of the heat flow and bulk pressure terms, via Eq. (6.3) one obtains

$$u^\mu \partial_\mu e \equiv \dot{e} = -(e+p) \Delta^{\mu\nu} \partial_\nu u^\mu + \pi^{\mu\nu} \partial_\nu u_\mu \,. \tag{6.28}$$

For the latter equation one uses the orthogonality property of the shear tensor $u_\mu \pi^{\mu\nu} = 0$ to eliminate its derivative from the equation.

Using the symmetry properties of the shear tensor, the ideal equation of state as well as the Bjorken flow velocity Eq. (5.9) one obtains from Eqs. (6.26) and (6.28)

$$\begin{aligned} \dot{n} &= -\frac{n}{\tau}\,, && (6.29)\\ \dot{e} &= -\frac{4}{3}\frac{e}{\tau} + \frac{\pi}{\tau}\,. && (6.30) \end{aligned}$$

From these two equations one easily deduces an evolution equation for the temperature

$$\dot{T} = -\frac{1}{3}\frac{T}{\tau} + \frac{1}{4}\frac{\pi T}{e\tau}\,. \tag{6.31}$$

Note that the evolution equation for the energy density does not *explicitly* depend on the details of microscopic processes considered in the system as long as these are energy-conserving, since Eq. (6.30) is obtained from the energy-momentum conservation equation (6.28). The particle production and annihilation will affect the evolution of e only *implicitly* via the shear viscosity coefficient η (comp. Eq. (4.8) and Refs. [42, 33]) which influences π via the corresponding evolution equation. Thus, Eq. (6.30) is applicable even if the particle number is not conserved. On the other hand, the particle density evolution will of course be explicitly affected by particle production and annihilation processes once these are considered in a consistent way.

6.3. Ideal hydrodynamics in Bjorken's model

Equations (6.29) and (6.30) constitute the local rest frame evolution equations for the particle and energy densities for a one-dimensionally expanding boost-invariant system of massless Boltzmann particles. Neglecting the shear pressure in Eq. (6.30) one obtains two independent ideal hydrodynamic equations, which are solved by

$$\begin{aligned} n &= n_0\frac{\tau_0}{\tau}\,, && (6.32)\\ e &= e_0\left(\frac{\tau_0}{\tau}\right)^{\frac{4}{3}}\,. && (6.33) \end{aligned}$$

One thus obtains for the effective temperature $T = \frac{e}{3n}$ of an ideal fluid

$$T = T_0\left(\frac{\tau_0}{\tau}\right)^{\frac{1}{3}}\,. \tag{6.34}$$

6.4. Dissipative hydrodynamics in Bjorken's model with conserved particle number

In order to solve Eq. (6.30) for a non-ideal fluid one needs a one-dimensional evolution equation for the shear pressure. The effect of dissipation is however qualitatively clear from Eq. (6.30) resp. (6.31). Since $\pi \geq 0$, the energy density and temperature decrease slower than in ideal case because the dissipated energy is turned into the inner energy of the system.

Evolution equations for π follow from Eqs. (3.13), (3.20) and (3.35). Introducing the symmetry properties of Bjorken flow into these equations and using the expressions for β_2 and α from Eqs. (6.22) and (6.23) one obtains first, second and third-order hydrodynamic equations for the shear pressure:

$$\text{first-order:} \quad \pi = \frac{4}{3}\frac{\eta}{\tau}\,, \tag{6.35}$$

$$\text{second-order:} \quad \dot{\pi} = -\frac{\pi}{\tau_\pi} - \frac{4}{3}\frac{\pi}{\tau} + \frac{8}{27}\frac{e}{\tau}\,, \tag{6.36}$$

$$\text{third-order:} \quad \dot{\pi} = -\frac{\pi}{\tau_\pi} - \frac{4}{3}\frac{\pi}{\tau} + \frac{8}{27}\frac{e}{\tau} - 3\frac{\pi^2}{e\tau}\,. \tag{6.37}$$

The power counting is based on the following considerations: both π/e and τ_π/τ have to be small to ensure validity of hydrodynamic approach. After multiplying the corresponding equation by τ_π/e on both sides, I consider terms of form $(\tau_\pi/\tau)^{q_1}(\pi/e)^{q_2}$ to be of q-th order. In an equation of q-th order terms of all higher orders are omitted. This kind of power-counting was applied in Ref. [34, 35].

For a system with conserved particle number, each of the equations (6.35) – (6.37) is coupled to the evolution equations for the particle and energy densities, Eqs. (6.29) and (6.30). A complete overview of first, second and third-order hydrodynamic equations for boost-invariant one-dimensional one-component systems of massless particles with particle number conservation is given in Appendix C.1.

7. Partonic cascade BAMPS

Mind moves matter.

Virgil (70 BCE – 19 BCE), Roman poet.

7.1. Numerical solution of Boltzmann Equation

The abbreviation BAMPS is for **B**oltzmann **A**pproach to **M**ulti**P**arton **S**cattering. This model was developed to solve the Boltzmann Equation

$$p^{\mu}\partial_{\mu}f(x,p) = C[f(x,p)] \tag{7.1}$$

in presence of both elastic and inelastic processes [30]. The Boltzmann Equation (7.1) describes evolution of the single parton phase-space distribution function $f(x,p) = \frac{dN}{d^3pd^3x}$. Its evolution is on the one hand governed by drift and diffusion – formally described by the left hand side of Eq. (7.1) – and on the other hand by change of the phase space distribution due to scattering processes – which is given by the collision term on the right hand side of Eq.(7.1). The collision term contains all the information about structure of the interaction processes. Since $f(x,p)$ is interpreted as a single particle distribution function, Eq. (7.1) is a semi-classical formulation of parton dynamics. The partons are treated as particles with classical trajectories. The single-particle distribution function averages over correlations in a many-parton wave function of a single nucleon.

BAMPS is one of the most recent transport models and ranks among a number of approaches dealing with numerical solution of the Boltzmann Equation. The cascade models ZPC [28, 121] and MPC [29] implemented parton dynamics with elastic scattering and a geometric interpretation of the cross section. In the MPC model a parton subdivision technique is introduced, which is necessary to preserve covariance. The VNI partonic cascade model [27] for the first time implemented parton emission and fusion processes calculated in the framework of perturbative QCD. Further models studying the evolution of a quark and gluonic gas with pQCD based cross sections are introduced in [122, 123]. In contrast to the already introduced models, UrQMD[77, 78] is a hadronic transport algorithm describing hadronic interactions in terms of interactions between known hadrons and their resonances.

As already mentioned before, BAMPS is a semi-classical approach. The partonic degrees of freedom are treated as independent point-like particles in 6 dimensional phase space $(\vec{x}, \vec{p})$. The interactions between particles are implemented in BAMPS using the *stochastic* interpretation of the collision rate [124, 125, 126, 31]. At any time step a particle can undergo a scattering process with a certain probability which is calculated for a given number of participating particles dynamically. Since the stochastic interpretation of the collision rates in principal allows particles to interact without regarding their relative distance, the space has to be discretized into small cells in order to avoid acausal interactions between remote regions.

BAMPS implements three types of processes: elastic $2 \to 2$ scattering, *bremsstrahlung* process $2 \to 3$ and its reverse channel $3 \to 2$. Implementation of the reverse bremsstrahlung channel is essential to maintain detailed balance. The collision probabilities are calculated for the $2 \to n$ processes by the expression

$$P_{2n} = v_{rel} \frac{\sigma_{2n}}{N_{test}} \frac{\Delta t}{\Delta^3 x}, \tag{7.2}$$

where $n = 2, 3$ and σ_{2n} is the cross section, v_{rel} the relative velocity of the two participant in initial state, Δt the intrinsic time step and $\Delta^3 x$ the volume of a cell in which the collision happens. N_{test} denotes the number of test particles. The method of test particles increases the number of particles in the system by factor N_{test}, so that the physical observables calculated by averaging over the ensemble of particles have to be rescaled accordingly. The relative velocity of two particle is calculated via

$$v_{rel} = \frac{s}{E_1 E_2} = \frac{E_1 E_2 - \vec{p}_1 \vec{p}_2}{E_1 E_2} \tag{7.3}$$

with the invariant mass of particle pair s. For the $3 \to 2$ processes which are implemented in BAMPS the collision probability is given by the expression

$$P_{32} = \frac{1}{8 E_1 E_2 E_3} \frac{I_{32}}{N_{test}^2} \frac{\Delta t}{(\Delta^3 x)^2}. \tag{7.4}$$

The expression I_{32} replaces the cross section which cannot be defined for a process with three particles in initial state.

In presence of multi-particle processes the collision term $C[f]$ in the Boltzmann equation can be written as

$$C[f] = C_{22}[f] + C_{23}[f]. \tag{7.5}$$

For elastic $2 \to 2$ processes the collision term is given for a one-component system by

$$\begin{aligned} C_{22} &= \frac{1}{2} \int \frac{d\Gamma_2}{2} \frac{1}{2} \int \frac{d\Gamma'_1}{2} \frac{d\Gamma'_2}{2} f'_1 f'_2 \times \\ &\times |M_{1'2' \to 12}|^2 (2\pi)^4 \delta^{(4)} \left(p'_1 + p'_2 - p_1 - p_2\right) - \\ &- \frac{1}{2} \int \frac{d\Gamma_2}{2} \frac{1}{2} \int \frac{d\Gamma'_1}{2} \frac{d\Gamma'_2}{2} f_1 f_2 \times \\ &\times |M_{12 \to 1'2'}|^2 (2\pi)^4 \delta^{(4)} \left(p_1 + p_2 - p'_1 - p'_2\right). \end{aligned} \tag{7.6}$$

For the inelastic processes the corresponding expression reads

$$\begin{aligned}
C_{23} &= \frac{1}{2}\frac{1}{2!}\int \frac{d\Gamma_2}{2}\frac{d\Gamma_3}{2}\frac{1}{2!}\int \frac{d\Gamma'_1}{2}\frac{d\Gamma'_2}{2} f'_1 f'_2 \times \\
&\times \ |M_{1'2'\to 123}|^2 (2\pi)^4 \delta^{(4)} \left(p'_1 + p'_2 - p_1 - p_2 - p_3\right) + \\
&+ \ \frac{1}{2}\int \frac{d\Gamma_2}{2}\frac{1}{3!}\int \frac{d\Gamma'_1}{2}\frac{d\Gamma'_2}{2}\frac{d\Gamma'_3}{2} f'_1 f'_2 f'_3 \times \\
&\times \ |M_{1'2'3'\to 12}|^2 (2\pi)^2 \left(p'_1 + p'_2 + p'_3 - p_1 - p_2\right) - \\
&- \ \frac{1}{2}\frac{1}{2!}\int \frac{d\Gamma_2}{2}\frac{d\Gamma_3}{2}\frac{1}{2!}\int \frac{d\Gamma'_1}{2}\frac{d\Gamma'_2}{2} f_1 f_2 f_3 \times \\
&\times \ |M_{123\to 1'2'}|^2 (2\pi)^2 \left(p_1 + p_2 + p_3 - p'_1 - p'_2\right) - \\
&- \ \frac{1}{2}\int \frac{d\Gamma_2}{2}\frac{1}{3!}\int \frac{d\Gamma'_1}{2}\frac{d\Gamma'_2}{2}\frac{d\Gamma'_3}{2} f_1 f_2 f'_3 \times \\
&\times \ |M_{12\to 1'2'3'}|^2 (2\pi)^2 \left(p_1 + p_2 - p'_1 - p'_2 - p'_3\right) \ . \qquad (7.7)
\end{aligned}$$

The prefactors 1/2! and 1/3! in front of the integrals in Eqs. (7.6) and (7.7) indicate that particles in the initial and final state are identical. The Boltzmann Equation (1.2) is a one-particle equation, and thus one particle can be considered distinguished. In Eqs. (7.6) and (7.7) this is the particle with the four-momentum p_1. For all other particles both in initial and final state all possible permutations must be considered, which is done by the introduced prefactors (comp. Refs. [30, 41, 127]). The explicit expressions for the collision term components contain the usual definitions for the total cross sections [76]

$$\sigma_{22} = \frac{1}{2s}\frac{1}{2}\int \frac{d\Gamma'_1}{2}\frac{d\Gamma'_2}{2} |M_{12\to 1'2'}|^2 (2\pi)^4 \delta^{(4)} \left(p_1 + p_2 - p'_1 - p'_2\right) \ , \qquad (7.8)$$

$$\sigma_{23} = \frac{1}{2s}\frac{1}{3!}\int \frac{d\Gamma'_1}{2}\frac{d\Gamma'_2}{2}\frac{d\Gamma'_3}{2} |M_{12\to 1'2'3'}|^2 (2\pi)^4 \delta^{(4)} \left(p_1 + p_2 - p'_1 - p'_2 - p'_3\right) \ . \qquad (7.9)$$

For the 3 → 2 process the expression corresponding to the cross section is I_{32} defined as follows

$$I_{32} = \frac{1}{2!}\int \frac{d\Gamma'_1}{2}\frac{d\Gamma'_2}{2} |M_{123\to 1'2'}|^2 (2\pi)^4 \delta^{(4)} \left(p_1 + p_2 + p_3 - p'_1 - p'_2\right) \ . \qquad (7.10)$$

The matrix elements $M_{n\to m}$ are in general momentum dependent and given by the underlying field theory. They will be defined later in this work for a perturbative QCD approach. In case of momentum-independent matrix elements, i.e. for isotropic 2 → 3 cross sections, I_{32} is related to σ_{23} by the expression

$$I_{32} = 192/g\pi^2 \sigma_{23} \, . \qquad (7.11)$$

In a case of momentum-dependent matrix elements, i.e. non-isotropic cross section, the integration in Eq.(7.10) is calculated in BAMPS using numerical integration techniques (comp. Ref. [30] for details).

7.2. Boost-invariant expansion in BAMPS.

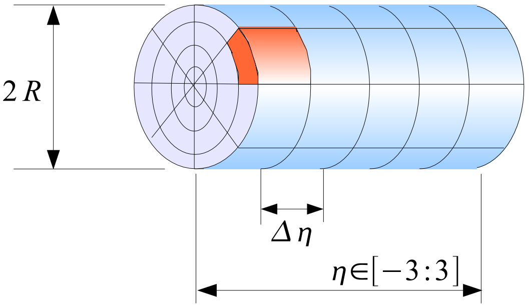

Figure 7.1.: Boost-invariant BAMPS box. In longitudinal direction the bin are constructed in rapidity space and have a fixed size $\Delta\eta$. All the cells have the same transverse area. Particles are reflected on a cylindric outer wall width fixed radius $R = 5fm$.

In this work BAMPS with a special geometry of the box, in which particles are confined, is used. The main focus of my work lies on investigation of hydrodynamic phenomena and comparisons with BAMPS for the case of boost-invariant expanding medium. The cells in the present BAMPS version are thus constructed not in the Cartesian coordinates (x, y, z) but in the coordinates (x, y, η). In longitudinal direction, which corresponds to the Cartesian z-axis the binning is done in terms of rapidity η: particles with rapidity $\eta \in [\bar{\eta} : \bar{\eta} + \Delta\eta]$ are found in a same bin of fixed size $\Delta\eta$. Rapidity interval $\eta \in [-3 : 3]$ is covered by initial sampling. In transverse direction the shape of the 'box' is circular with a *fixed* radius $R = 5fm$. The particles are reflected at the cylindric outer wall. In transverse direction the cells are constructed to have same transverse area. A schematic picture of this 'tube' geometry is given in Fig. 7.1.

Physical observables are calculated as average over an ensemble of particle in BAMPS in each cell (due to transverse isotropy in case of one-dimensional boost-invariant expansion the average can be built over all cells in a η-bin in order to suppress statistical fluctuations). The integration over the distribution function by four-momentum dependent weight $w(p)$ correspond to a discrete summation over the particles in a cell (bin):

$$\int d\Gamma \; w(p) f(x,p) \equiv \frac{1}{V_{cell}} \sum_{i}^{N_{cell}} \frac{w(p_i)}{E_i} \, . \tag{7.12}$$

If not stated otherwise the results presented in this work are extracted in the central rapidity bin $\eta \in [-0.1 : 0.1]$. Most results are obtained from simulations with a thermal initial condition

$$f(x,p) = \frac{g}{\pi^2} e^{-p_T \cdot \cosh y/T} \,. \tag{7.13}$$

7.3. Implementation of Leading Order pQCD processes in BAMPS

The stochastic interpretation of collision rates is a central feature of BAMPS. It allows to include both bremsstrahlung processes and the reverse process of gluon absorption in a consistent way. With geometrical interpretation of collision cross section a consistent implementation of the 3 → 2 process is not possible. Inclusion of both channels ensures that full detailed balance is maintained in the evolution. Implementation of leading-order (LO) pQCD processes in BAMPS is thus important to study chemical equilibration in a partonic matter as well as a number of further phenomena to be discussed later in this work.

For the differential cross section of pQCD elastic scattering among gluons BAMPS employs the expression [30, 128, 129]

$$\frac{d\sigma^{gg\to gg}}{dq_\perp^2} = \frac{9\pi\alpha_s}{(q_\perp^2 + m_D^2)^2} \,, \tag{7.14}$$

where $q_\perp^2$ is the transverse component of the momentum transfer in the center-of-mass frame of the colliding particles, α_s denotes the strong coupling constant. The total cross section is then obtained via

$$\sigma_{tot}^{gg\to gg} = \frac{1}{2}\int_0^{s/4} dq_\perp^2 \frac{d\sigma^{gg\to gg}}{dq_\perp^2} = \frac{9}{2}\frac{\pi\alpha_s^2}{m_D^2\left(1+4m_D^2/s\right)} \,. \tag{7.15}$$

The infrared divergence in the differential cross section is regularized by the effective screening mass m_D^2 [128] which is calculated in each cell dynamically in BAMPS via

$$m_D^2 = 16\pi\alpha_s \int d\Gamma N_c f(x,p) \tag{7.16}$$

with the choice of $N_c = 3$ for SU(3) of QCD throughout this work. The thus defined screening mass does not have a directional dependence, as it should be in general [130], but can rather be interpreted as an average over the transverse and the longitudinal screening masses.

The matrix elements for bremsstrahlung processes are of Gunion-Bertsch form[131, 128, 88]:

$$|M_{gg\to ggg}|^2 = \frac{9}{2}\frac{(4\pi\alpha_s^2)^2 \cdot s^2}{\left(q_\perp^2 + m_D^2\right)^2} \frac{48\pi\alpha_s^2 q_\perp^2}{k_\perp^2\left(\left(k_\perp - q_\perp\right)^2 + m_D^2\right)} \cdot \Theta\left(|k_\perp|\Lambda_g - \cosh y\right) \,. \tag{7.17}$$

The first part of the above expression is the already introduced differential cross section of elastic $gg \to gg$ process. The second part describes emission of one additional gluon with transverse momentum component $k_\perp$ and rapidity y in the center-of-mass frame of the two-body collision. In a dense partonic medium the radiation of an additional parton is suppressed by the Landau-Pomeranchuk-Migdal (LPM) effect[132], which reduces the bremsstrahlung cross section at high densities due to coherent interaction with scattering centers in the medium. Since the coherent effects cannot be taken into account within the semi-classical BAMPS approach, the LPM effect is accounted for by the Θ-function in Eq. (7.17). Inclusion of the Θ-function has the consequence that only independent processes (Bethe-Heitler regime) are considered in BAMPS. The formal treatment of the LPM effect is based on its following effective interpretation: the radiated gluon cannot scatter before its emission is completed. The emission (or formation) time of a gluon is typically given by $\tau \approx \frac{\cosh y}{k_\perp}$ and should be smaller than the mean free path in the medium Λ_g, leading to the requirement $\Lambda_g > \frac{\cosh y}{k_\perp}$. Such implementation of the LPM effect leads to a suppression of emission of soft (i.e. low $k_\perp$) gluons if mean free path Λ_g is large. Already from these qualitative arguments it becomes clear that inelastic processes will be important for isotropization of the momentum distribution, since large $k_\perp$ and thus large emission angles are preferred whereas small $k_\perp$ and angles are suppressed. In fact, this effect has been discussed in Refs. [41, 33] and will be addressed later in this work.

The strong coupling constant α_s is not dependent on the momentum transfer in present BAMPS calculations, i.e. the effect of *running coupling* (comp. Section 1.2) is not implemented. According to the recent experimental and theoretical estimates, as reviewed e.g. in Refs. [49, 133, 134], for a color glass condensate initial condition with $Q_s \sim 1-3$ GeV, which could apply for RHIC energies, the value of $\alpha_s(Q_s)$ is $0.25-0.5$. For studies of the elliptic flow and jet suppression in BAMPS [22, 135, 136] $\alpha_s = 0.3..0.6$ were applied.

7.4. Application of BAMPS to heavy-ion phenomenology

In this section I will review some of the applications of BAMPS to investigation of phenomena in relativistic heavy-ion collisions and briefly summarize the results of these studies. BAMPS is an appropriate tool to study off-equilibrium phenomena in a partonic medium. Since it solves the Boltzmann Equation exactly, deviations from equilibrium can be arbitrary large without exceeding the applicability limitations of the model. This is a major advantage of a kinetic transport model as compared to hydrodynamic models. The most interesting questions that can be addressed by BAMPS calculations are investigations of collective phenomena and dynamics of the equilibration processes in a QCD medium at weak coupling.

7.4.1. Thermalization of gluon matter in BAMPS

The issue of thermal and chemical equilibration of a quark-gluon plasma has been addressed in a number of studies, both analytic using relaxation time approximation [137, 138, 139, 128, 140] and numerical using Monte-Carlo techniques to solve the Boltzmann Equation in a cascade [27, 28, 29, 122, 123]. Thermalization process was also studied using analytic pQCD estimates of the collision rates, like e.g. in Refs. [141] and [142]. In BAMPS thermalization and onset of hydrodynamic behavior were studied in [30] using mini-jet initial conditions whereas thermalization of a color glass condensate (CGC) inspired initial configuration is investigated in [143, 32]. In the study reported in [32] the emphasis lies on detailed understanding of the thermalization mechanism and of the associated time scales. The question addressed there was whether the thermalization of the highly anisotropic, CGC inspired initial condition is well described by the 'bottom-up' scenario [142]. In this section I will summarize the review of 'bottom-up' scenario given in Ref. [32].

Color Glass Condensate was proposed as a possible state of hadrons at ultrarelativistic energies achieved in heavy ion collisions [70, 144]. The CGC calculation framework (see [145] and references therein) allows to calculate systematically n-point gluon correlation functions and their evolution with the momentum fraction x order by order in perturbation theory and thus gives access to understanding of the collective dynamics of QCD at high parton densities. The CGC formalism is embedded into the saturation scenario in which the density of partons per unit transverse area becomes very large at high energies leading to a saturation of partonic distributions due to unitarity constrains. When the saturation scale Q_s, which is given by the density of color sources per transverse area, becomes large compared to Λ_{QCD} the coupling constant $\alpha_S(Q_s)$ becomes weak and thus the high energy limit of QCD may be studied using weak coupling techniques. This way the behavior of the small x components of the hadronic wave function in QCD can be studied analytically in an effective theory which is the CGC.

The CGC initial condition used in BAMPS simulations consists of gluons with $p_T < Q_s$, which are produced by the non-perturbative part of the nucleus-nucleus interaction. The saturation momentum Q_s is the typical momentum of gluons in the CGC. It is close to 2 GeV at RHIC and is expected to be $4-6$ GeV at LHC [71, 146]. The Color Glass Condensate is a state with high parton occupation number where the transverse momenta reach up to Q_s, whereas the occupation number drops to 0 for transverse momenta much larger than Q_s. Initially, most gluons have transverse momenta close to Q_s, whereas the longitudinal momentum of gluons in the central rapidity bin is approximately zero.

As a possible scenario of thermalization of the CGC initial condition the "Bottom-Up" scenario was proposed [142]. According to this scenario the thermalization process goes through three stages. The first stage, $Q_s^{-1} \ll t \ll Q_s^{-1}\alpha_s^{-3/2}$, is dominated by hard gluons, i.e. gluons with transverse momenta $p_T \sim Q_s$, as is characteristic for the CGC initial state. The second stage, $Q_s^{-1}\alpha_s^{-3/2} \ll t \ll Q_s^{-1}\alpha_s^{-5/2}$, is the stage where soft gluons ($p_T \sim \alpha_s Q_s$) are produced in inelastic collisions. In the "Bottom-Up" picture the production of hard gluons is suppressed by the Landau-Pomeranchuk effect, discussed in Section 7.3. The multiplicity of soft gluons increases. The soft gluons thermalize among themselves and build up a thermal bath. In the third stage, $Q_s^{-1}\alpha_s^{-5/2} \ll t \ll Q_s^{-1}\alpha_s^{-13/2}$ the initially present hard gluons lose their energy to the thermal bath of soft particles and thus thermalize as well. The parametric estimate of the thermalization time scale in "Bottom-Up" scenario is $\tau_{th} \sim Q_s^{-1}\alpha_s^{-13/2}$. In this Section the thermalization process in BAMPS will be reviewed and the findings will be contrasted with "Bottom-Up" predictions.

For the initial gluon distribution of CGC we employ an idealized and boost-invariant form [147]

$$f(x,p) = \frac{c}{\alpha_s N_c}\frac{1}{\tau}\delta(y-\eta)\Theta(Q_s^2 - p_T^2)\,. \tag{7.18}$$

Because boost-invariance is assumed, the momentum and space-time rapidity are equal, i.e., $\eta = y$ for the initial gluons. $N_c = 3$ for SU(3) is used. The factor c in Eq. (7.18) is the "parton liberation coefficient" which accounts for the transformation of virtual partons in the initial state into on-shell partons in the final state, as introduced in [148]. SU(3) gauge theory calculations yield a value of $c \simeq 0.4$ [71, 146], which is employed for the following calculations. The initial particle density in the CGC approach is given by [147, 149, 150]

$$\frac{1}{\pi R^2}\frac{dN}{d\eta} = c\frac{N_c^2-1}{4\pi^2\alpha_s N_c}Q_s^2\,. \tag{7.19}$$

For the application of the Boltzmann equation, the phase space density has to be smaller than unity. If phase space density is high, Bose enhancement factors should be considered in the collision integrals, which is not done in BAMPS model.

The initial gluons are produced at proper time $\tau \sim \frac{1}{Q_s}$ and the initial phase space density $f(x,p)$ from Eq. (7.18) is infinite due to the delta function $\delta(p_z) \sim \frac{1}{\Delta p_z}$. Later the distribution in longitudinal momentum space broadens due to $2 \to 2$ (or $2 \to 3$) collisions and the occupation number becomes finite. BAMPS calculations start at time $\tau_0 = \frac{c}{\alpha_s N_c}\tau_i$ where $\tau_i \cong 1/Q_s$. At this time the parton distribution function in Eq. (7.18) is still larger than unity. The same initial time has been applied in [147]. In the "Bottom-Up" picture at a time $\tau \sim \alpha_s^{-3/2}Q_s^{-1}$ the distribution should become less than 1. One has to note that the Bose enhancement factor $(1+f)$ is not employed within the Boltzmann collision terms in BAMPS. Hence, as long as f is larger than 1 the collision rates are underestimated.

In the following the results of simulations for $Q_s = 3$ and $\alpha_s = 0.3$ are presented. A more detailed analysis can be found in [32]. The thermalization process is best illustrated by the time evolution of the normalized particle distribution in transverse momentum plane

$$\frac{dN}{N p_T dp_t} = \int p_0 f\, dy\, d\varphi\,. \tag{7.20}$$

The initial CGC distribution given by Eq. (7.18) is highly anisotropic. At early times the initially empty hard part of the spectrum ($p_T > Q_s$) is filled up with gluons. This is demonstrated in Fig.7.2 for BAMPS calculations with the initial time $\tau_0 = 0.04$ fm/c . From Fig.7.2 one observes that the spectrum of high momentum gluons achieves a nearly-exponential shape on a short time scale and almost as quick as the soft gluons. However, they have different slopes. At $\tau = 0.5$ fm/c the entire spectrum is to a good extent in agreement with a thermal fit using f_{eq} from Eq. (6.13) in Eq. (7.20) with $T \simeq 0.67$ GeV , which is indeed very close to the effective temperature of the system at this time [$T_{\text{eff}}(\tau = 0.5 \text{ fm/c}) = E/3N = 0.6$ GeV]. The transverse momentum spectrum achieves a thermal shape in hard and soft regions almost simultaneously. The subsequent

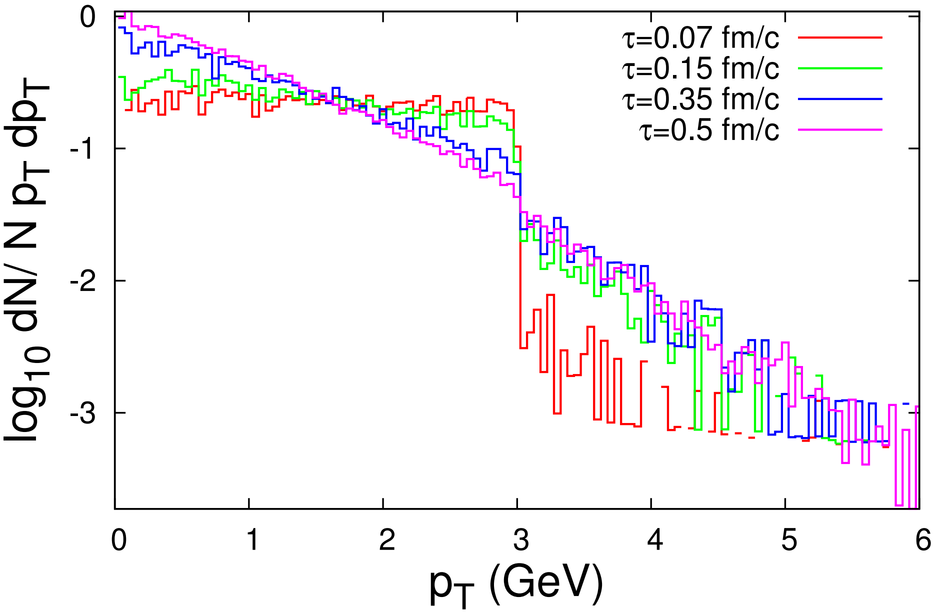

Figure 7.2.: Transverse momentum spectra in the central space time rapidity and at various *early* times. The initial condition for the BAMPS calculation is a CGC with $\alpha_s = 0.3$ and $Q_s = 3$ GeV.

time evolution of the transverse momentum distributions is shown in Fig. 7.3. At late times ($\tau > 0.5$ fm/c) the spectra are very good approximated by a thermal distribution, however the values of temperature which have to be chosen for the fit are slightly larger than the actual temperature of the system. This is explained by the fact that the system is still not completely equilibrated and the distribution function is better approximated by Grad's expression Eq. (6.12) rather than by the Boltzmann distribution. A higher temperature has to be chosen if off-equilibrium contribution to the distribution function is neglected.

The ratio of the numbers of the soft, medium and hard gluons to the total number of gluons is depicted in Fig. 7.4. The total gluon number is dominated by the medium sector until 0.5 fm/c and then by the soft sector after $\sim$ 1 fm/c. Contrary to the "Bottom-Up" picture, Fig. 7.4 shows that the soft gluon number increases over a long period of time at the cost of the primary "medium" gluons ($p_T \approx Q_s$). The production of soft gluons is effectively hindered by $3 \to 2$ processes and, thus, cannot exhibit a huge increase as predicted in the "Bottom-Up" scenario. The presence of a thermal bath of soft gluons seems not to be a necessary condition for the equilibration of hard gluons. The hard gluons produced in inelastic $3 \to 2$ collisions at early times are close to thermal distribution which underlines the importance of inelastic processes for kinetic equilibration in BAMPS. This leads, as discussed in Ref. [32] in more detail, to a faster

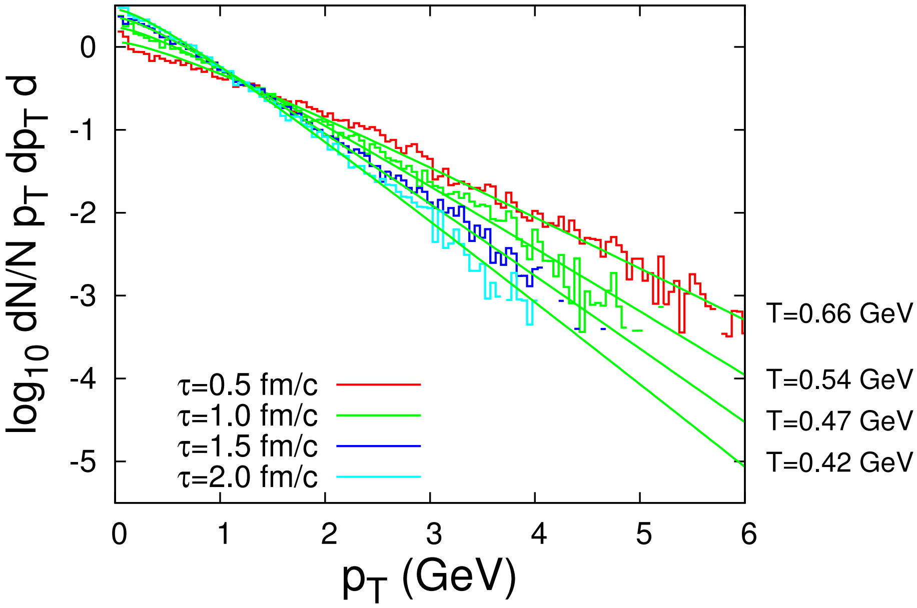

Figure 7.3.: Same as Fig.7.2 for later times.

thermalization than in ”Bottom-Up” picture.

The study presented in this Chapter demonstrates qualitatively how equilibration of an extremely anisotropic initial distribution is achieved in BAMPS. The role of inelastic collision processes will be quantified in the following in this work.

7.4.2. Jet suppression.

Studies of jet quenching in BAMPS simulations of $Au + Au$ collisions at RHIC were performed and reported by FOCHLER et. al. in Refs. [22, 135]. In BAMPS simulations the jet is represented by a high energetic gluon traversing the medium. Due to large energy scales involved, the energy loss of a jet can be studied by means of perturbative QCD, which is implemented in BAMPS. With the mini-jet initial conditions and applying free-streaming to model freeze-out in regions (cells) where the energy density drops below a critical value (gluon-hadron duality is used in BAMPS, i.e. one gluon correspond to one pion), the nuclear modification factor R_{AA} was found to be below the experimental results for neutral pions and charged hadrons for different centrality classes but at the same time in good agreement with other theoretical calculations for central collisions (c.f. Refs. [22, 135] for details). Studies of energy loss in a static medium in BAMPS demonstrated, that the pQCD bremsstrahlung process $gg \to ggg$ has a dominant contribution to the energy loss, leading to a large and linearly growing differential energy loss. The reason for this is the impact of LPM cut-off on momentum distribution of radiated particles. As

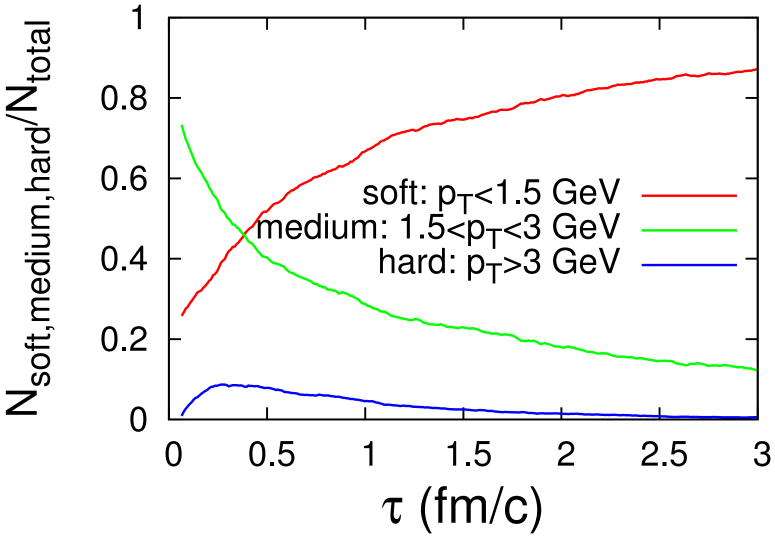

Figure 7.4.: Ratio of the numbers of the soft, medium and hard gluons to the total number.

already discussed in the previous Section, large-angle radiation is preferred if the LPM effect is taken into account via the Θ-function in the Gunion-Bertsch matrix elements (7.17). In addition, the influence of the particular implementation of the LPM cut-off was studied in more detail in Ref. [135].

7.4.3. Flow phenomena.

A major advantage of the kinetic transport model BAMPS is its ability to describe both low- and high-p_T regions of the spectrum, i.e. to provide a unified understanding of the bulk and jet properties of the QCD medium in perturbative coupling regime. Calculations of the elliptic flow v_2 with BAMPS were reported by Xu and Greiner in Ref. [136] for initial conditions which are a combination of the so-called 'mini-jets' scenario (for large momentum scale) and Glauber profile (for soft momentum scale). The results on integrated v_2 were found to be in good agreement with experimental data for the coupling regimes $\alpha_s = 0.3 \ldots 0.6$. For these calculations a simple picture of hadronization was employed, in which the gluons were turned into hadrons (pions) in a space region, where the energy density dropped below the specified critical value. In a further study of this problem the differential elliptic flow $v_2(p_T)$ was found to be slightly below the experimental data, which however could be corrected by a splitting (fragmentation) of a gluons into several hadrons (pions)[151] – a process which tends to increase average p_T of a particle. Whereas the elliptic flow calculations demonstrate a good agreement with experimental results, the nuclear modification factor $R_{AA}(p_T)$ is found to be below the data, although it was found to be sensitive to the details of implementation of the LPM effect in BAMPS. For both R_{AA} and v_2 the inelastic pQCD processes are important in order to reproduce the experimental results: implementation of only elastic processes leads to a significantly lower amount of suppression of jets and lower elliptic flow. These findings are consistent with the effect of inelastic processes on the η/s ratio calculated in Ref. [33, 42] and to be discussed in Chapter 9 of this work.

A very challenging task for dissipative hydrodynamic formalisms is solution of the Riemann problem. In the Riemann problem two fluids with different pressures are initially separated by a membrane. After the membrane is removed (in a *Gedankenexperiment* this can happen instantaneously), the matter is pushed from the region with higher pressure towards the lower pressure region. On the border of the regions a shock wave develops, which then propagates through the medium. This setup is connected with an infinitely large pressure gradient, which takes the existing numerical implementations of dissipative fluid dynamics formalisms to the limits of their applicability [85]. Evolution of shock waves in the afore-mentioned setup was investigated using the partonic model BAMPS [94]. This study demonstrated that BAMPS can be employed to investigate critical fluid dynamic phenomena, to which the Riemann problem and its variations [85] belong. BAMPS is able to reproduce ideal hydrodynamic solutions with high accuracy and at the same time to produce solutions of viscous hydrodynamic problems, which for the first time demonstrated that numerical solutions of relativistic kinetic transport theory can be regarded as benchmark for relativistic hydrodynamic calculations. Existence of shock waves in relativistic medium means that Mach Cone structures can be observed as well. Mach Cones are reaction of the medium to propagation of a super sonic object, like the jets in a quark-gluon plasma, and their surface is a shock front. Thus propagation of Mach Cones in a partonic medium with finite shear viscosity can also be studied using BAMPS. So far systematic fluid dynamic studies of Mach Cones were only within ideal hydrodynamic formalism [152].

8. Off-equilibrium distribution function in BAMPS.

In this section I evaluate with what accuracy Grad's approximation of the distribution function can reproduced the off-equilibrium distribution extracted from BAMPS calculations. Such comparison is in particular important in order to understand whether the derivations of hydrodynamic equations are based on correct assumptions, since the approximate form of the off-equilibrium distribution function is crucial for the derivations presented in Chapters 3.1.2 – 3.1.4.

The effect of viscous corrections to the distribution function on experimentally accessible observables like v_2, HBT radii and particle multiplicities has been investigated in Ref. [61]. There it is demonstrated that viscous corrections play an essential role already at $p_T \sim 1$ GeV even at small viscosity to entropy density ratio. The differential $v_2(p_T)$ is significantly suppressed, longitudinal pressure and HBT radius are reduced. There are as well significant corrections to particle multiplicities. Hence, it is important to evaluate the accuracy of the viscous corrections by a direct comparison of the analytic approximation with the kinetic transport results, as will be done here.

In one-dimensional boost-invariant geometry the off-equilibrium distribution of gluons is approximated by [comp. Eq. (6.12)]

$$f = 16\lambda e^{\frac{-p_T \cosh y}{T}} \left(1 + \frac{3}{8T^2} \frac{\pi}{e} p_T^2 \big(\frac{1}{2} - \sinh^2 y \big) \right) \tag{8.1}$$

The quality of this approximation is to be investigated in this chapter by comparing the normalized transverse particle distributions

$$\frac{dN}{N p_T dp_t} = \int p_0 f dy d\varphi \tag{8.2}$$

as calculated using Eq. (8.1) and by BAMPS.

8.1. Generic properties of Grad's approximation.

First it is interesting to discuss some generic properties of Grad's approximation. For this purpose I calculate the ratio of rapidity and angle averaged product $p_0 f_0 \phi$ and the rapidity and angle average of $p_0 f_0$: $\frac{\langle p_0 f_0 \phi \rangle_{y,\varphi}}{\langle p_0 f_0 \rangle_{y,\varphi}}$. This ratio quantifies the deviation of the off-equilibrium distribution given by Grad's approximation from equilibrium. If the ratio

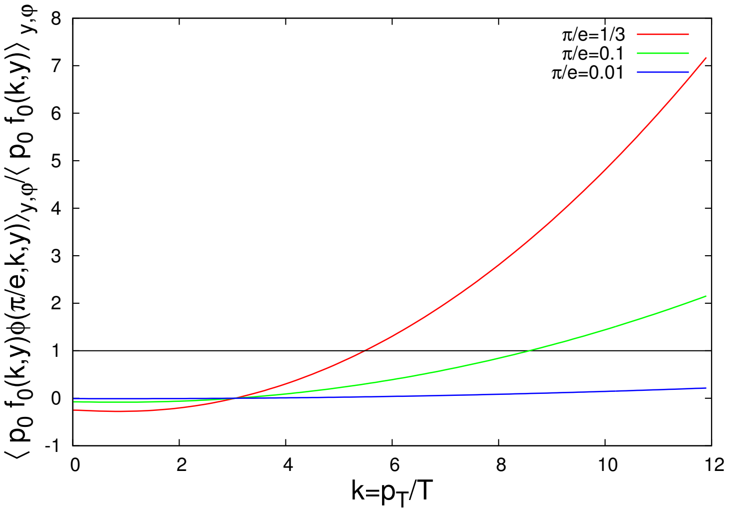

Figure 8.1.: Ratio of rapidity and angle average of the deviation function $f_0(y, p_T/T)\phi(\pi/e, y, p_T/T)$ to the rapidity and angle average of the equilibrium distribution function $f_0(y, p_T/T)$ by weight p_0 as function of p_T/T. Results are shown for different values of π/e.

is larger than 1, the deviation ϕ is too large and the expansion underlying Eq. (2.27) is not valid. Thus the criterion of validity of Grad's approach I investigate here is

$$\delta_{eq} = \frac{\langle p_0 f_0 \phi \rangle_{y,\varphi}}{\langle p_0 f_0 \rangle_{y,\varphi}} \ll 1. \tag{8.3}$$

For a one-dimensional problem with transverse isotropy the average over rapidity and angle yields the transverse distribution, $\frac{dN}{N p_T dp_t} = \langle p_0 f \rangle_{y,\varphi}$. Grad's ansatz for ϕ contains a $\frac{\pi}{e}$ dependence. For this study the value of $\frac{\pi}{e}$ is a free parameter. However its natural range for a system evolving toward kinetic equilibrium should be $0 \leq \frac{\pi}{e} \leq \frac{1}{3}$. The lower value describes a kinetically equilibrated system. The upper value guarantees that the effective pressure $p_{eff} = T_{33} = p - \pi = \frac{e}{3} - \pi$ is non-negative for a free evolving system. If the initial condition is such that $p_{eff} < 0$, one can expect that p_{eff} will become positive and relax to 0 after a certain time. In fact the phenomenon of negative effective pressure has been discussed in Ref. [153] as a possible criterion for evaluation of applicability limits of hydrodynamic description in heavy-ion systems. More discussion on evolution of the effective pressure in viscous one-dimensional systems will follow later in this work. In Fig. 8.1 the ratio is shown for $\frac{\pi}{e} = 0.01,\ 0.1,\ \frac{1}{3}$.

Figure 8.1 demonstrates that Grad's approximation fails for transverse momenta $p_T \gtrsim 5T$ if dissipation is strong. This failure is a generic property of Grad's approximation in the geometry considered here. For a partonic system the lower bound for the effective temperature is the phase transition temperature, i.e. roughly $T \gtrsim 0.2$ GeV. For the upper limit I will use an estimate based on the simple Color Glass Condensate model which was used in Ref. [149, 150, 32, 147]. For LHC conditions the simple CGC estimate is $T \lesssim 0.7$ GeV. Thus the break down of Grad's approximation is associated in a partonic system with the transverse momentum scale $p_T \sim 1-3$ GeV. This value increases with decreasing strength of dissipative effects, as Fig. 8.1 demonstrates for $\pi/e = 0.1$. In Fig. 8.1 the transition from $\pi/e = 1/3$ to $\pi/e = 0.01$ demonstrates the evolution of the deviations with ongoing thermalization of the system. With $\pi/e = 1/3$ the soft sector ($p_T \lesssim 2T$) is not thermal, the deviation of the distribution is around 20% but is considerably reduced with $\pi/e = 0.1$.

From the discussion of Fig. 8.1 one can draw a general conclusion that an evolution equation for the shear pressure π, or alternatively π/e, derived using Eq. (2.27) as demonstrated in Sections 3.1.3 – 3.1.4, will fail to describe dynamics of the system on all scales. Indeed, a transverse momentum scale p_T can be associated with a length scale $\lambda \sim 1/p_T$. The evolution equation for shear pressure has an intrinsic time scale τ_π, which is interpreted as a relaxation time, as discussed in Section 3.1.3. Since hydrodynamics is a macroscopic theory, the relaxation time is momentum independent. It is thus natural that a relaxation-type equation cannot describe dynamics on scales which are smaller than the intrinsic relaxation time, which applies to the hard part of the p_T spectrum.

8.2. Deviations of transverse particle distributions in BAMPS from equilibrium.

In this section the distributions extracted from BAMPS simulations are compared to equilibrium distributions in order to obtain a qualitative understanding of the evolution towards equilibrium. For this study a BAMPS simulation with constant isotropic elastic cross section (i.e. angle independent differential cross section) is used:

$$\sigma_{22} = \frac{6}{5} r \frac{T}{s}. \tag{8.4}$$

where T is the temperature and s the entropy density. In the above expression r is a constant parameter. This particular parametrization is inspired by the expression for the shear viscosity coefficient derived in Ref. [76] (and used for instance in Ref. [46, 34]) for applications with Israel-Stewart theory. The parameter r is identical with the ratio $\frac{\eta}{s}$[46, 34]. For the study presented here $r = \eta/s = 0.4$ is taken. BAMPS is initialized with thermal initial condition. In the kinetic theory, for a gas of massless Boltzmann particles (gluons), the thermal distribution function is given by

$$f_{eq} = d_g \lambda e^{-\beta u_\mu p^\mu} = d_g \lambda e^{-\frac{E}{T}} = d_g \lambda e^{-p_T \cdot \cosh y/T} \tag{8.5}$$

with T and E denoting temperature and energy of the particle in the local rest frame of a fluid element with four-velocity u^μ. $d_g = 16$ is the gluon degeneracy factor considering 3 flavors. The initial time is $\tau_0 = 0.4$ fm/c and the initial temperature $T_0 = T(\tau_0) = 0.5$ GeV. The system is initialized in chemical equilibrium, $\lambda(\tau_0) = 1$.

The initially equilibrated system evolves off-equilibrium due to the initial expansion and then starts relaxing towards equilibrium again. Throughout the evolution the temperature is decreasing which leads to a continuous "steepening" of the transverse spectrum.

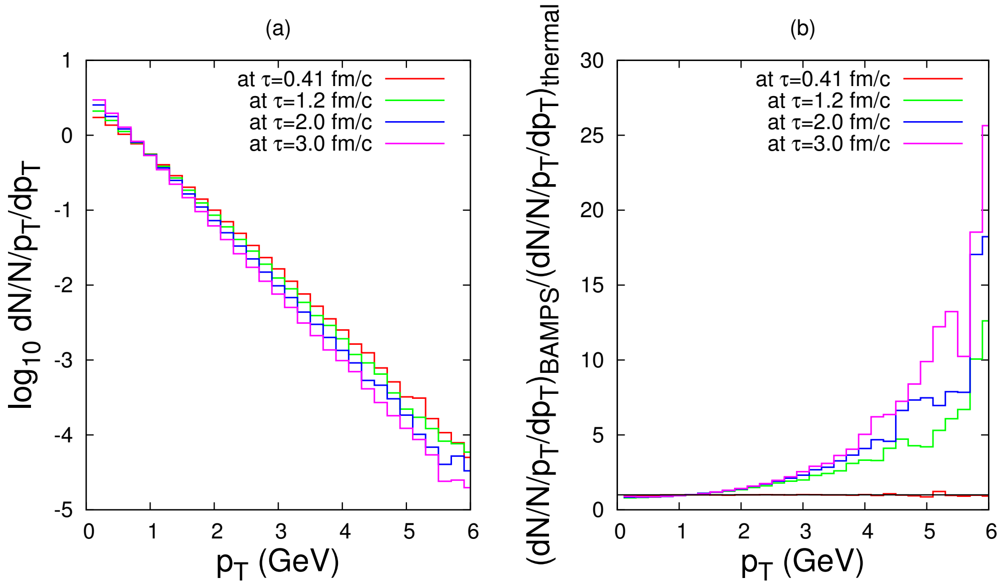

Figure 8.2.: Transverse spectra from BAMPS simulations at different times with initial thermal condition $\tau_0 = 0.4$ fm/c, $T_0 = 0.5$ GeV (a) and the relative deviation of BAMPS distribution from equilibrium calculated by Eq.(8.6) (b). Results are obtained with $r = \eta/s = 0.4$.

In Fig. 8.2(a) the transverse spectra from BAMPS at different times are depicted. The behavior observed here is analogous to the behavior discussed in section 7.4.1 around Fig. 7.3. The spectra in Fig. 8.2(a) can in principle be fitted by a thermal distribution using an effective temperature which is larger than the actual temperature of the system. However a thermal fit using the actual temperature is not possible. In Fig. 8.2(b) the ratio

$$\delta_{eq}^{BAMPS} = \frac{(dN/N/p_T/dp_T)_{BAMPS}}{(dN/N/p_T/dp_T)_{thermal}} = \frac{\langle p_0 f_{BAMPS}\rangle_{y,\varphi}}{\langle p_0 f_0\rangle_{y,\varphi}} \tag{8.6}$$

is plotted. An analogous ratio has been already defined in Eq. (8.3). For the analysis in Fig. 8.2(b) the numerator is calculated in BAMPS using the actual particle distribution. The denominator of Eq.(8.6) is calculated using Eq. (8.5) with effective temperature T and fugacity λ extracted from the same BAMPS calculation. Fig. 8.2(b) thus demonstrates the relative deviation of the particle distribution in BAMPS from equilibrium. Even at late times ($\tau = 3$ fm/c) the distribution is far from being thermal at high momenta. The time evolution of the deviation δ_{eq}^{BAMPS} at different momentum scales is shown in Fig. 8.3. At the soft momentum scale, $p_T = 0.4$ GeV, the ongoing thermalization can be observed as the deviation δ_{eq}^{BAMPS} starts relaxing towards 1 after going through a minimum. At larger momentum scales $p_T = 2,\ 4$ GeV the deviation growth with time. At this scales kinetic equilibration can be achieved only on a very long time scale exceeding the life span of the partonic medium in heavy-ion collisions.

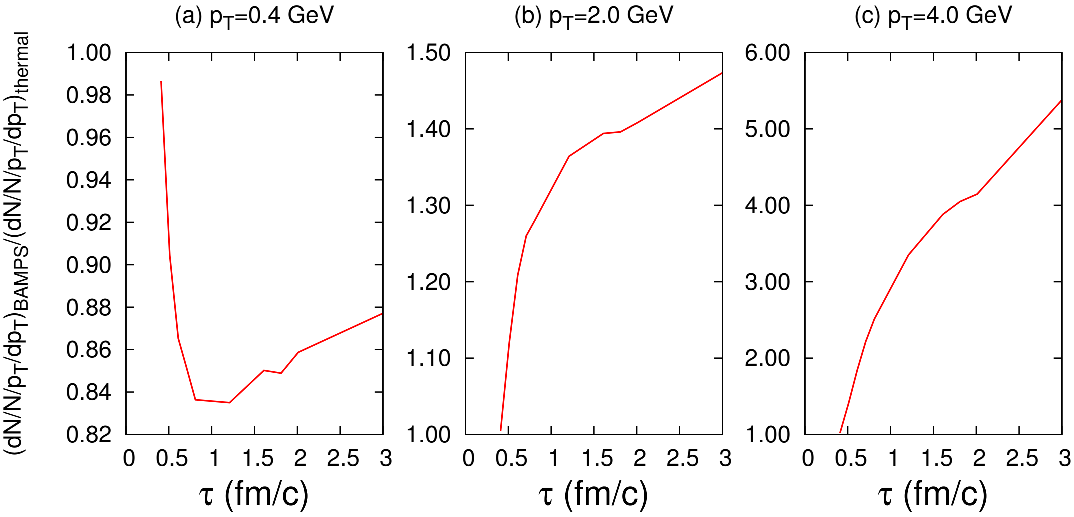

Figure 8.3.: Relative deviation of BAMPS distribution from equilibrium calculated by Eq.(8.6) at different values of p_T. Results are obtained with $r = \eta/s = 0.4$.

8.3. Deviations of transverse particle distributions in BAMPS from Grad's approximation.

In this section I address the question how accurate Grad's approximation describes off-equilibrium distributions in BAMPS. The differences between the BAMPS and thermal distributions observed in Fig. 8.2(b) underline the necessity of dissipative corrections to f_{eq}. These corrections are introduced in the Grad's approximation, as discussed in Section 2.4.1. The one-dimensional form of Grad's approximation is given by Eq. (8.1) earlier in this chapter. For the quantitative comparisons of Grad's approximation with BAMPS the thermodynamic quantities π, λ, e and T in Eq. (8.1) are extracted from BAMPS. In particular, the shear pressure π is extracted using

$$\pi = T_{33}^{eq} - T_{33}^{BAMPS} = p - T_{33}^{BAMPS} = \frac{e}{3} - T_{33}^{BAMPS}.$$

Fig. 8.4 demonstrates the transverse spectra from BAMPS compared to the ones calculated by Grad's approximation using Eq. (8.1) and BAMPS data. Clearly Grad's approximation fails to describe the high momentum region ($p_T \gtrsim 4$ GeV) of the spectrum at late times $\tau > 2$ fm/c. In order to quantify and understand the deviations observed at high momentum we introduce in Fig. 8.5(a) the ratio δ_{Grad}^{BAMPS} calculated as follows

$$\delta_{Grad}^{BAMPS} = \frac{(dN/N/p_T/dp_T)_{BAMPS}}{(dN/N/p_T/dp_T)_{Grad}} = \frac{\left\langle p_0 f_{BAMPS} \right\rangle_{y,\varphi}}{\left\langle p_0 16\lambda e^{\frac{-p_T \cosh y}{T}} \left(1 + \frac{3}{8T^2}\frac{\pi}{e} p_T^2 \left(\frac{1}{2} - \sinh^2 y\right)\right) \right\rangle_{y,\varphi}}. \tag{8.7}$$

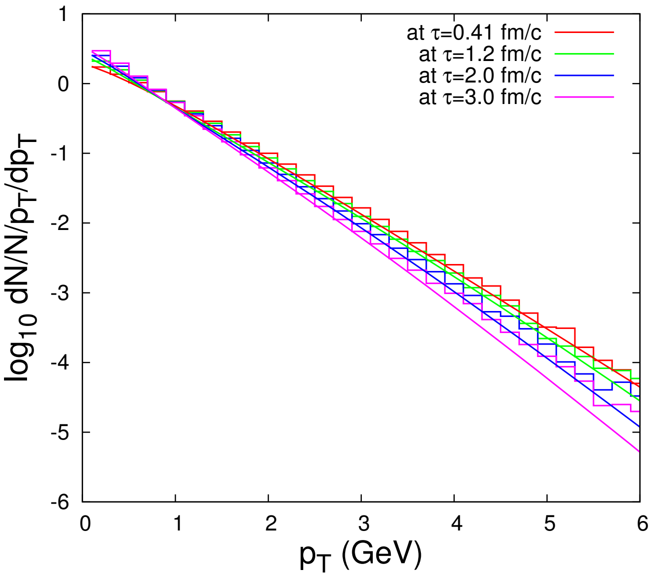

Figure 8.4.: Transverse spectra from BAMPS simulations at different times with initial thermal condition $\tau_0 = 0.4$ fm/c, $T_0 = 0.5$ GeV and the corresponding spectra from Grad's approximation. Results are obtained with $r = \eta/s = 0.4$.

In Fig. 8.5(a) we observe that the deviation between BAMPS and Grad's transverse distributions increases at high momentum at later times, however, comparing Fig. 8.5(a) and Fig. 8.2(b) one can conclude that it is considerably smaller than between BAMPS and thermal distribution at high momentum. The deviations at high momentum clearly indicate that this sector is far from complete thermalization whereas Grad's approximation is closer to a thermal distribution. Dissipative correction in Grad's approximation is proportional to the ratio $\frac{\pi}{e}$ (comp. Eq. (8.1)), which can be seen as a measure of overall degree of equilibration in the system. The time evolution of this ratio is shown in Fig. 8.5(b). As the system evolves the $\frac{\pi}{e}$ ratio reaches a maximum, indicating a strong deviation from equilibrium, and starts relaxing to 0 again. The value of $\frac{\pi}{e}$ is clearly dominated by the soft momentum sector of the spectrum since it contains the largest particle number. Hence a small $\frac{\pi}{e}$ indicates a high degree of equilibration of the soft sector, which dominates the overall multiplicity, but same is not true for hard momentum particles, which are still far from equilibrium. Thus, the correction in Grad's approximation is not large enough at high momentum since it is weighted by $\frac{\pi}{e}$. This explains the large deviations observed in Fig. 8.5(a).

Finally, in analogy to the study presented in Fig. 8.3, we can study time evolution of δ_{Grad}^{BAMPS} for a fixed value of p_T. This is presented in Fig. 8.6 for $p_T = 0.4$, 2 and 4 GeV. The conclusion that can be drawn from Fig. 8.6 is that Grad's approximation works remarkably good in the low momentum region and moreover provides a reasonably good

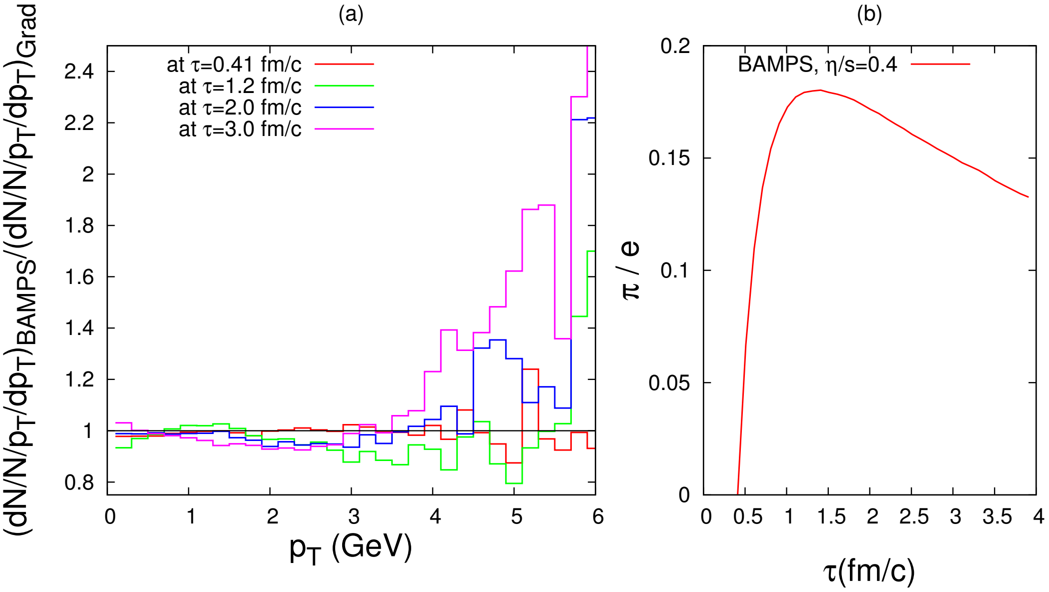

Figure 8.5.: (a) Ratio of transverse distribution from BAMPS simulations and the corresponding spectra from Grad's approximation and (b) the shear pressure to energy density ratio $\frac{\pi}{e}$ from same BAMPS simulation.

approximation of BAMPS distribution at intermediate $p_T = 2$ GeV, where the deviations are around 5% and large $p_T = 4$ GeV where the deviations are up to 20%. A fairly good agreement between BAMPS results and Grad's approximation even at high p_T is remarkable since Grad's approximation is known to become invalid at this momentum, as has been already discussed in section 8.1. To demonstrate the formal breakdown of Grad's approximation in the situation discussed here the ratio δ_{eq}^{Grad} as introduced in Eq. (8.3) is calculated using BAMPS data to reconstruct ϕ. The result is shown in Fig.8.7. Formally, Grad's approximation is not valid anymore at $p_T = 4$ GeV except at very early times since the (averaged) correction $\langle p_0 f_0 \phi \rangle_{y,\varphi}$ becomes larger than the corresponding average over the equilibrium function itself, $\langle p_0 f_0 \rangle_{y,\varphi}$. Nevertheless,Grad's approximation describes BAMPS distribution reasonably good at $p_T = 4$ GeV as Fig. 8.6(c) demonstrates.

Applicability of Grad's approximation for distribution function to kinetic transport results has been investigated in this Chapter using the transverse particle distributions. For this comparison BAMPS simulations with time dependent isotropic elastic cross section and constant particle number have been used corresponding to $\eta/s = 0.4$. Grad's approximation has been found to provide a good description of kinetic results for this moderately viscous system. For transverse momenta below 4 GeV the difference between BAMPS and Grad's approximation do not exceed 20%. Moreover, the agreement is still reasonably good in the momentum region where Grad's approximation formally becomes invalid ($p_T \sim 4$ GeV).

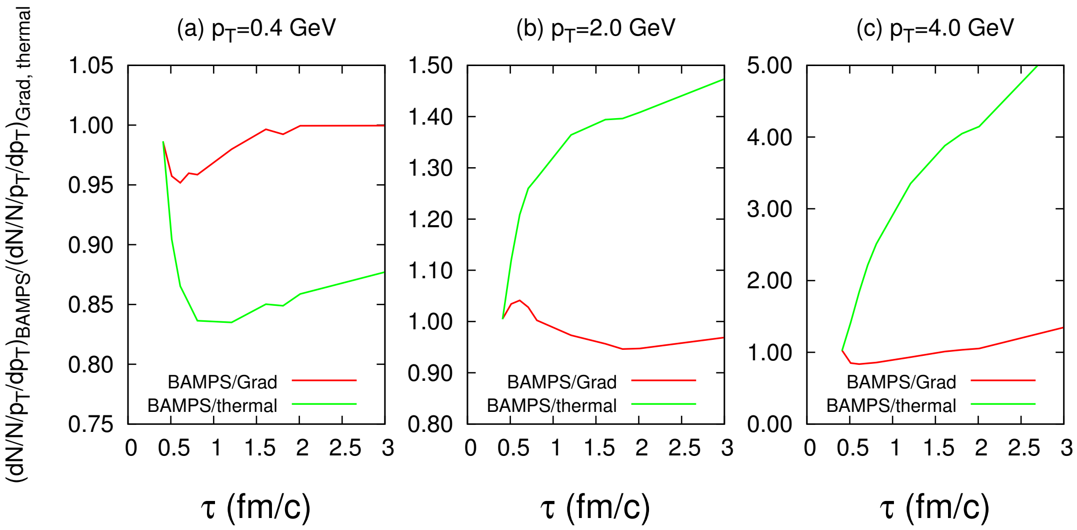

Figure 8.6.: Ratio of transverse distribution from BAMPS to the ones calculated by Grad's approximation and thermal distribution at different fixed values of p_T as function of time. Results are obtained with $r = \eta/s = 0.4$.

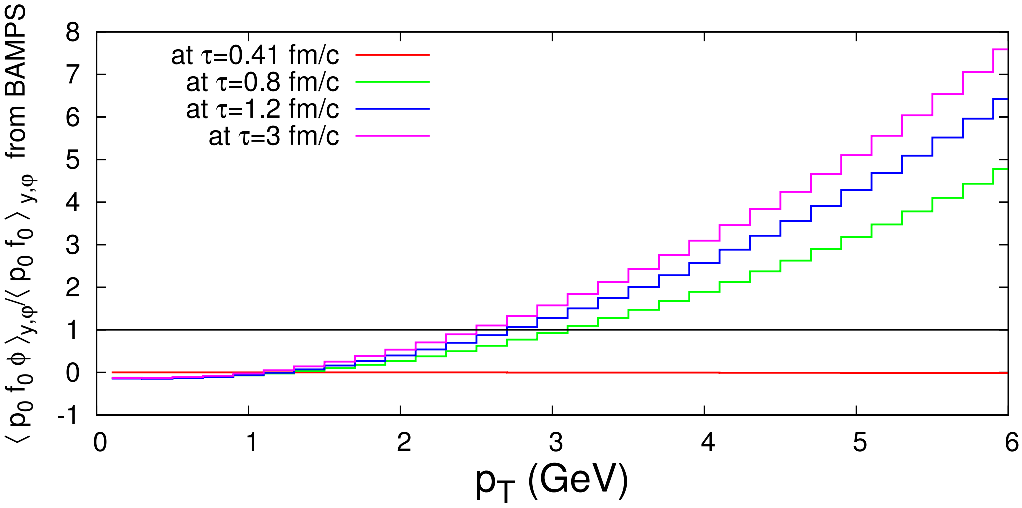

Figure 8.7.: Ratio of rapidity and angle average of the deviation function $f_0(y, p_T/T)\phi(\pi/e, y, p_T/T)$ to the rapidity and angle average of the equilibrium distribution function $f_0(y, p_T/T)$ by weight p_0 calculated using BAMPS data. Results are obtained with $r = \eta/s = 0.4$.

9. Shear viscosity of a pQCD interacting gluon gas.

In this Chapter, the formalism presented in Chapter 4.2.1 is applied to calculate the shear viscosity coefficient in a one-dimensionally expanding boost-invariant gluon gas. The interactions between the gluons are modelled using $2 \to 2$ and $2 \leftrightarrow 3$ leading order pQCD cross sections. The results presented here are obtained by two approaches, which both use the LO pQCD matrix elements as implemented in BAMPS and discussed in Chapter 7.3. Both approaches are dynamical and differ in the way the dynamics of the expansion is implemented.

9.1. Shear viscosity of a gluon gas from BAMPS.

I first present results on extraction of the shear viscosity coefficient from BAMPS calculations. The initial condition for these calculations is a kinetically and chemically equilibrated gluon gas, with the distribution given by the Boltzmann distribution (8.5) with $\lambda = 1$. The initial time τ_0 is chosen to be 0.4 fm/c and the initial temperature T_0 is 500 MeV for the results presented here.

The shear viscosity is calculated by Eq. (4.8). For a one dimensional system, if the third spatial coordinate is chosen as the expansion axis, in the local rest frame the shear tensor takes the form

$$\pi^{\mu\nu} = \begin{pmatrix} 0 & 0 & 0 & 0 \\ 0 & \frac{\pi}{2} & 0 & 0 \\ 0 & 0 & \frac{\pi}{2} & 0 \\ 0 & 0 & 0 & -\pi \end{pmatrix} \tag{9.1}$$

Due to the transverse isotropy, an inherent property of the boost invariant scenario considered here, and for a massless gas the $P^{\mu\nu}$ tensor, being the second moment of the collision term, is traceless and has a diagonal form with two degenerate components:

$$P^{\mu\nu} = \begin{pmatrix} P_{00} & 0 & 0 & 0 \\ 0 & \frac{1}{2}(P_{00} - P_{33}) & 0 & 0 \\ 0 & 0 & \frac{1}{2}(P_{00} - P_{33}) & 0 \\ 0 & 0 & 0 & P_{33} \end{pmatrix} \tag{9.2}$$

With the value of C_0 from Eqs. (6.15) resp. (A.31) the expression for shear viscosity reduces to

$$\eta = 4n \frac{-T^2 \pi}{P^{33} - \frac{1}{3} P^{00}} \,. \tag{9.3}$$

Figure 9.1 shows η/s extracted within the space time rapidity interval $\eta_s \in [-0.1:0.1]$, where $\eta_s = \frac{1}{2}\ln[(t+z)/(t-z)]$. The entropy density is calculated using the kinetic equilibrium expression $s = 4n - n\ln\lambda$. The three values of α_s shown in Fig. 9.1 demonstrate the transition between a weakly coupled and a strongly coupled gluon system. For $\alpha_s = 0.3$ and 0.6 the extracted η/s value is in a good approximation constant in time:

$$\begin{aligned}
\frac{\eta}{s} &\approx 0.08 \ (\alpha_s = 0.6) \\
\frac{\eta}{s} &\approx 0.17 \ (\alpha_s = 0.3) \\
\frac{\eta}{s} &\approx 2.6 \ - \ 3.2 \ (\alpha_s = 0.05)
\end{aligned} \tag{9.4}$$

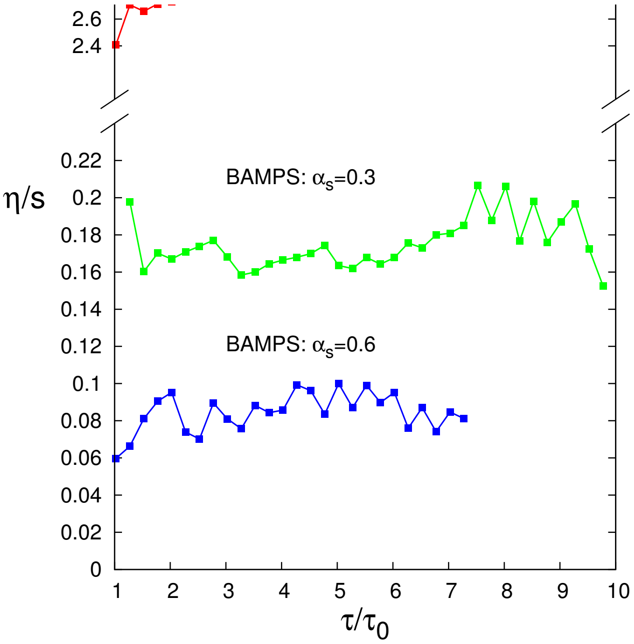

Figure 9.1.: Shear viscosity to entropy density ratio extracted from BAMPS using Eq. 9.3 and the kinetic equilibrium expression $s = 4n - n\ln\lambda$. BAMPS results are calculated with the initial conditions given by $\tau_0 = 0.4$ fm/c, $T_0 = 500$ MeV. Both elastic and inelastic pQCD processes are included with constant values of α_s.

For $\alpha_s = 0.6$, the obtained value is approximately 0.08 and thus very close to the conjecture bound for relativistic quantum field theories at finite temperature, $\eta/s = \frac{1}{4\pi}$ [154]. Thus, the results for $\alpha_s = 0.3$ and 0.6 indicate that the pQCD interacting gluonic matter behaves in BAMPS like a strongly coupled system. The fact that already at finite coupling within a perturbative QCD description BAMPS calculations yield a low, close to the lower bound, value of η/s ratio is the result of high efficiency of the inelastic $2 \leftrightarrow 3$ processes in driving the system to isotropy in the momentum space. For the first time this was discussed by XU and GREINER in Ref. [41] and investigated in various applications of BAMPS in Refs. [22, 135, 33, 42]. For instance in Refs. [22, 135] the energy loss of gluon jets in BAMPS is demonstrated to be larger if pQCD interactions are implemented in comparison with BAMPS simulations with only elastic processes with isotropic differential cross section. Comparable values of energy loss can be achieved if the isotropic elastic cross section is scaled by a considerable factor. In a pQCD interacting medium, the energy loss is found to be clearly dominated by radiative processes. Correspondingly, the nuclear modification factor R_{AA} is found to be small but comparable to recent calculations based on GLV formalism. Simultaneously, a sizable amount of elliptic flow can be observed in BAMPS simulations [135, 151, 136], which is not possible with elastic only processes [22]. The observed collectiveness in BAMPS simulations is consistent with the low values of η/s ratio, as obtained in this work and earlier publications [33, 42].

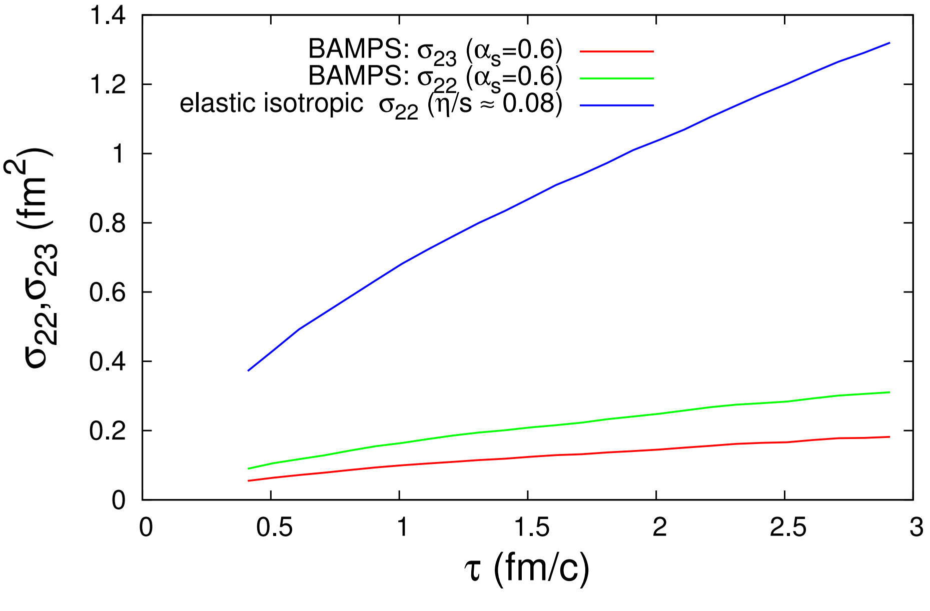

Figure 9.2.: PQCD cross sections, σ_{22} and σ_{23}, extracted from BAMPS simulations with $\alpha_s = 0.6$. The value of elastic isotropic cross section, corresponding to $\eta/s \approx 0.08$, which was extracted from BAMPS simulations, is calculated using BAMPS data.

The high efficiency of inelastic processes in BAMPS is demonstrated in Fig. 9.2, where the pQCD cross sections are extracted from BAMPS simulation with $\alpha_s = 0.6$. From this run the value $\eta/s \approx 0.08$ was extracted. On the other hand, Eq. (8.4) can be used to calculate an elastic isotropic cross section which would support this η/s value. The results of such calculation, for which actual temperature and particle density from BAMPS run are used, is demonstrated in Fig. 9.2 together with the values of pQCD cross sections. In order to obtain a medium with properties close to a strongly interacting system ($\eta/s \sim 1/(4\pi)$) with isotropic angle distribution, the elastic cross section has to be chosen almost factor 10 larger than the inelastic σ_{23} cross section in BAMPS. The reason for this is the angle distribution of the particles produced in inelastic $2 \to 3$ collisions. This distribution indicates that in BAMPS the large-angle radiation is favored [41, 135]. This increases the transport cross section[41], $\sigma^{tr} \sim \int \sin^2\theta \frac{d\sigma}{d\Omega}$, and thus essentially speeds up isotropization in momentum space. In our study of thermalization of the Color Glass Condensate initial conditions in BAMPS, presented in Chapter 7.4.1 and Refs. [143, 32], we found that thermalization of hard momentum sector proceeds on a short time scale, which is explained by the large angle dominance of radiated particle distributions. The conclusion, that a large value of elastic cross section is needed to describe the collective behavior observed in experiment by STAR was as well obtained by Molnar and Gyulassy in Ref. [155] from calculations of elliptic flow by kinetic transport model MPC [28, 29].

9.2. Shear viscosity to entropy density ratio as function of α_s.

In this Section the shear viscosity to the entropy density ratio η/s is calculated for a gluonic system, which undergoes a one-dimensional expansion with Bjorken boost invariance, i.e., a (0+1) dimensional expansion. In contrast to the results presented in Section 9.1, BAMPS will not be employed for calculations presented here. Instead, an iterative and self-consistent prescription to calculate the η/s ratio using Grad's approximation for the distribution function, second-order hydrodynamic equations and LO pQCD matrix elements will be introduced. This prescription was reported in Ref. [33].

In Sections 4.2.1 and 9.1 the expression for the shear viscosity coefficient was derived using Grad's approximation for the distribution function, Eqs. (2.42) resp. (8.1). The obtained expression, as given for a one dimensional system of massless gluons by Eq. (9.3), depends on macroscopic observables π, e, n and on the moments of the collision term P_{00} and P_{33}. Since the collision term itself, Eqs. (7.6) and (7.7), is a (complicated) functional of the distribution function, it as well depends on π, e, n if the distribution function is replaced by Grad's approximation. Thus, once the values of π, e, n are known and the matrix elements, entering the collision term are given, the shear viscosity coefficient can be calculated using Eq. (9.3). In the previous Section the time evolution of the macroscopic quantities π, e and n was obtained from BAMPS calculations. But since the derivation of Eq. (9.3) is based on Grad's approximation, for which compatibility with kinetic transport results is limited, as discussed in Section 8.2, it is a natural choice to obtain the time evolution of π, e and n from hydrodynamic equations and not from kinetic transport calculations. Derivation of second-order, Israel-Stewart equations was discussed in Section 3.1.3. For a one-dimensional system of massless Boltzmann particles they read (comp. Section 6)

$$\dot{n} = -\frac{n}{\tau} \tag{9.5}$$

$$\dot{e} = -\frac{4}{3}\frac{e}{\tau} + \frac{\pi}{\tau} \tag{9.6}$$

$$\dot{\pi} = -\frac{\pi}{\tau_\pi} - \frac{4}{3}\frac{\pi}{\tau} + \frac{8}{27}\frac{e}{\tau} \tag{9.7}$$

$$\tau_\pi = \frac{9\eta}{2e}$$

Evolution equation for shear pressure π depends explicitly on the shear viscosity coefficient η and is coupled to the evolution equation for the energy density. Thus the problem of calculation of η by Eq. (9.3) via Eqs. (9.5) – (9.7) and Grad's approximation becomes *iterative.*

Considering the self-iterative nature of the problem, the following algorithm is proposed:

1. Equations (9.5) – (9.7) are solved with a guessed value of η. The guessed value can be chosen arbitrarily because the final result does not depend on it. η/n is assumed to be a constant of time (i.e. the system is assumed to be close to chemical equilibrium).
2. The obtained $n(\tau)$, $e(\tau)$ and $\pi(\tau)$ at a time τ are used to calculate $\eta(\tau)$ according to (9.3). For doing so, first the moments P^{00} and P^{33} are calculated using $f(x,p)$ in Eq. (8.1) with given $n(\tau), e(\tau)$ and $\pi(\tau)$ and the cross sections in Eqs. (7.14), (7.9), (7.10) and (7.17).
3. Averaging over the η values calculated in several previous steps is done to obtain the actual $\eta(\tau)$. The algorithm turns back to step 1. The actual $\eta(\tau)$ is used to solve Eqs. (9.5) – (9.7).

In the second step of the iterative algorithm the collision term $C[f]$ is evaluated using the approximated distribution function, Eq. (8.1), according to which particles are sampled, and the matrix elements as implemented in BAMPS, which allow to simulate collision processes between pairs of sampled particles. The sampling according to Eq. (8.1) faces the problem, that the distribution function becomes negative at a certain value of p_T, as demonstrated in the discussion around Fig. 8.1. For p_T larger than the critical value, a cut-off is applied, i.e. no particles are sampled in this region. The critical momentum depends on actual values of π, e and T and is of order of 3 GeV for the situation considered here. But since the distribution function becomes small at this momentum, as BAMPS transverse spectra, Fig. 8.2, demonstrate, the effect of the cut-off is negligible.

The particle number is assumed to be constant in the algorithm presented here. Indeed, Eq. (9.5) is solved by $n(\tau) = n_0\tau_0/\tau$. Since the volume is proportional to τ, the

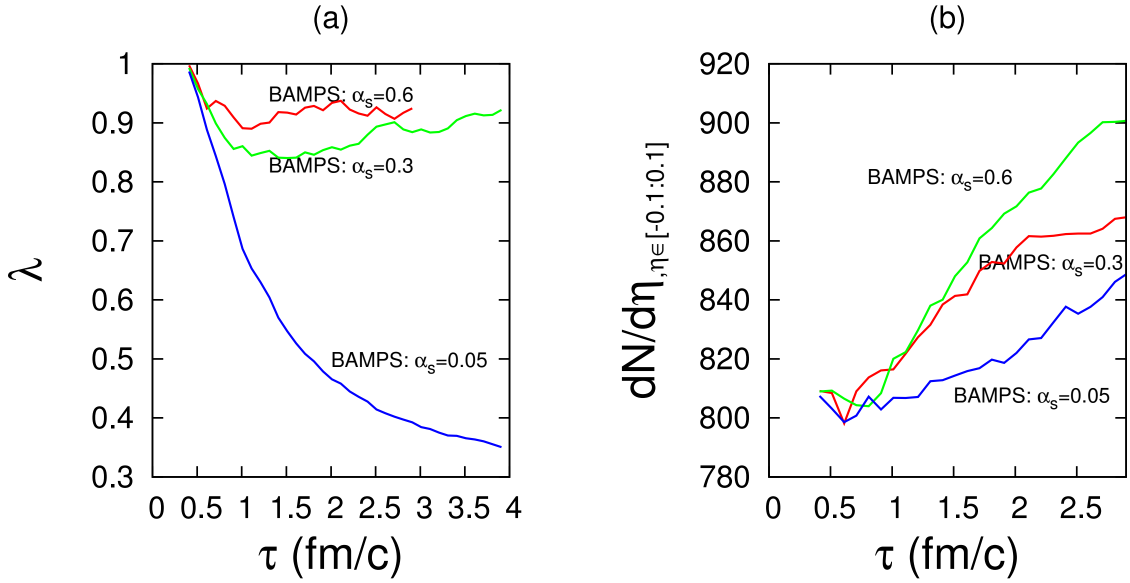

Figure 9.3.: Fugacity (a) and particle multiplicity (b) extracted from BAMPS simulations with different values of α_s.

particle number $N = nV \sim n_0\tau_0$ is constant. This assumption is not valid if one takes into account particle production and annihilation processes. In presence of particle number changing processes the initial expansion will drive the system off kinetic and chemical equilibrium. This can be illustrated by BAMPS calculations. In Fig. 9.3 the fugacity $\lambda = n/n_{eq}$ and the particle multiplicity in central rapidity bin from BAMPS simulations are demonstrated. Time evolution of the fugacity, Fig. 9.3(a) reflects the ongoing chemical equilibration in the system which is driven off equilibrium initially. The fugacity relaxes to 1 at strong coupling $\alpha_s \sim 0.3-0.6$). For $\alpha_s = 0.05$ the relaxation does not set in on time scale shown in the figure. The particle multiplicity increases due to ongoing particle production, which accompanies chemical and kinetic equilibration of the system.

BAMPS results presented in Fig. 9.3 demonstrate that the assumption of chemical equilibrium and constant particle number is in a certain approximation valid at very early times. Thus, the iterative calculation of η by the algorithm presented earlier has to be done at a early time point within proximity of the initial equilibrium state. The convergence of iterative calculations is demonstrated in Fig. 9.4, where the values of η/s calculated at each iteration step are shown. Calculations are performed at different time steps. At small coupling, $\alpha_s = 0.08$ the choice of the time point becomes important: at later time points the system is far from kinetic and chemical equilibrium; nevertheless, at each of the time points a fast convergence is observed.

Finally, η/s as function of α_s, as calculated by the iterative algorithm within proximity of initial equilibrium state, $\tau = 2\tau_0 = 0.8$ fm/c, is shown in Fig. 9.5. To demonstrate

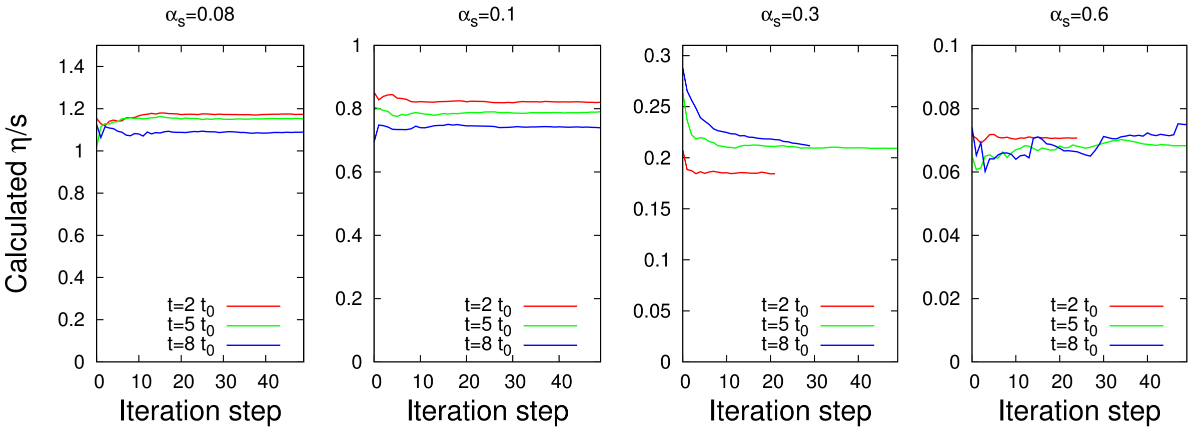

Figure 9.4.: Results of iterative calculations of η/s for different α_s and time steps.

the influence of the inelastic processes on η/s, its value is calculated iteratively both with and without taking into account inelastic processes. For the calculations with elastic, $2 \to 2$, pQCD processes only, the moments of the collision term in Eq. (9.3) are $P^{\mu\nu} = \int d\Gamma p^\mu p^\nu C_{22}[f_{Grad}]$. If both elastic and inelastic, $2 \leftrightarrow 3$, processes are considered, the moments are calculated according to $P^{\mu\nu} = \int d\Gamma p^\mu p^\nu \left(C_{22}[f_{Grad}] + C_{23}[f_{Grad}]\right)$. As demonstrated in Fig. 9.5, with elastic processes only, the η/s value is large – roughly by factor 7 compared to values obtained implementing both elastic and inelastic processes. Thus, elastic pQCD processes are clearly not efficient enough to support small η/s values close to the lower bound $1/(4\pi)$. Only if an isotropic angle distribution and large values of cross section are implemented, the η/s ratio can become low, as was already demonstrated in Fig. 9.2. This conclusion is consistent with the results on η/s in Ref. [115], where the obtained η/s ratio was shown to be much larger than $1/(4\pi)$ for elastic pQCD processes only. Note that at weak coupling, $\alpha_s \lesssim 0.05$, the dominance of $2 \leftrightarrow 3$ collisions becomes weaker; for small α_s the difference between $2 \to 2$ and full calculations becomes smaller. This is because at weak coupling the bremsstrahlung, $2 \to 3$, processes become collinear, i.e. small angle dominated[42, 156].

A similar approach to calculation of the shear viscosity coefficient was introduced in Ref. [42], though there are important conceptual differences between the formalisms presented there and the one discussed in this work. For the formalism in Ref. [42], the Navier-Stokes equation (3.13) was considered, which is a *first-order equation*, whereas the formalism presented here and in Ref. [33] is fully consistent with Israel and Stewart's *second-order* theory. Nevertheless, the expression obtained in Ref. [42] has a form similar to Eq. (4.8). The differences between this work and Ref. [42] are definitions of the moments of the collision term and a term $\propto \partial_t \ln \lambda$, which appears in the denominator of the expression in Ref. [42], but is missing in the formalism presented here. As Fig. 9.5 demonstrates, values calculated by present formalism are systematically larger than in Ref. [42] but converge with increasing α_s. At large α_s, the difference between second-order and Navier-Stokes based calculations is approximately 50% ($\alpha_s = 0.2$), 20% ($\alpha_s =$

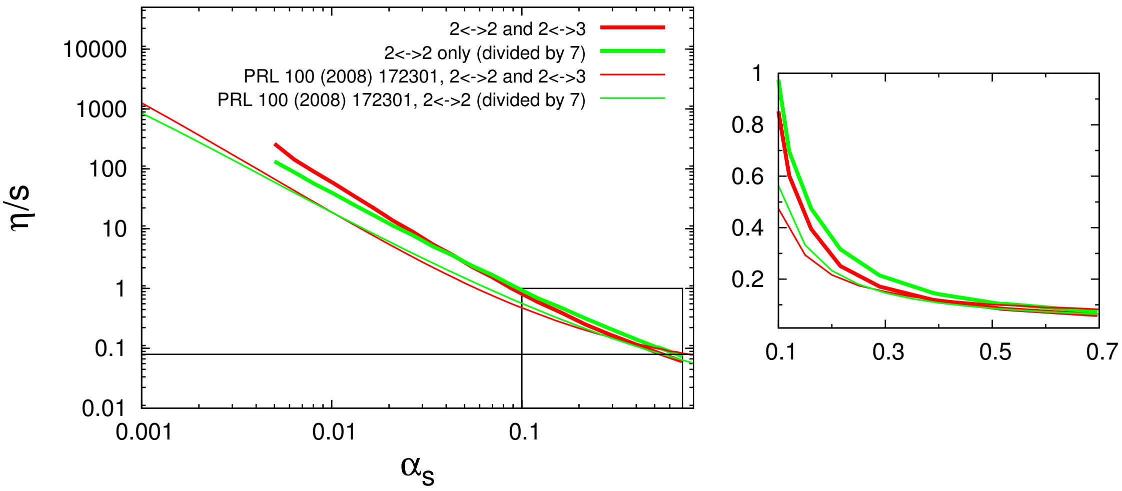

Figure 9.5.: η/s as function of α_s. The results are calculated implementing both elastic and inelastic processes (red lines) and with elastic processes only (green lines).

0.3) and 0% ($\alpha_s = 0.6$). If the η/s value, extracted from BAMPS, is to be employed in second-order hydrodynamic equations, it is more consistent to calculate it by Eq. (4.8), since it is consistent with the second-order Israel-Stewart formalism.

9.3. Applicability limits of the second-order hydrodynamic formalism.

The formalism presented in previous section is based on Grad's approximation and second-order dissipative hydrodynamic equations. Since both are truncated expansions in terms of dissipative fluxes, and in particular, for the problems considered here, in term of $\pi^{\mu\nu}$, the applicability of the formalism is limited.

The time evolution of π, e and n can be calculated by the iterative algorithm discussed above. With the obtained solutions, the deviations from equilibrium can be quantified using the following observable, proposed by us in Ref. [33]:

$$\sigma_\phi = \sqrt{\langle \phi^2 \rangle_{eq}} = \frac{1}{n} \int d\Gamma p_0 f_{eq} \phi^2. \tag{9.8}$$

In the latter expression, ϕ denotes the dissipative correction to the equilibrium distribution function, as given by Eq. (8.1). In chapter 8 I have demonstrated that ϕ can be both positive and negative, dependent on the momentum. The positive-definite observable σ_ϕ is a measure of the absolute deviation from equilibrium. When averaged over the momentum, ϕ should be smaller than unity to guarantee validity of both Grad's approximation, which is linear in ϕ, and of second-order hydrodynamic equations, which are obtained from the expansion of the entropy current.

Inserting $\phi = \frac{3}{8T^2}\frac{\pi}{e}p_T^2\left(\frac{1}{2} - \sinh^2 y\right)$ (comp. Eq. (8.1)) into the definition of σ_ϕ, Eq. (9.8), one obtains

$$\sigma_\phi = \frac{9\sqrt{2}}{4}\frac{|\pi|}{e}, \tag{9.9}$$

The value of σ_ϕ, as calculated by the iterative algorithm, is presented in Fig. 9.6.

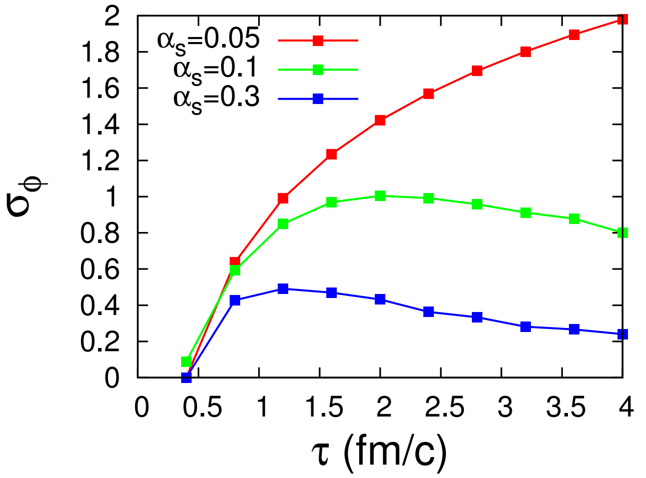

Figure 9.6.: Deviation from equilibrium, σ_ϕ, calculated using solutions of the iterative algorithm for different values of α_s.

Formally, for initial conditions chosen here, the second-order formalism breaks down for $\alpha_s \lesssim 0.1$, as Fig. 9.6 demonstrates. Although σ_ϕ is still below 1 for $\alpha_s = 0.1$, it grows larger than unity already at $\tau \sim 1$ fm/c for $\alpha_s = 0.05$. With $\sigma_\phi > 1$, the hydrodynamic equations are well outside their validity range, and the entire algorithm becomes invalid.

Considering Fig. 9.6, one has to keep in mind that strictly speaking the iterative algorithm is only applicable at early times, because the net particle number is assumed to be constant which leads to a loss of chemical equilibrium and continuous decrease of the fugacity at late times. Thus, the results of iterative hydrodynamic calculations cannot be directly compared with BAMPS results, since particle production and annihilation lead to restoration of chemical equilibrium in BAMPS. Nevertheless, it is interesting to quantify the equilibrium deviations in BAMPS by calculating σ_ϕ. This is shown in Fig. 9.7. In BAMPS σ_ϕ cannot grow larger than 1.06 since $\frac{\pi}{e} \leq \frac{1}{3}$ in kinetic theory for an expanding one-dimensional system. Even with $\alpha_s = 0.05$ the value of σ_ϕ is still slightly below unity and definitely below the maximum value of 1.06. It is necessary to mention, that the value $\alpha_s = 0.05$ employed for some analysis in this work, is rather unphysical, since it corresponds to extremely large momentum transfer, as follows from recent experimental and theoretical results[49, 133]. One can thus regard $\alpha_s \sim 0.05$ as a limit of applicability of the expression in Eq. (9.3).

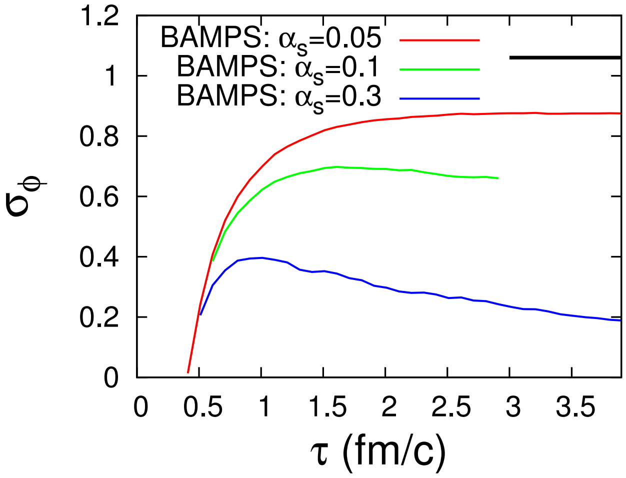

Figure 9.7.: Deviation from equilibrium, σ_ϕ, calculated using solutions of the iterative algorithm for different values of α_s.

9.4. Limits of the transport approach.

The transport approach itself is limited in its applicability. The particular implementation of the Boltzmann Equation (7.1) in BAMPS does not include quantum statistic effects which become important in a dense and strongly interacting system. The partonic degrees of freedom in BAMPS are represented by 'quasi-particles', obeying a fixed dispersion relation. The spectral functions of quasi-particles are δ-functions, describing infinitely long living, i.e. stable objects. For heavy-ion collisions at high energies the applicability 'quasi-particle' model is rather questionable in the high density and/or high energy regime, where particles are expected to achieve a finite width due to collision processes. For a strongly coupled system, the quasi-particle picture is appropriate in the limit of high temperature, at which the coupling becomes small. An effective kinetic treatment of such a system was given for example by ARNOLD,MOORE and YAFFE in Ref. [157]. In the collision term of the Boltzmann Equation as implemented in BAMPS, explicitly given in Eq. (7.6) and (7.7), the broadening is neglected. The quasi-particle picture becomes inapplicable if the mean free path λ, which is the inverse of the collision rate R, $\lambda = R^{-1}$, becomes of order of the thermal size of the particles, which is given by the inverse of the mean energy per particle $\langle E \rangle = 3T$.

The ratio of the mean free path to the thermal size of particles extracted from BAMPS simulations is demonstrated in Fig. 9.8. At large coupling, $\alpha_s \gtrsim 0.6$ the quasi-particle picture in BAMPS becomes rather questionable.

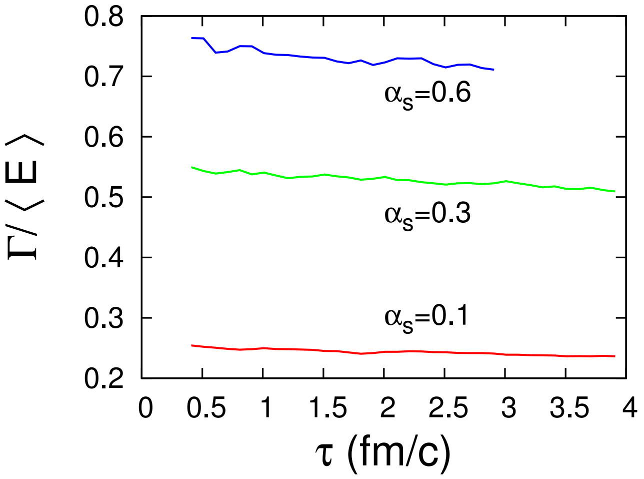

Figure 9.8.: Ratio of the collisional broadening to mean energy per particle.

Conclusion

To conclude, the η/s has been calculated in this chapter as function of α_s using a self-consistent iterative algorithm. The core of this algorithm are second-order Israel-Stewart hydrodynamic equations and the expression for shear viscosity, which was derived, in full consistency with Israel-Stewart equations, using Grad's approximation for distribution function. For the calculation of the shear viscosity coefficient, LO pQCD matrix elements were employed. The obtained results on $\eta/s(\alpha_s)$ are in good agreement with the earlier published Navier-Stokes based calculations [42]. The inelastic pQCD processes are demonstrated to be much more efficient for restoration of isotropy in the momentum space than the elastic ones thus leading to a low values of the η/s ratio extracted from BAMPS. For the realistic effective coupling values $\alpha_s = 0.3..0.6$ the ratio η/s is found to be in the range 0.18..0.08, thus close to the lower value for a infinitely strongly coupled system.

10. Comparison of dissipative hydrodynamic calculations with BAMPS results for a one-component system with conserved particle number.

In this chapter solutions of the dissipative hydrodynamic equations with conserved particle four-current, as derived in Sections 3.1.3 and 3.1.4 and summarized in section 6 and C.1, will be compared with results of BAMPS calculations. The main objective of this comparison is to evaluate the applicability limitations of hydrodynamic equations. For the comparison introduced in this chapter, only elastic processes with angle independent (i.e. isotropic) differential cross sections are considered. In order to compare the results of hydrodynamic and kinetic transport calculations, a correspondence between the transport coefficients on the hydrodynamic side and scattering cross section on the other side has to be established. For isotropic cross section, such a correspondence was found by de Groot, van Leeuwen and van Weert in Ref. [76]. For instance, in Ref. [76] the shear viscosity coefficient is given in terms of the elastic transport cross section:

$$\eta = \frac{4T}{5\sigma_{tr}}\,. \tag{10.1}$$

The transport cross section σ_{tr} is defined in terms of a weighted integral over the differential cross section $\frac{d\sigma}{d\Omega}$ in the center-off-mass frame:

$$\sigma_{tr} = \int_{cm} d\Omega \; sin^2\theta \frac{d\sigma}{d\Omega}\,. \tag{10.2}$$

If the differential cross section is angle independent, i.e. isotropic, the transport cross section is proportional to the total cross section

$$\sigma_{22}^{tr} = \frac{2}{3}\sigma_{22}\,, \tag{10.3}$$

and the shear viscosity coefficient becomes

$$\eta = \frac{6}{5}\frac{T}{\sigma_{22}}\,. \tag{10.4}$$

In the latter two expressions σ_{22} denotes the total elastic cross section.

The expression in Eq. (10.4) was obtained in Ref. [76] for the *second-order*, Israel-Stewart, hydrodynamic theory. In Ref. [46] HUOVINEN and MOLNAR employed this functional dependence between the shear viscosity coefficient and the total cross section for a detailed comparison of Israel-Stewart results for one-dimensional boost-invariant system with kinetic transport calculations by MPC [28, 29, 155]. In this chapter I will introduce an analogous comparison employing the BAMPS model. In addition to the second-order Israel-Stewart equations, I will present the solutions of third-order equations, derived in Section 3.1.4 and in Refs. [34, 158]. Comparison of the two hydrodynamic approaches with BAMPS will, on the one hand, help finding the applicability limits of Israel-Stewart and third-order equations; on the other hand, it will demonstrate the effect of inclusion of higher-order terms into the equations and advantage of higher-order equations compared with Israel-Stewart theory.

Unless otherwise stated, the initial conditions for both BAMPS and hydrodynamic calculations will be of thermal type and given by Eq. (8.5). Like for the results presented in sections 8.2 and 9.1, the initial time and temperature are chosen to be $\tau_0 = 0.4$ fm/c and $T_0 = T(\tau_0) = 0.5$ GeV. The results presented in this section are extracted from the central rapidity region $\eta \in [-0.1 : 0.1]$. For BAMPS as well as hydrodynamic calculations the local rest frame entropy density s is calculated using the kinetic equilibrium expression $s = 4n - n \ln \lambda$.

10.1. Relevant observables.

To obtain a quantitative measure for the strength of dissipation in a system, a set of proper observable should be introduced. The case to be studied here, a one-dimensional boost-invariant expansion of a Boltzmann gas, has the advantage of simple geometry leading to a relatively simple structure of hydrodynamic equations, as given in Section 6 and Section C.1 of Appendix C.1. For the derivation of hydrodynamic equations in Sections 3.1.2 – 3.1.4 and Appendix B, the entropy current is constructed for a disequilibrated system by introducing a small deviation ϕ of the distribution function from its equilibrium from [comp. Eqs. (3.16) and (3.24) and discussion around Eq. (B.3)]. For a one-dimensional system, the deviation ϕ can be found in Eq. (8.1). The expansion leading to the expressions (3.16) and (3.24) clearly breaks down if ϕ becomes larger than 1. Since ϕ is a momentum-dependent quantity, for a macroscopic theory like hydrodynamics it is natural to introduce a momentum averaged measure of the deviation from the equilibrium distribution, σ_ϕ, which was introduced in Eq. (9.8). Both ϕ and σ_ϕ are proportional to the ratio of the shear pressure to energy density $\frac{\pi}{e}$, resp. $\frac{\pi}{p}$ using the ideal gas equation of state, which is thus a *smallness parameter* of the expansion (comp. the discussion in Section 3.1.4).

The formal role of the ratio $\frac{\pi}{e}$ can alternatively be motivated by a closer investigation of the one-dimensional second-order evolution equation for the shear pressure π [comp.

Eqs. (3.20) resp. (6.36)]:

$$\dot{\pi} = -\frac{\pi}{\tau_\pi} - \frac{4}{3}\frac{\pi}{\tau} + \frac{8}{27}\frac{e}{\tau}\,. \tag{10.5}$$

Note, that in the first-order, Navier-Stokes theory, the corresponding equation is not a dynamical equation and contains only two terms [comp. Eqs. (3.13) resp. (6.35)]:

$$\pi = \frac{4}{3}\frac{\eta}{\tau}\,. \tag{10.6}$$

Dividing the first-order equation by the relaxation time $\tau_\pi = 2\eta\beta_2$, which appears in the second-order equation, and using the expression (6.22) for β_2, one obtains

$$\frac{\pi}{\tau_\pi} = \frac{8}{27}\frac{e}{\tau}\,. \tag{10.7}$$

Thus the terms $\frac{\pi}{\tau_\pi}$ and $\frac{8}{27}\frac{e}{\tau}$ on the right-hand side of Eq. (10.5) are first-order terms originating from a first-order term in the entropy current. The term $\frac{4}{3}\frac{\pi}{\tau}$ is a second-order term. The ratio of the second-order term and the both first-oder terms, one obtains

$$\frac{4/3 \cdot \pi/\tau}{8/27 \cdot e/\tau} = \frac{9}{2}\frac{\pi}{e}\,, \quad \frac{4/3 \cdot \pi/\tau}{\pi/\tau_\pi} = \frac{4}{3}\frac{\tau_\pi}{\tau}\,. \tag{10.8}$$

The expressions obtained this way are indicators of the *formal break down* of hydrodynamic approach. Indeed, if the conditions

$$\frac{\pi}{e} \geq \frac{2}{9} \quad \text{and} \quad \frac{\tau_\pi}{\tau} \geq \frac{3}{4} \tag{10.9}$$

are fulfilled, the second-order terms become larger than the first-order ones and thus the series of terms cannot be truncated. On the other hand, one realizes that the second-order theory is well applicable if the conditions

$$\frac{\pi}{e} \ll \frac{2}{9} \quad \text{and} \quad \frac{\tau_\pi}{\tau} \ll \frac{3}{4} \tag{10.10}$$

hold, since then the series of terms can be expected to converge.

The ratios $\frac{\pi}{e}$ and $\frac{\tau_\pi}{\tau}$ are thus smallness parameters for hydrodynamic equations and control their applicability. Their meaning can as well be understood from the kinetic theory point of view. The shear stress tensor is the anisotropic part of the energy-momentum tensor, as follows from its definition in Section 2.1. The ratio $\frac{\pi}{e}$ thus can be rewritten as $\frac{|\delta T^{33}|}{T^{00}}$ and thus quantifies the deformation of the energy-momentum tensor. From the kinetic theory point of view, the ratio $\frac{\tau_\pi}{\tau}$ can be identified with the Knudsen number (comp. discussion in section 3.1.4 and Refs. [94, 34])

$$Kn = \frac{\lambda_{mfp}}{\tau}\,. \tag{10.11}$$

In the latter expression λ_{mfp} denotes the *microscopic* scale of the system, which is the mean free path. For a one-dimensional boost-invariant system the expansion scalar θ

(comp. discussion in section 3.1.4) is given by $\partial_\mu u^\mu = 1/\tau$. Thus, the ratio $\frac{\tau_\pi}{\tau}$ can be understood as the product $\lambda \cdot \partial_\mu u^\mu$ describing a competition between the microscopic scale λ_{mfp}, which drives the system towards *local* equilibrium due to collisions, and the macroscopic expansion rate θ driving the system off equilibrium *globally.* If $\frac{\tau_\pi}{\tau} \propto \lambda_{mfp}\theta$ is small, the equilibration process dominates over the expansion. Otherwise, the expansion prevails, the local equilibration due to collisional processes is slower than the loss of global equilibrium due to expansion and the system cannot equilibrate. In this regime hydrodynamic description breaks down, which follows from Eq. (10.9). This line of argumentation was already applied in this work in section 3.1.4 and in Ref. [34], where derivation of third-order hydrodynamic equations is introduced.

Another observable which can be used to quantify the degree of disequilibration of the system is the *pressure isotropy* [153], i.e. the ratio of the longitudinal and transverse components of the energy-momentum tensor

$$\mathcal{P} = \frac{p_L}{p_T} = \frac{T^{33}}{(T^{11}+T^{22})/2} = \frac{p-\pi}{p+\pi/2}\,. \tag{10.12}$$

For a free expanding system, as considered in Bjorken model, π is usually positive so that the third component of the shear stress tensor, $\pi^{33} = -\pi$, is negative. This is in particular true for an initially equilibrated system undergoing the expansion, which reduces the longitudinal pressure. Throughout the evolution towards equilibrium π should not become larger than $p = \frac{e}{3}$, which is equivalent to the restriction that the third diagonal component of the energy-momentum tensor,

$$T^{33} = \int d\Gamma f(p_T, p_z)\; p_z^2 = p - \pi\,, \tag{10.13}$$

is always non-negative. For a disequilibrated system with a longitudinal expansion direction the third energy-momentum tensor component is often called the *longitudinal pressure*, $p_L = T^{33} = p - \pi$ [159, 153]. Accordingly, the transverse components of the energy-momentum tensor are related to the transverse pressure, $p_T = (T^{11}+T^{22})/2 = p + \pi/2$. The longitudinal pressure may become negative as the system undergoes a phase transition as a result of expansion and cooling, as for example discussed in Ref. [159]. In this case, the reason for a negative pressure can be the attractive nuclear interaction. Another scenario in which the longitudinal pressure can be negative is the coherent field picture of the quark-gluon plasma with instabilities, which are analogous to the Weibel instabilities in non-relativistic plasmas. The coherent field description in presence of instabilities is relevant for the early-time evolution of the quark-gluonic system; its evolution was studied in Refs. [160, 161, 162, 74]. RAJAGOPAL and TRIPURANENI argued in Ref. [163] that a transition between positive and non-negative longitudinal pressure can be interpreted as an onset of cavitation with subsequent hadronization of a system fallen apart.

However, in a system with homogeneous phase structure without attractive interactions among the (quasi-) particles, i.e. a system which is typically considered in the kinetic transport theory, the occurrence of negative longitudinal pressure is *not physical.* Dissipative hydrodynamic equations derived in this work in Sections 3.1.2 – 3.1.4 for an ideal gas equation of state should not lead to negative longitudinal pressure. This conclusion was used by Martinez and Strickland in Ref. [153] to evaluate constrains on initial conditions for second-order dissipative hydrodynamic equations. Thus the pressure isotropy defined in Eq. (10.12) can be an indicator either of a high degree of equilibration in the system ($\mathcal{P} = 1$) or of a breakdown of hydrodynamic description ($\mathcal{P} < 0$).

10.2. Comparison of numerical results.

The parameters of BAMPS resp. dissipative hydrodynamic hydrodynamic calculations, which results are to be presented in this section, are summarized in the following table:

Parameter		Value
τ_0		0.1, 0.4, 1.0 fm/c
$T_0(\tau_0)$		0.5 GeV
Type of interactions		Elastic processes, isotropic cross section
Hydro	η/s	0.05, 0.2, 0.4, 1.0, 3.0
BAMPS	σ_{22}	$\frac{6}{5}\left(\frac{\eta}{s}\right)^{-1}\frac{T}{n(4-\ln\lambda)}$

10.2.1. Effect of initial time.

In this subsection the initial time is varied whereas the parametrization of the elastic cross section resp. the η/s value are fixed in BAMPS resp. hydrodynamic calculations. In Fig. 10.1(a) – (c) energy per unit transverse area and unit rapidity $\frac{dE}{dAd\eta} = e \cdot \tau$, effective temperature $T = e/(3n)$ and the π/e ratio from BAMPS, second and third-order hydrodynamic calculations with $\eta/s = 1$ are presented.

A good agreement is observed between BAMPS and hydrodynamic calculations considering the energy in Fig. 10.1(a). The depicted observable is directly related to the energy density, which thus exhibits very weak sensitivity to dissipative corrections. On the other hand, second-order hydrodynamics fails to describe evolution of the effective temperature with reasonable accuracy except if the initial time is large. The combination of very low initial time $\tau_0 = 0.1$ fm/c and strong dissipation $\eta/s = 1$ leads in BAMPS calculations to a behavior which is very similar to free-streaming: the effective temperature decreases initially and stays approximately constant later on. Indeed, in the free-streaming limit in one-dimension both energy and particle densities scale with the inverse of the proper time, $e = e_0\tau_0/\tau$ and $n \propto n_0\tau_0/\tau$, leading to $T = const$. Accordingly, the π/e ratio saturates at $\pi/e \approx 1/3$. This is consistent with the observed saturation of the temperature considering Eqs. (6.30) and (6.29). Such free-streaming similar behavior cannot be described by hydrodynamic equations, which produce unphysical solutions, as Fig. 10.1(b) demonstrates: second-order hydrodynamics leads to increase of the temperature, i.e. reheating. This happens because the system becomes over-stressed, since π/e grows larger than 1/3 and consequently the shear pressure π exceeds the isotropic pressure $p = e/3$. Such anomalies are not observed in the solutions of third-order hydrodynamics. In the extreme limit of free-streaming similar behavior, $\tau_0 = 0.1$ fm/c, third-order hydrodynamics fails as well, although its solutions are still physically valid. However, for larger

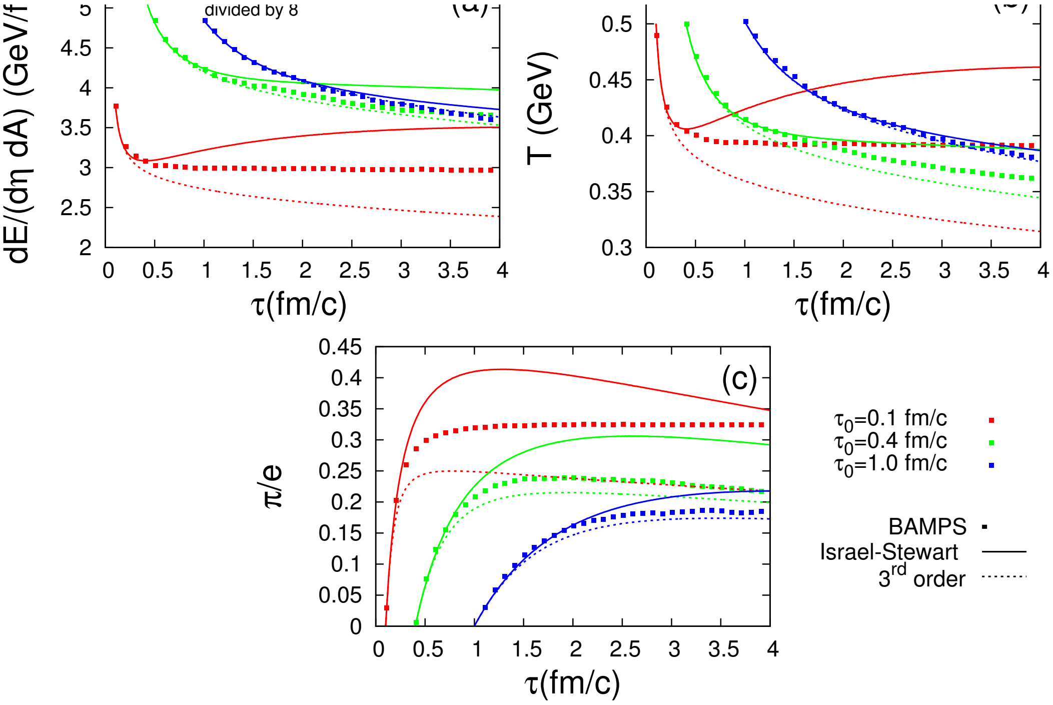

Figure 10.1.: Evolution of energy per unit transverse area and rapidity (a), effective temperature (b) and shear pressure to energy density ratio (c) from BAMPS and hydrodynamic calculations with different initial times τ_0 and $\eta/s = 1.0$.

initial time the differences between BAMPS and hydrodynamic results are *considerably reduced* if third-order equations are considered.

The pressure isotropy from BAMPS and hydrodynamic calculations is shown in Fig. 10.2(a). BAMPS results for $\tau_0 = 0.1$ fm/c demonstrate that in the free-streaming limit longitudinal pressure vanishes since the pressure isotropy saturates at 0; at the same time the second-order hydrodynamics leads to negative pressure isotropy due to negative longitudinal pressure. For neither of the demonstrated initial times an onset of relaxation towards equilibrium can be observed. The reason for this can be understood from Fig. 10.2(b), where the hydrodynamic relaxation time to expansion time ratio τ_π/τ is demonstrated. Using Eqs. (3.21) and (6.22) the τ_π/τ ratio can be rewritten as

$$\frac{\tau_\pi}{\tau} = \frac{3}{2}\frac{1}{T\tau}\left(\frac{\eta}{s}\right) \cdot (4 - \ln\lambda) \; , \tag{10.14}$$

where the entropy density was approximated by its kinetic equilibrium value $s = 4n - n\ln\lambda$. Thus, for a fixed η/s the initial value of τ_π/τ ratio is inversely proportional to the initial time and temperature. A sufficiently small τ_0 can make relaxation towards equilibrium on a reasonable time scale impossible even for small η/s. The hydrodynamic

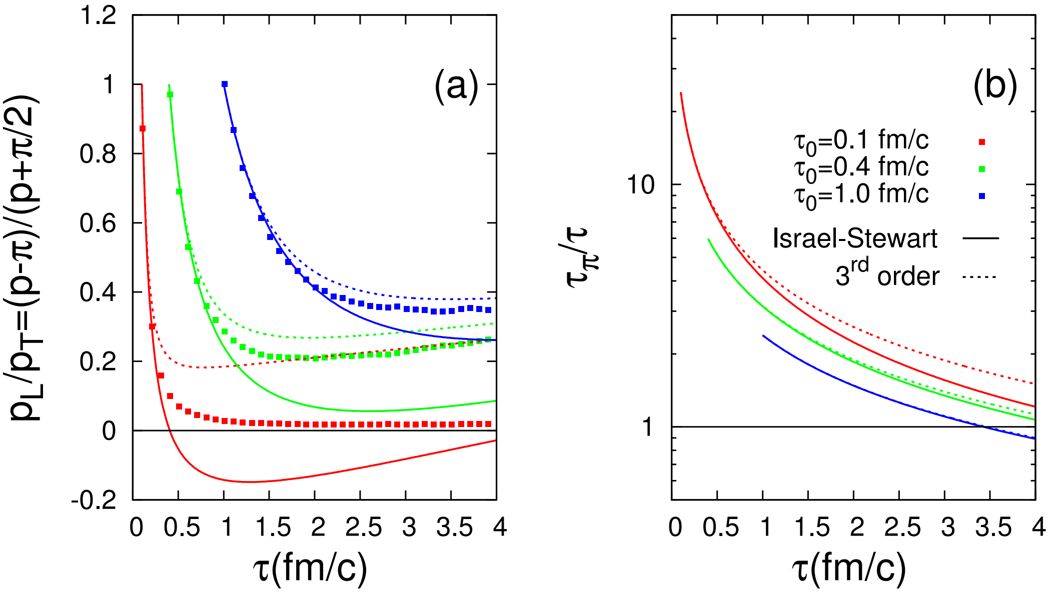

Figure 10.2.: Evolution of pressure isotropy (a) and the Knudsen number $\frac{\tau_\pi}{\tau}$ (b) from BAMPS and hydrodynamic calculations with different initial times τ_0 and $\eta/s = 1.0$.

evolution in Fig. 10.2(b) is dominated by expansion for $\tau_0 \leq 1$ fm/c. The consequence is a strong increase of the shear pressure, as observed and discussed earlier.

In fact, Eq. (10.14) allows to make a rough estimate of the possible value of the initial time τ_0, for which a partonic system will be able to start to relax towards equilibrium immediately, i.e. will be initialized within the applicability limit of hydrodynamic description. Imposing the condition $\frac{\tau_\pi}{\tau_f} \leq 1$ and setting $\lambda = 1$, one obtains from Eq. (10.14) the constraint

$$T\tau \gtrsim 6\frac{\eta}{s}\,. \tag{10.15}$$

Taking $\eta/s = 0.2$ – approximately the value we extracted from BAMPS for $\alpha_s = 0.3$ in chapter 9 – one obtains $T\tau \geq 1.2$. For the initial temperature in range $T_0 = 0.2..0.6$ GeV – where the upper value might be characteristic temperature of the color glass condensate initial temperature at RHIC (comp. chapter 7.4.1) – one obtains $\tau_0 = 0.4..1.2 fm$ for the time at which hydrodynamic description is formally correct. This simple estimate is in agreement with the results obtained by Martinez and Strickland in Ref. [153]. At the same time, this estimate for τ_0 agrees with the range of thermalization times $\sim 0.5 - 2$ fm/c used in Refs. [8, 9, 10, 164, 116] to initialize hydrodynamic calculations, which were found to be able to describe the collective flow at RHIC. With $\eta/s = 1$, the minimal τ_0 is smaller for the chosen temperature range, $0.08 - 0.24$, which is consistent with the observation in Fig. 10.2(b). Also, contrary to the assumption leading to Eq. (10.15), the fugacity is not 1 if particle number is conserved, which additionally increases τ_0.

In order to obtain a more quantitative comparison of hydrodynamic and kinetic transport results, the relative deviations, obtained as ratio of hydrodynamic results and BAMPS results, are shown in Fig. 10.3(a)–(d). The observables presented there are the diagonal components of the energy momentum tensor in the local rest frame, $T^{00} = e$, $1/2(T^{11} + T22) = p + \pi/2$ and $T^{33} = p - \pi$, as well as the momentum isotropy $\mathcal{P}$. Since the particle number is the same in hydrodynamic and kinetic transport calculations, the deviations of the effective temperature are given by the deviations of energy density and are not shown. Considering the energy density, Fig. 10.3(a), and the trans-

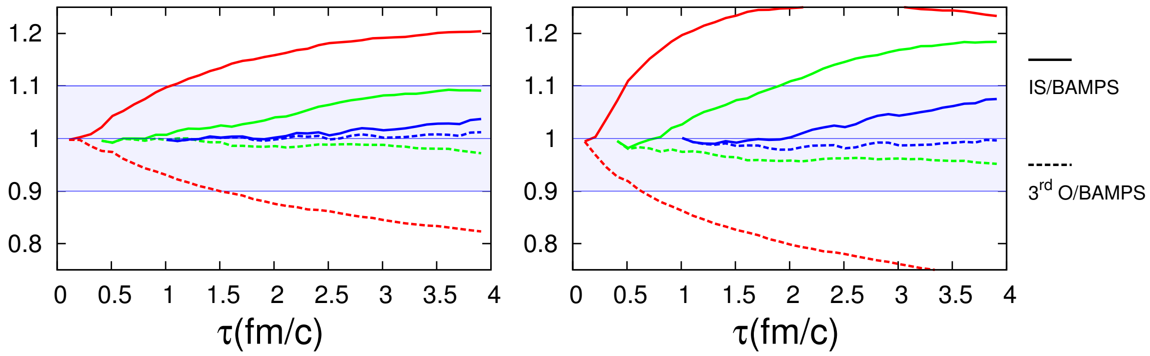

(c) longitudinal pressure, T^{33}=p-π

(d) pressure isotropy, $2T^{33}/(T^{11}+T^{22})$

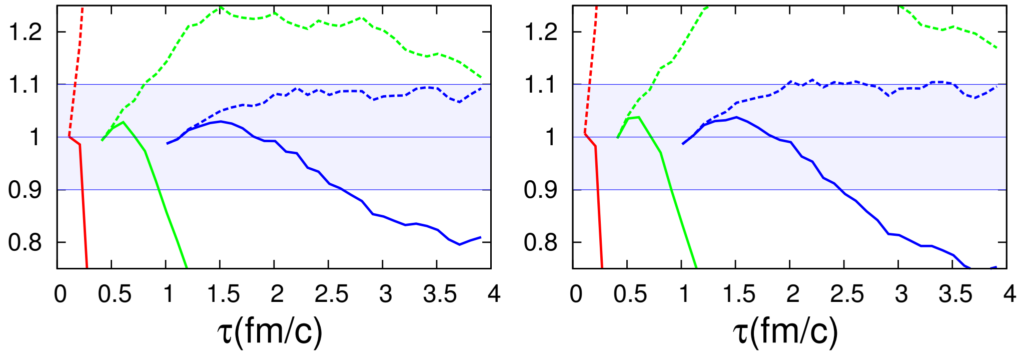

Figure 10.3.: Relative difference between hydrodynamic and BAMPS results for components of the energy momentum tensor for $\eta/s = 1$ and different τ_0.

verse pressure, Fig. 10.3(b), second-order hydrodynamic results are within 10% accuracy only for $\tau_0 = 1$ fm/c with the chosen value of $\eta/s = 1$. However, considering the longitudinal pressure, Fig. 10.3(c), and the pressure isotropy, Fig. 10.3(d), applicability of second-order hydrodynamics becomes questionable even for $\tau_0 = 1$ fm/c. One can conclude that the second-order hydrodynamic description is clearly beyond the edge of its applicability for $\tau_0 \approx 1$ fm/c, $T_0 = 0.5$ GeV and $\eta/s = 1$ and cannot be considered applicable for the shown initial times. At the same time, inclusion of third-order terms into the evolution equation for shear pressure leads to a significant reduction of deviation between hydrodynamic results and BAMPS calculations. Even for lower initial times, $\tau_0 = 0.4$ fm/c, third-order hydrodynamic calculations lead to less than 10% deviations from kinetic transport results considering energy density and transverse pressure. Deviations are around 20% for the longitudinal pressure and pressure isotropy. Thus, third-order hydrodynamic description becomes inapplicable for $\tau_0 \approx 0.4$ fm/c, $T_0 = 0.5$ GeV and $\eta/s = 1$ but is still well applicable for $\tau_0 \approx 1$ fm/c.

Applicability of hydrodynamic description was investigated by HUOVINEN and MOLNAR in Ref. [46] with respect to the variable

$$K = \tau/\lambda^{tr} \,. \tag{10.16}$$

K is the inverse of the Knudsen number used in this work, if defined via the *transport mean free path* λ^{tr} instead of the usual mean free path λ:

$$K = 1/Kn^{tr} = \frac{\tau}{\lambda^{tr}} \,. \tag{10.17}$$

The transport mean free path is given in terms of the *transport cross section* σ^{tr} as defined by Eq. (10.2). For the elastic isotropic collisional processes, that are implemented in BAMPS for the results presented here, the transport mean free path $\lambda^{tr} = 1/\langle n\sigma^{tr}\rangle$ is simply proportional to the usual mean free path, $\lambda^{tr} = 3/2\lambda$. From a comparison of second-order hydrodynamic calculations with kinetic transport calculation by MPC HUOVINEN and MOLNAR concluded in [46] that second-order hydrodynamics is applicable if the initial conditions are such that $K_0 = K(\tau_0, T_0, \eta/s) \gtrsim 2$. Their conclusion was based on the requirement that the relative deviations of pressure isotropy must be below 10% for hydrodynamics to be well applicable. In particular, the relative deviations were found to be $\sim 20\%$ for $K_0 = 1$ and $\sim 10\%$ for $K_0 = 2$. The values of $K_0(\tau_0)$ corresponding to the initial conditions employed here are

$$K_0(0.1 \text{ fm/c}) = 0.05, \quad \mathrm{K}_0(0.4 \text{ fm/c}) = 0.2, \quad \mathrm{K}_0(1.0 \text{ fm/c}) = 0.5 \,. \tag{10.18}$$

From the comparisons demonstrated in this section in Figs. 10.2 and 10.3 we can conclude that second-order hydrodynamic description is already inapplicable for $K_0 \lesssim 0.5$, whereas the *third-order* description is still well applicable for $K_0 = 0.5$.

The relative deviation of second-order hydrodynamics from kinetic transport results observed in Ref. [46] are larger than the ones reported here for same values of K_0. In particular, we observe a $\sim 20\%$ deviation of momentum isotropy for $K_0 = 0.5$, whereas in Ref. [46] this magnitude of deviation is observed already for $K_0 = 1$, which corresponds to a larger initial time. This difference can be explained by a slightly different form of second-order hydrodynamic equations. Whereas Eq. (6.36) – resp. the full set of equations as given in section C.1 of Appendix C – is strictly of second order in small quantities π/e and τ_π/τ, the evolution equation for π used in Ref. [46] explicitly contains a term of third order, $\sim \pi^2/(e\tau)$, which should be neglected for consistency, unless other terms of same order are included into the equations, like it is done in this work in scope of third-order formalism. In a regime, where π/e is large but still below 1/3, the third-order term kept in Ref. [46] is not small and positive, thus increasing $\dot{\pi}$ and driving the system further away from equilibrium. Note that if *all* third-order terms are consistently included, as done here – comp. Eq. (6.37) – their effect on $\dot{\pi}$ is opposite, i.e. damping instead enhancing thus leading to a smaller shear pressure as compared to solutions of second-order equations. Thus, the equations used in Ref. [46] have to lead to a larger critical value of K_0. This will be verified in the next section.

Finally, it is interesting to note that inclusion of third-order terms into the evolution equation for shear pressure leads to a significant reduction of deviations from kinetic transport results even in the regime of Kn being larger than unity, as demonstrated for $\tau_0 = 0.4$ fm/c in this section. This might indicate that the (truncated) higher-order terms in the evolution equation for shear pressure π are proportional to powers of π/e rather than τ_π/τ. This is certainly true for the third-order term derived in this work.

10.2.2. Effect of shear viscosity to entropy density ratio.

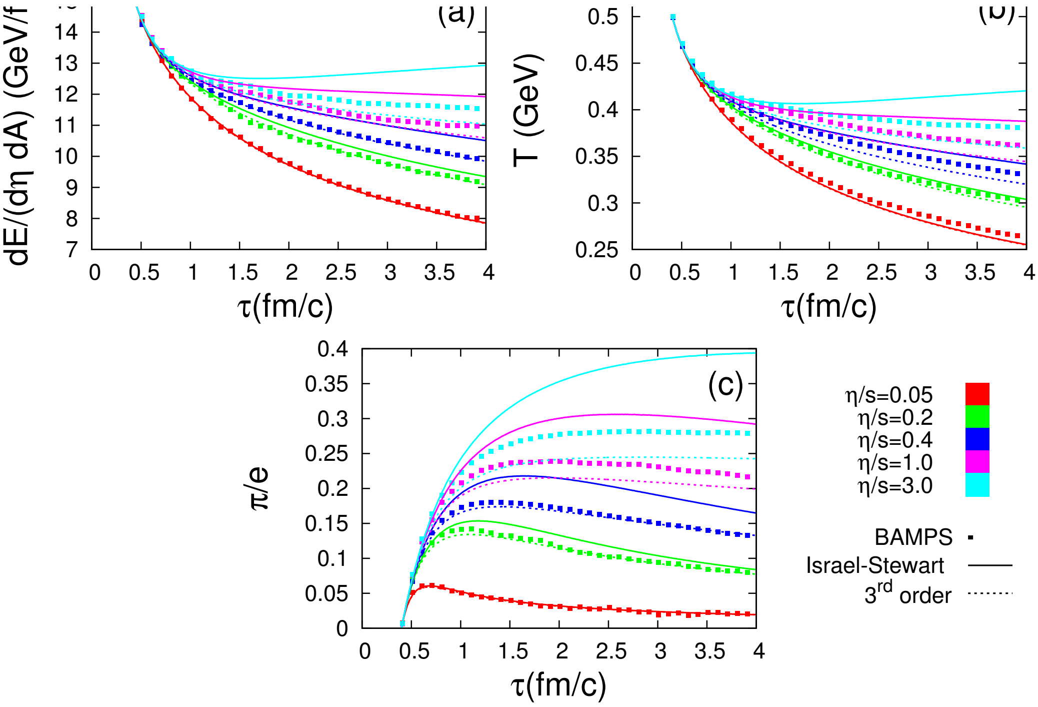

Figure 10.4.: Evolution of energy per unit transverse area and rapidity (a), effective temperature (b) and shear pressure to energy density ratio (c) from BAMPS and hydrodynamic calculations with different values of η/s and initial time $\tau_0 = 0.4$ fm/c.

In this subsection the initial time is fixed, $\tau_0 = 0.4$ fm/c, whereas the parametrization of the elastic cross section resp. the η/s value is varied in BAMPS resp. hydrodynamic

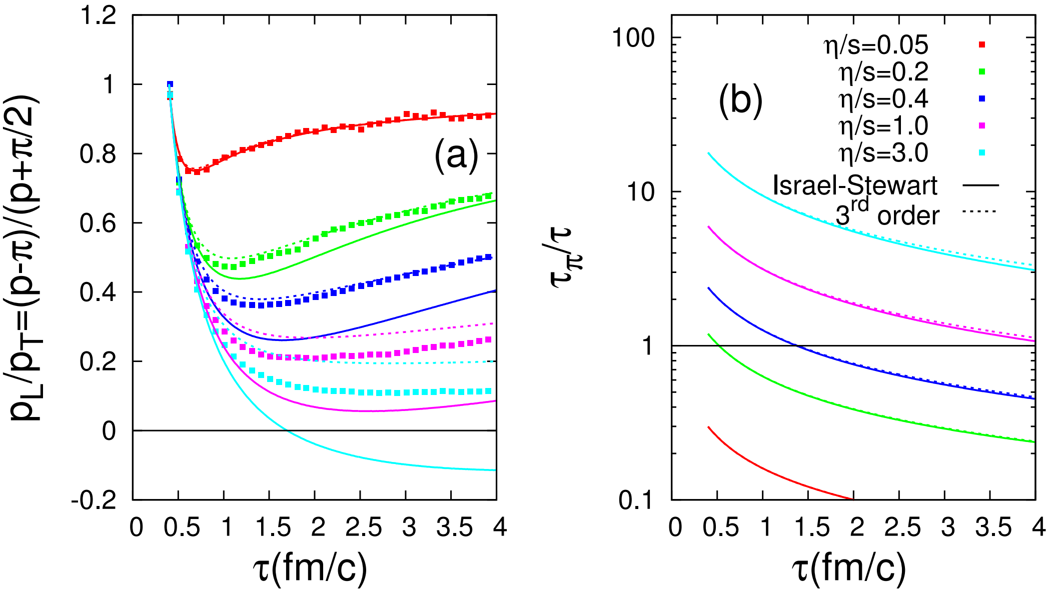

Figure 10.5.: Evolution of pressure isotropy (a) and the Knudsen number $\frac{\tau_\pi}{\tau}$ (b) from BAMPS and hydrodynamic calculations with initial time $\tau_0 = 0.4$ fm/c and different η/s values.

calculations. The scheme for the analysis presented here is similar to the one in previous subsection.

In Fig. 10.4(a)-(c) energy per unit transverse area and unit rapidity $\frac{dE}{dAd\eta} = e \cdot \tau$, effective temperature $T = e/(3n)$ and the π/e ratio from BAMPS, second and third-order hydrodynamic calculations with $\eta/s = 0.05 - 3$ are presented. The second-order hydrodynamic solution becomes unphysical for $\eta/s = 3$, leading to increase of energy density and effective temperature. This behavior was already observed in Fig.10.1 (a)-(b) in previous subsection for $\eta/s = 1$ and $\tau_0 = 0.1$ fm/c. Accordingly, the pressure isotropy, shown in Fig. 10.5(a), becomes negative in second-order hydrodynamic calculations for $\eta/s = 3$. However, in kinetic transport calculations the free-streaming similar behavior, which was observed in Fig. 10.1, is still not observed even with $\eta/s = 3$. The third-order results are closer to kinetic transport and the unphysical reheating is prevented. Evolution of the Knudsen number $Kn = \tau_\pi/\tau$ is shown in Fig. 10.5(b). For $\eta/s = 0.05$ the system is initialized within the relaxation regime – accordingly, the deviations between kinetic transport and both second and third-order hydrodynamic equations are marginal.

The relative deviations of dissipative hydrodynamic results from BAMPS calculations are shown in Fig. 10.6 for the components of energy-momentum tensor. This allows to constrain the applicability of hydrodynamic description using the same criteria as in previous subsection: all four energy momentum components must be described by hydrodynamics within 10% accuracy. This criterion is still fulfilled in *second-order*

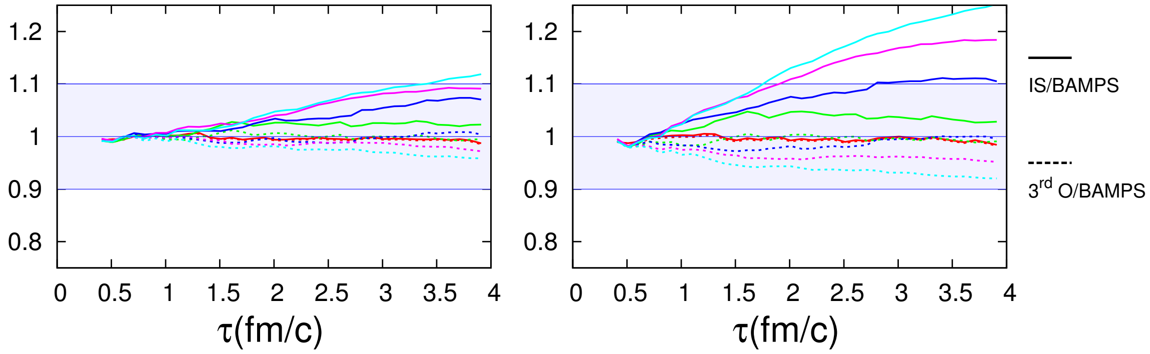

(c) longitudinal pressure, T^{33}=p-π

(d) pressure isotropy, $2T^{33}/(T^{11}+T^{22})$

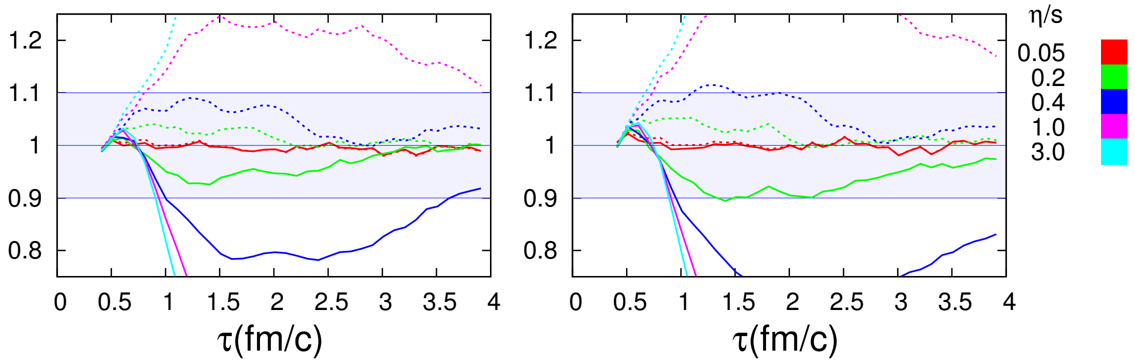

Figure 10.6.: Relative difference between hydrodynamic and BAMPS results for components of the energy momentum tensor with $\tau_0 = 0.4$ fm/c and different η/s values.

theory for $\eta/s \lesssim 0.2$, which is corresponding to $K_0 \gtrsim 1$ for $\tau_0 = 0.4$ fm/c chosen in this section. This value is smaller than the one obtained by Huovinen and Molnar in Ref. [46] for reasons discussed at the end of previous section. The *third-order* description is sufficiently accurate for $\eta/s \lesssim 0.4$, corresponding to $K_0 \gtrsim 0.5$, as already concluded in previous section.

Again, the fact that hydrodynamics is applicable (with less than 10% accuracy) even in the regime of $Kn \geq 1$ (comp. Fig. 10.5(b) for $\eta/s = 0.2 - 0.4$) might indicate that the omitted higher-order terms are a converging series of powers of π/e, which is still below 1/3 (comp. Fig. 10.4(d) for $\eta/s = 0.2 - 0.4$) rather than τ_π/τ. Indeed, in Refs. [34] and [158] we have demonstrated that the series of higher-order terms, omitted in Eqs. (6.36) resp. (6.37), can be effectively resummed in free-streaming limit and thus included into hydrodynamic equations. This procedure will be discussed in the next chapter.

10.2.3. Inclusion of beyond-third-order terms into one-dimensional hydrodynamic equations

In Chapter 3.1.4 I demonstrate how the standard Israel-Stewart formalism can be extended to a third-order formalism. The corresponding equations are obtained from the divergence of the third-order entropy current according to the second-law of thermodynamics. The effect of third-order terms is shown to be considerable in the regime where the second-order formalism is not accurate enough in comparison to kinetic theory. The question thus arises, how strong is the effect of fourth and higher-order terms, not included into the equations discussed here.

An attempt to construct an effective equation, containing terms which are usually neglected in the standard, Israel-Stewart, formalism is the so-called *effective hydrodynamics*, introduced recently by Shuryak and Lubinsky in Ref. [165] and considered for application in calculations of shock waves in a strongly coupled plasmas in Ref. [166]. Effective hydrodynamic approach attempts to include the higher-order terms in the gradient expansion of $T^{\mu\nu}$ in an effective way by introducing terms that are of high order in derivatives but linear in velocity – i.e. terms like $\nabla^2 u$ but not $(\nabla u)^2$. The strategy of the effective hydrodynamic approach is to introduce a hydrodynamic-like representation of $T^{\mu\nu}$ containing all possible terms including terms of different orders in gradients of the velocity. Effectively these terms are included into the expansion of $T^{\mu\nu}$ by introducing a generalized transport coefficient, dependent on operators of form ∇^n, in front of the gradient ∇u. Using the linear response theory the generalized shear coefficient can be expressed in terms of the retarded correlator of the energy-momentum tensor. By virtue of the AdS/CFT correspondence[117], the result of such calculations can be compared with the solutions of linearized gravity equations in the background of the AdS-Schwarzschild black hole.

The approach I introduce here is different in its philosophy; in the form introduced here it is applicable only for one-dimensional boost-invariant expansion. As the starting point, the following phenomenological evolution equation for the shear pressure can be considered:

$$\dot{\pi} = -\frac{\pi}{\tau_\pi} - \frac{4}{3}\frac{\pi}{\tau} + \frac{8}{27}\frac{e}{\tau} + \sum_{n=2}^{\infty} x_n \left(\frac{\pi}{e}\right)^n \frac{e}{\tau} . \tag{10.19}$$

The latter expression is just the standard Israel-Stewart, i.e. second-order, equation (6.36) with an infinite series of higher-order terms added. The functional form of these terms is inspired by the third-order term in Eq. (6.37) and the coefficients x_n are supposed to be time-independent. Thus Eq. (10.19) is supposed to contain *all orders* of corrections to the standard causal dissipative hydrodynamic formalism.

Since all orders of corrections are included into it, Eq. (10.19) can be applied to the *free-streaming* limit. From th kinetic theory point of view, the free-streaming limit is the limit of vanishing collision rate or, in other words, vanishing cross section, $\sigma \to 0$. A free-streaming similar behavior can be observed if the mean free path is large in comparison to the expansion scale, $\lambda/\tau \gg 1$, as was demonstrated in Fig. 10.2 for $\tau_0 = 0.1$ fm/c and $\eta/s = 1$. In hydrodynamics the mean free path corresponds to the relaxation time

τ_π – and the free-streaming limit is the $\tau_\pi \to \infty$ limit. In the free-streaming limit the longitudinal pressure $p_L = p - \pi$ is zero since it cannot be built up by interactions. This means $\pi = p = \frac{e}{3}$. Together with Eqs. (6.29) and (6.30) the conclusions obtained above lead to the following equations in the free-streaming limit:

$$\frac{\pi}{e} = \frac{1}{3} \Leftrightarrow \dot{\left(\frac{\pi}{e}\right)} = 0, \quad \dot{e} = -\frac{e}{\tau}, \quad \dot{T} = 0\,. \tag{10.20}$$

Before proceeding further, one rewrites Eq. (10.19) as follows

$$\dot{\pi} = -\frac{\pi}{\tau_\pi} - \frac{4}{3}\frac{\pi}{\tau} + \frac{8}{27}\frac{e}{\tau} + \frac{\pi^2}{e\tau}\underbrace{\sum_{n=0}^{\infty} x_n \left(\frac{\pi}{e}\right)^n}_{=\mathcal{X}} = -\frac{\pi}{\tau_\pi} - \frac{4}{3}\frac{\pi}{\tau} + \frac{8}{27}\frac{e}{\tau} + \mathcal{X}\frac{\pi^2}{e\tau}\,, \tag{10.21}$$

where $\mathcal{X}$ is a new, in general time-dependent, coefficient. Inserting the relations from Eq. (10.20) into Eq. (10.21) in the $\tau_\pi \to \infty$ limit one obtains

$$\mathcal{X} = -\frac{5}{3}\,. \tag{10.22}$$

In this value the series $\sum_{n=0}^{\infty} x_n \left(\frac{\pi}{e}\right)^n$ is resummed using the free-streaming limit relation $\pi/e = 1/3$. For the resummation scheme presented here, the exact form of the coefficients x_n is not important. The evolution equation for shear pressure takes the form

$$\dot{\pi} = -\frac{\pi}{\tau_\pi} - \frac{4}{3}\frac{\pi}{\tau} + \frac{8}{27}\frac{e}{\tau} - \frac{5}{3}\frac{\pi^2}{e\tau}\,. \tag{10.23}$$

The latter equations will be referred to as "all orders" equations since the value $\mathcal{X} = -\frac{5}{3}$ effectively takes into account all orders of dissipative corrections, which are resummed using their maximum values. One can expect that Eq. (10.23) will be well applicable as long as dissipation is strong and the behavior tends towards free-streaming, i.e. when $Kn = \frac{\tau_\pi}{\tau}$ is large.

To investigate the solutions of Eq. (10.23), in Fig. 10.7 I show the pressure isotropy in comparison with second and third-order hydrodynamics and BAMPS calculations. If the initial time is fixed (Fig. 10.7(a)), solution of Eq. (10.23) seems to be in best agreement with kinetic transport for the largest η/s ratio – this is the regime of largest Kn. However, on a time scale long enough in comparison to the initial time, i.e. the deviation between kinetic transport and "all orders" solutions starts growing and third-order solutions gives a better description of kinetic transport results. This is because as soon as the system is in relaxation regime the ratio π/e, which is a measure of the strength of dissipation, starts decreasing and thus the higher-order corrections should become weaker – but they are included into $\mathcal{X} = -\frac{5}{3}$ by their maximum, $\pi/e = 1/3$, values and the "all orders" solution relaxes slower than the kinetic transport one. On the other hand, terms of the form $(\pi/e)^n \cdot e/\tau_\pi$ are not included into the ansatz Eq. (10.19) and, furthermore, the coefficients in front of these terms cannot be determined in the $\tau_\pi \to \infty$ limit. Such terms might be important in the regime $\tau_\pi \lesssim \tau$, which

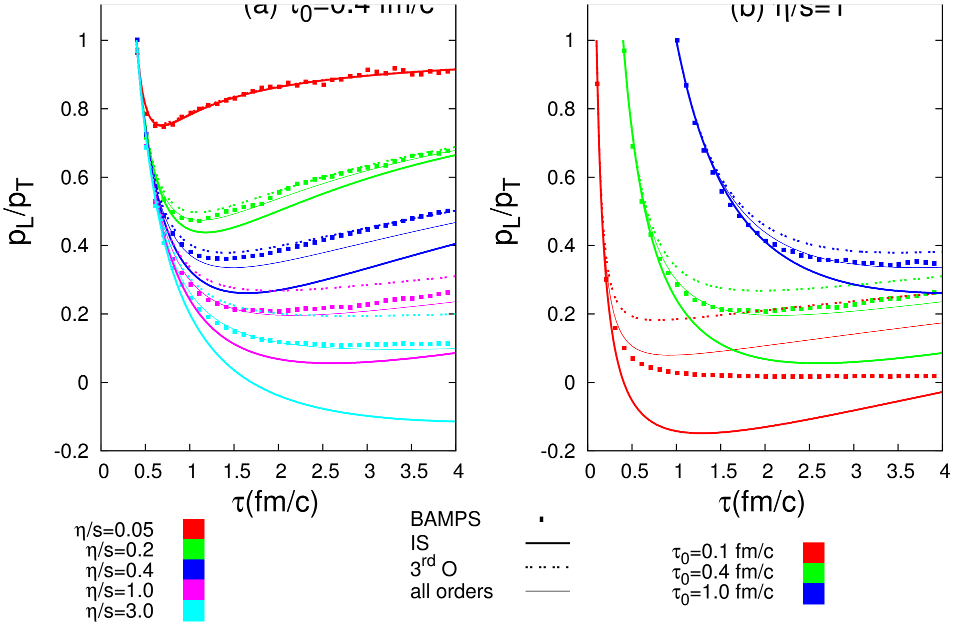

Figure 10.7.: Pressure isotropy from BAMPS, second, third-order and "all orders" hydrodynamic calculations.

again can explain the deviation between "all orders" and kinetic transport calculations for $\eta/s < 0.4$ in Fig. 10.7(a). Note, that a second-order term of form $(\pi/e)^2 \cdot e/\tau_\pi$ indeed was found in a some publications, where hydrodynamic equations were derived from the Boltzmann equation – as e.g. in Refs. [93, 101]. Despite of its phenomenological nature, the "all-orders" equation offers an interesting possibility to push hydrodynamics to the free-streaming limit and to investigate the impact of higher-order terms on the hydrodynamic evolution in a one-dimensional system.

Although the "all-orders" equation includes the effect of higher orders of dissipative corrections, it is still a relaxation-type equation, in which the higher-order terms play the role of damping, which is weakest in the Israel-Stewart's equation. To make the relaxation type nature of Eqs. (6.36) – (6.37) clear, it is instructive to rewrite them in the following form:

$$\dot{\left(\frac{\pi}{e}\right)} = \frac{\frac{\pi_{NS}}{e} - \frac{\pi}{e}}{\tau_\pi} - (\mathcal{X}+1)\frac{\pi^2}{e^2\tau}\,. \tag{10.24}$$

In the latter equation $\mathcal{X} = 0$ for Israel-Stewart equation, so that the last, third-order, term cancels with the one originating from the proper time derivative of e on the left hand side; $\mathcal{X} = 3$ for the third-order equation and $\mathcal{X} = 5/3$, as obtained before. π_{NS} denotes the first-order expression for π, given by Eqs. (3.11) resp. (6.35). The relaxation form of the evolution equation for π leads to a clear interpretation of the higher-order terms: they damp relaxation of the shear pressure π towards the Navier-Stokes solution.

This damping is not present in the Israel-Stewart form of equation ($\mathcal{X} = 0$), and in the third-order equation it is stronger ($\mathcal{X} = 3$) than if all orders are included ($\mathcal{X} = 5/3$), which indicates a possibility of oscillating behavior of the higher-order terms.

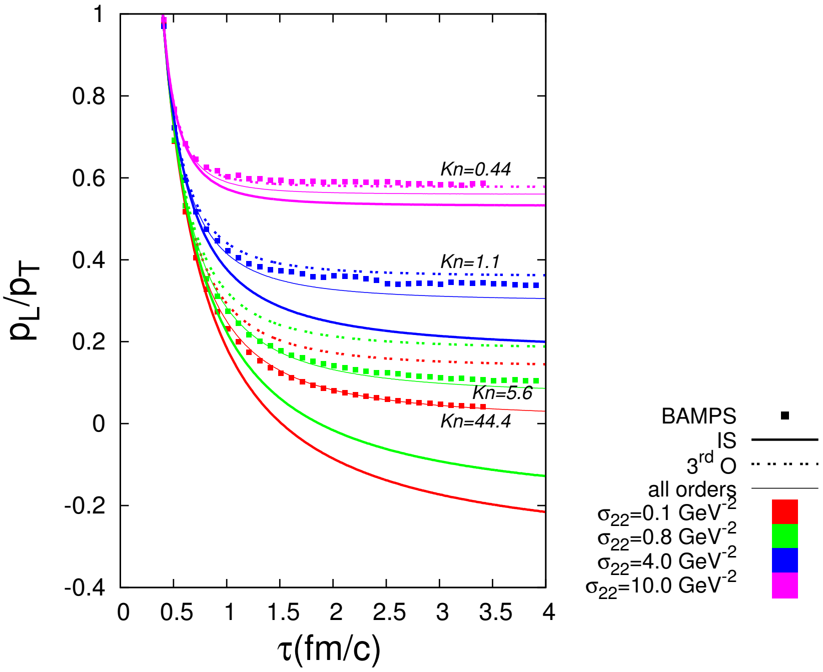

Figure 10.8.: Pressure isotropy from BAMPS, second, third-order and "all orders" hydrodynamic calculations from calculations with constant isotropic cross section.

An interesting test case for a relaxation-type equation of this kind is the case of constant cross section, $\sigma_{22} = const$. If the isotropic cross section is held constant, the relaxation is 'frozen', since the Knudsen number is constant, according to Eqs. (3.21) and (10.4):

$$Kn = \frac{\tau_\pi}{\tau} = \frac{9}{5}(n\sigma_{22}\tau)^{-1} = const\,. \tag{10.25}$$

Since the relaxation towards equilibrium is not possible, π/e ratio and pressure isotropy p_L/p_T will saturate at a certain value. The transition from the "all-orders" towards the third-order solution can be illustrated using the constant cross section regime. Fig. 10.8 demonstrates that at large Kn, which in this study is constant, the "all-orders" formalism is in best agreement with kinetic transport, whereas the third-order solution is over-damped, leading to larger values for pressure isotropy. At $Kn \lesssim 1$ the third-order calculations are much closer to kinetic transport than both "all-orders" and second-order formalism, which is in agreement with the conclusions made earlier in this chapter.

Conclusions.

A direct comparison of the second-oder Israel-Stewart and novel third-order dissipative hydrodynamic and kinetic transport calculations for systems with conserved net particle number has demonstrated that consistent inclusion of third-order terms into hydrodynamic formalism extends its applicability range and helps preventing unphysical behavior of the solutions. If the initial conditions are characterized by value K according to Eq. (10.16), the second-order formalism deviates from kinetic transport calculations by less than 10% for $K \gtrsim 1$, which corresponds to $\eta/s \lesssim 0.2$ for $\tau_0 = 0.4$ fm/c. Third-order calculations can be performed at $\eta/s \lesssim 0.4$, corresponding to $K_0 \gtrsim 0.5$. An effective way to include all orders of corrections into hydrodynamic equations has been introduced. In the limit of large Kn the solutions of this formalism reproduce the solutions of kinetic transport theory remarkably good. However, this so-called "all-orders" formalism is restricted to the one-dimensional case. The novel third-order equations can be applied in a general geometry.

11. Hydrodynamic evolution of a chemically equilibrating Gluon Plasma.

A kinetically equilibrated one-component system is a system with isotropic momentum space distribution, described by a appropriate distribution function. For a gas of ultra-relativistic massless particles (gluons) this is the Boltzmann distribution, which in a most general case can be written as

$$f(x,p) = \frac{dN}{d^3pd^3x} = d \cdot e^{\frac{\mu - u_\alpha p^\alpha}{T}} \tag{11.1}$$

with the degeneracy factor d chemical potential μ and temperature T. The factor $e^{\mu/T}$ often appears under the name of fugacity

$$\lambda \equiv e^{\mu/T} \tag{11.2}$$

and the Boltzmann distribution is then rewritten in the form already given by Eq. (8.5). The fugacity factor is the degree of undersaturation of the phase-space density. In QCD medium the phase space is populated in leading order by the inelastic, $2 \leftrightarrow 3$, processes, which were already introduced in chapter 7. In the particular example of a CGC initial condition, discussed in section 7.4.1, the momentum space contained a oversaturated hard sector and a undersaturated soft sector, which both relaxed – in a almost synchronous way – towards equilibrium via the inelastic pQCD processes.

A chemically equilibrated one-component system is a system of vanishing chemical potential $\mu = 0$ corresponding to $\lambda = 1$. The usual assumption of the most hydrodynamic models is the one of permanent chemical equilibrium, $\lambda = const = 1$ [167]. Historically, this assumption was supported by the success of statistical (thermal) models to reproduce hadron multiplicities by assuming their origin to be a thermal source with a temperature $T \approx 170$ MeV and a nearly zero light quark chemical potential. (see Refs. [168] and [169] for comprehensive overviews). The assumption that the quark-gluonic medium achieves a state close to chemical and kinetic equilibrium prior to the phase transition is supported by the recent observations of saturation of the strange sector particle yields. It was observed in Refs. [170, 171, 172] that the fugacity factor of strangeness rises from approximately 0.7 to 1 if going from peripheral to central $Au + Au$ collisions at RHIC, which indicates that a complete chemical equilibration might be achieved as the density and interaction rate in the system increases.

However, on what time scale an almost complete chemical and kinetic equilibration of quarks and gluons can be achieved in heavy-ion systems – and thus what is the initial time for hydrodynamic approaches which assume chemical and kinetic equilibration – is not completely clear. Moreover, light quarks are expected to be less abundant than gluons in the systems produced in ultrarelativistic heavy-ion collisions and thus the initial quark phase space distribution is far from equilibrium both kinetically and chemically. However, the first attempts to describe the dynamics of a initially disequilibrated quark-gluon system neglected kinetic off-equilibrium effects. Evolution of a chemically disequilibrated but kinetically equilibrated partonic plasma was first studied by MATSUI, SVATITSKY and MCLERRAN in Ref. [173], by BIRO et. al. in Ref. [88] and by SRIVASTAVA et. al. in Ref. [174]. Employing this scenario numerous studies of heavy-ion phenomenology were performed, like e.g. studies of hard photon production rate [175], strangeness [176, 177, 178, 179], open charm [180] and dilepton production [181]. The quite strong assumption of permanent kinetic equilibrium was dropped in the late 90th: dissipative effects [182] and photon and lepton pair production [183, 184, 185] in a chemically and kinetically disequilibrated quark-gluon plasma were studied employing a first-order hydrodynamic formalism. The first application of second-order hydrodynamics to study of a disequilibrated plasma was reported by MURONGA in Ref. [87]. A connection to kinetic theory was attempted by WONG who introduced a study of kinetic and chemical equilibration of a quark-gluonic system employing a relaxation time approximation of the Boltzmann Equation [140]. A Fokker-Planck equation based approach to study shifts of hadron transverse spectra due to collisional energy loss of high energy partons passing through a chemically equilibrating quark-gluon plasma was reported in Ref. [186]. Alternatively, GELIS, KAJANTIE and LAPPI demonstrated how the quark–anti-quark pair production rate – and thus chemical equilibration of the quark sector – can be calculated by numerical integration of the Dirac equation using a classical gluon field model with an ensemble of initial conditions, as demonstrated in Ref. [187].

The issue of chemical equilibration is of central importance for multi-component systems, i.e. mixtures of quarks and gluons in the heavy-ion phenomenology. An approach to hydrodynamic description of relativistic dissipative multi-component systems was reported by MONNAI and HIRANO in Ref. [100]. A multi-component hydrodynamic formalism is important, since different component of a quark-gluon mixture are expected to equilibrate chemically and kinetically on different time scales [88, 89] – in particular the gluonic sector is expected to equilibrate on a shorter time scale. However, the formalism presented in Ref. [100] cannot describe kinetic evolution of each separate component. An alternative multi-component formalism, solving this problem, was derived in this work in Section 3.1.5, but does not include inelastic, i.e. particle number changing, processes.

To what degree chemical equilibration of quark and gluons is achieved at the phase transition might be crucial for modelling of the hadronization process using recombination models [66, 65, 188, 68, 67, 189, 190], which are sensitive to the phase space distribution of quarks and gluons. Since the effect of chemical equilibration will influence the temperature of the system (as Eqs. (11.8) and (11.13) indicate and as will be demonstrated later in this Chapter), it is important for such experimental observables as dilepton [174, 191, 103, 192, 193] and photon [194, 195] yields in heavy-ion collisions.

11.1. Dissipative hydrodynamics in Bjorken's model including particle production and annihilation processes

11.1.1. Rate equation for particle production in anisotropic systems.

In this section I will consider Eq. (2.43) with non-vanishing source term, i.e. the particle number will not be conserved. Particle number changing processes are essential for the chemical equilibration in the system. They are in particular of great importance for modelling of a quark-gluon plasma, since partons can be created in 'bremsstrahlung' pQCD processes and annihilated in the reverse channel.

The importance of radiative processes for an expanding partonic system can be easily understood as follows. In an initially thermalized expanding system with conserved particle number the particle density decreases with time, $n \propto \tau^{-1}$. For an ideal fluid the temperature would evolve according to Eq.(6.34), $T \propto \tau^{-1/3}$, and the fugacity would thus stay constant, $\lambda \propto n/T^3 = const.$ If dissipation is present, the dissipated energy is turned into the inner energy of the system, i.e. into heat, as follows from Eq.(6.31), and the temperature decreases slower than in ideal hydrodynamics: $T \propto \tau^{-1/3+\delta}$ with $\delta > 0$. This leads to a continuous decrease of the fugacity: $\lambda \propto n/T^3 \propto \tau^{-3\delta}$. The system is thus driven off chemical equilibrium, which is the $\lambda = 1$ state. Chemical equilibrium can be restored if the particle number increases and thus the particle density decreases slower than τ^{-1}, i.e. if particles are produced in inelastic processes.

As already discussed in Section 2.4.3, in presence of inelastic particle number changing processes – which are in lowest order QCD the $2 \to 3$ and reverse processes – the particle number four-current N^μ is not conserved. From the point of view of kinetic theory the particle number current is defined as the 1st moment of the phase space distribution $f(x,p)$:

$$N^\mu \equiv \int p^\mu f(x,p) d\Gamma \, . \tag{11.3}$$

The divergence of the particle four-current $\partial_\mu N^\mu$ can be written as 0th moment of the collision term, as already demonstrated earlier in Eq. (2.43):

$$\partial_\mu N^\mu = \int d\Gamma C[f] = J \, . \tag{11.4}$$

The explicit form of the collision term is given in Eqs. (7.6) and (7.7). For a one-dimensional boost-invariant expansion the left hand side of the latter equation can be rewritten as follows

$$\partial_\mu N^\mu = \dot{n} + \frac{n}{\tau} = J \, . \tag{11.5}$$

If particle number conservation is considered, the source term J is identical 0. From the kinetic theory point of view, the origin of J is the inelastic part of the collision term C_{23}, comp. Eq. (7.7). As demonstrated in Appendix D, if one considers the differential cross section $d\sigma_{23}/d\Omega$ for the inelastic 2 → 3 processes to be angle independent (isotropic), Eq. (11.5) can be written for a one-dimensional boost-invariant system in the following form:

$$\dot{n} + \frac{n}{\tau} = \frac{1}{2} n R_{23} - \frac{1}{3} n R_{32} = \frac{1}{2} n^2 \left(1 - \lambda\right) \sigma_{23} \,, \tag{11.6}$$

with σ_{23} being the total – i.e. angle integrated – cross section.

Equation (11.6) constitutes the evolution equation for the particle density in a anisotropic system in presence of inelastic processes. The derivation of Eq. (11.6) given in Appendix D is consistent with Grad's approximation for the off-equilibrium, anisotropic, distribution function, which means that it can be included into the set of second and third-order dissipative hydrodynamic equations derived in this work. However, before I discuss the hydrodynamic equations including particle production, I remark that the concept of particle density and particle number, as used here, is an "artifact" of the microscopic, kinetic picture of the QGP. In numerous implementations of dissipative hydrodynamics [62, 47, 116, 196, 197] the authors do not introduce an independent evolution equation for the particle number density for each particle species. Rather, the temperature T is often defined via the energy density e:. For a Boltzmann gas this means

$$T = \left(\frac{\pi^2}{3g} \cdot e \right)^{1/4} \,. \tag{11.7}$$

This definition implies full chemical equilibration of the system, $\lambda = 1$, at all times during the evolution. However, this assumption leads to a contradiction with the assumption of non-vanishing viscosity, as demonstrated in the following. For a one dimensional boost-invariant system from Eqs. (11.7) and (6.30) follows

$$\frac{\dot{T}}{T} = -\frac{1}{3\tau} + \frac{1}{4} \frac{\pi}{e\tau} \,. \tag{11.8}$$

On the other hand, using the Boltzmann distribution (6.13) with $\lambda = 1$ one obtains $n/T^3 = const$, which leads using Eq. (11.8) to

$$\frac{\dot{n}}{n} = 3\frac{\dot{T}}{T} = -\frac{1}{\tau} + \frac{3}{4} \frac{\pi}{e\tau} \,. \tag{11.9}$$

If $\lambda = 1$ the latter equation is only consistent with Eq. (11.6) if $\pi/e = 0$, i.e. if the evolution of the medium is in fact ideal. Thus, Eq. (11.7) – and the $\lambda = const = 1$ assumption – is inconsistent with the assumption of finite shear viscosity or relaxation time, which means it is only applicable in the limit of infinitely large inelastic collision rates. In this sense $\lambda = 1$ scenario can be interpreted as instantaneous chemical equilibration scenario.

11.1.2. Second-order hydrodynamic evolution equations including number changing processes.

For a one-dimensional boost-invariant system Eq. (3.19) can be written using Eq. (6.30) as

$$\dot{\pi} = -\frac{\pi}{\tau_\pi} + \frac{8}{27}\frac{e}{\tau} - \frac{1}{2}\frac{\pi}{\tau} + + \frac{1}{2}\pi\frac{\dot{e}}{e} + \frac{1}{2}\pi\frac{\dot{T}}{T}\,. \tag{11.10}$$

Dependent on the considered scenario of chemical evolution, either Eq. (11.8) or $T = e/(3n)$ together with Eq. (11.6) can be used in the evolution equation for π. However, one finds that for the both scenarios – the one of instantaneous chemical equilibration $\lambda(\tau) = 1$ and the one of chemical equilibration via particle production and annihilation with a given inelastic cross section σ_{23} – the second-order evolution equation for π can be written in a universal way.

$$\dot{\pi} = -\frac{\pi}{\tau_\pi} - \frac{4}{3}\frac{\pi}{\tau} + \frac{8}{27}\frac{e}{\tau} - \frac{1}{4}\pi n\,(1-\lambda)\,\sigma_{23}\,. \tag{11.11}$$

I refer to the latter equation as the second-order equation. The case of *instantaneous chemical equilibration* is realized by setting $\lambda = 1$ in Eq. (11.11), which has to be solved together with Eq. (6.30). If only elastic processes are considered, the inelastic cross section σ_{23} is identical 0 and Eq. (11.11) is identical with Eq. (6.36). In the case of *finite inelastic cross section*, i.e. in a system with particle production and annihilation processes, Eq. (11.11) is coupled to Eqs. (6.30) and (11.6). A compact overview of the different scenarios and corresponding equations is given in Appendix C.

11.1.3. Third-order hydrodynamic evolution equations including number changing processes.

For a one-dimensional system of Boltzmann particles the general third-order equation (3.33) can be written as

$$\dot{\pi} = -\frac{\pi}{\tau_\pi} + \frac{8}{27}\frac{e}{\tau} - \frac{1}{2}\frac{\pi}{\tau} + \frac{1}{2}\pi\frac{\dot{T}}{T} + \frac{1}{2}\pi\frac{\dot{e}}{e} + \frac{3}{2}\frac{\pi^2}{e\tau} + \frac{3}{2}\frac{\pi^2}{e}\frac{\dot{T}}{T} + \frac{3}{2}\frac{\pi^2}{e}\frac{\dot{e}}{e} - 4\frac{\pi^2}{e\tau}\,. \tag{11.12}$$

In the third-order formalism the scenario of instantaneous chemical equilibration will not be considered. Indeed, since instantaneous chemical equilibration implies infinite inelastic collision rates and small π/e ratio (as demonstrated in the discussion after Eq. (11.9)) the use of the third-order formalism is rather inconsistent in this case. In a chemically equilibrating system in presence of inelastic processes the temperature $T = e/(3n)$ evolves according to

$$\frac{\dot{T}}{T} = \frac{\dot{e}}{e} - \frac{\dot{n}}{n} = -\frac{1}{3\tau} + \frac{\pi}{e\tau} - \frac{1}{2}n\,(1-\lambda)\,\sigma_{23}\,. \tag{11.13}$$

Keeping only terms up to third order one thus obtains

$$\dot{\pi} = -\frac{\pi}{\tau_\pi} - \frac{4}{3}\frac{\pi}{\tau} + \frac{8}{27}\frac{e}{\tau} - 3\frac{\pi^2}{e\tau} - \frac{1}{4}\left(1 + 3\frac{\pi}{e}\right)\pi n(1-\lambda)\sigma_{23}\,. \tag{11.14}$$

I refer to the latter equation as the third-order equation. It has to be solved together with Eqs. (6.30) and (11.6). The scenario of conserved particle number is realized by setting $\sigma_{23} = 0$, in which case Eq. (11.14) is identical with Eq. (6.37) obtained earlier.

11.2. Results of hydrodynamic calculations.

In this Section I discuss solutions of the hydrodynamic equations derived previously for systems with non-conserved net particle number. The production and annihilation channels $2 \leftrightarrow 3$ are included via the rate equation (11.6). In order to calculate the rates inelastic cross section has to be introduced. In the calculations presented here the total isotropic inelastic cross section σ_{23} is parametrized as follows

$$\sigma_{23} = \frac{k}{\lambda T^2 (4 - \ln \lambda)} , \tag{11.15}$$

where T denotes the effective temperature, λ the fugacity and k is a numerical factor which can be chosen arbitrary. With the inelastic cross section parametrized this way, the η/s ratio is approximately a constant, as demonstrated in Ref. [35] and will be discussed later in this work. However, the value of η/s is not completely determined by the inelastic cross section (or, to be more precise, transport rate), since the elastic processes do contribute to it as well. Although it was demonstrated in Chapter 9 in this work and in Refs. [41, 33] that within pQCD framework the contribution from inelastic processes is dominant, with isotropic cross sections considered in this Section this is not necessary the case. Thus, the value of η/s can be chosen arbitrary for the hydrodynamic calculations which will be presented here. In calculations with constant η/s the value 0.35 is chosen, i.e. roughly the upper limit deduced from comparisons with elliptic flow measurements at RHIC [116]. The solutions presented in this section are obtained using the setups summarized in the following table:

Type of initial condition	Parameters
I. Chemically and kinetically equilibrated with constant τ_π/τ and σ_{23}	$\tau_\pi/\tau = 0.5$, $\tau_0 = 0.4$ fm/c $T_0 = 0.5$ GeV, $\lambda_0 = 1$, $\pi_0/e_0 = 0$
II. Chemically and kinetically equilibrated	$\eta/s = 0.35$, $\tau_0 = 0.4$ fm/c, $T_0 = 0.5$ GeV, $\lambda_0 = 1$, $\pi_0/e_0 = 0$
III. Chemically and kinetically disequilibrated	$\eta/s = 0.35$, $\tau_0 = 0.4$ fm/c, $T_0 = 0.5/0.2^{1/4}$ GeV, $\lambda_0 = 0.2$, $\pi_0/e_0 = 0.1$

The solutions to be discussed in the following Sections are obtained employing second and third-order hydrodynamics equations including particle production processes. In addition, the particle number conservation and instantaneous chemical equilibration scenarios are considered within the second-order formalism.

11.2.1. Constant Knudsen number and inelastic cross section with chemically and kinetically equilibrated initial condition.

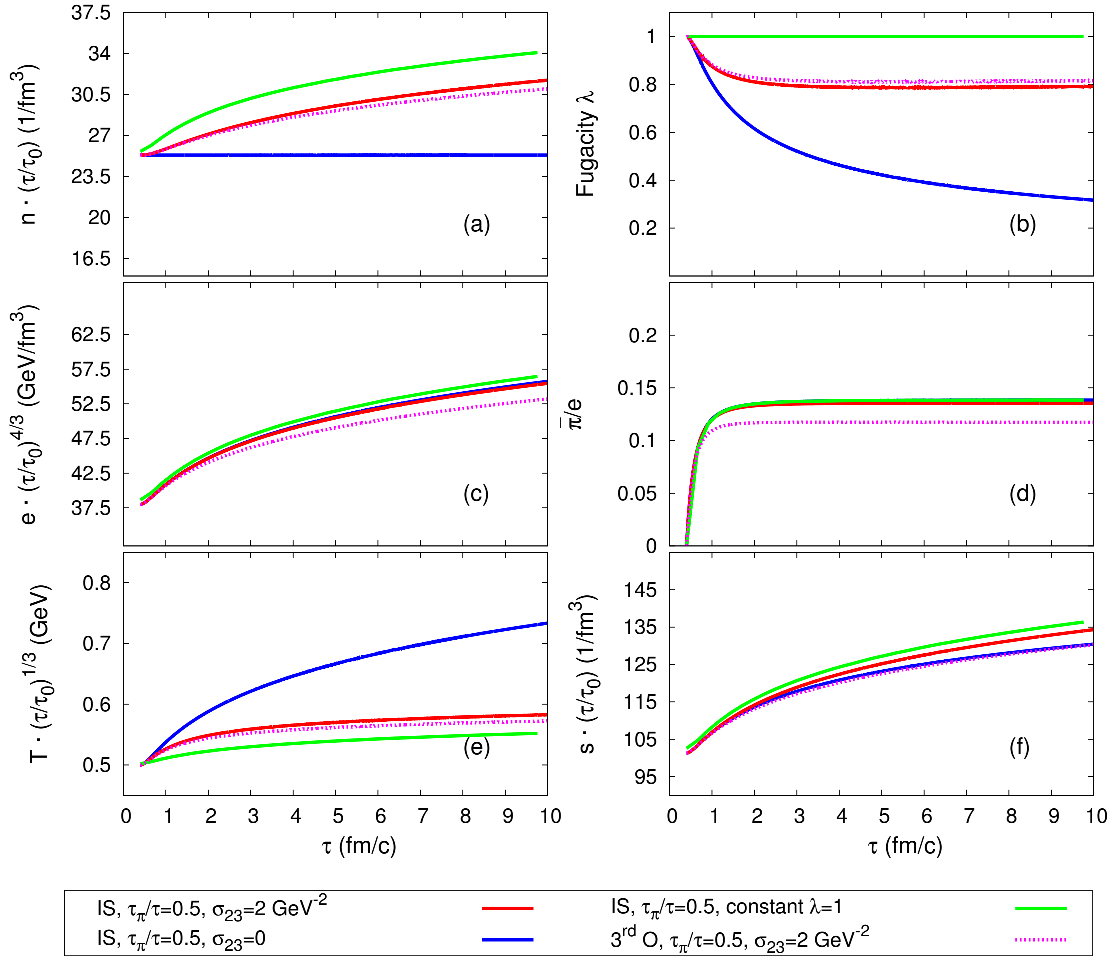

Figure 11.1.: Rescaled particle density (a), fugacity b), energy density (c), π/e ratio (d), effective temperature (e) and entropy density (f) from solutions of second and third-order hydrodynamic equations with chemically and kinetically equilibrated initial condition, constant $Kn = \tau_\pi/\tau = 0.5$ and constant inelastic cross section $\sigma_{23} = 2$ GeV^{-2}.

With the setup chosen here the interplay between the chemical and kinetic equilibration processes can be studied. For the one-dimensional system considered throughout this work, the relaxation time $\tau_\pi = Kn \cdot \tau$ is the same for all scenarios to be discussed here – due to the choice of a constant Knudsen number the relaxation time is independent of the dynamics. Since the inelastic cross section is constant, the possible differences of the solutions can only be due to different forms of equations. The scenario of constant

Knudsen number and constant inelastic cross section is rather academic, as the results of BAMPS calculations including pQCD processes, presented in Chapter 9, indicate.

For the results presented in Fig. 11.1 the second-order formalism is solved considering particle number changing processes (solid red lines), particle number conservation (solid blue lines) and instantaneous chemical equilibration (solid green lines). The third-order formalism is solved including particle number changing processes (dashed magenta lines). The results on n, e and T are rescaled by the ideal hydrodynamic evolution factors [comp. Eqs. (6.32)-(6.34)]. Comparing the results on shear pressure to energy density ration in Fig. 11.1(d) one can conclude that kinetic equilibration is rather independent of the chemical processes in the system. If τ_π is the same, both particle conservation and particle production scenarios lead to nearly same values of π/e. Same is observed for the energy density in Fig. 11.1(c), since its evolution is determined by π/e according to Eq. (6.30). The solutions of the third-order formalism are closer to kinetic equilibrium, as indicated by the smaller π/e ratio in 11.1(d) and a smaller rescaled energy density in 11.1(c). This is the effect of the additional, third-order damping term in the evolution equation for π, as already discussed in Chapter 10.

On the other hand, the chemical evolution of the system is only slightly affected by the degree of kinetic equilibration, as demonstrated by the particle number density evolution in Fig. 11.1(a) for second and third order calculations with non-vanishing inelastic cross section. The particle number density is nearly the same although a more significant difference is observed for π/e from second and third-order calculations. Accordingly, the effective temperature and the fugacity are nearly the same in both cases.

Inclusion of particle number changing processes has of course a significant effect on particle number density, fugacity and temperature if they are compared to the results obtained from the particle number conservation and instantaneous chemical equilibration scenarios. A constant $\lambda = 1$ is associated to the largest amount of particle and entropy production, as shown in Fig. 11.1(a) and (e). Temperature decreases much slower if particle number is conserved, as shown in Fig. 11.1(e). This, together with π/e being insensitive to particle production, should have a significant effect on transverse spectra, according to Eq. (8.1). The effect of hydrodynamic evolution on the spectra will be studied later in this Chapter.

Main conclusion that can be drawn from the comparison of the results presented in this Section for constant Kn and σ_{23} is that the chemical and kinetic evolution of the system are only weakly coupled to each other in scope of the formalism considered here.

11.2.2. Constant η/s and time-dependent inelastic cross section with chemically and kinetically equilibrated initial condition.

The results presented in Fig. 11.2 are obtained using a constant η/s value and a time-dependent inelastic cross section, parametrized according to Eq. (11.15) with $k = 1$ (comp. discussion in Ref. [35], where Fig. 11.2 was first published). The results are rescaled in the same manner as in Fig. 11.1. With the time-dependent inelastic cross section and constant η/s the system is able to relax towards equilibrium chemically and kinetically after a certain time, as indicated by increasing fugacity in 11.2(b) and

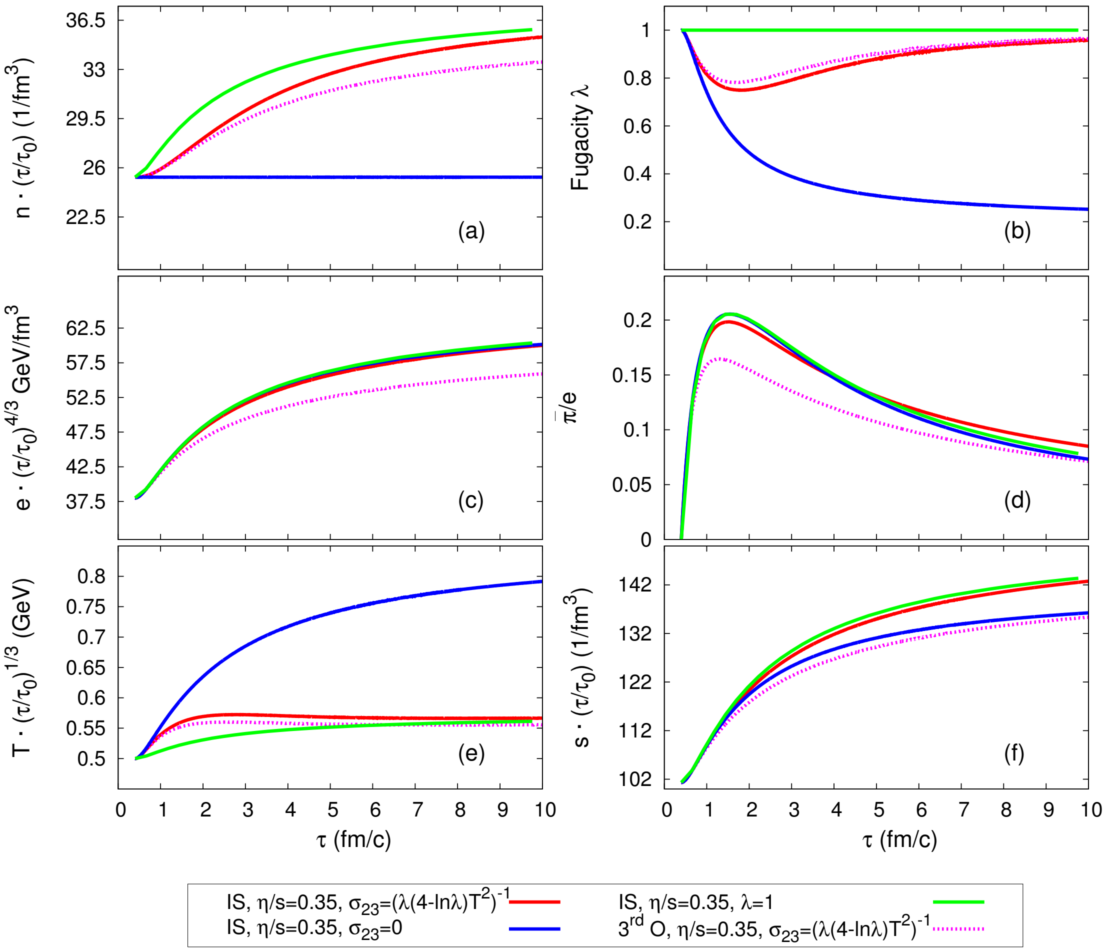

Figure 11.2.: Solution of second and third-order hydrodynamic equations with chemically and kinetically equilibrated initial condition, constant $\eta/s = 0.35$ and time dependent inelastic cross section given by Eq. (11.15) with $k = 1$.

decreasing π/e ratio in 11.2(d). Similar to the situation in Fig. 11.1, the kinetic evolution is marginally influenced by the details of microscopic interactions, since the scenarios with conserved and time-dependent particle number lead to approximately same values of π/e, as demonstrated in Fig. 11.2(d). Correspondingly, the energy density in 11.2(c) is insensitive to the chemical evolution of the system.

The particle number density evolution is only weakly sensitive to the kinetic equilibration process, as follows from the comparison of second and third-order calculations in Fig. 11.2(a) and (b). This is consistent with the observations from previous Section. The effect of chemical equilibration on evolution of the temperature is significant – a runaway loss of chemical equilibrium observed in Fig. 11.2(b) for the $\sigma_{23} = 0$ scenario leads to a significantly slower decrease of the temperature in Fig. 11.2(e) in comparison to the scenario with non-vanishing σ_{23}. The possibility of particle production and annihilation leads to an increased entropy density; at the same time, inclusion of third-order terms decreases the entropy density, as demonstrated in Fig. 11.2(f). If particle number changing processes are included, the solutions converge to the solutions obtained for the scenario of instantaneous chemical equilibration after a certain time. However, there are observable differences in the temperature and particle density evolution.

Comparison of the results obtained with constant η/s and time-dependent σ_{23} confirms the conclusion made from the analysis of constant Kn and σ_{23} scenario. The chemical and kinetic evolutions are weakly coupled to each other. Inclusion of chemical equilibration via particle number changing processes has a significant effect on the temperature of the system.

11.2.3. Constant η/s, chemically and kinetically disequilibrated initial condition.

If the initial condition is chemically and kinetically equilibrated, the evolution of the system goes through a phase of disequilibrium to a phase of relaxation towards equilibrium. In this case evolution of the instantaneous chemical equilibration scenario differs only marginally from evolution of a chemically equilibrating system, as one could observe in the previous Section. However, the assumption of an equilibrated initial state for the QGP is a strong assumption. An examples of chemically and kinetically disequilibrated initial conditions is the color glass condensate discussed in Chapter 7.4.1 and in Refs. [147, 142, 150, 198, 199, 71, 72]. In this section I consider a system with constant η/s , time-dependent σ_{23} and a disequilibrated initial condition with $\pi(\tau_0)/e(\tau_0) = 0.1$ and $\lambda(\tau_0) = 0.2$ in order to demonstrate the sensitivity of the results to the initial loss of equilibrium. The results are shown in Fig. 11.3 and are rescaled like in the previous two sections.

With the disequilibrated initial condition the difference between the instantaneous chemical equilibration scenario and and a scenario with finite inelastic cross section becomes more pronounced than in previous two sections. The particle, energy and entropy densities from calculations with finite inelastic cross section converge slower towards the $\lambda = 1$ result, as shown in Fig. 11.3(a), (c) and (f).

The particle number conservation scenario leads to a significantly larger temperature than the chemical equilibration scenarios – comp. Fig. 11.3(c). This difference is even larger than the one observed with equilibrated initial conditions. This again stresses the importance of the proper treatment of particle number evolution in scope of hydrodynamic formalisms.

The differences between second and third-order calculations also become more pronounced with disequilibrated initial conditions. The particle, energy and entropy densities calculated with third-order formalism are smaller than the second-order results, as shown in Fig. 11.3(a), (c) and (f).

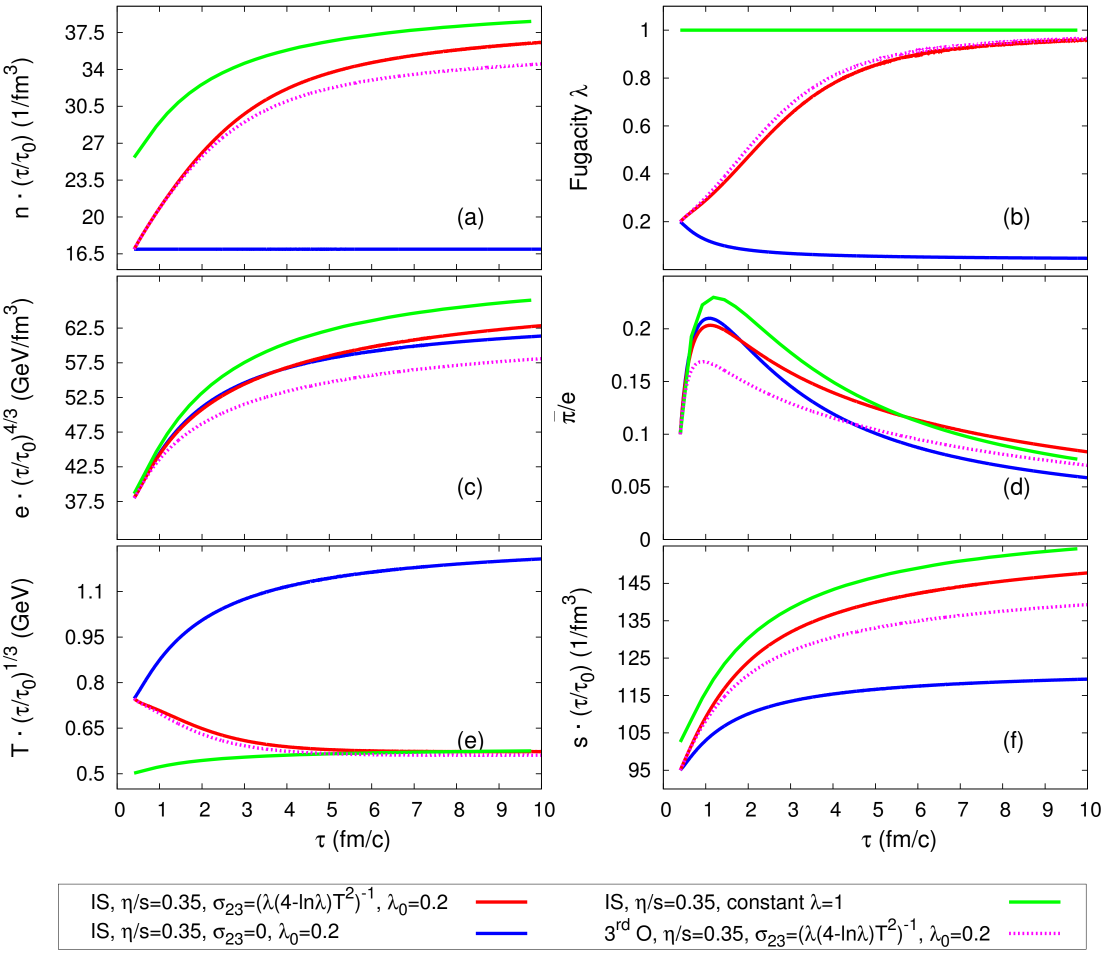

Figure 11.3.: Solution of second and third-order hydrodynamic equations with chemically and kinetically disequilibrated initial condition, constant $\eta/s = 0.35$ and time dependent inelastic cross section given by Eq. (11.15) with $k = 1$.

11.2.4. Effect of chemical evolution on transverse spectra.

In the previous three Sections a proper treatment of chemical evolution in hydrodynamic formalism was shown to have a significant effect on the effective temperature T. This observable is accessible in the heavy-ion experiments via the transverse spectra of such electromagnetic probes as photons or dileptons, which do not interact with the system after the production time point and for this reason already in the late 70s were considered a good probe of the early stage of heavy-ion collisions [200, 3]. The effect of momentum-space anisotropy on the dilepton spectra was studied by Martinez and Strickland employing second-order hydrodynamic formalism with conserved particle number in Ref. [103].

In this section I present the transverse spectra reconstructed from hydrodynamic calculations presented in Sections 11.2.2 and 11.2.3. Hydrodynamic evolution equations (11.11), (11.14) and (11.6) were derived using the off-equilibrium distribution from Eq. (8.1). The normalized transverse spectrum

$$\frac{dN}{N p_T dp_T} = \int p_0 f \, dy d\varphi \tag{11.16}$$

can be calculated by a numerical integration of Eq. (8.1) using the results of second-order hydrodynamic calculations presented in Figs. 11.2 and 11.3.

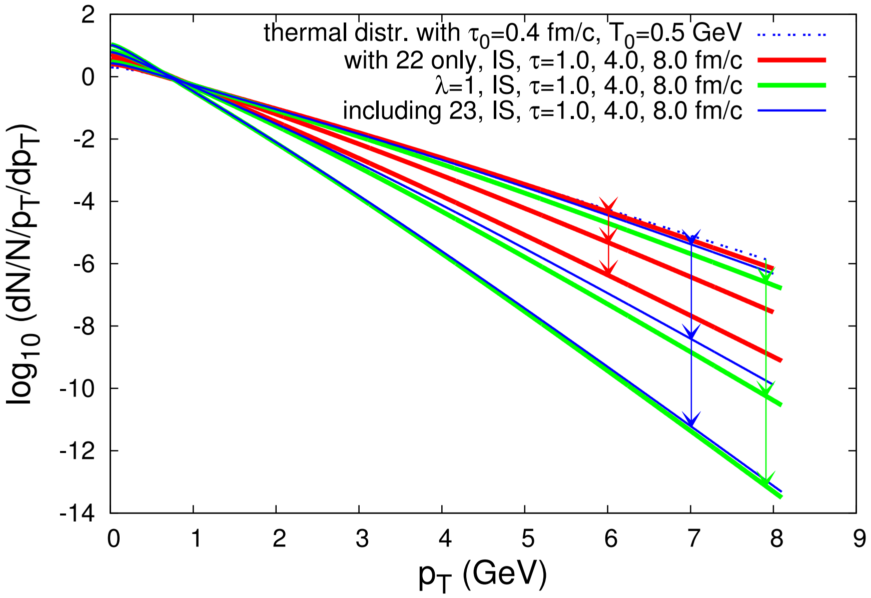

Figure 11.4.: Transverse spectra reconstructed from the results presented in Fig. 11.2 at $\tau = 0.4$, 1.0, 4.0 and 8.0 fm/c. Initial condition is equilibrated chemically and kinetically and thus unique for all three scenarios. Arrows indicate the transitions between sequential time points.

The normalized transverse spectra at different time points obtained from calculations with equilibrated initial conditions for different scenarios of chemical evolution (particle number conservation, particle production and annihilation and instantaneous chemical equilibration) are shown in Fig. 11.4. In all three scenarios the evolution starts with the same, equilibrated, initial condition. One observes that the spectra are sensitive to the chemical evolution of the system: without the inelastic collisions (red lines) a strong deviation from chemical equilibrium leads to a significantly flatter spectrum. The difference between the spectra obtained with and without inclusion of inelastic processes (blue and red lines) becomes more pronounced at later times ($\tau = 8$ fm/c). The spectra obtained with the scenario of instantaneous chemical equilibration (red lines) are nearly identical with the ones of a chemically equilibrating system (blue lines) although small differences are observable at intermediate time $\tau = 4$ fm/c.

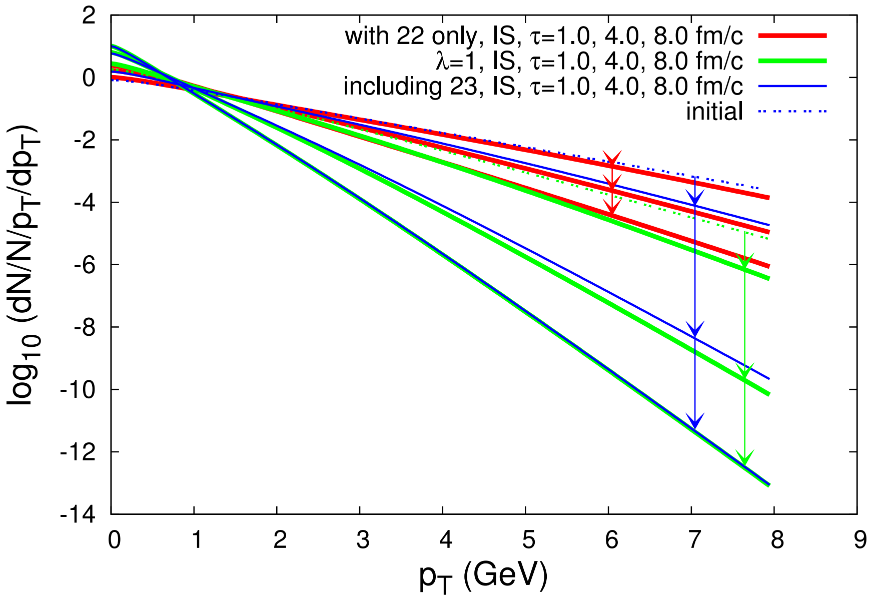

Figure 11.5.: Transverse spectra reconstructed from the results presented in Fig. 11.3 at $\tau = 0.4$, 1.0, 4.0 and 8.0 fm/c. Initial condition is disequilibrated both chemically and kinetically. For the $\lambda = 1$ scenario the initial condition is disequilibrated only kinetically. Arrows indicate the transitions between sequential time points.

If a chemically and kinetically disequilibrated initial condition is considered, as for the results presented in Fig. 11.3, the difference between the spectra from the three scenarios becomes larger than in the case of fully equilibrated initial conditions. Fig. 11.5 demonstrates the spectra reconstructed using the results from Fig.11.3. If the initial state is chemically disequilibrated, there is a clear difference between the spectra from the scenarios of instantaneous (green lines) and dynamical (blue lines) chemical equilibration at early ($\tau = 1.0$ fm/c) times. At late times ($\tau = 8.0$ fm/c), as equilibrium is nearly restored, both scenarios are again almost indistinguishable. Again, if only elastic scatterings are considered (red lines), the spectra are considerably flatter throughout the evolution, since the deviation from chemical equilibrium increases dramatically.

The observed differences of the spectra obtained using Grad's approximation from Eq. (8.1) are clearly due to different evolution of the effective temperature, which is mainly sensitive to the evolution of the particle number density (since π/e ratio shows only weak sensitivity to the chemical evolution of the system, as shown in Figs. 11.1, 11.2 and 11.3).

Conclusions I.

To conclude, the inclusion of chemical equilibration via particle production and annihilation processes into hydrodynamic formalism proves to be important – in the first place with respect to evolution of the effective temperature T. This observable reveals the strongest sensitivity to the details of microscopic processes considered in an expanding system with finite interaction rates, such as the QGP. The transverse spectra are highly sensitive to the degree of chemical equilibration in the system. Strong deviations from chemical equilibration lead to strong modifications of the temperature T and thus of the slopes of transverse spectra, which are both important observables with respect to electromagnetic probes in heavy-ions collisions.

11.3. Comparison between dissipative hydrodynamic calculations and BAMPS results for a system with non-conserved particle number.

In this section the results of hydrodynamic calculations including particle production and annihilation are compared to the results obtained from kinetic transport model BAMPS, which was introduced in Chapter 7. The comparisons presented in this section are analogous to the ones presented in Chapter 10, where the particle number in the system was assumed to be constant. The results presented in this Section were previously published in Ref. [35].

In BAMPS we consider isotropic cross sections. For the inelastic processes the total cross section is calculated via Eq. (11.15) and for the $3 \to 2$ channel one obtains $\mathcal{I}_{32} = 12 g \pi^2 \sigma_{23}$. For the elastic channel $2 \to 2$ the cross section is chosen to be identical with the inelastic one: $\sigma_{22} = \sigma_{23}$. The choice of isotropic cross sections for the collision processes makes a comparison with hydrodynamic formalism easier, since the rates R_{23} and R_{32} in the rate equation (11.6) can be calculated analytically and Eq. (11.6) can be solved directly without any input from BAMPS.

In order to find a parametrization for the shear viscosity coefficient η, the η/s ratio is extracted from BAMPS calculations. This is done via Eq. (9.3) with $s = 4n - n \ln \lambda$ in the same manner as for pQCD cross sections in Section 9.1. The results on η/s as function of proper time τ in BAMPS calculations with $k = 0.5,\ 1,\ 3$ and 6 in Eq. (11.15) are shown in Fig. 11.6. The extracted η/s ratio is in a good approximation constant in time.

The values

$$\eta/s\ (k) = 0.05\ (6), \quad 0.1\ (3), \quad 0.35\ (1), \quad 0.75\ (0.5)$$

are used together with Eq. (11.15) to solve the set of hydrodynamic equations (11.6), (6.30), (11.11) and (11.14). The solutions of second (Israel-Stewart) and third-order hydrodynamic equations are compared with the corresponding BAMPS calculations in Figs.11.7-11.11.

In Figs. 11.7 and 11.8 we observe that the energy density and the shear pressure from

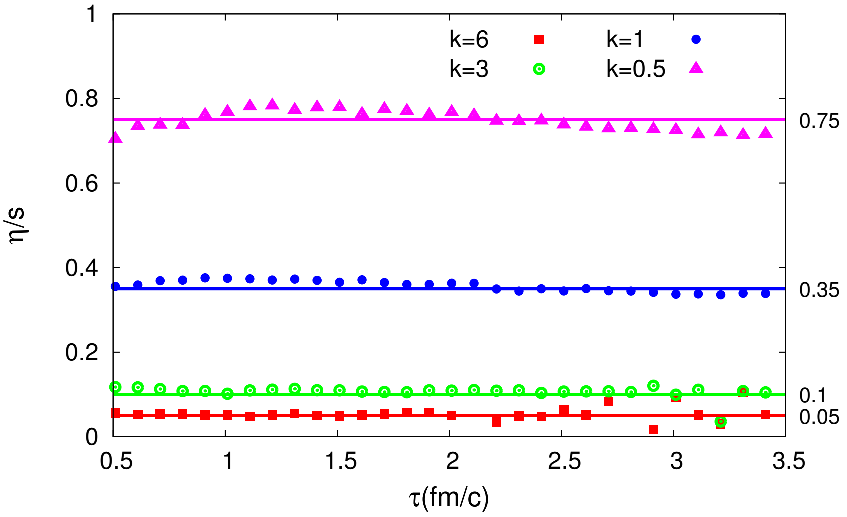

Figure 11.6.: Shear viscosity to entropy density ratio as function of time extracted from BAMPS calculations using Eq. (9.3). In BAMPS calculations isotropic elastic and inelastic cross sections $\sigma_{22} = \sigma_{23}$ are parametrized via Eq. (11.15) with $k = 0.5,\ 1,\ 3$ and 6.

the third-order hydrodynamic calculations agree perfectly with the BAMPS results even for large η/s values. In contrast, the viscous effect is overestimated by the second-order equations. This becomes significant for large η/s values, which mark the applicability boundary of the second-order approach. These findings are in line with observations in Chapter 10 and in Ref. [34], where particle changing processes were not taken into account.

The difference in the particle number density (Fig. 11.9) between the hydrodynamic and BAMPS results is large at large η/s values. Although both second and third-order equations give larger densities than those in BAMPS, the third-order results are closer to the ones from BAMPS . On the other hand, looking at the temperature T (Fig. 11.10) and the fugacity λ (Fig. 11.11) one observes that the second-order results show better agreement with the BAMPS results than the third-order ones. However, it is difficult to make conclusions about applicability of a hydrodynamic approach based on the observables T and λ. These quantities are defined via e and n, but not solved directly from the hydrodynamic equations. If we consider the particle number conservation, the results on T and λ from the third-order calculations are in very good agreement with those from BAMPS, as can be concluded from the observations in Chapter 10 and Ref. [34]. In the situation considered here, small differences between hydrodynamic and kinetic transport results on both key observables e and n translate into differences in T and λ in a non-trivial way.

To understand the differences in particle number densities between the hydrodynamic and BAMPS results, I examine Eq. (11.6), which is valid by virtue of Grad's approxi-

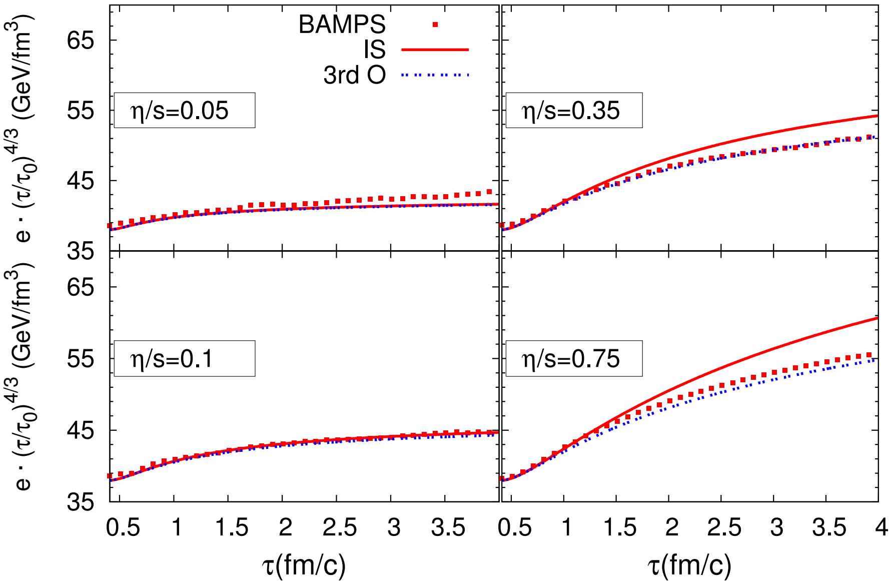

Figure 11.7.: Rescaled energy density e from BAMPS, second and third-order hydrodynamic calculations. Particle production included via isotropic cross section given by Eq. (11.15).

mation (8.1). For this calculate the difference of the rates and the right hand side of Eq. (11.6) are calculated using the actual values of R_{23}, R_{32}, n, λ, and σ_{23} extracted from the BAMPS. The results are shown in Fig. 11.12. Except for the case of $\eta/s = 0.05$, $n^2(1-\lambda)\sigma_{23}/2$ is always larger than $n \cdot R_{23}/2 - n \cdot R_{32}/3$, which leads to a stronger particle production in the hydrodynamic than in the transport approach, as seen in Fig. 11.9. This indicates that the approximate distribution (8.1) must deviate from the one extracted from BAMPS. In fact, the deviations between Grad's approximation and the particle distribution extracted from BAMPS were already quantified and discussed in Chapter 8. In Fig. 11.13 the differences between BAMPS and hydrodynamic spectra are shown for calculations with $k = 0.5$, 1 and 3. The hydrodynamic spectra are reconstructed using the results of BAMPS calculations together with Eq. (8.1). With the values of $k = 0.5 - 1$, the deviations are of order of 10% for $p_T < 3$ GeV, which is consistent with the observations in Chapter 8. For these values of k, corresponding to $\eta/s = 0.35 - 0.75$, Eq. (11.6) is not exactly satisfied, as demonstrated in Fig. 11.12. Thus, the differences in evolution of the particle number density in hydrodynamic formalism and in BAMPS can be explained due to insufficient accuracy of Grad's approximation for the off-equilibrium distribution function. Since the evolution equations for the shear pressure π and the expression for the viscosity coefficient η are derived using Grad's approximation, the observed non-conformance between the latter and the actual off-equilibrium distribution in kinetic transport calculation leads to non-conformance of the macroscopic observables.

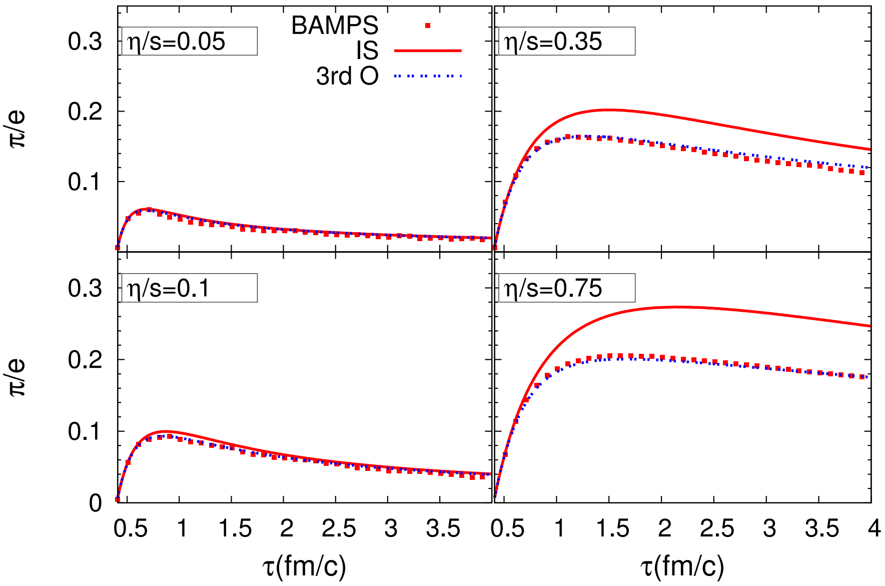

Figure 11.8.: Shear pressure to energy density ratio π/e from BAMPS, second and third-order hydrodynamic calculations. Particle production included via isotropic cross section given by Eq. (11.15).

Conclusions II.

In this section the shear viscosity to entropy density ratio η/s was extracted from BAMPS calculations with isotropic elastic and inelastic cross sections and employed to solve hydrodynamic equations for systems with non-constant particle number. Comparisons between hydrodynamic and kinetic transport calculations demonstrated a reasonably good agreement concerning the bulk observables e and n. The visible deviations in particle number are due to insufficient accuracy of the rate equation (11.6). The third-order equations provide a better description of kinetic transport results considering the energy and particle densities e and n and the shear pressure to energy density ratio π/e; they lead to a faster decrease of the temperature and larger values of fugacity. The second-order equations provide a better description of T and λ, but lead to larger deviations considering all other observables.

Since the approximation-based evolution equations for n, e and π are solved directly in hydrodynamic formalism, these quantities should be used to quantify the accuracy of hydrodynamic description. However, the interplay between the values of π, e and n is non-trivial and a straight-forward quantitative analysis of deviations between hydrodynamic and BAMPS results like in Chapter 10 becomes complicated. Quantitatively, the third-order formalism provides a better description of kinetic transport results on the key observables n, e and π/e. Considering these three observables the deviations do not exceed 10% even for $\eta/s = 0.75$ ($k = 0.5$) which is larger than the critical values of η/s found in Chapter 10 for identical initial condition. The possible explanation for smaller

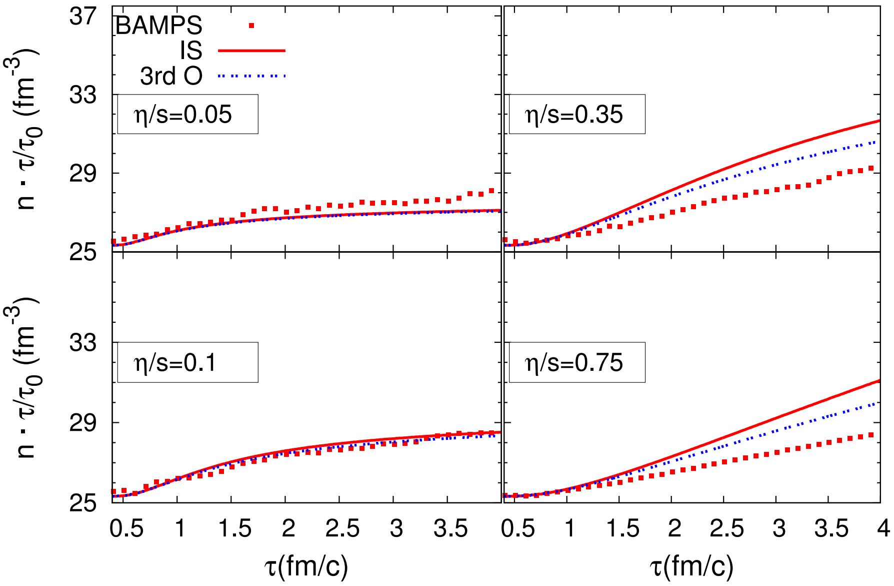

Figure 11.9.: Rescaled particle number density n from BAMPS, second and third-order hydrodynamic calculations. Particle production included via isotropic cross section given by Eq. (11.15).

deviations might be in fact the possibility of particle production, which is an additional mechanism of cooling and thus a counter-weight to the reheating due to energy dissipation in the hydrodynamic formalism.

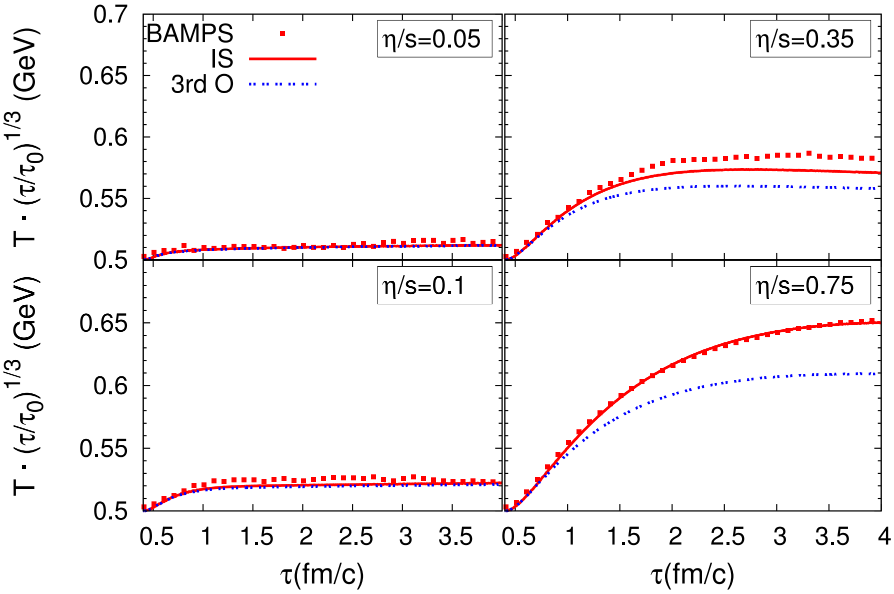

Figure 11.10.: Rescaled effective temperature T from BAMPS, second and third-order hydrodynamic calculations. Particle production included via isotropic cross section given by Eq. (11.15).

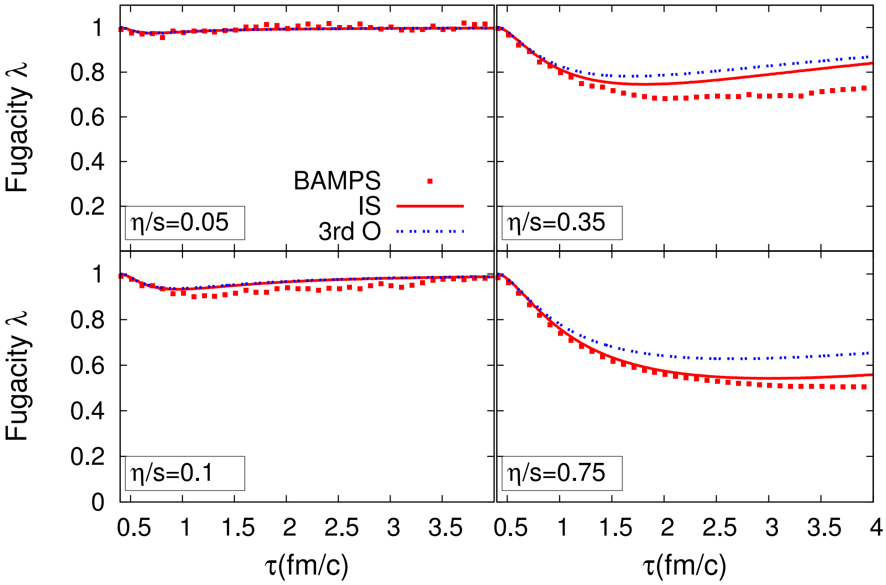

Figure 11.11.: Fugacity λ from BAMPS, second and third-order hydrodynamic calculations. Particle production included via isotropic cross section given by Eq. (11.15).

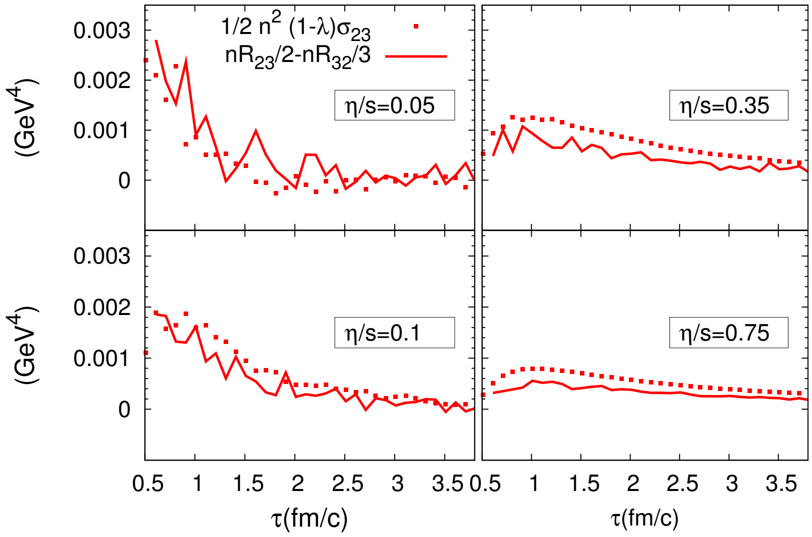

Figure 11.12.: Verification of Eq. (11.6). The values $nR_{23}/2 - nR_{32}/3$ on the left hand side and $1/2n^2(1-\lambda)\sigma_{23}$ on the right hand side are calculated using the actual values of R_{23}, R_{32}, n, λ and σ_{23} from BAMPS.

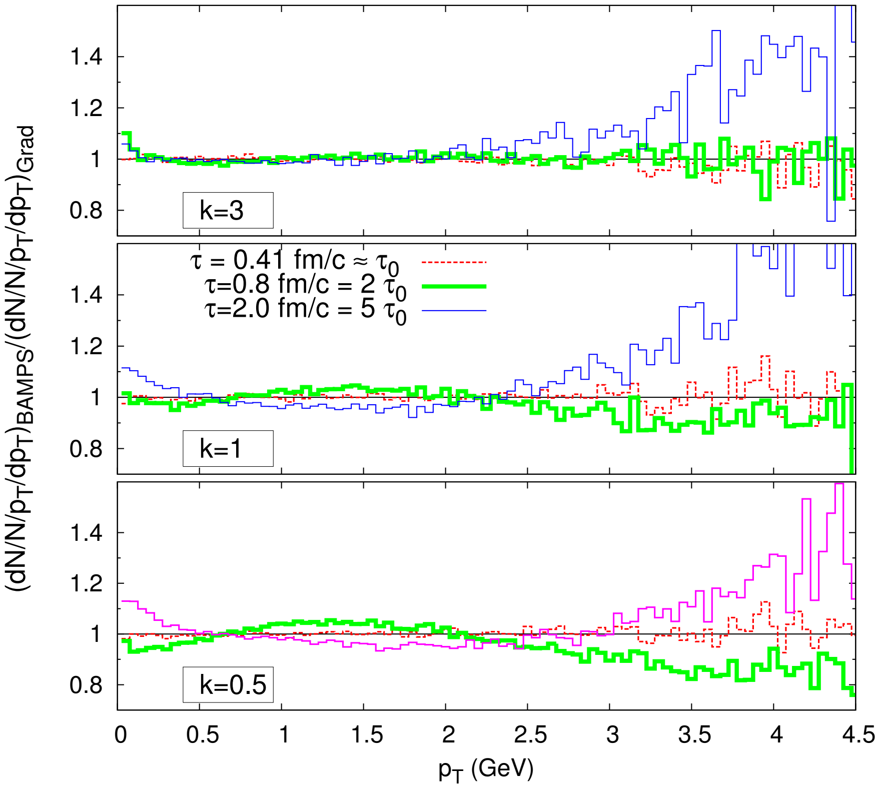

Figure 11.13.: Ratio of transverse distribution from BAMPS to the ones calculated by Grad's approximation based on actual values of e, π, λ and T extracted from BAMPS.

12. Hydrodynamic evolution of a two-component system with conserved particle numbers.

In this Chapter dissipative hydrodynamic equations for a two-component system will be given for a one-dimensional system with transverse symmetry, following the same premises as in Chapter 6. The shear viscosity coefficients for the two components, given in a general form by Eq. (4.12), will be evaluated for a one-dimensional system using Grad's ansatz for the distribution functions and isotropic elastic cross sections. The results of hydrodynamic calculations will be compared with kinetic transport ones. In addition I will discuss whether the obtained evolution equations for the components of a mixture can be summed up into a effective, one-component equation. The question to be addressed in this respect is whether a one-component hydrodynamic theory can be applied to describe a multi-component system. This is of course highly relevant for heavy-ion systems produced in experiments at RHIC and LHC, since the QGP is a mixture of quarks and gluons.

Note that hydrodynamics of mixtures is a highly interesting topic not for for the heavy-ion research community (comp. for instance the discussion of hadronic mixture in Ref. [99]), but also in physics of materials (like physics of polymeric fluids [96]), biophysics [97] and plasma physics [98], just to name some.

12.1. Hydrodynamic equations for a two-component system in one dimension.

Let us consider a system of two components, *Flavor 1* and *Flavor 2*. In analogy to Chapter 6, Bjorken flow is assumed, i.e. $\partial_\mu u^\mu = 1/\tau$. The evolution equations for the particle densities follow from the conservation of the partial particle flow vectors (3.50):

$$\dot{n}_i = -\frac{n_i}{\tau}\,. \tag{12.1}$$

The evolution equations for the energy densities cannot be obtained for a general situation, since the partial energy-momentum tensors are not conserved and the form of the source terms, describing energy-momentum exchange between components are not known in scope of the approach discussed in this work. However, assuming same effective temperature for all components, as expressed by Eq. (3.51), one can obtain evolution equations for the partial energy densities. Since Eq. (3.49), expressing total energy conservation, leads to

$$\dot{e} = -\frac{4}{3}\frac{e}{\tau} + \frac{\pi}{\tau} \tag{12.2}$$

for the total energy density e (as already discussed in Section 6.2), and since from Eq. (3.52) follows that

$$e_i = e\frac{n_i}{n}\,, \tag{12.3}$$

one obtains for the partial energy densities

$$\dot{e_i} = -\frac{4}{3}\frac{e}{\tau}\frac{n_i}{n} + \frac{\pi_i}{\tau}\frac{n_i}{n} \tag{12.4}$$

where n denotes the total particle density.

To complete the set of hydrodynamic equations, $\beta_{2,i}$ first must be specified. Since the Grad's ansatz for the off-equilibrium distribution function is formally identical for one- and multi-component case, the $\beta_{2,i}$ are analogous to the one-component coefficient β_2, calculated in Section 6.1 and Appendix B:

$$\beta_{2,i} = \frac{9}{4e_i}\,. \tag{12.5}$$

From Eq. (3.56) now follows

$$\dot{\pi}_i = -\frac{\pi_i}{2\beta_i\eta_i} - \frac{4}{3}\frac{\pi_i}{\tau} + \frac{8}{27}\frac{e_i}{\tau}\,. \tag{12.6}$$

Finally, the expression (4.12) for the shear viscosity coefficients η_i must be evaluated for a one-dimensional system. The integrals in Eq. (4.12) can be evaluated analytically for the case of binary cross sections with isotropic angle distributions. Only this case will be considered here. The details of this calculation are given in Appendix E. One obtains [201, 36]

$$\eta_i = T\left(\frac{5}{6}\sigma_{ii} + \frac{7}{6}\frac{n_j}{n_i}\sigma_{ij} - \frac{1}{3}\frac{\pi_j}{\pi_i}\sigma_{ij}\right)^{-1}\,. \tag{12.7}$$

In the latter equation σ_{11} and σ_{22} denote total cross sections for scattering of particles of same Flavor (self-collisions), whereas $\sigma_{12} = \sigma_{21}$ refers to scattering of particles of different Flavors (inter-collisions).

Inserting Eq. (12.7) into (12.6) one finally obtains the evolution equations for partial shear pressures in a two-component system [36]:

$$\dot{\pi}_i = -\pi_i\cdot\left(\frac{5}{9}n_i\sigma_{ii} + \frac{7}{9}n_j\sigma_{ij}\right) + \pi_j\cdot\left(\frac{2}{9}n_i\sigma_{ij}\right) - \frac{4}{3}\frac{\pi_i}{\tau} + \frac{8}{27}\frac{e_i}{\tau}\,. \tag{12.8}$$

The equations are coupled, as one would expect, via the inter-collision cross section. In the limit of two identical species, which can be realized either by setting $\sigma_{11} = \sigma_{22} = 0$ or by setting $\lambda_1 = \lambda_2$, Eq. (12.8) is identical with the one-component Israel-Stewart equation (6.36).

12.2. Effective shear viscosity of a multi-component system.

The deconfined state of QCD matter produced at early stages of ultrarelativistic heavy-ion collisions at RHIC and LHC is a multi-component system with quark and gluon degrees of freedom. Although the initially produced quark-gluon plasma (QGP) might be dominated by gluons, as follows from the CGC framework [202], a considerable amount of quarks is produced on the way to thermal and chemical equilibration [187, 89, 88]. However, most of the presently known relativistic dissipative hydrodynamic formalisms [40, 80, 93, 39] and their applications are based on a one-component picture of the QGP. From comparisons with experimental results on the elliptic flow v_2 at RHIC [7] and LHC [203] the shear viscosity to entropy density ratio of the QGP was extracted in Refs. [47, 204, 205, 206] using one-component formalisms. Still it is now clear whether a multi-component system behaves like a one-component system. In case it does not, the shear viscosity to entropy density ratio cannot be chosen freely and can be expected to have a complicated time dependence due to complicated dynamics of the mixture.

A dissipative hydrodynamic formalism reported recently in Ref. [100] allows to calculate global properties of a multi-component system, but does not allow for describing each component separately. Since the equilibration time scales for quarks and gluons in QGP might be significantly different, as pQCD based kinetic transport calculations indicate [30], it is important to consider a multi-component hydrodynamic formalism which is able to describe the dissipative properties of each component properly and thus able to describe the complicated dynamics of the mixture. Such formalism was for the first time reported in Ref. [36] and in this work.

In this section I will discuss hydrodynamic behaviour of a mixture of two components. This means the system as a whole will be considered. Adding up Eqs. (12.8) for all components one obtains the evolution equation for the total shear pressure $\pi = \pi_1 + \pi_2$, which can be written as follows:

$$\dot{\pi} = -\frac{2}{9}\frac{\pi e}{\eta_{eff}} - \frac{4}{3}\frac{\pi}{\tau} + \frac{8}{27}\frac{e}{\tau}\,. \tag{12.9}$$

In the latter equation the *effective* shear viscosity of the mixture η_{eff} is defined via

$$\frac{\pi e}{\eta_{eff}} = \frac{5}{2}\left(\pi_1 n_1 \sigma_{11} + \pi_1 n_2 \sigma_{12} + \pi_2 n_2 \sigma_{22} + \pi_2 n_1 \sigma_{12}\right)\,. \tag{12.10}$$

Using the expressions for the mean free paths $\lambda_1 = n_1\sigma_{11} + n_2\sigma_{12}$ and $\lambda_2 = n_2\sigma_{22} + n_1\sigma_{12}$ one thus can write

$$\eta_{eff} = \frac{2}{5} e \left(\alpha_1 \lambda_1^{-1} + \alpha_2 \lambda_2^{-1}\right)^{-1} \tag{12.11}$$

with the coefficients

$$\alpha_i = \frac{\pi_i}{\pi}\,. \tag{12.12}$$

The effective shear viscosity (12.11) explicitly depends on the partial shear pressures. Thus in general it is not a unique characteristic of the mixture, but rather depends on the dynamics.Nevertheless it is possible to apply Eq. (12.11) in the quasi-stationary limit, i.e. in proximity of equilibrium, when the coefficients α_i become constant. The expectation that α_i become constant is reasonable, since the partial shear pressures approach zero as the system approaches equilibrium, whereas the shear viscosity can be defined for a equilibrated medium by means of the Green-Kubo relation [207].

Let us now consider the (quasi-) stationary limit

$$\dot{\alpha_i} = 0 \Leftrightarrow \frac{\partial}{\partial\tau}\left(\frac{\pi_1}{\pi_2}\right) = 0\,. \tag{12.13}$$

Using Eqs. (12.8) and neglecting any terms explicitly proportional to $1/\tau$ (i.e. in the $\tau \to \infty$ limit) one obtains the stationary solution for π_1/π_2:

$$\left.\frac{\pi_1}{\pi_2}\right|_{\dot{\alpha_1}=\dot{\alpha_2}=0} = \sqrt{\gamma^2 + \frac{n_1}{n_2}} - \gamma\,, \tag{12.14}$$

where

$$\gamma = \frac{5}{4n_2\sigma_{12}}\left(\frac{1}{\lambda_1} - \frac{1}{\lambda_2}\right) + \frac{1}{2}\left(1 - \frac{n_1}{n_2}\right)\,. \tag{12.15}$$

With π_1/π_2 from Eq. (12.14) the effective shear viscosity (12.11) can be calculated in terms of the energy and particle densities and cross sections only.

12.3. Comparison with kinetic transport calculations.

Static setup.

Dissipative hydrodynamic equations for multi-components systems presented in this work are novel. For the first time they were reported in Ref. [36]. In the kinetic transport theory multi-component systems were studied for example in Refs. [140, 30]. In this Section solutions of hydrodynamic equations are compared with kinetic transport results obtained from BAMPS. All calculations are done for the case of isotropic distribution of scattering angles.

We first consider a spatially isotropic medium. This means, all gradients $\partial_\mu u^\mu$ vanish and terms explicitly proportional to $1/\tau$ are neglected in Eqs. (12.8), (12.4) and (12.1). In such static setup the energy and particle densities are conserved, $\dot{e} = 0$ and $\dot{n} = 0$. In BAMPS this is realized by confining the medium in a static box. This setup allows to verify validity of the transition between kinetic transport theory and hydrodynamics, since all non-vanishing terms in Eq. (12.8) originate from kinetic transport theory.

Solutions of Eq. (12.8) are compared with BAMPS calculations in Fig. 12.1. The results are shown for following initial conditions: $\sigma_{11} = 10$ GeV^{-2}, $\sigma_{12} = \sigma_{11}/2$, $\sigma_{22} = \sigma_{11}/4$, $T = 0.4$ GeV, $\pi_1/e_1 = 0.3$. In Fig. 12.1(a) $\pi_2/e_2 = 0$ and $n_1/n_2 = 1$. In Fig. 12.1(b) $\pi_2/e_2 = \pi_1/e_1 = 0.3$ and $n_1/n_2 = 5$. The solid gray lines show a one-component solution, given by Eq. (6.36), with the effective shear viscosity calculated according to Eq. (12.11). A good agreement – with deviations below 10% – between hydrodynamic and kinetic transport calculations can be observed for both initial conditions, which demonstrates validity of the derived hydrodynamic equations. One clearly observes

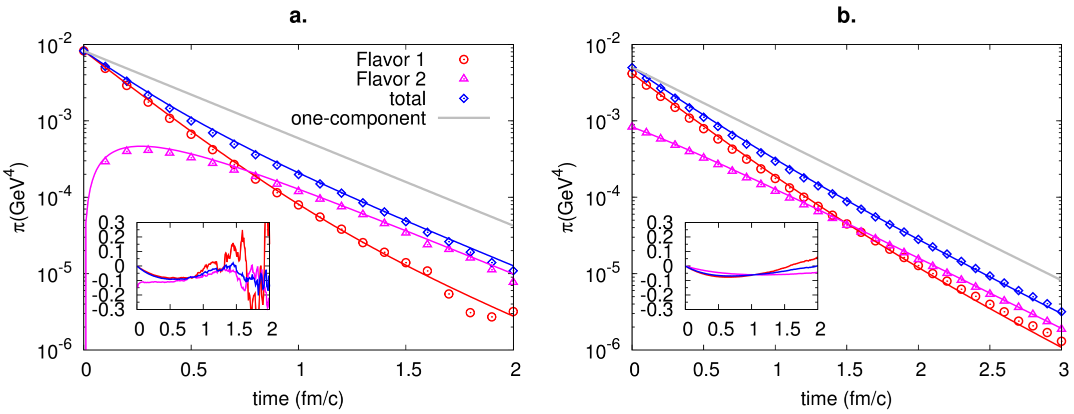

Figure 12.1.: Evolution of partial and total shear pressures from multi-component hydrodynamic (lines) and BAMPS (symbols) calculations. Solid gray lines show solutions of one-component equations with an effective shear viscosity of the mixture. Initial conditions are $\pi_2/e_2 = 0$, $n_1/n_2 = 1$ (a) and $\pi_2/e_2 = \pi_1/e_1$, $n_1/n_2 = 5$ (b). See text for further details. Inlays demonstrate relative deviation between hydrodynamic results and BAMPS.

development of shear pressure in the initially equilibrated Flavor 2 in Fig. 12.1(a). The one-component solution cannot describe evolution of the total shear pressure at all times. Only after a certain time, which is needed to achieve a quasi-stationary state, the system can be described by a one-component equation with an effective shear viscosity coefficient. One can draw this conclusion since the one-component solution and total shear pressure from BAMPS become parallel at late times. Existence of quasi-stationary limit in kinetic transport calculations is demonstrated in Fig. 12.2, where the ratio π_2/π_1 is shown for the situation depicted in Fig. 12.1. Note that due to low values of the partial shear pressure, at late times BAMPS results are fluctuating strongly, although the results presented here are obtained with very large, $\sim 10^7$, particle numbers per run.

To give a stronger proof of applicability of the one-component description at late times one can consider a system where the initial π_1/π_2 ratio is exactly the one in stationary limit. This is done for example for the situation depicted in Fig. 12.1(b) and the result is demonstrated in Fig. 12.3. One clearly observes that a one-component description is applicable only in the quasi-static limit defined via Eq. (12.14).

Note that the shear viscosities η_i of the components of the mixture are not positive definite, as follows from Eq. (12.7). The initial conditions can be chosen such that one of them becomes negative in a two-component mixture. Thus η_i cannot always be interpreted as transport coefficients in the usual sense. Still, negative values do have a physical meaning: a negative viscosity η_i means, according to Eq. (12.6), that the corresponding partial shear pressure increases, i.e. the component of the mixture is brought from equilibrium. This can happen if the shear pressures of the two components are very different, so that one of the components is brought out of equilibrium during the

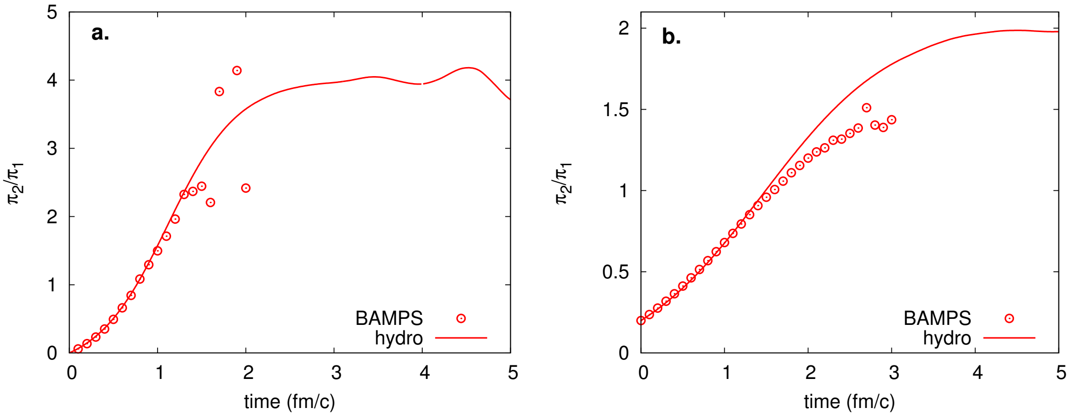

Figure 12.2.: Ratio of partial shear pressures shown in Fig. 12.1 from hydrodynamic (lines) and BAMPS (symbols) calculations.

other one relaxes towards equilibrium. In fact, the shear viscosity η_2 becomes negative in the situation shown in Fig. 12.1 (a), and as long as it is negative shear pressure π_2 increases. As η_2 becomes positive, π_2 starts decreasing. Evolution of η_2 is shown in Fig. 12.4. The viscosity coefficients η_2 has a divergence, which means that the corresponding relaxation rate $1/(2\eta_2\beta_{2,2})$ becomes zero and changes its sign. Note that in the quasi-static limit $\pi_1/\pi_2 = const$ both coefficients η_1 and η_2 are strictly non-negative and thus only then attain the usual meaning of viscosity coefficients.

Longitudinal expansion.

In an expanding system the energy density is not conserved due to volume change. In addition to expansion, also dissipation has an effect on evolution of the energy density, as Eq. (12.4) states. Thus the assumption of equal temperatures in a mixture in general cannot hold as soon as expansion is considered. For a comparison with kinetic transport calculation I consider the following initial conditions: $\tau_0 = 0.4$ fm/c, $T(\tau_0) = 420$ MeV. The degeneracy of both Flavors is chosen to be 16 and the initial fugacities are $\lambda_1 = \lambda_2 = 1$. The cross sections are $\sigma_{11} = 20\ \mathrm{GeV}^{-2} \approx 7.8$ mb and $\sigma_{22} = 0.2 \cdot \sigma_{11}$ together with $\sigma_{12} = 0.5 \cdot \sigma_{11}$ resp. $\sigma_{12} = 0.001 \cdot \sigma_{11}$. The results on shear pressure and temperature are shown in Fig. 12.5. One observes that the temperatures of the two components indeed evolve differently in the case of non-equal cross sections for self-collisions, though the difference of the temperatures is significantly reduced as the inter-collision cross section becomes larger (as follows from comparison of Fig. 12.5 (a) and (b)).

The obtained hydrodynamic equations can be applied to estimate dissipative effects in a quark-gluonic system. In order to mimic the gluons and quarks in a QGP I choose the degeneracy factors to be $d_1 = 16$ and $d_2 = 24$, thus considering two flavours, $N_f = 2$. Only momentum-independent differential cross sections and elastic processes can be

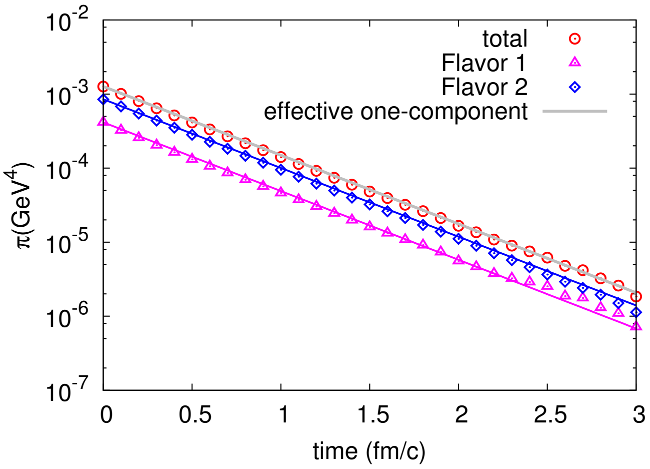

Figure 12.3.: Evolution of shear pressure with initial conditions corresponding to the quasi-static limit defined by Eq. (12.14). Cross sections and densities are same as for Fig. 12.1(b).

considered. The cross sections are parametrized as follows:

$$\sigma_{ij} = k_{ij}/T^2\,. \tag{12.16}$$

These cross sections are meant to mimic the following processes: $gg \leftrightarrow gg$, $gq \leftrightarrow gq$ and $qq \leftrightarrow qq$. Quarks and anti-quarks are considered indistinguishable for these studies. For these processes the existing leading order pQCD calculations yield the following ratios of differential cross sections [30, 208]:

$$\left(\frac{d\sigma_{gg\leftrightarrow gg}}{dt}\right) / \left(\frac{d\sigma_{gq\leftrightarrow gq}}{dt}\right) \approx 9/4\,, \tag{12.17}$$

$$\left(\frac{d\sigma_{gg\leftrightarrow gg}}{dt}\right) / \left(\frac{d\sigma_{qq\leftrightarrow qq}}{dt}\right) \approx (9/4)^2\,. \tag{12.18}$$

These ratios will be used to mimic the elastic processes in a quark-gluon plasma using parametrization (12.16).

To gauge the initial conditions for RHIC and LHC energies, the charged particle multiplicity in the central rapidity region can be used. For the initial fugacities λ_1 and λ_2 of gluons and quarks accordingly the two cases $\lambda_1 = \lambda_2 = 1$ and $\lambda_1 = 1$, $\lambda_2 = 0.2$ will be used for both RHIC and LHC conditions. For sake of simplification parton-hadron duality will be assumed, i.e. at the phase transition one parton will correspond to one hadron. For RHIC energies the initial time $\tau_0 = 0.4$ fm/c is used. The initial temperature at initial time $\tau_0 = 0.4$ fm/c is chosen to be such that the final total transverse energy per unit rapidity at mid-rapidity is $dE_T/dy \approx 600$ GeV[209] at $\tau \approx 4$ fm/c. At this time the energy density drops below 1 GeV/fm^3 and thus the phase transition can be expected to take place. Assuming initial thermal equilibrium one then obtains the

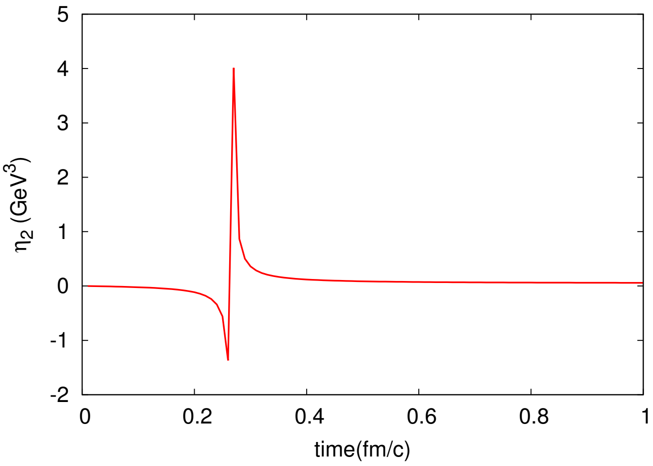

Figure 12.4.: Evolution of shear viscosity coefficients η_2 for situation shown in Fig. 12.1(a).

initial temperatures $T_0 = 300$ MeV with $\lambda_1(\tau_0) = \lambda_2(\tau_0) = 1$ and $T_0 = 340$ MeV with $\lambda_1(\tau_0) = 1, \lambda_2(\tau_0) = 0.2$.

Currently no data on average transverse energy per particle in the LHC experiments with center-of-mass energy $\sqrt{s} = 2760$ GeV is available. To estimate the initial temperature for this scenario one can use the observation, that average transverse energy per particle E_T/N saturates for SPS and RHIC energies [210] and thus one can assume that the value $dE_T/dy \approx 600$ GeV observed at RHIC can be rescaled with the ratio of multiplicities at LHC and RHIC. Using $dN/dy \approx 1600$ at LHC [211] and $dN_{ch}/dy \approx 700$ at RHIC [209] one obtains

$$\left.\frac{dE_T}{dy}\right|_{LHC} = \left.\frac{dE_T}{dy}\right|_{RHIC} \cdot \frac{dN/dy|_{LHC}}{dN/dy|_{RHIC}} . \tag{12.19}$$

Assuming the lifetime of QGP at LHC to be ≈ 9 fm/c (which is the final time 4 fm/c for RHIC conditions rescaled with the ratio of multiplicities) and the initial time $\tau_0 = 0.25$ fm/c, we obtain for the initial temperature $T_0 = 450$ MeV with $\lambda_1 = \lambda_2 = 1$ resp. $T_0 = 510$ MeV with $\lambda_1 = 1$, $\lambda_2 = 0.2$.

Using Eq. (12.11) discussed in Section 12.2 one can calculate the effective η/s ratio of the quark-gluon mixture for the conditions discussed so far in this Section. For both RHIC and LHC conditions one obtains $\eta/s = 0.23$ in case $\lambda_1 = \lambda_2$ and $\eta/s = 0.28$ in case $\lambda_1 = 1$, $\lambda_2 = 0.2$. These values are within the range currently discussed in literature for both RHIC and LHC experiments [206, 116, 204].

The results presented in Fig. 12.5 demonstrate that the temperature (and thus the energy density as well) does not differ much for the two components of the mixture in case the inter-cross section is not too small. Thus for the parametrization of cross sections (12.16) and (12.18) chosen here to mimic LO pQCD processes the strongest effect is expected to be observed in evolution of the shear pressure. The shear pressure is in turn

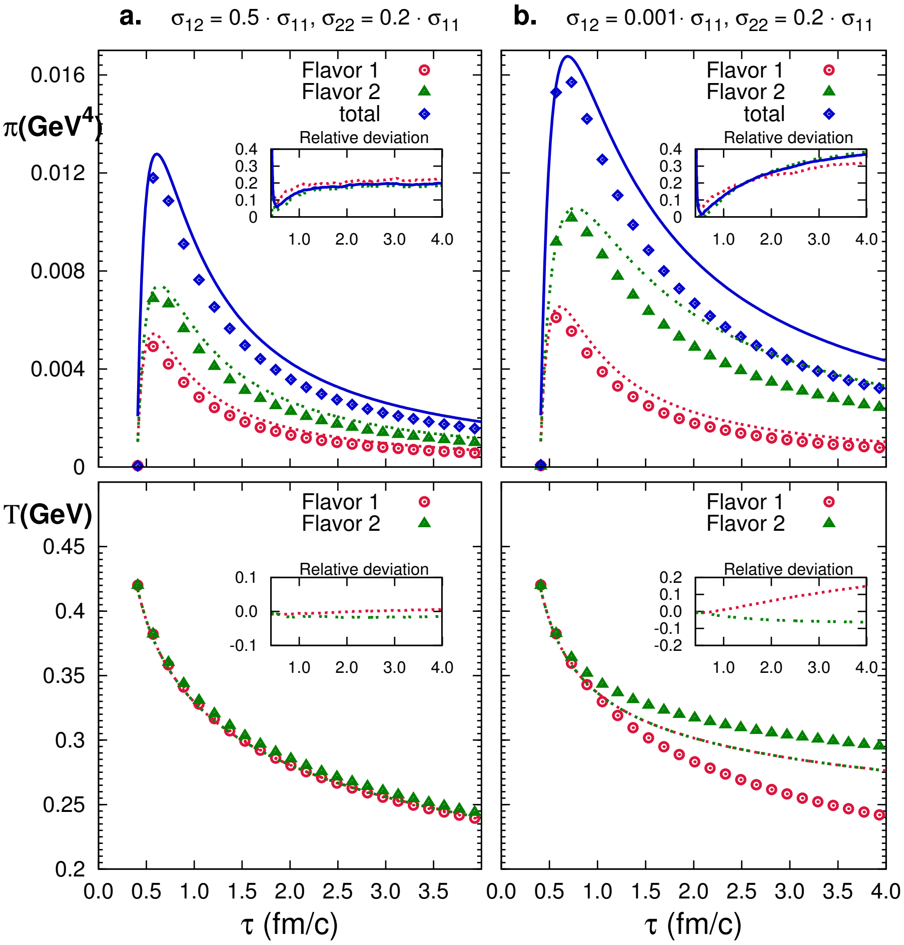

Figure 12.5.: Evolution of partial shear pressures and effective temperatures in a expanding system with two components. Results in panels (a) and (b) are obtained with different inter-collision cross sections.

relevant for dissipative corrections to the transverse spectra, as already demonstrated in Section 8 of this work and in Refs. [33, 35]. Here the dissipative corrections to transverse spectra for a quark-gluonic mixture will be quantified using the model assumptions discussed above. A quantitative measure of the dissipative corrections to transverse spectra can be defined as follows:

$$\frac{\delta dN}{dN_{th}}(p_T) \equiv \frac{(dN/p_T/dp_T)_{Grad}}{(dN/p_T/dp_T)_{thermal}} - 1 = \frac{\int p_T \cosh y \ f_0 \phi \ dy d\varphi}{\int p_T \cosh y \ f_0 \ dy d\varphi}\,, \tag{12.20}$$

where ϕ is the off-equilibrium correction to the distribution function according to Grad's ansatz given by Eq. (8.1) (with the degeneracy factor 24 for quarks and 16 for gluons). The ratio (12.20) describes change multiplicity due to dissipative correction relative to the thermal yield.

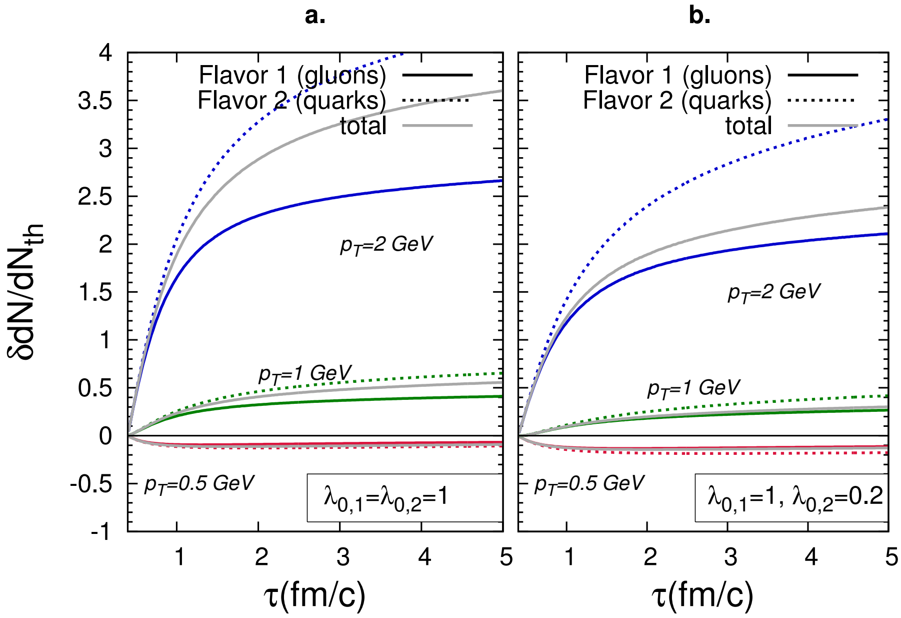

Figure 12.6.: Ratio defined in Eq. (12.20) extracted from hydrodynamic calculations with RHIC typical initial conditions (see text) for different values of p_T. Results are shown for *Flavour 1* (solid lines) and *Flavour 2* (dashed lines) and the total system (grey solid lines). The initial values of fugacities are $\lambda_{0,1} = \lambda_{0,2} = 1$ (a) and $\lambda_{0,1} = 1$, $\lambda_{0,2} = 0.2$ (b). The cross sections are time dependent according to Eqs. (12.16) and (12.18) with $k_{11} = 0.9$.

Results on $\frac{\delta dN}{dN_{th}}(p_T)$ with the cross sections parametrized according to Eqs. (12.16) and (12.18) with $k_{gg} \equiv k_{11} = 0.9$ are shown in Fig. 12.6 and 12.7 for RHIC respectively LHC initial conditions as discussed above. The results are shown for different values of the transverse momentum p_T. Panel (a) demonstrates the results for initial $\lambda_1 = \lambda_2 = 1$ and panel (b) for initial $\lambda_1 = 1$, $\lambda_2 = 0.2$. Significant effects of dissipation are observed in both quark and gluonic distributions already for $p_T = 1$ GeV $\approx 3\mathrm{T}_0$ (with T_0 being the initial temperature) for RHIC conditions and $p_T = 2$ GeV $\approx 4\mathrm{T}_0$ for LHC setup. The dissipative effects are stronger for quarks due to larger mean free path. At the times at which the phase transition is expected to take place (4 fm/c for RHIC and 9 fm/c for LHC conditions) the difference between dissipative corrections to quark and gluonic spectra is almost factor of 2. The transverse spectra are important for the so-called recombination and coalescence models of hadronization [65, 66, 67, 68], in which the hadrons are built up from partons which are close to each other in the phase space. It is not sufficient to assume a thermal distribution at the freeze-out, since the parton yields are significantly different in a dissipative QGP at moderately large $p_T \sim 3 - 4T_0$. It is furthermore important to properly account for the dissipative effects on quark and gluonic spectra, since the yields are a gain different for the both species, as demonstrated

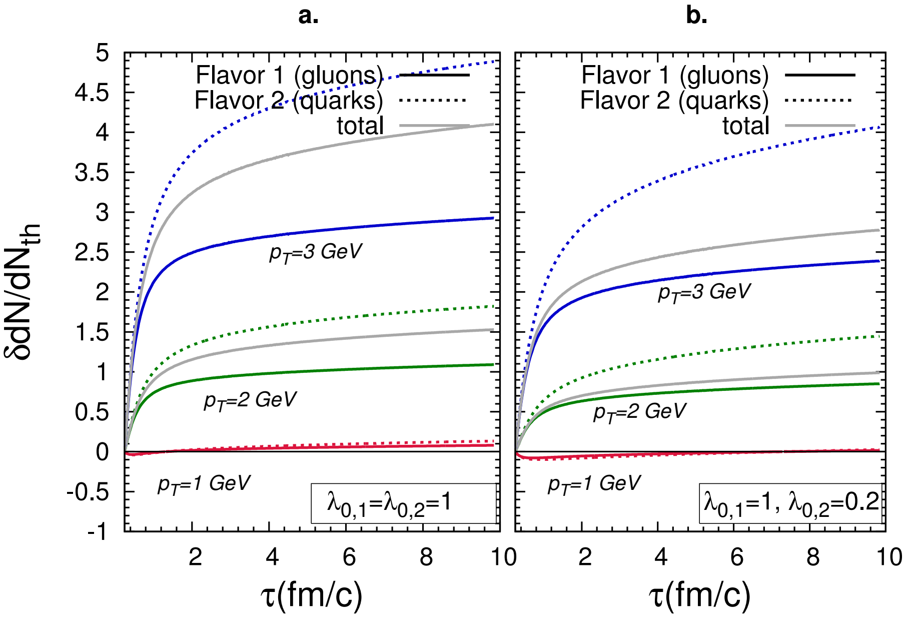

Figure 12.7.: Same as in Fig. 12.6 for LHC typical initial conditions (see text) and different values of p_T.

in this Section. Same applies to calculations of yields for direct photons and dileptons [195, 193].

Conclusions.

The analysis presented in this Chapter demonstrates the importance of a proper treatment of the hydrodynamic evolution in a multi-component medium. The global behaviour of a multi-component fluid in general cannot be described by the standard one-component formalisms, since a certain time is needed for the medium to establish an effective one-component behaviour. At early time the evolution can only be understood in terms of a multi-component hydrodynamic formalism, such as the one derived and applied in this work. The effective shear viscosity to entropy density ratio, η/s, is a characteristic of a medium very close to equilibrium. For a multi-component medium the effective η/s ratio can be consistently defined only after a certain time, before which the evolution does not follow the known one-component descriptions. Since the Quarks-Gluon Plasma produced in heavy-ion collisions at RHIC and LHC is a multi-component fluid, it is essential to solve multi-component hydrodynamic equations instead of treating it as a one-component system. The dissipative effects on quark and gluonic spectra differ significantly for conditions typical for RHIC resp. LHC experiments which is of great significance for modelling of the hadronization process.

13. Summary, Conclusions and Outlook

Education is a progressive discovery of our ignorance.

Will Durant (1885 – 1981), American writer, historian, and philosopher.

Summary

The intention of this work was to investigate the correspondence between the kinetic transport theory, based on the relativistic Boltzmann equation, and relativistic dissipative hydrodynamics.

These two theories are widely accepted and applied tools for modelling the space-time evolution of the quark-gluonic plasma produced during the early stages of heavy-ion collisions at the experimental facilities RHIC and LHC. Whereas the kinetic theory allows to model the microscopic dynamics of a system, the hydrodynamic theory is of macroscopic nature and thus averages over the intrinsic microscopic scales. Furthermore, the hydrodynamic equations are obtained considering a small deviation from the equilibrium state and thus their solutions become unreliable as the departure from equilibrium becomes too large.

In this work possibilities of extension of the standard dissipative hydrodynamic formalism by Israel and Stewart were explored. The discussed extensions are inclusion of particle production and annihilation processes into the hydrodynamic formalism, inclusion of higher-order terms, neglected in the standard approach, and the construction of a hydrodynamic formalism for a multi-component mixture. The limits of applicability of dissipative hydrodynamic formalisms wre studied by direct comparisons of the relevant observables with results of kinetic transport calculations. Another aspect of this work was calculation of the shear viscosity coefficient as a function of the microscopic cross sections and extraction of this coefficient from kinetic transport calculations.

The main pillars on which this work is based are publications in Refs. [32], [33], [34], [35] and [36].

Dissipative hydrodynamic equations can be obtained from using the so-called entropy principle together with balance equations for the particle flow vector and energy-momentum tensor. The entropy principle was used to derive the standard dissipative hydrodynamic formalism by Israel and Stewart [40]. In scope of this formalism the entropy four-current is calculated using a heuristic ansatz for the phase-space distribution for a non equilibrium system. The construction of the off-equilibrium distribution function was discussed in this work in Chapter 2 in order to lay a foundation for further calculations.

In the entropy principle based formalism, the hydrodynamic equations for dissipative currents are obtained by applying the second law of thermodynamics to the divergence of the entropy current, which is also referred to as entropy production. In this work, in Chapter 3, an extended form of the entropy current from the Israel-Stewart theory was used to obtain hydrodynamic equations, which contain terms of higher (third) order in dissipative currents than the Israel-Stewart theory. Another extension of the standard hydrodynamic formalism presented in this work is inclusion of particle number-changing processes into hydrodynamic formalism. This was done using inelastic cross sections with isotropic angle distributions and in consistency with the Boltzmann Equation based kinetic theory. Finally, the entropy principle was applied to derive a set of dissipative hydrodynamic equations for a multi-component system.

In Chapter 4 a formal expression for the shear viscosity coefficient η was derived in terms of the collision integral from the Boltzmann equation. This derivation was again based on the entropy principle and established a direct connection between the hydrodynamic and kinetic theories. The obtained expression was applied in Chapter 9 to calculate the shear viscosity to entropy density ratio of a gluonic gas using leading order perturbative QCD scattering cross sections. For the values of the strong coupling constant $\alpha_s = 0.3 \ldots 0.6$ typical for quark-gluonic systems produced in RHIC and LHC experiments the obtained η/s values lie within the range $0.18 \ldots 0.08$, in consistentcy with the recent estimates from dissipative hydrodynamic calculations [206, 116, 204]. The obtained expression was also applied to calculate the shear viscosity coefficients for the components of a multi-component mixture. This calculation can be done analytically for the special case of isotropic angle distribution, i.e. angle-independent differential cross sections.

Solutions of the derived hydrodynamic equations were compared with the results of kinetic transport calculations by the partonic cascade BAMPS [30, 41] in Chapters 10, 11 and 12. This comparisons were done for the special case of a one-dimensional boost-invariant system, which was introduced in Chapter 5 and can be used as a simplified model for the early stage of a heavy-ion collision [45]. These comparisons demonstrated that the standard second-order hydrodynamic formalism can be applied if $\eta/s \lesssim 0.2$ and the initial time $\tau_0 = 0.4$ fm/c. Earlier initial times require an even smaller η/s ratio. At the same time, the third-order formalism derived in this work is applicable if $\eta/s \lesssim 0.4$. Thus inclusion of higher-order terms extends the applicability limits of the hydrodynamic formalism. If particle number changing processes are included into the third-order hydrodynamic formalism, it can be considered applicable even for $\eta/s = 0.75$. This can be explained by the fact that particle production is an additional mechanism of cooling and thus a counter-weight to the reheating due to dissipation in the hydrodynamic formalism.

The reason for systematic deviations between dissipative hydrodynamic and kinetic transport results can be found in the ansatz for the off-equilibrium distribution function, which is underlying the derivation of hydrodynamic equations. By extracting the particle distributions from kinetic transport calculations on the one hand and calculating the distribution using analytic expression on the other hand, it was demonstrated that the heuristic analytic ansatz for the distribution function, which is used for derivation of hydrodynamic equations, does not exactly describe the actual solution of the Boltzmann Equation. The deviations are moderate if isotropic cross sections are used, but become more pronounced if the perturbative QCD interactions are considered.

The obtained dissipative hydrodynamic equations for the components of a multi-component mixture reveal an interesting feature – in a general situation they cannot be summed up into a one-component hydrodynamic equation of the standard form known from the Israel-Stewart [40] formalism. In the formalism presented here both the viscosity coefficients for each component and the viscosity coefficient for the whole system depend on the partial shear pressures. Only in the stationary limit $t \to \infty$ the shear viscosity coefficients do become independent of the partial shear pressures and thus attain a physical meaning. For this reason a one-component hydrodynamic formalism can be applied to a mixture only after a certain time, which is needed to establish an effective one-component behaviour and depends on the intrinsic microscopic scales and initial conditions. Whereas the one-component formalism fails to describe hydrodynamic evolution of the system as whole, evolution of each single component can be described by the obtained multi-component equations with good accuracy, as was verified by consistent comparisons with kinetic transport results from BAMPS in Chapter 12. The findings in Chapter 12 put certain constrains on the initial conditions for one-component dissipative hydrodynamic formalisms. These constrains on applicability of one-component dissipative hydrodynamics are a step towards a more detailed understanding of the early phase of heavy-ion collisions, since the initial conditions for dissipative hydrodynamic calculations are still unknown and the medium produced in early stages is a mixture of quarks and gluons.

Outlook

The extensions of standard hydrodynamic formalism presented in this work are a step towards a higher versatility of dissipative hydrodynamic as a tool to investigation of heavy-ion phenomenology. Inclusion of thir-order terms has corrected the problem of occurance of negative pressure in hydrodynamic calculations and helped to reduce deviations between the results of hydrodynamic and kinetic transport calculations. However, in the formalisms presented here the effects of heat flow and bulk viscosity were neglected. Their inclusion into the third-order formalism was completed just recently by different authors [95, 201]. It is important to implement the obtained thrid-order equations in a full three dimensional hydrodynamic algorithm.

Inclusion of heat transport and bulk pressure into the multi-component hydrodynamic formalism is a topic for future work. It is also important to modify the multi-component hydrodynamic formalism in such a way that it can be coupled to different equations of state. This will allow to apply the multi-component hydrodynamic formalism to systems of massive particles, such as hadronic mixtures. In this context it is also necessary to extract the bulk viscosity coefficients from kinetic transport calculations, in a similar way as was done in this work for the shear viscosity.

The ability to describe a medium with a realisitc equation of state is one of the advantages of the hydrodynamic approach. In the quasi-particle model like BAMPS the equation of state can be modified by implementing a temperature-dependent mass of the particles. This is a challenging task, since a temperature-dependent mass also means that evolution of each individual quasi-particle will be affected by the global properties of the medium. Formally, this leads to an additional term in the Boltzmann Equation, which than becomes th Vlasov-Boltzmann Equation. The additional Vlasov term accounts for the effect of the medium on evolution of a single-particle distribution. This effect can be interpreted as presence of a 'mean-field', which is an effective field acting on particles and influencing their dynamics. Implementation of temperature-dependent mass in BAMPS will lead to a higher versatility of this kinetic model and will help to cover yet another gap between kinetic transport and hydrodynamic formalisms.

For the simulations of heavy-ion collisions, kinetic transport and dissipative hydrodynamics have different rages of applicability. Kinetic transport can be applied for initial states which are more extreme than those available for hydrodynamics. However it is important to mention that up to now there is no clarity on how the initial conditions for dissipative hydrodynamic calculations of early stages of heavy-ion collisions should look like. This leads to a very promising possibility to use kinetic transport calculations in order to generate energy density, temperature, pressure and flow velosity profiles which can be used as initial conditions for hydrodynamic formalisms. This can be accoplished using the standard initial conditions of Glauber type or Color Glass Condensate, which can be used within a kinetic transport model even at early times, at which hydrodynamic approach might become invalid due to presence of large gradients, that cannot be resolved by hydrodynamic equations. Also for mixtures the very early stage must be simulated using the kinetic transport theory up to a point, where either multi-component or standard one-component hydrodynamic calculations can be initialized.

To summarize, the ultimate goal must be to establish the kinetic transport theory as a standard approach to simulate the early, far-from-equilibrium phase of the heavy ion collisions and to obtain more realistic and reliable initial conditions for hydrodynamic calculations.

A. Components of the off-equilibrium distribution function in Grad's 14-moment theory.

For the calculations presented here the Eckart frame is chosen. This choice leads to a vanishing particle flow and the following form of the energy-momentum tensor:

$$
\begin{aligned}
T^{\mu\nu} &= eu^\mu u^\nu - (p+\Pi)\Delta^{\mu\nu} + q^\mu u^\nu + u^\mu q^\nu + \pi^{\mu\nu}\,, && \text{(A.1)}\\
N^\mu &= nu^\mu\,, && \text{(A.2)}\\
\Pi &= -\frac{1}{3}\Delta^{\mu\nu}\delta T^{\mu\nu}\,, && \text{(A.3)}\\
q^\mu &= u_\nu \Delta^\mu_\lambda \delta T^{\nu\lambda}\,, && \text{(A.4)}\\
\pi^{\mu\nu} &= \delta T^{\langle\mu\nu\rangle}\,. && \text{(A.5)}
\end{aligned}
$$

Using the velocity field four-vector u^μ, an orthogonal tensorial basis can be constructed and the moments of the equilibrium distribution can be decomposed in this basis as follows:

$$
\begin{aligned}
\tilde{N}^{\mu\nu}_{eq} &= \int p^\mu f_{eq} d\Gamma = b_{10} u^\mu\,, && \text{(A.6)}\\
\tilde{T}^{\mu\nu}_{eq} &= \int p^\mu p^\nu f_{eq} d\Gamma = b_{20} u^\mu u^\nu + b_{21}\Delta^{\mu\nu}\,, && \text{(A.7)}\\
\tilde{F}^{\alpha\mu\nu}_{eq} &= \int p^\alpha p^\mu p^\nu f_{eq} d\Gamma = b_{30} u^\alpha u^\mu u^\nu + b_{31}\left(u^\alpha\Delta^{\mu\nu} + u^\mu\Delta^{\alpha\nu} + u^\nu\Delta^{\mu\alpha}\right)\,. && \text{(A.8)}\\
\tilde{R}^{\alpha\beta\mu\nu}_{eq} &= \int p^\alpha p^\beta p^\mu p^\nu f_{eq} d\Gamma = b_{40} u^\alpha u^\beta u^\mu u^\nu + \\
&+ b_{41}\Big(u^\alpha u^\beta\Delta^{\mu\nu} + u^\alpha u^\mu\Delta^{\beta\nu} + u^\alpha u^\nu\Delta^{\mu\beta} + u^\beta u^\mu\Delta^{\alpha\nu} + u^\beta u^\nu\Delta^{\mu\alpha} + u^\mu u^\nu\Delta^{\alpha\beta}\Big) + \\
&+ b_{42}\Big(\Delta^{\alpha\beta}\Delta^{\mu\nu} + \Delta^{\mu\alpha}\Delta^{\beta\nu} + \Delta^{\alpha\nu}\Delta^{\mu\beta}\Big)\,. && \text{(A.9)}
\end{aligned}
$$

The coefficients b_{ij} can be obtained by taking appropriate projections of the integrals in Eqs. (A.6) – (A.9). Using the Boltzmann distribution for massless particles, Eq. (6.13), and the identities $\Delta^{\mu}_{\mu} = 3$, $u_\mu p^\mu = p_0$ and $p_\mu p^\mu = 0$ one obtains:

$$\begin{aligned}
b_{10} &= u_\mu \tilde{N}^{\mu}_{eq} = \int p_0 f_{eq} d\Gamma = n && \text{(A.10)}\\
b_{20} &= u_\mu u_\nu \tilde{T}^{\mu\nu}_{eq} = \int p_0^2 f_{eq} d\Gamma = e && \text{(A.11)}\\
b_{21} &= \frac{1}{3}\Delta_{\mu\nu}\tilde{T}^{\mu\nu}_{eq} = -\frac{1}{3}\int p_0^2 f_{eq} d\Gamma = -\frac{1}{3}e && \text{(A.12)}\\
b_{30} &= u_\alpha u_\mu u_\nu \tilde{F}^{\alpha\mu\nu}_{eq} = \int p_0^3 f_{eq} d\Gamma = 4eT && \text{(A.13)}\\
b_{31} &= \frac{1}{3}u_\alpha \Delta_{\mu\nu}\tilde{F}^{\alpha\mu\nu}_{eq} = -\frac{1}{3}\int p_0^3 f_{eq} d\Gamma = -\frac{4}{3}eT && \text{(A.14)}\\
b_{40} &= u_\alpha u_\beta u_\mu u_\nu \tilde{R}^{\alpha\beta\mu\nu}_{eq} = \int p_0^4 f_{eq} d\Gamma = 20eT^2 && \text{(A.15)}\\
b_{41} &= \frac{1}{3}u_\alpha u_\beta \Delta_{\mu\nu}\tilde{R}^{\alpha\beta\mu\nu}_{eq} = -\frac{1}{3}\int p_0^4 f_{eq} d\Gamma = -\frac{20}{3}eT^2 && \text{(A.16)}\\
b_{42} &= \frac{1}{15}\Delta_{\alpha\beta}\Delta_{\mu\nu}\tilde{R}^{\alpha\beta\mu\nu}_{eq} = \frac{1}{15}\int p_0^4 f_{eq} d\Gamma = \frac{4}{3}eT^2 && \text{(A.17)}\\
& && \text{(A.18)}
\end{aligned}$$

The non-ideal parts $\delta T^{\mu\nu}$ and δN^μ of the energy-momentum tensor and the particle flow vector can be written in terms of $\tilde{N}^{\mu}_{eq}$, $\tilde{T}^{\mu\nu}_{eq}$, $\tilde{F}^{\alpha\mu\nu}_{eq}$ and $\tilde{R}^{\alpha\beta\mu\nu}_{eq}$ according to Eqs. (2.31) and (2.30). Without loss of generality one can assume the following form for the tensors $\epsilon_{\mu\nu}$, ϵ_μ and ϵ:

$$\begin{aligned}
\epsilon_{\mu\nu} &= A_2(3u_\mu u_\nu - \Delta_{\mu\nu})\Pi - \frac{1}{2}B_1\left(u_\mu q_\nu + u_\nu q_\mu\right) + C_0\pi_{\mu\nu} && \text{(A.19)}\\
\epsilon_\nu &= A_1 u_\nu \Pi - B_0 q_\nu && \text{(A.20)}\\
\epsilon &= A_0 \Pi && \text{(A.21)}
\end{aligned}$$

In the latter set of equations $\epsilon_{\mu\nu}$ was assumed to be traceless, since its trace can always be absorbed into the scalar ϵ. The coefficients A_i, B_i, C_i are to be determined yet. To do so one first inserts (A.19) – (A.21) into the decompositions of δN^μ and $\delta T^{\mu\nu}$, (2.30) and (2.31). Then one can insert δN^μ and $\delta T^{\mu\nu}$ into the definitions of the dissipative fields (A.3) – (A.5). In addition one will have to use the Landau matching coditions

$$u_\mu u_\nu \delta T^{\mu\nu} = 0\,, \tag{A.22}$$
$$u_\mu \delta N^\mu = 0\,, \tag{A.23}$$

and the constitutive equation of Eckart's frame

$$\Delta^{\nu}_{\mu} N^\mu = 0\,. \tag{A.24}$$

The sets of equations to be solved are:

For A_0, A_1, A_2 (after inserting $\delta T^{\mu\nu}$ into the definition of Π and using the Landau conditions)

$$\begin{aligned}
&\Pi + \frac{1}{3}\Delta^{\mu\nu}\delta T^{\mu\nu}(b_{ij}, \epsilon, \epsilon_\mu, \epsilon_{\mu\nu}) = 0\,,\\
&u_\mu u_\nu \delta T^{\mu\nu}(b_{ij}, \epsilon, \epsilon_\mu, \epsilon_{\mu\nu}) = 0\,,\\
&u_\mu \delta N^\mu(b_{ij}, \epsilon, \epsilon_\mu, \epsilon_{\mu\nu}) = 0\,,
\end{aligned}$$

For B_0, B_1 (after inserting $\delta T^{\mu\nu}$ into the definition of q^μ and using the constitutive equation of Eckart's frame)

$$\begin{aligned}
&q^\alpha + u_\mu \Delta^\alpha_\nu \delta T^{\mu\nu}(b_{ij}, \epsilon, \epsilon_\mu, \epsilon_{\mu\nu}) = 0\,,\\
&\Delta^\alpha_\mu \delta N^\mu(b_{ij}, \epsilon, \epsilon_\mu, \epsilon_{\mu\nu}) = 0\,,
\end{aligned}$$

For C_0 (after inserting $\delta T^{\mu\nu}$ into the definition of $\pi^{\mu\nu}$):

$$\pi^{\mu\nu} - \delta T^{\langle\mu\nu\rangle}(b_{ij}, \epsilon, \epsilon_\mu, \epsilon_{\mu\nu}) = 0 \qquad \text{(A.25)}$$

It is now a matter of straight-forward algebraic operations to obtain the expressions for the coefficients A_i, B_i, C_i, which prove to be complicated functions of b_{ij}:

$$\begin{array}{rcl}
A_0 & = & -\left(b_{30}^2 - b_{30}b_{31} + b_{20}b_{40} - b_{20}b_{41}\right) \times \\
\left(\, b_{21}b_{30}^2 \right. & - & b_{20}b_{30}b_{31} - b_{21}b_{30}b_{31} + b_{20}b_{31}^2 + b_{20}b_{21}b_{40} \\
 & + & \left. b_{10}b_{31}b_{40} - b_{20}^2 b_{41} - b_{20}b_{21}b_{41} - b_{10}b_{30}b_{41} - b_{10}b_{31}b_{41} + \frac{5}{3}b_{20}^2 b_{42} + \frac{5}{3}b_{10}b_{30}b_{42}\, \right)^{-1}
\end{array} \qquad \text{(A.26)}$$

$$\begin{array}{rcl}
A_1 & = & -\left(b_{20}b_{30} - b_{20}b_{31} - b_{10}b_{40} + b_{10}b_{41}\right) \times \\
\left(\, b_{21}b_{30}^2 \right. & - & b_{20}b_{30}b_{31} - b_{21}b_{30}b_{31} + b_{20}b_{31}^2 + b_{20}b_{21}b_{40} \\
 & + & \left. b_{10}b_{31}b_{40} - b_{20}^2 b_{41} - b_{20}b_{21}b_{41} - b_{10}b_{30}b_{41} - b_{10}b_{31}b_{41} + \frac{5}{3}b_{20}^2 b_{42} + \frac{5}{3}b_{10}b_{30}b_{42}\, \right)^{-1}
\end{array} \qquad \text{(A.27)}$$

$$\begin{array}{rcl}
A_2 & = & -\left(b_{20}^2 + b_{10}b_{30}\right) \times \\
\left(\, -3b_{21}b_{30}^2 \right. & + & 3b_{20}b_{30}b_{31} + 3b_{21}b_{30}b_{31} - 3b_{20}b_{31}^2 - 3b_{20}b_{21}b_{40} \\
 & - & \left. 3b_{10}b_{31}b_{40} + 3b_{20}^2 b_{41} + 3b_{20}b_{21}b_{41} + 3b_{10}b_{30}b_{41} + 3b_{10}b_{31}b_{41} - 5b_{20}^2 b_{42} - 5b_{10}b_{30}b_{42}\, \right)^{-1}
\end{array} \qquad \text{(A.28)}$$

$$B_0 = -\frac{b_{31}}{b_{31}^2 + b_{21}b_{41}} \qquad \text{(A.29)}$$

$$B_1 = -\frac{b_{21}}{\left(b_{31}^2 + b_{21}b_{41}\right)} \qquad \text{(A.30)}$$

$$C_0 = \frac{1}{2b_{42}} \qquad \text{(A.31)}$$

B. Entropy current up to third order in shear stress tensor.

In this Appendix the entropy current is derived up to third order in shear tensor using Grad's ansatz for the off-equilibrium distribution function and kinetic definition of the entropy.

The entropy current s^μ can be calculated according to the kinetic definition:

$$s^\mu = -\int d\Gamma p^\mu f(\ln f - 1)\,. \tag{B.1}$$

In Grad's approach the off-equilibrium distribution function $f(x,p)$ is expanded up to linear order in deviations from equilibrium (comp. discussion in Section 2.4.1):

$$f = f_0(1+\phi) \tag{B.2}$$

Using the linear order approximation for the distribution function we expand the logarithm in Eq. (B.1) up to third order in ϕ and obtain

$$s^\mu \approx -\int d\Gamma f_0 p^\mu \left(\ln f_0 - 1 + \phi + \phi \ln f_0 + \frac{\phi^2}{2} - \frac{\phi^3}{6}\right) = s_0^\mu + s_1^\mu + s_2^\mu + s_3^\mu\,. \tag{B.3}$$

with

$$\begin{aligned} s_0^\mu &= -\int d\Gamma f_0 p^\mu \left(\ln f_0 - 1\right)\,, \\ s_1^\mu &= -\int d\Gamma f_0 p^\mu \left(\phi + \phi \ln f_0\right)\,, \\ s_2^\mu &= -\int d\Gamma f_0 p^\mu \frac{\phi^2}{2}\,, \\ s_3^\mu &= \int d\Gamma f_0 p^\mu \frac{\phi^3}{6}\,. \end{aligned}$$

The 0th order contribution is the equilibrium entropy current in kinetic equilibrium and is given for massless Boltzmann gas by[33]

$$s_0^\mu = s_0 u^\mu = \left(4n - n\ln\lambda\right) u^\mu \tag{B.4}$$

with the fugacity $\lambda = \frac{n}{n_{eq}}$. The first-order contributions vanish due to the properties of ϕ, as discussed in Ref. [33].

For the second-order contribution s_2^ω one obtains

$$\begin{aligned} s_2^\omega &= -\frac{1}{2}\int d\Gamma f_0 p^\omega \phi^2 = -\frac{1}{2}C_0^2 \int d\Gamma (\pi_{\mu\nu}p^\mu p^\nu)^2 p^\omega f_0 = \\ &= -\frac{1}{2}C_0^2 \pi_{\mu\nu}\pi_{\alpha\beta}\int p^\mu p^\nu p^\alpha p^\beta p^\omega f_0 = -\frac{1}{2}C_0^2 \pi_{\mu\nu}\pi_{\alpha\beta}\mathcal{I}^{\mu\nu\alpha\beta\omega}\,, \end{aligned} \tag{B.5}$$

with

$$\mathcal{I}^{\mu\nu\alpha\beta\omega} = \int d\Gamma p^\mu p^\nu p^\alpha p^\beta p^\omega f_0\,. \tag{B.6}$$

The moment $\mathcal{I}^{\mu\nu\alpha\beta\omega}$ of the equilibrium distribution can be decomposed into orthogonal parts with thermodynamic coefficients a_{nk} as follows:

$$\begin{aligned} \mathcal{I}^{\mu\nu\alpha\beta\omega} &= \mathcal{I}_1^{\mu\nu\alpha\beta\omega} + \mathcal{I}_2^{\mu\nu\alpha\beta\omega} + \mathcal{I}_3^{\mu\nu\alpha\beta\omega} = \\ &= a_{50}u^\mu u^\nu u^\alpha u^\beta u^\omega + \\ &+ a_{51}\left(\Delta^{\mu\nu}u^\alpha u^\beta u^\omega + \text{permutations}\right) + \\ &+ a_{52}\left(\Delta^{\mu\nu}\Delta^{\alpha\beta}u^\omega + \text{permutations}\right)\,. \end{aligned}$$

We realize that the products $\pi_{\mu\nu}\pi_{\alpha\beta}\mathcal{I}_1^{\mu\nu\alpha\beta\omega}$ and $\pi_{\mu\nu}\pi_{\alpha\beta}\mathcal{I}_2^{\mu\nu\alpha\beta\omega}$ vanish because shear tensor is traceless and component-wise orthogonal to the flow velocity, $\pi_{\alpha\beta}u^\alpha = 0$ and $\pi_{\alpha\beta}\Delta^{\alpha\beta} = 0$. Thus the only relevant contribution is $\mathcal{I}_3^{\mu\nu\alpha\beta\omega}$, though here all permutations containing explicitly $u^\mu, u^\nu, u^\alpha, u^\beta$ will vanish immediately after contraction with the shear tensor due the orthogonality properties discussed above. Thus the relevant parts of $\mathcal{I}_3^{\mu\nu\alpha\beta\omega}$ are

$$\mathcal{I}_3^{\mu\nu\alpha\beta\omega} \equiv a_{52}\cdot\left(\Delta^{\mu\nu}\Delta^{\alpha\beta}u^\omega + \Delta^{\mu\alpha}\Delta^{\beta\nu}u^\omega + \Delta^{\mu\beta}\Delta^{\alpha\nu}u^\omega\right). \tag{B.7}$$

In order to obtain a_{52} one uses Eq. (B.7) to calculate the projection

$$u_\omega\Delta_{\mu\nu}\Delta_{\alpha\beta}\mathcal{I}^{\mu\nu\alpha\beta\omega} = u_\omega\Delta_{\mu\nu}\Delta_{\alpha\beta}\mathcal{I}_3^{\mu\nu\alpha\beta\omega} = a_{52}\cdot\left(3^2+3+3\right) = 15a_{52}. \tag{B.8}$$

Note, that products involving $\mathcal{I}_1^{\mu\nu\alpha\beta\gamma\delta\omega}\ldots\mathcal{I}_2^{\mu\nu\alpha\beta\gamma\delta\omega}$ vanish in this contraction because of $\Delta^{\mu\nu}u_\nu = 0$. On the other hand one obtains using Eq. (B.6)

$$\Delta_{\mu\nu}\Delta_{\alpha\beta}u_\omega\mathcal{I}^{\mu\nu\alpha\beta\omega} = \int d\Gamma\left(\Delta_{\mu\nu}p^\mu p^\nu\right)^2 u_\alpha p^\alpha f_0 = \int d\Gamma p_0^5 f_0\,. \tag{B.9}$$

which leads to

$$a_{52} = \frac{\int d\Gamma p_0^5 f_0}{15} = 8eT^3\,. \tag{B.10}$$

If the decomposition Eq. (B.7) is contracted with $\pi_{\mu\nu}\pi_{\alpha\beta}$ only the last 2 summands contribute and give identical results. One obtains

$$\pi_{\mu\nu}\pi_{\alpha\beta}\mathcal{I}^{\mu\nu\alpha\beta\omega} = 2\cdot a_{52}\cdot\pi_{\alpha\beta}\pi^{\alpha\beta}u^\omega. \tag{B.11}$$

Using the value of C_0 we realize that the contribution to the entropy density second order in shear stress is

$$s_2^\omega = -\frac{9}{8}\frac{1}{eT}\pi_{\alpha\beta}\pi^{\alpha\beta}u^\omega\,. \tag{B.12}$$

This corresponds to the expression in Eq. (3.24) with $\beta_2 = \frac{9}{4e}$ which is the value obtained by Israel and Stewart[40].

Now I evaluate the third-order contribution in Eq. (B.3), which is analogous to the calculation of the second-order term.

$$\begin{aligned} s_3^\omega &= \frac{1}{6}\int d\Gamma f_0 p^\omega \phi^3 = \frac{1}{6}C_0^3\int d\Gamma(\pi_{\mu\nu}p^\mu p^\nu)^3 p^\omega f_0 = \\ &= \frac{1}{6}C_0^3\pi_{\mu\nu}\pi_{\alpha\beta}\pi_{\gamma\delta}\int p^\mu p^\nu p^\alpha p^\beta p^\gamma p^\delta p^\omega f_0 = \frac{1}{6}C_0^3\pi_{\mu\nu}\pi_{\alpha\beta}\pi_{\gamma\delta}\mathcal{I}^{\mu\nu\alpha\beta\gamma\delta\omega} \end{aligned} \tag{B.13}$$

with

$$\mathcal{I}^{\mu\nu\alpha\beta\gamma\delta\omega} = \int d\Gamma p^\mu p^\nu p^\alpha p^\beta p^\gamma p^\delta p^\omega f_0\,. \tag{B.14}$$

The moment $\mathcal{I}^{\mu\nu\alpha\beta\gamma\delta\omega}$ of the equilibrium distribution is decomposed into orthogonal parts with thermodynamic coefficients a_{nk} as follows:

$$\begin{aligned} \mathcal{I}^{\mu\nu\alpha\beta\gamma\delta\omega} &= \mathcal{I}_1^{\mu\nu\alpha\beta\gamma\delta\omega} + \mathcal{I}_2^{\mu\nu\alpha\beta\gamma\delta\omega} + \mathcal{I}_3^{\mu\nu\alpha\beta\gamma\delta\omega} + \mathcal{I}_4^{\mu\nu\alpha\beta\gamma\delta\omega} = \\ &= a_{70}u^\mu u^\nu u^\alpha u^\beta u^\gamma u^\delta u^\omega + \\ &+ a_{71}\left(\Delta^{\mu\nu}u^\alpha u^\beta u^\gamma u^\delta u^\omega + \text{permutations}\right) + \\ &+ a_{72}\left(\Delta^{\mu\nu}\Delta^{\alpha\beta}u^\gamma u^\delta u^\omega + \text{permutations}\right) + \\ &+ a_{73}\left(\Delta^{\mu\nu}\Delta^{\alpha\beta}\Delta^{\gamma\delta}u^\omega + \text{permutations}\right)\,. \end{aligned} \tag{B.15}$$

Like in the derivation of the second-order component, we realize that the products $\pi_{\mu\nu}\pi_{\alpha\beta}\pi_{\gamma\delta}\mathcal{I}_1^{\mu\nu\alpha\beta\gamma\delta\omega} \ldots \pi_{\mu\nu}\pi_{\alpha\beta}\pi_{\gamma\delta}\mathcal{I}_3^{\mu\nu\alpha\beta\gamma\delta\omega}$ vanish because shear tensor is traceless and component-wise orthogonal to the flow velocity. Thus the only relevant contribution is now $\mathcal{I}_4^{\mu\nu\alpha\beta\gamma\delta\omega}$, though also here some permutations vanish if contracted with the shear tensor. For instance, all permutations containing explicitly $u^\mu, u^\nu, u^\alpha, u^\beta, u^\delta, u^\gamma$ will vanish immediately after contraction as discussed above. The relevant parts of $\mathcal{I}_4^{\mu\nu\alpha\beta\gamma\delta\omega}$ are

$$\begin{aligned} \mathcal{I}_4^{\mu\nu\alpha\beta\gamma\delta\omega} &\equiv a_{73}\cdot(\Delta^{\alpha\beta}\Delta^{\gamma\delta}\Delta^{\mu\nu}u^\omega + \Delta^{\alpha\gamma}\Delta^{\beta\delta}\Delta^{\mu\nu}u^\omega + \Delta^{\alpha\delta}\Delta^{\gamma\beta}\Delta^{\mu\nu}u^\omega \\ &+ \Delta^{\mu\alpha}\Delta^{\gamma\delta}\Delta^{\beta\nu}u^\omega + \Delta^{\alpha\nu}\Delta^{\gamma\delta}\Delta^{\mu\beta}u^\omega + \\ &+ \Delta^{\alpha\beta}\Delta^{\mu\gamma}\Delta^{\delta\nu}u^\omega + \Delta^{\alpha\beta}\Delta^{\gamma\nu}\Delta^{\mu\delta}u^\omega + \\ &+ \Delta^{\alpha\delta}\Delta^{\gamma\nu}\Delta^{\mu\beta}u^\omega + \Delta^{\alpha\nu}\Delta^{\gamma\beta}\Delta^{\mu\delta}u^\omega + \\ &+ \Delta^{\mu\alpha}\Delta^{\gamma\nu}\Delta^{\beta\delta}u^\omega + \Delta^{\alpha\delta}\Delta^{\mu\gamma}\Delta^{\beta\nu}u^\omega + \\ &+ \Delta^{\alpha\gamma}\Delta^{\beta\nu}\Delta^{\mu\delta}u^\omega + \Delta^{\alpha\nu}\Delta^{\mu\gamma}\Delta^{\beta\delta}u^\omega + \\ &+ \Delta^{\alpha\gamma}\Delta^{\mu\beta}\Delta^{\delta\nu}u^\omega + \Delta^{\mu\alpha}\Delta^{\gamma\beta}\Delta^{\delta\nu}u^\omega)\,. \end{aligned} \tag{B.16}$$

The total number of relevant permutations is 15. To calculate the thermodynamic coefficient a_{73} one evaluates the contraction $\Delta_{\mu\nu}\Delta_{\alpha\beta}\Delta_{\gamma\delta}u_\omega\mathcal{I}^{\mu\nu\alpha\beta\gamma\delta\omega}$ using Eq. (B.16) (note, that products involving $\mathcal{I}_1^{\mu\nu\alpha\beta\gamma\delta\omega}\ldots\mathcal{I}_3^{\mu\nu\alpha\beta\gamma\delta\omega}$ vanish in this contraction):

$$\Delta_{\mu\nu}\Delta_{\alpha\beta}\Delta_{\gamma\delta}u_\omega\mathcal{I}^{\mu\nu\alpha\beta\gamma\delta\omega} = a_{73}\cdot(3^3+6\cdot 3^2+8\cdot 3) = 105a_{73} \tag{B.17}$$

On the other hand one can use Eq. (B.14) to obtain

$$\Delta_{\mu\nu}\Delta_{\alpha\beta}\Delta_{\gamma\delta}u_\omega\mathcal{I}^{\mu\nu\alpha\beta\gamma\delta\omega} = \int d\Gamma\,(\Delta_{\mu\nu}p^\mu p^\nu)^3\,u_\alpha p^\alpha f_0 = -\int d\Gamma p_0^7 f_0\,. \tag{B.18}$$

One thus obtains for a_{73}

$$a_{73} = -\frac{\int d\Gamma p_0^7 f_0}{105} = 192eT^5\,. \tag{B.19}$$

Now the product $\pi_{\mu\nu}\pi_{\alpha\beta}\pi_{\gamma\delta}\mathcal{I}^{\mu\nu\alpha\beta\gamma\delta\omega} = \pi_{\mu\nu}\pi_{\alpha\beta}\pi_{\gamma\delta}\mathcal{I}_4^{\mu\nu\alpha\beta\gamma\delta\omega}$ can be completely evaluated. If the decomposition Eq. (B.16) is contracted with $\pi_{\mu\nu}\pi_{\alpha\beta}\pi_{\gamma\delta}$ only the last 8 summands contribute and give identical results. One obtains

$$\pi_{\mu\nu}\pi_{\alpha\beta}\pi_{\gamma\delta}\mathcal{I}^{\mu\nu\alpha\beta\gamma\delta\omega} = 8\cdot a_{73}\cdot\pi_{\alpha\beta}\pi^\beta_\sigma\pi^{\alpha\sigma}u^\omega\,. \tag{B.20}$$

Thus the contribution to the entropy density third order in shear stress is

$$s_3^\omega = -\frac{9}{2}\frac{1}{e^2T}\pi_{\alpha\beta}\pi^\beta_\sigma\pi^{\alpha\sigma}u^\omega\,. \tag{B.21}$$

This corresponds to the expression in Eq. (3.24) with $\beta_2 = \frac{9}{4e}$ and $\alpha = -\frac{8}{9}$ which is consistent with the values in Eqs. (6.22) and (6.23).

Up to third order in shear stress the entropy current calculated directly using Grad's approximation thus reads

$$s^\mu = s_0 - \frac{9}{8}\frac{1}{eT}\pi_{\alpha\beta}\pi^{\alpha\beta}u^\mu - \frac{9}{2}\frac{1}{e^2T}\pi_{\alpha\beta}\pi^\beta_\sigma\pi^{\alpha\sigma}u^\mu\,. \tag{B.22}$$

C. Hydrodynamic equations for one-dimensional boost-invariant systems

I consider longitudinally expanding boost-invariant systems of massless Boltzmann particles (gluons). The equations are given in the local rest frame of the fluid.

C.1. Systems with conserved particle number

$$\dot{n} = -\frac{n}{\tau} \tag{C.1}$$

$$\dot{e} = -\frac{4}{3}\frac{e}{\tau} + \frac{\pi}{\tau} \tag{C.2}$$

$$\text{first-order:} \quad \pi = \frac{4}{3}\frac{\eta}{\tau} \tag{C.3}$$

$$\text{second-order:} \quad \dot{\pi} = -\frac{\pi}{\tau_\pi} - \frac{4}{3}\frac{\pi}{\tau} + \frac{8}{27}\frac{e}{\tau} \tag{C.4}$$

$$\text{third-order:} \quad \dot{\pi} = -\frac{\pi}{\tau_\pi} - \frac{4}{3}\frac{\pi}{\tau} + \frac{8}{27}\frac{e}{\tau} - 3\frac{\pi^2}{e\tau} \tag{C.5}$$

$$\tau_\pi = \frac{9\eta}{2e} \tag{C.6}$$

C.2. Systems with particle creation and annihilation processes

Here the case of isotropic inelastic cross section is considered, $\sigma_{23} = \sigma_{23}(T)$.

$$\dot{n} = -\frac{n}{\tau} + \frac{1}{2} n^2 (1-\lambda)\, \sigma_{23} \tag{C.7}$$

$$\dot{e} = -\frac{4}{3}\frac{e}{\tau} + \frac{\pi}{\tau} \tag{C.8}$$

$$\text{first-order:} \quad \pi = \frac{4}{3}\frac{\eta}{\tau} \tag{C.9}$$

$$\text{second-order:} \quad \dot{\pi} = -\frac{\pi}{\tau_\pi} - \frac{4}{3}\frac{\pi}{\tau} + \frac{8}{27}\frac{e}{\tau} - \frac{1}{4}\pi n\, (1-\lambda)\, \sigma_{23} \tag{C.10}$$

$$\text{third-order:} \quad \dot{\pi} = -\frac{\pi}{\tau_\pi} - \frac{4}{3}\frac{\pi}{\tau} + \frac{8}{27}\frac{e}{\tau} - 3\frac{\pi^2}{e\tau} - \frac{1}{4}\left(1 + 3\frac{\pi}{e}\right) \pi n\, (1-\lambda)\, \sigma_{23} \tag{C.11}$$

$$\tau_\pi = \frac{9\eta}{2e} \tag{C.12}$$

$$\lambda = \frac{n}{n_{eq}} = \frac{n}{\frac{16}{\pi^2} T^3} \tag{C.13}$$

$$T = \frac{e}{3n} \tag{C.14}$$

The following scenarios of chemical evolution are considered:

- Instantaneous chemical equilibration: Eqs. (C.9)-(C.10) coupled to Eq. (C.8) with $\lambda = 1$.
- Chemical equilibration via particle production and annihilation with finite inelastic collision rate: Eqs. (C.9)-(C.11) coupled to Eqs. (C.7) and (C.8) with $\lambda = \frac{n}{\frac{16}{\pi^2}T^3}$ and $T = \frac{e}{3n}$.

The case of instantaneous chemical equilibration is not considered within the third-order formalism since it requires an infinitely large inelastic collision rates corresponding to infinitely small dissipative corrections.

C.3. System of two components with conserved particle numbers.

A system consisting of two components with isotropic elastic cross sections is considered.

$$n = n_1 + n_2 \tag{C.15}$$

$$e = e_1 + e_2 \tag{C.16}$$

$$\pi = \pi_1 + \pi_2 \tag{C.17}$$

$$\dot{n}_1 = -\frac{n_1}{\tau} \tag{C.18}$$

$$\dot{n}_2 = -\frac{n_2}{\tau} \tag{C.19}$$

$$\dot{e}_1 = -\frac{4}{3}\frac{e}{\tau}\frac{n_1}{n} + \frac{\pi}{\tau}\frac{n_1}{n} \tag{C.20}$$

$$\dot{e}_2 = -\frac{4}{3}\frac{e}{\tau}\frac{n_2}{n} + \frac{\pi}{\tau}\frac{n_2}{n} \tag{C.21}$$

$$\dot{\pi}_1 = -\frac{5}{9}\pi_1 n_1 \sigma_{11} - \frac{7}{9}\pi_1 n_2 \sigma_{12} + \frac{2}{9}\pi_2 n_1 \sigma_{12} - \frac{4}{3}\frac{\pi_1}{\tau} + \frac{8}{27}\frac{e_1}{\tau} \tag{C.22}$$

$$\dot{\pi}_2 = -\frac{5}{9}\pi_2 n_2 \sigma_{22} - \frac{7}{9}\pi_2 n_1 \sigma_{12} + \frac{2}{9}\pi_1 n_2 \sigma_{12} - \frac{4}{3}\frac{\pi_2}{\tau} + \frac{8}{27}\frac{e_2}{\tau} \tag{C.23}$$

D. Evolution equation for particle density in presence of inelastic processes.

In this appendix I derive the evolution equation for the particle number in presence of particle production and annihilation processes.

$$\partial_\mu N^\mu = \int \frac{d^3p}{(2\pi)^3 E} C[f] = \int \frac{d^3p}{(2\pi)^3 E} \left(C_{22}[f] + C_{23}[f] \right) = J$$

In the following, the phase space distribution function $f(x,p)$ is denoted by f_i in case it is related to the particle with the four-momentum p_i. Integrating the inelastic part $C_{23}[f]$, given in Eq. (7.7), over momentum p_1 one obtains

$$\begin{aligned}
&\int \frac{d^3p}{(2\pi)^3 E} C_{23} = \\
&\frac{1}{2}\int dw_1 dw_2 dw_3 \frac{1}{2}\int dw'_1 dw'_2 f'_1 f'_2 |M_{1'2'\to 123}|^2 (2\pi)^4 \delta^{(4)}(p'_1 + p'_2 - p_1 - p_2 - p_3) + \\
+ &\int dw_1 dw_2 \frac{1}{6}\int dw'_1 dw'_2 dw'_3 f'_1 f'_2 f'_3 |M_{1'2'3'\to 12}|^2 (2\pi)^4 \delta^{(4)}(p'_1 + p'_2 + p'_3 - p_1 - p_2) - \\
- &\frac{1}{2}\int dw_1 dw_2 dw_3 \frac{1}{2}\int dw'_1 dw'_2 f_1 f_2 f_3 |M_{123\to 1'2'}|^2 (2\pi)^4 \delta^{(4)}(p_1 + p_2 + p_3 - p'_1 - p'_2) - \\
- &\int dw_1 dw_2 \frac{1}{6}\int dw'_1 dw'_2 dw'_3 f_1 f_2 |M_{12\to 1'2'3'}|^2 (2\pi)^4 \delta^{(4)}(p_1 + p_2 - p'_1 - p'_2 - p'_3)
\end{aligned} \tag{D.1}$$

with the integration measure $dw = \frac{d^3p}{(2\pi)^3 2E}$. The first and the last summands contain an integration over the transition matrix element squared $|M_{2\to 3}|^2$ and the momenta of the final three-particle state. This integration can be absorbed into the definition of the total cross section σ_{23} of an inelastic two-particle process[76, 41]:

$$2 \cdot s \cdot \sigma_{23} \equiv \frac{1}{3!}\int dw'_1 dw'_2 dw'_3 |M_{12\to 1'2'3'}|^2 (2\pi)^4 \delta^{(4)}(p_1 + p_2 - p'_1 - p'_2 - p'_3) \tag{D.2}$$

with $s = p_{1\mu} p_2^\mu = E_1 \cdot E_2 - \vec{p}_1 \cdot \vec{p}_2$ being the invariant center of mass energy of the two colliding particles. The prefactor 1/3! indicates that the three particles in the final state are identical and thus all possible 3! permutations have to be taken into account. The origin of other numerical prefactors in front of the integrals in the collision term was already discussed after Eqs. (7.6) and (7.7) in Section 7.1. In the remaining part of the first and the last summands in Eq. (D.1) the relative velocity of the two colliding particles can be introduced

$$v_{rel} = \frac{s}{2E_1E_2}\,. \tag{D.3}$$

With Eq. (D.3) the first and the last summand can be written as

$$\begin{aligned} &\frac{1}{2}\int dw_1 dw_2 dw_3 \frac{1}{2}\int dw'_1 dw'_2 f'_1 f'_2 |M_{1'2'\to 123}|^2 (2\pi)^4 \delta^{(4)}(p'_1 + p'_2 - p_1 - p_2 - p_3) - \\ -\ &\int dw_1 dw_2 \frac{1}{6}\int dw'_1 dw'_2 dw'_3 f_1 f_2 |M_{12\to 1'2'3'}|^2 (2\pi)^4 \delta^{(4)}(p_1 + p_2 - p'_1 - p'_2 - p'_3) = \\ =\ &\frac{1}{2}\int d^3p_1 d^3p_2 f_1 f_2 v_{rel}\sigma_{23} \equiv \frac{1}{2} n^2 \langle v_{rel}\sigma_{23}\rangle_2\,. \end{aligned} \tag{D.4}$$

In the latter equation the angular brackets denote an average over all possible multiplets (pairs, triplets) of particles (c.f. Refs. [41, 127, 35]):

$$\langle \mathcal{Q}\rangle_m \equiv \frac{1}{n^m}\int \frac{d^3p_1}{(2\pi)^3}\cdots\frac{d^3p_m}{(2\pi)^3} f_1 \ldots f_m \mathcal{Q}\,. \tag{D.5}$$

Analogously, the second and the third summands in Eq. (D.1) can be rewritten absorbing integration over the final two-particle states into the definition

$$\mathcal{I}_{32} = \frac{1}{2}\int dw_1 dw_2 |M_{1'2'3'\to 12}|^2 (2\pi)^4 \delta^{(4)}(p'_1 + p'_2 + p'_3 - p_1 - p_2)\,. \tag{D.6}$$

One then obtains

$$\begin{aligned} &\int dw_1 dw_2 \frac{1}{6}\int dw'_1 dw'_2 dw'_3 f'_1 f'_2 f'_3 |M_{1'2'3'\to 12}|^2 (2\pi)^4 \delta^{(4)}(p'_1 + p'_2 + p'_3 - p_1 - p_2) - \\ -\ &\frac{1}{2}\int dw_1 dw_2 dw_3 \frac{1}{2}\int dw'_1 dw'_2 f_1 f_2 f_3 |M_{123\to 1'2'}|^2 (2\pi)^4 \delta^{(4)}(p_1 + p_2 + p_3 - p'_1 - p'_2) = \\ -\ &\frac{1}{6}\int d^3p_1 d^3p_2 d^3p_3 f_1 f_2 f_3 \frac{\mathcal{I}_{32}}{8E_1E_2E_3} \equiv \frac{1}{6} n^3 \langle \frac{\mathcal{I}_{32}}{8E_1E_2E_3}\rangle_3\,. \end{aligned} \tag{D.7}$$

Putting together Eqs. (D.4)-(D.7) one thus can write

$$\int C_{23}[f(x,p)]\frac{d^3p}{(2\pi)^3E} = \frac{1}{2} n^2 \langle v_{rel}\sigma_{23}\rangle - \frac{1}{6} n^3 \langle \frac{\mathcal{I}_{32}}{8E_1E_2E_3}\rangle_3\,. \tag{D.8}$$

With the definitions of the inelastic collision rates

$$R_{23} = n\langle v_{\mathrm{rel}}\sigma_{23}\rangle_2\,, \quad R_{32} = \frac{1}{2} n^2 \left\langle \frac{I_{32}}{8E_1E_2E_3}\right\rangle_3\,, \tag{D.9}$$

one thus obtains a rate equation for the divergence of the particle number current:

$$\partial_\mu N^\mu = \frac{1}{2} n R_{23} - \frac{1}{3} n R_{32}\,. \tag{D.10}$$

In Eq. (D.5) f_i represent the *off-equilibrium* phase space distribution, which in this work is approximated by introducing a small deviation from the isotropic equilibrium distribution f_{0i}:

$$f_i = f_{0i}\left(1+\phi_i\right) \tag{D.11}$$

with $f_0 \equiv g\lambda e^{-E/T}$. g denotes the degeneracy factor and is 16 for applications presented in this work. λ is the fugacity, describing deviations from chemical equilibrium. The deviation ϕ_i describes deformation of the momentum space distribution.

In order to obtain an evolution equation for the particle number in a anisotropic system, the rates R_{23} and R_{32} have to be evaluated using the approximated distribution function. In particular, one has to evaluate the averages $\langle \ldots \rangle_2$ and $\langle \ldots \rangle_3$. Inserting Eq. (D.11) into the definition Eq. (D.5, one obtains

$$\begin{aligned}\langle v_{\mathrm{rel}}\sigma_{23}\rangle_2 &= \frac{1}{n^2}\int \frac{d^3p_1}{(2\pi)^3}\frac{d^3p_2}{(2\pi)^3}\frac{s}{2E_1E_2}\sigma_{23} f_{01} f_{02}\left(\phi_1+\phi_2+\phi_1\phi_2+1\right) = \\ &= \frac{1}{n^2}\frac{1}{(2\pi)^6}\int \frac{d^3p_1}{E_1}\frac{d^3p_2}{E_2}\sigma_{23} f_{01} f_{02}(\underbrace{\phi_1}_{\textcircled{2a}}+\underbrace{\phi_2}_{\textcircled{2b}}+\underbrace{\phi_1\phi_2}_{\textcircled{2c}}+\underbrace{1}_{\textcircled{2d}})\cdot\left(E_1E_2 - p_{x1}p_{x2} - p_{y1}p_{y2} - p_{z1}p_{z2}\right)\end{aligned} \tag{D.12}$$

$$\begin{aligned}\langle \frac{I_{32}}{8E_1E_2E_3}\rangle_3 &= \frac{1}{n^3}\frac{1}{8\cdot(2\pi)^9}\int \frac{d^3p_1}{E_1}\frac{d^3p_2}{E_2}\frac{d^3p_3}{E_3}\mathcal{I}_{32} f_{01} f_{02} f_{03}\,\times \\ &\times\left(\underbrace{\phi_1}_{\textcircled{3a}}+\underbrace{\phi_2}_{\textcircled{3b}}+\underbrace{\phi_3}_{\textcircled{3c}}+\underbrace{\phi_1\phi_2}_{\textcircled{3d}}+\underbrace{\phi_2\phi_3}_{\textcircled{3e}}+\underbrace{\phi_1\phi_3}_{\textcircled{3f}}+\underbrace{\phi_1\phi_2\phi_3}_{\textcircled{3g}}+\underbrace{1}_{\textcircled{3h}}\right).\end{aligned} \tag{D.13}$$

The total cross section σ_{23} and $\mathcal{I}_{32}$ can be put in front of the integral. Due to symmetry of the indices, there three groups of identical integrals – these are integrals containing the following terms:
(2a) and(2b);
(3a),(3b) and(3c);
(3d),(3e) and(3f).
First, it is necessary to evaluate the integrals(2a) and(3a). This will be done in the following.

The equilibrium deviation ϕ_i needed to evaluate(2a) and(3a) is modeled using Grad's method, discussed in chapters 2.4.1 and 8. In particular I will employ its one-dimensional form, given in Eq. (8.1). Evaluating the integral containing (2a) one obtains

$$(2a) = \frac{g^2\lambda^2}{n^2(2\pi)^6}\sigma_{23}\frac{\bar{\pi}}{16eT^2}\int dp_{T1}dp_{T2}d\varphi_1 d\varphi_2 dy_1 dy_2 p_{T1}^4 p_{T2}^2 e^{-p_{T1}/T\cosh y_1} e^{-p_{T2}/T\cosh y_2} \times$$
$$\times\left(\cosh y_1\cosh y_2-\cos\varphi_1\cos\varphi_2-\sin\varphi_1\sin\varphi_2-\sinh y_1\sinh y_2\right)\cdot\left(\sinh^2 y_1-\frac{1}{2}\right) = 0\,. \tag{D.14}$$

By analogy to Eq. (D.14), parts (2b) and (2c) evaluate to 0 as well. The reason for this are the properties of the deviation functions ϕ_1 and ϕ_2, which have to satisfy the matching conditions Eqs. (2.36) and (2.37), as discussed in section 2.4.2, and which are symmetric, due to the particular form Eq.(8.1) used here, under the transformation $\vec{p}\to-\vec{p}$. The only non-vanishing parts of Eq. (D.12) is the part which does not contain either ϕ_1 or ϕ_2. Thus, Eq. (D.12) reduces to averaging over the equilibrium distribution functions f_{0i} of the two incoming particles.

The term (3a) describes a three-particle initial state. Evaluating it one obtains

$$(3a) = \frac{1}{8}\frac{\bar{\pi}}{eT^2}\frac{g^3\lambda^3}{(2\pi)^9}\int dp_{T1}dy_1 d\varphi_1 p_{T1}^3 e^{-p_{T1}/T\cosh y_1}\left(\sinh^2 y_1-\frac{1}{2}\right)\int d\Gamma_2 d\Gamma_3 f_{02}f_{03} = 0\,.$$

Note that all integrals in Eq. (D.13) factorize into products of three independent integrals. Since (3a) vanishes, seven of eight integrals, in particular (3a)-(3g), in Eq. (D.13) vanish as well. The non-vanishing part of Eq. (D.13) does not contain the deviations functions ϕ_i from Grad's approximation but only f_{0i}.

Thus, Eq. (D.13) reduces, just like Eq. (D.12), to averaging over the equilibrium distribution functions f_{0i} of the three incoming particles. I.e. we obtain the identity

$$\int\frac{d^3p}{(2\pi)^3E}C_{23}[f_{Grad}] = \frac{d^3p}{(2\pi)^3E}C_{23}[f_0]\,. \tag{D.15}$$

Evaluating the non-vanishing parts of Eqs. (D.12) and (D.13) using the equilibrium distribution for gluons $f_0 = 16\lambda e^{-E/T}$ one obtains

$$\partial_\mu N^\mu = \int\frac{d^3}{(2\pi)^3E}C_{23}[f_0] = 128\frac{\lambda^2T^6}{\pi^4}\sigma_{23}-\frac{32}{3}\frac{\lambda^3T^6}{\pi^6}\mathcal{I}_{32}\,. \tag{D.16}$$

With isotropic cross sections the integrals in $\mathcal{I}_{32}$ can be evaluated analytically and one obtains for a gluon gas[30, 41]

$$\mathcal{I}_{32} = 12\pi^2\sigma_{23}\,. \tag{D.17}$$

Using Eq. (D.16) together with (D.17) one thus obtains the evolution equation for the particle density for the Bjorken scenario considered in this work:

$$\partial_\mu N^\mu = \dot{n}+\frac{n}{\tau} = \frac{1}{2}n^2(1-\lambda)\sigma_{23}\,. \tag{D.18}$$

which is the same as in Refs. [89, 88, 87, 174, 182]. The kinetic off-equilibrium effects, corresponding to the deviation function $\phi(x,p)$ do not explicitly affect the particle production.

E. Shear viscosity coefficients for a multi-component fluid.

In this Chapter the integrals in Eq. (4.12) will be evaluated assuming a one-dimensional setup. Let us consider a system with isotropic momentum distribution in transverse xy plane and anisotropy in longitudinal z dirction. The shear stress tensor is then diagonal

$$\pi^{\mu\nu} = diag(0, \pi/2, \pi/2, -\pi)\,, \tag{E.1}$$

with π denoting the shear pressure. Without the heat and bulk contributions the off-equilibirum distributions can be written in local rest frame as

$$f_i(x,p) = f_{0,i}\,(1 + \phi_i(x,p)) = \lambda_i d_i e^{-E_i}\left(1 + C_{0,i}\pi_i(p_z^2 - \frac{1}{2}p_T^2)\right)\,. \tag{E.2}$$

Two components – which will be denoted as Flavor a and Flavor b – and only elastic binary processes will be considered since we have used particle number conservation for all components to obtain Eq. (4.12). We will calculate η_a here. Using the binary collision term $C_{bin}[..]$ [30] one now can write contraction of its second moment with the shear tensor as follows:

$$\begin{aligned}
&\pi_{\mu\nu}\int p^\mu p^\nu\Big(C_{bin}[f_a] + C_{bin}[f_a,f_b]\Big)\frac{d^3p}{E(2\pi)^3} = \\
&= \pi\int (p_z^2 - \frac{1}{2}p_T^2)\Big(C_{bin}[f_a] + C_{bin}[f_a,f_b]\Big)\frac{d^3p}{E(2\pi)^3} = \\
&= \int (p_{1,z}^2 - \frac{1}{2}p_{2,T}^2)d\Gamma_1 d\Gamma_2\cdot\frac{1}{\nu_{aa}}\int d\Gamma_1' d\Gamma_2' f_{a,1}' f_{a,2}'|M_{1'2'\to 12}|^2(2\pi)^4\delta^{(4)}(p_1+p_2-p_1'-p_2') - \\
&- \int (p_{1,z}^2 - \frac{1}{2}p_{1,T}^2)d\Gamma_1 d\Gamma_2\cdot\frac{1}{\nu_{aa}}\int d\Gamma_1' d\Gamma_2' f_{a,1} f_{a,2}|M_{12\to 1'2'}|^2(2\pi)^4\delta^{(4)}(p_1+p_2-p_1'-p_2') + \\
&+ \int (p_{1,z}^2 - \frac{1}{2}p_{1,T}^2)d\Gamma_1 d\Gamma_2\cdot\frac{1}{\nu_{ab}}\int d\Gamma_1' d\Gamma_2' f_{a,1}' f_{b,2}'|M_{1'2'\to 12}|^2(2\pi)^4\delta^{(4)}(p_1+p_2-p_1'-p_2') - \\
&- \int (p_{1,z}^2 - \frac{1}{2}p_{1,T}^2)d\Gamma_1 d\Gamma_2\cdot\frac{1}{\nu_{ab}}\int d\Gamma_1' d\Gamma_2' f_{a,1} f_{b,2}|M_{12\to 1'2'}|^2(2\pi)^4\delta^{(4)}(p_1+p_2-p_1'-p_2')\,.
\end{aligned} \tag{E.3}$$

with $d\Gamma \equiv d^3p/(2E)/(2\pi)^3$. The factors $\nu_{aa} = 2$ and $\nu_{ab} = 1$ account for the fact that particles are indistinguishable in case of two identical Flavors and distinguishable in case their Flavors are different.

Now the distribution functions $f_a(\lambda_a, e_a, \pi_a, T, p^\mu)$ and $f_b(\lambda_b, e_b, \pi_b, T, p^\mu)$ must be inserted into Eq. (E.3). In the integrals expressions of the following from will appear:

$$\mathfrak{I} \equiv \int\int d\Gamma_1 d\Gamma_2 \cdot \mathfrak{g}(p_1')|M_{1'2'\to 12}|^2 \cdot \delta^{(4)}(p_1 + p_2 - p_1' - p_2') \tag{E.4}$$

These integrals can be transformed to the following form [76, 212]:

$$\mathfrak{I} = \frac{2s\nu}{4\pi} \int \mathfrak{g}(p'_{1TR}) \frac{d\sigma_{22}}{d\Omega^*} d\Omega^* \,. \tag{E.5}$$

In the latter equation p'_{1TR} denotes Lorentz transformation from the center-of-mass (CM) frame of two particles with four-momenta p_1 and p_2 into the lab frame. This transformation is given by the Loretz faktor $\vec{\beta} = (\vec{p}_1 + \vec{p}_2)/(E_1 + E_2)$. In the CM frame the momentum p_1' is given by $p_1' = \frac{\sqrt{s}}{2}(1, \cos\theta^* \cos\phi^*, \cos\theta^* \sin\phi^*, \sin\theta^*)$, with $\sqrt{s}$ being the center-of-mass energy of the colliding particles, $s = (p_1 + p_2)^2$. The integral (E.5) can be evaluated if the differental cross section $d\sigma_{22}/d\Omega$ is momentum independent. This means that the scattering angle is isotropically distributed.. Here only this type of scattering processes is considered.

For the trivial case $\mathfrak{g}(p_1') = 1$ one obtains $\mathfrak{I} = 2s\nu\sigma_{22}$. In case of non-trivial $\mathfrak{g}(p_1')$ the integral $\mathfrak{I}$ additionally depends on four-momenta p_1 and p_2, which are relevant for evaluation of the remaining integrals in Eq. (E.3).

After all integrals are solved in Eq. (E.3) one obtains by inserting (E.3) into (4.12) the following expression for the shear viscosity coefficient of component a:

$$\eta_a = T\left(\frac{5}{6}\sigma_{aa} + \frac{7}{6}\frac{n_b}{n_a}\sigma_{ab} - \frac{1}{3}\frac{\pi_b}{\pi_a}\sigma_{ab}\right)^{-1} \,. \tag{E.6}$$

This result, reported in Refs. [201] and [36] is only valid for systems with binary collision processes and isotropic scattering angle distribution.

Bibliography

[1] E. V. Shuryak, *Quantum chromodynamics and the theory of superdense matter*, Physics Reports **61** (1980), no. 2 71 – 158.

[2] W. Scheid, H. Muller and W. Greiner, *Nuclear Shock Waves in Heavy-Ion Collisions*, Phys.Rev.Lett. **32** (1974) 741–745.

[3] E. V. Shuryak, *Quark-Gluon Plasma and Hadronic Production of Leptons, Photons and Psions*, Phys. Lett. **B78** (1978) 150.

[4] T. Rentzsch, G. Graebner, J. Maruhn, H. Stoecker and W. Greiner, *(3+1)-dimensional relativistic hydrodynamic space-time evolution of the reaction o (200-gev/n) —&gt; pb*, Mod.Phys.Lett. **A2** (1987) 193–198.

[5] J. Brachmann, A. Dumitru, J. Maruhn, H. Stoecker, W. Greiner et. al., *Nonequilibrium fluid dynamics in the early stage of ultrarelativistic heavy ion collisions*, Nucl.Phys. **A619** (1997) 391–412 [`nucl-th/9703032`].

[6] **STAR** Collaboration, K. H. Ackermann et. al., *Elliptic flow in Au + Au collisions at s(N N)**(1/2) = 130-GeV*, Phys. Rev. Lett. **86** (2001) 402–407 [`nucl-ex/0009011`].

[7] **PHENIX Collaboration** Collaboration, S. S. Adler et. al., *Elliptic flow of identified hadrons in Au+Au collisions at s(NN)**(1/2) = 200-GeV*, Phys.Rev.Lett. **91** (2003) 182301 [`nucl-ex/0305013`].

[8] P. Huovinen, P. F. Kolb, U. W. Heinz, P. V. Ruuskanen and S. A. Voloshin, *Radial and elliptic flow at RHIC: further predictions*, Phys. Lett. **B503** (2001) 58–64 [`hep-ph/0101136`].

[9] T. Hirano and K. Tsuda, *Collective flow and two pion correlations from a relativistic hydrodynamic model with early chemical freeze out*, Phys. Rev. **C66** (2002) 054905 [`nucl-th/0205043`].

[10] M. J. Tannenbaum, *Recent results in relativistic heavy ion collisions: From ' a new state of matter ' to ' the perfect fluid '*, Rept. Prog. Phys. **69** (2006) 2005–2060 [`nucl-ex/0603003`].

[11] H. Song and U. W. Heinz, *Suppression of elliptic flow in a minimally viscous quark- gluon plasma*, Phys. Lett. **B658** (2008) 279–283 [`0709.0742`].

[12] M. Luzum, *Relativistic Heavy Ion Collisions: Viscous Hydrodynamic Simulations and Final State Interactions*, `0908.4100`.

[13] T. Matsui and H. Satz, *J/psi Suppression by Quark-Gluon Plasma Formation*, Phys. Lett. **B178** (1986) 416.

[14] L. Bravina et. al., *Can the RHIC J/psi puzzle(s) be settled at LHC?*, Eur. Phys. J. **C61** (2009) 865–870 [`0811.0790`].

[15] R. Rapp, D. Blaschke and P. Crochet, *Charmonium and bottomonium in heavy-ion collisions*, Progress in Particle and Nuclear Physics **65** (2010), no. 2 209 – 266.

[16] X.-N. Wang and M. Gyulassy, *Gluon shadowing and jet quenching in A + A collisions at s**(1/2) = 200-GeV*, Phys. Rev. Lett. **68** (1992) 1480–1483.

[17] **STAR** Collaboration, C. Adler et. al., *Centrality dependence of high* p_T *hadron suppression in Au+Au collisions at* $\sqrt{s}_{NN}$ *= 130-GeV*, Phys. Rev. Lett. **89** (2002) 202301 [`nucl-ex/0206011`].

[18] **PHENIX** Collaboration, S. S. Adler et. al., *Suppressed pi0 production at large transverse momentum in central Au + Au collisions at s(NN)**(1/2) = 200-GeV*, Phys. Rev. Lett. **91** (2003) 072301 [`nucl-ex/0304022`].

[19] **STAR** Collaboration, J. Adams et. al., *Transverse momentum and collision energy dependence of high p(T) hadron suppression in Au + Au collisions at ultrarelativistic energies*, Phys. Rev. Lett. **91** (2003) 172302 [`nucl-ex/0305015`].

[20] M. Gyulassy, I. Vitev, X.-N. Wang and B.-W. Zhang, *Jet quenching and radiative energy loss in dense nuclear matter*, `nucl-th/0302077`.

[21] A. Kovner and U. A. Wiedemann, *Gluon radiation and parton energy loss*, `hep-ph/0304151`.

[22] O. Fochler, Z. Xu and C. Greiner, *Towards a unified understanding of jet-quenching and elliptic flow within perturbative QCD parton transport*, Phys. Rev. Lett. **102** (2009) 202301 [`0806.1169`].

[23] T. Schafer, *Nearly perfect fluidity*, Physics **2** (Oct, 2009) 88.

[24] T. Schafer and D. Teaney, *Nearly Perfect Fluidity: From Cold Atomic Gases to Hot Quark Gluon Plasmas*, Rept. Prog. Phys. **72** (2009) 126001 [`0904.3107`].

[25] P. Kovtun, D. T. Son and A. O. Starinets, *Viscosity in strongly interacting quantum field theories from black hole physics*, Phys. Rev. Lett. **94** (2005) 111601 [`hep-th/0405231`].

[26] *The Frontiers of Nuclear Science, A Long Range Plan*, `0809.3137`.

[27] K. Geiger and B. Mueller, *Dynamics of parton cascades in highly relativistic nuclear collisions*, Nuclear Physics B **369** (1992), no. 3 600 – 654.

[28] B. Zhang, *ZPC 1.0.1: A parton cascade for ultrarelativistic heavy ion collisions*, Comput. Phys. Commun. **109** (1998) 193–206 [`nucl-th/9709009`].

[29] D. Molnar and M. Gyulassy, *New solutions to covariant nonequilibrium dynamics*, Phys. Rev. **C62** (2000) 054907 [`nucl-th/0005051`].

[30] Z. Xu and C. Greiner, *Thermalization of gluons in ultrarelativistic heavy ion collisions by including three-body interactions in a parton cascade*, Phys. Rev. **C71** (2005) 064901 [`hep-ph/0406278`].

[31] G. Ferini, M. Colonna, M. Di Toro and V. Greco, *Scalings of Elliptic Flow for a Fluid at Finite Shear Viscosity*, Phys. Lett. **B670** (2009) 325–329 [`0805.4814`].

[32] A. El, Z. Xu and C. Greiner, *Thermalization of a color glass condensate and review of the 'Bottom-Up' scenario*, Nucl. Phys. **A806** (2008) 287–304 [`0712.3734`].

[33] A. El, A. Muronga, Z. Xu and C. Greiner, *Shear viscosity and out of equilibrium dynamics*, Physical Review C (Nuclear Physics) **79** (2009), no. 4 044914.

[34] A. El, Z. Xu and C. Greiner, *Extension of relativistic dissipative hydrodynamics to third order*, Phys. Rev. **C81** (2010) 041901 [`0907.4500`].

[35] A. El, A. Muronga, Z. Xu and C. Greiner, *A Relativistic dissipative hydrodynamic description for systems including particle number changing processes*, Nucl.Phys. **A848** (2010) 428–442 [`1007.0705`].

[36] A. El, I. Bouras, F. Lauciello, Z. Xu and C. Greiner, *Dissipative hydrodynamics for relativistic multi-component systems*, `1103.4038`.

[37] R. Baier, P. Romatschke and U. A. Wiedemann, *Dissipative hydrodynamics and heavy ion collisions*, Phys. Rev. **C73** (2006) 064903 [`hep-ph/0602249`].

[38] B. Betz, D. Henkel and D. H. Rischke, *From kinetic theory to dissipative fluid dynamics*, Prog. Part. Nucl. Phys. **62** (2009) 556 [`0812.1440`].

[39] G. S. Denicol, T. Koide and D. H. Rischke, *Dissipative relativistic fluid dynamics: a new way to derive the equations of motion from kinetic theory*, `1004.5013`.

[40] W. Israel and J. M. Stewart, *Transient relativistic thermodynamics and kinetic theory*, Ann. Phys. **118** (1979) 341–372.

[41] Z. Xu and C. Greiner, *Transport rates and momentum isotropization of gluon matter in ultrarelativistic heavy-ion collisions*, Phys. Rev. **C76** (2007) 024911 [`hep-ph/0703233`].

[42] Z. Xu and C. Greiner, *Shear viscosity in a gluon gas*, Phys. Rev. Lett. **100** (2008) 172301 [`0710.5719`].

[43] C. Wesp, A. El, F. Reining, Z. Xu, I. Bouras et. al., *Calculation of shear viscosity using Green-Kubo relations within a parton cascade*, `1106.4306`. * Temporary entry *.

[44] F. Reining, I. Bouras, A. El, C. Wesp, Z. Xu et. al., *Extraction of shear viscosity in stationary states of relativistic particle systems*, `1106.4210`. * Temporary entry *.

[45] J. D. Bjorken, *Highly relativistic nucleus-nucleus collisions: The central rapidity region*, Phys. Rev. D **27** (Jan, 1983) 140–151.

[46] P. Huovinen and D. Molnar, *The applicability of causal dissipative hydrodynamics to relativistic heavy ion collisions*, Phys. Rev. **C79** (2009) 014906 [`0808.0953`].

[47] H. Song and U. W. Heinz, *Causal viscous hydrodynamics in 2+1 dimensions for relativistic heavy-ion collisions*, Phys. Rev. **C77** (2008) 064901 [`0712.3715`].

[48] S. Bethke, *Determination of the QCD coupling* α_s, J. Phys. **G26** (2000) R27 [`hep-ex/0004021`].

[49] S. Bethke, *The 2009 Wolrd Average of* $\alpha_s(M_Z)$, Eur. Phys. J. **C64** (2009) 689–703 [`0908.1135`].

[50] "http://www.gsi.de/fair/experiments/CBM/1intro.html."

[51] J. Cleymans, H. Oeschler, K. Redlich and S. Wheaton, *Comparison of chemical freeze-out criteria in heavy-ion collisions*, Phys. Rev. **C73** (2006) 034905 [`hep-ph/0511094`].

[52] J. Randrup and J. Cleymans, *Exploring high-density baryonic matter: Maximum freeze-out density*, `0905.2824`.

[53] C. R. Allton et. al., *The equation of state for two flavor QCD at non-zero chemical potential*, Phys. Rev. **D68** (2003) 014507 [`hep-lat/0305007`].

[54] F. Karsch, E. Laermann and A. Peikert, *The pressure in 2, 2+1 and 3 flavour QCD*, Phys. Lett. **B478** (2000) 447–455 [`hep-lat/0002003`].

[55] F. Karsch, *Lattice QCD at high temperature and density*, Lect. Notes Phys. **583** (2002) 209–249 [`hep-lat/0106019`].

[56] **BRAHMS** Collaboration, I. Arsene et. al., *Quark Gluon Plasma an Color Glass Condensate at RHIC? The perspective from the BRAHMS experiment*, Nucl. Phys. **A757** (2005) 1–27 [`nucl-ex/0410020`].

[57] B. B. Back et. al., *The PHOBOS perspective on discoveries at RHIC*, Nucl. Phys. **A757** (2005) 28–101 [`nucl-ex/0410022`].

[58] **STAR** Collaboration, J. Adams et. al., *Experimental and theoretical challenges in the search for the quark gluon plasma: The STAR collaboration's critical assessment of the evidence from RHIC collisions*, Nucl. Phys. **A757** (2005) 102–183 [`nucl-ex/0501009`].

[59] **PHENIX** Collaboration, K. Adcox et. al., *Formation of dense partonic matter in relativistic nucleus nucleus collisions at RHIC: Experimental evaluation by the PHENIX collaboration*, Nucl. Phys. **A757** (2005) 184–283 [`nucl-ex/0410003`].

[60] J.-Y. Ollitrault, *Anisotropy as a signature of transverse collective flow*, Phys. Rev. **D46** (1992) 229–245.

[61] D. Teaney, *Effect of shear viscosity on spectra, elliptic flow, and hanbury brown–twiss radii*, Phys. Rev. C **68** (Sep, 2003) 034913.

[62] P. Romatschke and U. Romatschke, *Viscosity Information from Relativistic Nuclear Collisions: How Perfect is the Fluid Observed at RHIC?*, Phys. Rev. Lett. **99** (2007) 172301 [`0706.1522`].

[63] K. Dusling and D. Teaney, *Simulating elliptic flow with viscous hydrodynamics*, Phys. Rev. **C77** (2008) 034905 [`0710.5932`].

[64] **PHENIX** Collaboration, A. Adare et. al., *Scaling properties of azimuthal anisotropy in Au + Au and Cu + Cu collisions at s(NN)**(1/2) = 200-GeV*, Phys. Rev. Lett. **98** (2007) 162301 [`nucl-ex/0608033`].

[65] R. J. Fries, B. Muller, C. Nonaka and S. A. Bass, *Hadron production in heavy ion collisions: Fragmentation and recombination from a dense parton phase*, Phys. Rev. **C68** (2003) 044902 [`nucl-th/0306027`].

[66] R. J. Fries, B. Muller, C. Nonaka and S. A. Bass, *Hadronization in heavy ion collisions: Recombination and fragmentation of partons*, Phys. Rev. Lett. **90** (2003) 202303 [`nucl-th/0301087`].

[67] V. Greco, C. M. Ko and P. Levai, *Parton coalescence at RHIC*, Phys. Rev. **C68** (2003) 034904 [`nucl-th/0305024`].

[68] V. Greco, C. M. Ko and P. Levai, *Parton coalescence and antiproton/pion anomaly at RHIC*, Phys. Rev. Lett. **90** (2003) 202302 [`nucl-th/0301093`].

[69] S. A. Bass, *Microscopic reaction dynamics at SPS and RHIC*, Nucl. Phys. **A698** (2002) 164–170 [`nucl-th/0104040`].

[70] L. D. McLerran and R. Venugopalan, *Computing quark and gluon distribution functions for very large nuclei*, Phys. Rev. **D49** (1994) 2233–2241 [`hep-ph/9309289`].

[71] A. Krasnitz, Y. Nara and R. Venugopalan, *Coherent gluon production in very high energy heavy ion collisions*, Phys. Rev. Lett. **87** (2001) 192302 [`hep-ph/0108092`].

[72] A. Krasnitz, Y. Nara and R. Venugopalan, *Gluon production in the color glass condensate model of collisions of ultrarelativistic finite nuclei*, Nucl. Phys. **A717** (2003) 268–290 [`hep-ph/0209269`].

[73] S. Mrowczynski, *Plasma instability at the initial stage of ultrarelativistic heavy ion collisions*, Phys. Lett. **B314** (1993) 118–121.

[74] A. Rebhan, M. Strickland and M. Attems, *Instabilities of an anisotropically expanding non-Abelian plasma: 1D+3V discretized hard-loop simulations*, Phys. Rev. **D78** (2008) 045023 [`0802.1714`].

[75] A. Dumitru and Y. Nara, *QCD plasma instabilities and isotropization*, Phys. Lett. **B621** (2005) 89–95 [`hep-ph/0503121`].

[76] C. G. v. W. S. R. de Groot, W. A. van Leeuwen, Relativistic Kinetic Theory: Principles and Applications. North Holland, Amsterdam, 1980.

[77] S. A. Bass et. al., *Microscopic models for ultrarelativistic heavy ion collisions*, Prog. Part. Nucl. Phys. **41** (1998) 255–369 [`nucl-th/9803035`].

[78] M. Bleicher et. al., *Relativistic hadron hadron collisions in the ultra- relativistic quantum molecular dynamics model*, J. Phys. **G25** (1999) 1859–1896 [`hep-ph/9909407`].

[79] W. Ehehalt and W. Cassing, *Relativistic transport approach for nucleus-nucleus collisions based on a NJL Lagrangian*, `hep-ph/9507274`.

[80] A. Muronga, *Causal Theories of Dissipative Relativistic Fluid Dynamics for Nuclear Collisions*, Phys. Rev. **C69** (2004) 034903 [`nucl-th/0309055`].

[81] Z. Fodor and S. D. Katz, *The phase diagram of quantum chromodynamics*, `0908.3341`.

[82] H. Grad Commun. Pure Appl. Math. **2** (1949) 331.

[83] A. Muronga, *Relativistic dynamics of non-ideal fluids: Viscous and heat-conducting fluids. ii. transport properties and microscopic description of relativistic nuclear matter*, Physical Review C (Nuclear Physics) **76** (2007), no. 1 014910.

[84] D. H. Rischke. PhD thesis, University of Frankfurt, 1992.

[85] I. Bouras et. al., *Investigation of shock waves in the relativistic Riemann problem: A comparison of viscous fluid dynamics to kinetic theory*, Phys. Rev. **C82** (2010) 024910 [`1006.0387`].

[86] M. Martinez and M. Strickland, *Dissipative Dynamics of Highly Anisotropic Systems*, `1007.0889`.

[87] A. Muronga, *Viscous hydrodynamics*, J. Phys. **G31** (2005) S1035–S1039 [`0710.3277`].

[88] T. S. Biro, E. van Doorn, B. Muller, M. H. Thoma and X. N. Wang, *Parton equilibration in relativistic heavy ion collisions*, Phys. Rev. **C48** (1993) 1275–1284 [`nucl-th/9303004`].

[89] D. M. Elliott and D. H. Rischke, *Chemical equilibration of quarks and gluons at RHIC and LHC energies*, Nucl. Phys. **A671** (2000) 583–608 [`nucl-th/9908004`].

[90] W. A. Hiscock and L. Lindblom, *Stability and causality in dissipative relativistic fluids*, Annals Phys. **151** (1983) 466–496.

[91] W. A. Hiscock and L. Lindblom, *Generic instabilities in first-order dissipative relativistic fluid theories*, Phys. Rev. **D31** (1985) 725–733.

[92] W. A. Hiscock and L. Lindblom, *Linear plane waves in dissipative relativistic fluids*, Phys. Rev. **D35** (1987) 3723–3732.

[93] P. Romatschke, *New developments in relativistic viscous hydrodynamics*, `0902.3663`.

[94] I. Bouras, E. Molnár, H. Niemi, Z. Xu, A. El, O. Fochler, C. Greiner and D. H. Rischke, *Relativistic shock waves in viscous gluon matter*, Physical Review Letters **103** (2009), no. 3 032301.

[95] A. Muronga, *New developments in relativistic dissipative fluid dynamics*, J. Phys. G: Nucl. Part. Phys. **37** (2010) 094008.

[96] H. Pleiner and J. L. Harden, *General nonlinear 2-fluid hydrodynamics of complex fluids and soft matter*, AIP Conference Proceedings **708** (2004), no. 1 46–51.

[97] M. M. Dupin, I. Halliday and C. M. Care, *Multi-component lattice boltzmann equation for mesoscale blood flow*, Journal of Physics A: Mathematical and General **36** (2003), no. 31 8517.

[98] M. Gavrikov and V. Savelev, *Plasmastatic problems in two-fluid magnetohydrodynamics with allowance for the electron inertia*, Fluid Dynamics **45** (2010) 325–341. 10.1134/S0015462810020171.

[99] M. Prakash, M. Prakash, R. Venugopalan and G. Welke, *Nonequilibrium properties of hadronic mixtures*, Phys.Rept. **227** (1993) 321–366.

[100] A. Monnai and T. Hirano, *Relativistic Viscous Hydrodynamic Equations at the Second Order for Multi-Component Systems with Multiple Conserved Currents*, `1003.3087`.

[101] R. Baier, P. Romatschke, D. T. Son, A. O. Starinets and M. A. Stephanov, *Relativistic viscous hydrodynamics, conformal invariance, and holography*, JHEP **04** (2008) 100 [`0712.2451`].

[102] G. S. Denicol, X.-G. Huang, T. Koide and D. H. Rischke, *Consistency of field-theoretical and kinetic calculations of viscous transport coefficients for a relativistic fluid*, `1003.0780`.

[103] M. Martinez and M. Strickland, *Pre-equilibrium dilepton production from an anisotropic quark-gluon plasma*, Phys. Rev. **C78** (2008) 034917 [`0805.4552`].

[104] F. Reif, Grundlagen der physikalischen Statistik und der Physik der Wärme. Berlin, New York : de Gruyter, 1976.

[105] F. Reining, *Untersuchung von scherfluss und -viskosität in einer partonischen kaskade*, Master's thesis, University of Frankfurt, 2009.

[106] A. Hosoya, M.-a. Sakagami and M. Takao, *NONEQUILIBRIUM THERMODYNAMICS IN FIELD THEORY: TRANSPORT COEFFICIENTS*, Ann. Phys. **154** (1984) 229.

[107] A. Hosoya and K. Kajantie, *Transport coefficients of qcd matter*, Nuclear Physics B **250** (1985), no. 1-4 666 – 688.

[108] S. Chakrabarty, *TRANSPORT COEFFICIENTS OF QUARK - GLUON PLASMA*, Pramana **25** (1985) 673–683.

[109] W. Czyz and W. Florkowski, *KINETIC COEFFICIENTS FOR QUARK - ANTI-QUARK PLASMA*, Acta Phys. Polon. **B17** (1986) 819–837.

[110] D. W. von Oertzen, *Transport coefficients in quantum chromodynamics*, Phys. Lett. **B280** (1992) 103–108.

[111] M. H. Thoma, *Viscosity coefficient of the quark - gluon plasma in the weak coupling limit*, Phys. Lett. **B269** (1991) 144–148.

[112] S. V. Ilin, A. D. Panferov and Y. M. Sinyukov, *THE VISCOSITY COEFFICIENT IN TEMPERATURE GAUGE THEORIES. QCD PLASMA*, Phys. Lett. **B227** (1989) 455–460.

[113] G. Baym, H. Monien, C. J. Pethick and D. G. Ravenhall, *Transverse interactions and transport in relativistic quark-gluon and electromagnetic plasmas*, Phys. Rev. Lett. **64** (Apr, 1990) 1867–1870.

[114] H. Heiselberg, *Viscosities of quark - gluon plasmas*, Phys. Rev. **D49** (1994) 4739–4750 [`hep-ph/9401309`].

[115] P. B. Arnold, G. D. Moore and L. G. Yaffe, *Transport coefficients in high temperature gauge theories: (I) Leading-log results*, JHEP **11** (2000) 001 [`hep-ph/0010177`].

[116] M. Luzum and P. Romatschke, *Conformal Relativistic Viscous Hydrodynamics: Applications to RHIC results at* $sqrt(s_NN) = 200GeV.$, Phys. Rev. **C78** (2008) 034915 [`0804.4015`].

[117] G. Policastro, D. T. Son and A. O. Starinets, *From AdS/CFT correspondence to hydrodynamics*, JHEP **09** (2002) 043 [`hep-th/0205052`].

[118] H. T. Elze, J. Rafelski and L. Turko, *Entropy production in relativistic hydrodynamics*, Phys. Lett. **B506** (2001) 123–130 [`hep-ph/0103066`].

[119] **UA5** Collaboration, K. Alpgard et. al., *First Results on Complete Events from p anti-p Collisions at the Center-of-Mass Energy of 540-GeV*, Phys. Lett. **B107** (1981) 310.

[120] I. G. Bearden, D. Beavis, C. Besliu, B. Budick, H. Bøggild, C. Chasman, C. H. Christensen, P. Christiansen, J. Cibor, R. Debbe, E. Enger, J. J. Gaardhøje, M. Germinario, K. Hagel, O. Hansen, A. Holm, A. K. Holme, H. Ito, A. Jipa, F. Jundt, J. I. Jørdre, C. E. Jørgensen, R. Karabowicz, E. J. Kim, T. Kozik, T. M. Larsen and J. H. Lee, *Charged meson rapidity distributions in central* $au + au$ *collisions at* $snn = 200gev$, Phys. Rev. Lett. **94** (Apr, 2005) 162301.

[121] L.-W. Chen, V. Greco, C. M. Ko and P. F. Kolb, *Pseudorapidity dependence of anisotropic flows in relativistic heavy-ion collisions*, Phys. Lett. **B605** (2005) 95–100 [`nucl-th/0408021`].

[122] V. Borchers, J. Meyer, S. Gieseke, G. Martens and C. C. Noack, *A Poincare covariant parton cascade model for ultrarelativistic heavy ion reactions*, Phys. Rev. **C62** (2000) 064903 [`hep-ph/0006038`].

[123] S. A. Bass, B. Muller and D. K. Srivastava, *Parton rescattering and screening in Au + Au collisions at RHIC*, Phys. Lett. **B551** (2003) 277–283 [`nucl-th/0207042`].

[124] P. Danielewicz and G. F. Bertsch, *Production of deuterons and pions in a transport model of energetic heavy ion reactions*, Nucl. Phys. **A533** (1991) 712–748.

[125] A. Lang, H. Babovsky, W. Cassing, U. Mosel, H.-G. Reusch and K. Weber, *A new treatment of boltzmann-like collision integrals in nuclear kinetic equations*, Journal of Computational Physics **106** (1993), no. 2 391 – 396.

[126] W. Cassing, *Antibaryon production in hot and dense nuclear matter*, Nucl. Phys. **A700** (2002) 618–646 [`nucl-th/0105069`].

[127] Z. Xu and C. Greiner, *Dependence of elliptic flow on number of parton degrees of freedom*, Phys. Rev. **C81** (2010) 054901 [`1001.2912`].

[128] S. M. H. Wong, *Thermal and chemical equilibration in a gluon plasma*, Nucl. Phys. **A607** (1996) 442–456 [`hep-ph/9606305`].

[129] J. F. Owens, E. Reya and M. Gluck, *Detailed Quantum Chromodynamic Predictions for High p(T) Processes*, Phys. Rev. **D18** (1978) 1501.

[130] T. S. Biro, B. Muller and X.-N. Wang, *Color screening in relativistic heavy ion collisions*, Phys. Lett. **B283** (1992) 171–173.

[131] J. F. Gunion and G. Bertsch, *HADRONIZATION BY COLOR BREMSSTRAHLUNG*, Phys. Rev. **D25** (1982) 746.

[132] A. B. Migdal, *Bremsstrahlung and pair production in condensed media at high-energies*, Phys. Rev. **103** (1956) 1811–1820.

[133] **D0** Collaboration, V. M. Abazov et. al., *Determination of the strong coupling constant from the inclusive jet cross section in ppbar collisions at sqrt(s)=1.96 TeV*, Phys. Rev. **D80** (2009) 111107 [`0911.2710`].

[134] G. M. Prosperi, M. Raciti and C. Simolo, *On the running coupling constant in QCD*, Prog. Part. Nucl. Phys. **58** (2007) 387–438 [`hep-ph/0607209`].

[135] O. Fochler, Z. Xu and C. Greiner, *Energy loss in a partonic transport model including bremsstrahlung processes*, `1003.4380`.

[136] Z. Xu, C. Greiner and H. Stocker, *PQCD calculations of elliptic flow and shear viscosity at RHIC*, Phys. Rev. Lett. **101** (2008) 082302 [`0711.0961`].

[137] G. Baym, *THERMAL EQUILIBRATION IN ULTRARELATIVISTIC HEAVY ION COLLISIONS*, Phys. Lett. **B138** (1984) 18–22.

[138] H. Heiselberg and X.-N. Wang, *Thermal Equilibration in an Expanding Parton Plasma*, Nucl. Phys. **B462** (1996) 389–414 [`hep-ph/9601247`].

[139] H. Heiselberg and X.-N. Wang, *Expansion, thermalization and entropy production in high- energy nuclear collisions*, Phys. Rev. **C53** (1996) 1892–1902 [`hep-ph/9504244`].

[140] S. M. H. Wong, *Thermal and chemical equilibration in relativistic heavy ion collisions*, Phys. Rev. **C54** (1996) 2588–2599 [`hep-ph/9609287`].

[141] E. V. Shuryak, *Two stage equilibration in high-energy heavy ion collisions*, Phys. Rev. Lett. **68** (1992) 3270–3272.

[142] R. Baier, A. H. Mueller, D. Schiff and D. T. Son, *'Bottom-up' thermalization in heavy ion collisions*, Phys. Lett. **B502** (2001) 51–58 [`hep-ph/0009237`].

[143] A. El, *Untersuchung des 'bottom-up' szenarios der thermalisierung im rahmen einer pqcd basierten partonischen kaskadesimulation*, Master's thesis, University of Frankfurt, 2006.

[144] A. Krasnitz and R. Venugopalan, *The initial energy density of gluons produced in very high energy nuclear collisions*, Phys. Rev. Lett. **84** (2000) 4309–4312 [`hep-ph/9909203`].

[145] F. Gelis, E. Iancu, J. Jalilian-Marian and R. Venugopalan, *The Color Glass Condensate*, `1002.0333`.

[146] A. Krasnitz, Y. Nara and R. Venugopalan, *Classical gluodynamics of high energy nuclear collisions: An erratum and an update*, Nucl. Phys. **A727** (2003) 427–436 [`hep-ph/0305112`].

[147] J. Bjoraker and R. Venugopalan, *From colored glass condensate to gluon plasma: Equilibration in high energy heavy ion collisions*, Phys. Rev. **C63** (2001) 024609 [`hep-ph/0008294`].

[148] D. Kharzeev and M. Nardi, *Hadron production in nuclear collisions at RHIC and high density QCD*, Phys. Lett. **B507** (2001) 121–128 [`nucl-th/0012025`].

[149] A. H. Mueller, *The Boltzmann equation for gluons at early times after a heavy ion collision*, Phys. Lett. **B475** (2000) 220–224 [`hep-ph/9909388`].

[150] A. H. Mueller, *Toward equilibration in the early stages after a high energy heavy ion collision*, Nucl. Phys. **B572** (2000) 227–240 [`hep-ph/9906322`].

[151] Z. Xu and C. Greiner, *Elliptic flow of gluon matter in ultrarelativistic heavy- ion collisions*, Phys. Rev. **C79** (2009) 014904 [`0811.2940`].

[152] B. Betz, M. Gyulassy, D. H. Rischke, H. Stocker and G. Torrieri, *Jet Propagation and Mach Cones in (3+1)d Ideal Hydrodynamics*, J. Phys. **G35** (2008) 104106 [`0804.4408`].

[153] M. Martinez and M. Strickland, *Constraining relativistic viscous hydrodynamical evolution*, Phys. Rev. **C79** (2009) 044903 [`0902.3834`].

[154] P. Kovtun, D. T. Son and A. O. Starinets, *Viscosity in strongly interacting quantum field theories from black hole physics*, Phys. Rev. Lett. **94** (2005) 111601 [`hep-th/0405231`].

[155] D. Molnar and M. Gyulassy, *Saturation of elliptic flow at RHIC: Results from the covariant elastic parton cascade model MPC*, Nucl. Phys. **A697** (2002) 495–520 [`nucl-th/0104073`].

[156] P. B. Arnold, G. D. Moore and L. G. Yaffe, *Transport coefficients in high temperature gauge theories. II: Beyond leading log*, JHEP **05** (2003) 051 [`hep-ph/0302165`].

[157] P. B. Arnold, G. D. Moore and L. G. Yaffe, *Effective kinetic theory for high temperature gauge theories*, JHEP **01** (2003) 030 [`hep-ph/0209353`].

[158] A. El, Z. Xu and C. Greiner, "Third-order dissipative hydrodynamics from the entropy principle." 2010.

[159] L. P. Csernai, *Introduction to relativistic heavy ion collisions*, . Chichester, UK: Wiley (1994) 310 p.

[160] P. Romatschke and A. Rebhan, *Plasma Instabilities in an Anisotropically Expanding Geometry*, Phys. Rev. Lett. **97** (2006) 252301 [`hep-ph/0605064`].

[161] R. J. Fries, *Early time evolution of high energy heavy ion collisions*, J. Phys. **G34** (2007) S851–854 [`nucl-th/0702026`].

[162] Y. V. Kovchegov and A. Taliotis, *Early time dynamics in heavy ion collisions from AdS/CFT correspondence*, Phys. Rev. **C76** (2007) 014905 [`0705.1234`].

[163] K. Rajagopal and N. Tripuraneni, *Bulk Viscosity and Cavitation in Boost-Invariant Hydrodynamic Expansion*, JHEP **03** (2010) 018 [`0908.1785`].

[164] P. F. Kolb and U. W. Heinz, *Hydrodynamic description of ultrarelativistic heavy-ion collisions*, `nucl-th/0305084`.

[165] M. Lublinsky and E. Shuryak, *Improved Hydrodynamics from the AdS/CFT*, Phys. Rev. **D80** (2009) 065026 [`0905.4069`].

[166] S. Khlebnikov, M. Kruczenski and G. Michalogiorgakis, *Shock waves in strongly coupled plasmas*, `1004.3803`.

[167] P. Huovinen and P. V. Ruuskanen, *Hydrodynamic Models for Heavy Ion Collisions*, Ann. Rev. Nucl. Part. Sci. **56** (2006) 163–206 [`nucl-th/0605008`].

[168] P. Braun-Munzinger, K. Redlich and J. Stachel, *Particle production in heavy ion collisions*, `nucl-th/0304013`.

[169] P. BRAHMS, PHENIX and S. Collaboration, Hunting the Quark Gluon Plasma: Results from the First 3 Years at RHIC. (Upton, NY: Brookhaven National Laboratory report No. BNL-73847-2005, 2005.

[170] **STAR** Collaboration, J. Adams et. al., *Multi-strange baryon production in Au Au collisions at s(NN)**(1/2) = 130-GeV*, Phys. Rev. Lett. **92** (2004) 182301 [`nucl-ex/0307024`].

[171] **STAR** Collaboration, O. Y. Barannikova, *Probing collision dynamics at RHIC*, `nucl-ex/0403014`.

[172] J. Cleymans, B. Kampfer, M. Kaneta, S. Wheaton and N. Xu, *Centrality dependence of thermal parameters deduced from hadron multiplicities in Au + Au collisions at s(NN)**(1/2) = 130-GeV*, Phys. Rev. **C71** (2005) 054901 [`hep-ph/0409071`].

[173] T. Matsui, B. Svetitsky and L. D. McLerran, *Strangeness production in ultrarelativistic heavy-ion collisions. i. chemical kinetics in the quark-gluon plasma*, Phys. Rev. D **34** (Aug, 1986) 783–793.

[174] D. K. Srivastava, M. G. Mustafa and B. Muller, *Expanding quark-gluon plasmas: Transverse flow, chemical equilibration, and electromagnetic radiation*, Phys. Rev. **C56** (1997) 1064–1074 [`nucl-th/9611041`].

[175] C. T. Traxler and M. H. Thoma, *Photon emission from a parton gas at chemical nonequilibrium*, Phys. Rev. **C53** (1996) 1348–1352 [`hep-ph/9507444`].

[176] D. Pal, A. Sen, M. G. Mustafa and D. K. Srivastava, *Evolution of strangeness in equilibrating and expanding quark-gluon plasma*, Phys. Rev. **C65** (2002) 034901 [`nucl-th/0105032`].

[177] P. Levai and X.-N. Wang, *Strangeness production in chemically non-equilibrated parton plasma*, `hep-ph/9504214`.

[178] J. Letessier and J. Rafelski, *Strangeness chemical equilibration in QGP at RHIC and LHC*, Phys. Rev. **C75** (2007) 014905 [`nucl-th/0602047`].

[179] Z. J. He, J. L. Long, Y. G. Ma, G. L. Ma and B. Liu, *Strangeness in a chemically equilibrating quark gluon plasma*, Phys. Rev. **C69** (2004) 034906.

[180] P. Levai, B. Muller and X.-N. Wang, *Open charm production in an equilibrating parton plasma*, Phys. Rev. **C51** (1995) 3326–3335 [`hep-ph/9412352`].

[181] Z. He, J. Long, W. Jiang, Y. Ma and B. Liu, *Dileptons from a chemically equilibrating quark-gluon plasma*, Phys. Rev. **C68** (2003) 024902.

[182] D. Dutta, A. K. Mohanty, K. Kumar and R. K. Choudhury, *Dissipative phenomena in chemically non-equilibrated quark gluon plasma*, Phys. Rev. **C61** (2000) 034902 [`hep-ph/9908359`].

[183] A. K. Chaudhuri, *Chemical equilibration in viscous quark-gluon plasma and electromagnetic signals*, J. Phys. **G26** (2000) 1433 [`nucl-th/9808074`].

[184] B. Kampfer, O. P. Pavlenko, A. Peshier and G. Soff, *Dilepton production in a chemically equilibrating, expanding, and hadronizing quark - gluon plasma*, Phys. Rev. **C52** (1995) 2704–2713.

[185] D. Dutta, A. K. Mohanty, K. Kumar and R. K. Choudhury, *Effect of baryon density on parton production, chemical equilibration and thermal photon emission from quark gluon plasma*, Phys. Rev. **C61** (2000) 064911 [`hep-ph/9912352`].

[186] B. K. Patra and M. Mishra, *Quenching of hadron spectra in a chemically equilibrating quark-gluon plasma*, `hep-ph/0703302`.

[187] F. Gelis, K. Kajantie and T. Lappi, *Chemical thermalization in relativistic heavy ion collisions*, Phys. Rev. Lett. **96** (2006) 032304 [`hep-ph/0508229`].

[188] Z.-w. Lin and C. M. Ko, *Flavor ordering of elliptic flows at high transverse momentum*, Phys. Rev. Lett. **89** (2002) 202302 [`nucl-th/0207014`].

[189] D. Molnar and S. A. Voloshin, *Elliptic flow at large transverse momenta from quark coalescence*, Phys. Rev. Lett. **91** (2003) 092301 [`nucl-th/0302014`].

[190] R. C. Hwa and C. B. Yang, *Scaling distributions of quarks, mesons and proton for all p(T), energy and centrality*, Phys. Rev. **C67** (2003) 064902 [`nucl-th/0302006`].

[191] K. Dusling and S. Lin, *Dilepton production from a viscous QGP*, Nucl. Phys. **A809** (2008) 246–258 [`0803.1262`].

[192] H. van Hees and R. Rapp, *Dileptons in Heavy-Ion Collisions*, Nucl. Phys. **A827** (2009) 341c–346c [`0901.2316`].

[193] **PHENIX** Collaboration, A. Adare et. al., *Detailed measurement of the e+e- pair continuum in p+p and au+au collisions at* $sqrt(s_nn) = 200$ *gev and implications for direct photon production*, Phys. Rev. **C81** (2010) 034911 [`0912.0244`].

[194] B. Schenke and M. Strickland, *Photon production from an anisotropic quark-gluon plasma*, Phys. Rev. **D76** (2007) 025023 [`hep-ph/0611332`].

[195] **PHENIX** Collaboration, S. S. Adler et. al., *Centrality dependence of direct photon production in s(NN)**(1/2) = 200-GeV Au + Au collisions*, Phys. Rev. Lett. **94** (2005) 232301 [`nucl-ex/0503003`].

[196] E. Molnar, *Comparing the first and second order theories of relativistic dissipative fluid dynamics using the 1+1 dimensional relativistic flux corrected transport algorithm*, Eur. Phys. J. **C60** (2009) 413–429 [`0807.0544`].

[197] E. Molnar, H. Niemi and D. H. Rischke, *Numerical tests of causal relativistic dissipative fluid dynamics*, Eur. Phys. J. **C65** (2010) 615–635 [`0907.2583`].

[198] H.-J. Drescher, A. Dumitru, A. Hayashigaki and Y. Nara, *The eccentricity in heavy-ion collisions from color glass condensate initial conditions*, Phys. Rev. **C74** (2006) 044905 [`nucl-th/0605012`].

[199] D. Kharzeev and M. Nardi, *Hadron production in nuclear collisions at RHIC and high density QCD*, Phys. Lett. **B507** (2001) 121–128 [`nucl-th/0012025`].

[200] E. L. Feinberg, *Direct Production of Photons and Dileptons in Thermodynamical Models of Multiple Hadron Production*, Nuovo Cim. **A34** (1976) 391.

[201] F. Lauciello Master's thesis, University of Frankfurt, 2011.

[202] E. Iancu and R. Venugopalan, *The Color glass condensate and high-energy scattering in QCD*, `hep-ph/0303204`. To be published in QGP3, Eds. R.C. Hwa and X.N.Wang, World Scientific.

[203] **The ALICE Collaboration** Collaboration, K. Aamodt et. al., *Elliptic flow of charged particles in Pb-Pb collisions at 2.76 TeV*, `1011.3914`. * Temporary entry *.

[204] H. Song, S. A. Bass and U. W. Heinz, *Elliptic flow in 200 A GeV Au+Au collisions and 2.76 A TeV Pb+Pb collisions: insights from viscous hydrodynamics + hadron cascade hybrid model*, `1103.2380`.

[205] M. Luzum and P. Romatschke, *Conformal Relativistic Viscous Hydrodynamics: Applications to RHIC results at s(NN)**(1/2) = 200-GeV*, Phys.Rev. **C78** (2008) 034915 [`0804.4015`].

[206] D. A. Teaney, *Viscous Hydrodynamics and the Quark Gluon Plasma*, `0905.2433`.

[207] I. Fuini, John, N. S. Demir, D. K. Srivastava and S. A. Bass, *Shear Viscosity in a Perturbative Quark-Gluon-Plasma*, J.Phys.G **G38** (2011) 015004 [`1008.2306`].

[208] B. L. Combridge, J. Kripfganz and J. Ranft, *Hadron production at large transverse momentum and qcd*, Physics Letters B **70** (1977), no. 2 234 – 238.

[209] **PHENIX** Collaboration, A. Bazilevsky, *Charged particle multiplicity and transverse energy measurements in Au Au collisions in PHENIX at RHIC*, Nucl. Phys. **A715** (2003) 486 [`nucl-ex/0209025`].

[210] J. Cleymans, R. Sahoo, D. P. Mahapatra, D. K. Srivastava and S. Wheaton, *Saturation of E_T/N_{ch} and Freeze-Out Criteria in Heavy-Ion Collisions*, J. Phys. **G35** (2008) 104147 [`0803.3940`].

[211] **The ALICE** Collaboration, K. Aamodt et. al., *Charged-particle multiplicity density at mid-rapidity in central Pb-Pb collisions at sqrt(sNN) = 2.76 TeV*, Phys. Rev. Lett. **105** (2010) 252301 [`1011.3916`].

[212] E. Byckling and K. Kajantie, Particle Kinematics. Wiley, 1973.

Index

”Bottom-Up” scenario, 55, 57

Asymptotic freedom, 2

BAMPS, 63
Bjorken scenario of heavy-ion collisions, 39
  Bjorken flow velocity, 41
Boltzmann Equation
  in a multi-component system, 36
Boltzmann equation, 49
Boost-invariance, 39
Bremsstrahlung (pQCD), 50
Bulk pressure, 12

Chapman-Enskog method, 34
Chemical equilibration, 100, 102, 103
  instantaneous, 98
Collision term, 50, 147
Color confinement, 2
Color Glass Condensate, 54, 55
Cross section
  isotropic, 79, 148
  total, 51, 79
  transport, 79
  transport , 72, 86

Distribution function, 14
  off-equilibrium, 14

Eckart frame, 13
Elliptic flow
  differential, 6
  integrated, 6
  scaling of, 7
Energy density, 12
Energy flow, 12
Energy frame, see Landau frame
Entropy current, 20, 21
  in a multi-component system, 27
Equilibrium pressure, 12
Expansion scalar, 81

Free-streaming limit, 90
Full stopping in heavy-ion collisions, 39

Gibbs-Duham relation, 20
Grad’s approximation, 61, 62, 64, 109
Gunion-Bertsch matrix elements, 53

Hadronization, 96
Heat flow, 12
High energy physics research facilities
  BEVALAC, Berkley, 3
  FAIR, GSI, 4
  LHC, CERN, 3, 4
  NICA, JINR, 4
  RHIC, BNL, 3, 4
Hydrodynamics
  ”all orders” equation, 91
  comparisons with kinetic transport, 107
  effective, 89
  first-order, 20
  multi-component, 26
  second-order, 21
  third-order, 23

Instantaneous chemical equilibration, 98
Inter-collisions, 36
Israel-Stewart equation, see second-order hydrodynamics
  truncated, 23

Jet quenching, 5

Kubo-Green formalism, 34

Landau frame, 13
Landau matching conditions, 16
Landau-Pomeranchuk-Migdal effect, 53
Longitudinal pressure, 44, 82

Mean free path, 78, 81
  transport, 86

Navier-Stockes equation, see first-order hydrodynamics
Nuclear modification factor, 5

Particle density, 12
Particle flow, 12
Particle frame, see Eckart frame
Partonic Cascade Models, 7
pQCD bremsstrahlung, 53
Pressure isotropy, 81
Proper time, 40

QCD, see Quantum Chromodynamics
Quantum Chromodynamics, 1
Quasi-particles, 78

Rapidity
  momentum, 41
  space-time, 40
Recombination model, 7, 96
Relaxation time, 22
Running coupling, 2, 54

Saturation momentum scale, 55
Self-collisions, 36
Shear stress tensor, 12
Shear viscosity, 21
  classical definition, 33
  effective, of a mixture, 117
  multi-component system, 36, 116
  of a pQCD medium, 69
  one-component system, 35
Single particle distribution function, 49
Smallness parameter, 80
Standard Model, 1
Statistical model, 95
Stochastic interpretation of collision rates, 49
Strong coupling constant, 54
Strongly coupled system, 70

Thermalization, 55
Transparency in heavy-ion collisions, 4, 39
Transport coefficients, 21
Transverse spectrum, 61, 63, 104

UrQMD, 8

Vorticity, 23

Curriculum Vitae

Andrej El

Goethe-Universität Frankfurt am Main
Institut für Theoretische Physik
Max-von-Laue Str. 1
60438 Frankfurt am Main
Telefon: (069) 798 47855
Email: el@th.physik.uni-frankfurt.de

Persönliche Daten

19.Juni 1980 geboren in Minsk, Belarus (ehem. UdSSR).

Seit 1997 in Deutschland wohnhaft

Seit 2006 deutscher Staatsbürger

Schulbildung

1986 – 1997 Allgemeine Hochschulreife (als Realschulabschluss anerkannt) an der Minsker Schule Nr.165, Minsk, Belarus.

1998 – 2001 Allgemeine Hochschulreife (Abitur), Ludwig-Geissler Schule, Hanau.

Studium und wissenschftlicher Werdegang

2001 – 2006 Studium der Physik an der Goethe-Universität Frankfurt am Main.

2002 – 2006 Mitglied der Studienstiftung des Deutschen Volkes

2006 Studium mit Diplom abgeschlossen.
Thema der Diplomarbeit: 'Untersuchung des Bottom-Up Szenarios der Thermalisierung im Rahmen einer pQCD basierten partonischen Kaskadesimulation'.
Betreuer der Diplomarbeit: Prof. Dr. C. Greiner

2006 Aufnahme als Doktorand an der Goethe-Universität Frankfurt am Main unter Betreuung von Prof. Dr. C. Greiner

Berufliche Tätigkeit

seit 2006 Wiss. Mitarbeiter der Goethe-Universität Frankfurt am Main.

Publikationen

Als Erstautor

Thermalization of a color glass condensate and review of the 'Bottom-Up' scenario.
A. El, Z. Xu, and C. Greiner, Nucl. Phys. A, 2008, 806, 287-304.

Shear viscosity and out of equilibrium dynamics.
A. El, A. Muronga, Z. Xu and C. Greiner, Physical Review C, 2009, 79, 044914.

Extension of relativistic dissipative hydrodynamics to third order.
A. El, Z. Xu and C. Greiner, Phys. Rev. C, 2010, 81, 041901

A Relativistic dissipative hydrodynamic description for systems including particle number changing processes.
A. El, A. Muronga, Z. Xu and C. Greiner, Nucl.Phys.A, 2010, 848, 428-442

Dissipative hydrodynamics for relativistic multi-component systems.
A. El,I. Bouras, F. Lauciello, Z. Xu and C. Greiner, 2011, arXiv: 1103.4038 [hep-ph]

Als Co-Autor

Relativistic Shock Waves in Viscous Gluon Matter.
I. Bouras, E. Molnár,H. Niemi, Z. Xu, A. El, O. Fochler, C. Greiner and D. Rischke, Physical Review Letters, 2009, 103, 032301

Investigation of shock waves in the relativistic Riemann problem: A comparison of viscous fluid dynamics to kinetic theory.
Bouras, I. et al, Phys. Rev. C, 2010, 82, 024910

Calculation of shear viscosity using Green-Kubo relations within a parton cascade.
C. Wesp et al, arXiv:1106.4306 [hep-ph]. Accepted for publication by PRC

Extraction of shear viscosity in stationary states of relativistic particle systems.
F. Reining et al, arXiv:1106.4210 [hep-th], submitted to PRE